

Determination of the rate of oceanic storage of anthropogenic CO<sub>2</sub>  
from measurements in the ocean interior:  
the South Atlantic Ocean

This thesis research was performed at the department of Ocean Ecosystems at the University of Groningen and the department of Biological and Chemical Oceanography at the Royal Netherlands Institute for Sea Research and was funded by the EU FP6 *Integrated Project* CarboOcean.

Printing of this thesis was supported by the Central Library and the Faculty of Mathematics and Natural Sciences of the University of Groningen.

Cover photo: *PFS Polarstern* breaking ice in the Weddell Sea, March 26<sup>th</sup>, 2008.

Lay-out: Steven van Heuven

Printed by: Ipskamp Drukkers, Enschede, The Netherlands

ISBN: 978-90-367-6012-6 (printed version)

978-90-367-6013-3 (electronic version)



RIJKSUNIVERSITEIT GRONINGEN

Determination of the rate of oceanic storage of anthropogenic CO<sub>2</sub>  
from measurements in the ocean interior:  
the South Atlantic Ocean

**Proefschrift**

ter verkrijging van het doctoraat in de  
Wiskunde en Natuurwetenschappen  
aan de Rijksuniversiteit Groningen  
op gezag van de  
Rector Magnificus, dr. E. Sterken,  
in het openbaar te verdedigen op  
vrijdag 8 februari 2013  
om 12:45 uur

door

Steven Marinus Adrianus Carolus van Heuven  
geboren op 15 maart 1980  
te Leiden

Promotores: Prof. dr. ir. H.J.W. de Baar  
Prof. dr. H.A.J. Meijer

Beoordelingscommissie: Prof. dr. L.G. Anderson  
Prof. dr. M. Rhein  
Prof. dr. ir. H. Ridderinkhof





# Contents

Chapter 1.	Introduction	1
Chapter 2.	Background	17
Chapter 3.	Shipboard methods and results	31
Chapter 4.	The CARINA data synthesis project: introduction and overview <i>Earth System Science Data, 2, 105-121, 2010 (co-author)</i>	57
Chapter 5.	Quality control procedures and methods of the CARINA database <i>Earth System Science Data, 2, 35-49, 2010 (co-author)</i>	83
Chapter 6.	Direct observation of increasing CO <sub>2</sub> in the Weddell Gyre along the Prime Meridian during 1973–2008 <i>Deep-Sea Research II, 58, 2613-2635, 2011 (first author)</i>	107
Chapter 7.	Determination of the rate of storage of anthropogenic CO <sub>2</sub> in the South Atlantic Ocean from 35 years of ocean interior observations <i>To be submitted to a scientific journal</i>	151
Chapter 8.	Synthesis and recommendations for future research	205
Chapter 9.	Summary	217
	Nederlandse samenvatting	225
	References	233
	Acknowledgements / dankwoord	249
	CV & Bibliography	255



# Chapter 1

## **Introduction**





## 1.1. The global carbon cycle

### *The natural steady state*

Carbon (C) is an element of fundamental importance to life on Earth. It is present in ubiquitous quantities: several tens of trillions of tonnes of carbon are contained in the air, sea, soil and living matter. This carbon is cycled between and within these *reservoirs* on time scales from days to millennia, driven by physical, chemical and biological processes. An atom of carbon may find itself as part of a plant leaf on one day, only to be released into the atmosphere the next, before being dissolved in the surface ocean where it may spend several decades before being released again. The rates of exchange are high, but because they are also reversing (seasonally or otherwise), there exists a dynamic equilibrium or *steady state*. The various reservoirs will, on average, contain approximately constant amounts of carbon. Figure 1.1 (Solomon et al., 2007) shows best estimates of the sizes of the reservoirs (*inventories*), and the exchanges between them (*fluxes*) for the 1990s.

The rapidly cycled, *biospheric* carbon, constitutes only a small fraction of the total amount of carbon on Earth. Much more carbon may be found as sedimentary formations of

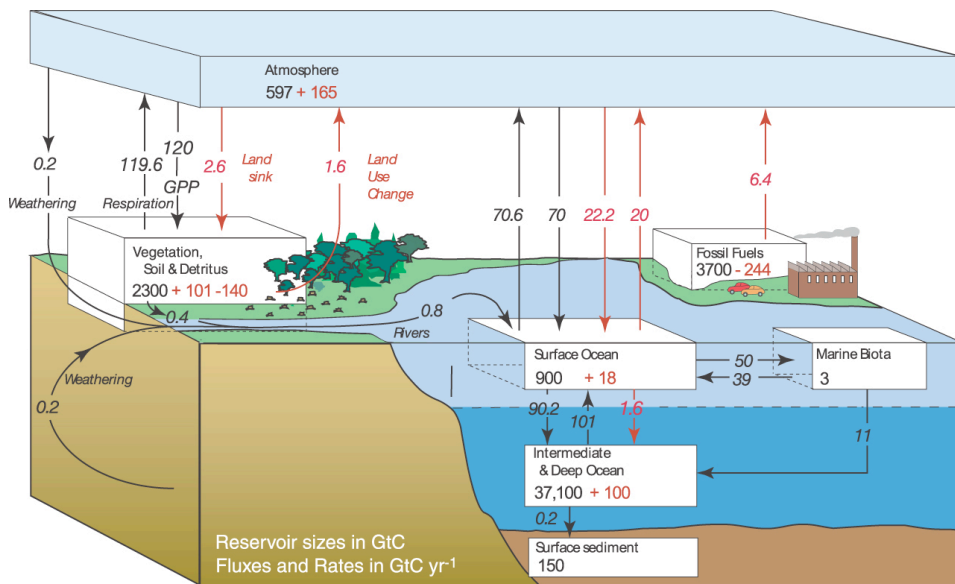


**Figure 1.1.** A schematic representation of reservoir and flux sizes of the perturbed global carbon cycle for the 1990s. Reservoir sizes are given in gigatonnes of carbon (PgC). Fluxes are given in PgC per year (PgC a<sup>-1</sup>). Black numerals represent reservoir sizes and fluxes of the pre-industrial 'natural' carbon cycle. Red numerals represent the size of the anthropogenic perturbation. Gross fluxes generally have uncertainties of more than  $\pm 20\%$ . Not shown are the very large reservoirs of sedimentary CaCO<sub>3</sub> deposits (i.e., limestones,  $\sim 60$  million PgC) and sedimentary organic carbon deposits ( $\sim 12$  million PgC). The latter pool contains the relatively small pool of recoverable fossil fuels (mainly coal, oil, methane gas), which is currently estimated to be in the order of  $\sim 6000$  PgC. Source: Solomon et al., 2007.

## Chapter 1

limestone deposits ( $\text{CaCO}_3$ ; 60 million PgC; see Panel 1.1 for explanation of used units) and as organic sedimentary deposits (12 million PgC). The latter contains the various forms of *fossil fuels* (coal, oil, methane gas; ~6000 PgC). Moreover, carbon may be found within the igneous rock (i.e., of volcanic origin).

For all practical considerations, the above sedimentary deposits of carbon have no significant *natural* contact with the biosphere on the times scales relevant to human society. Only a very modest natural exchange is known to take place between the biospheric and deep-earth reservoirs as slow chemical weathering of sedimentary and igneous rocks, and in context of the geological process of plate tectonics and associated volcanism (Varekamp, 1992).

### *The perturbed global carbon cycle*

In a very strong departure from the natural *steady state* of the carbon cycle, humanity has taken to the rapid extraction of fossil fuels from geological reservoirs to drive, by their combustion in heat engines and furnaces, the unparalleled economic expansion that has been taking place since the middle of the 18th century. The combusted carbon is emitted to the atmosphere as carbon dioxide ( $\text{CO}_2$ ), adding to the natural concentration of this gas in the atmosphere. Additional sources of 'human-caused' or *anthropogenic*  $\text{CO}_2$  ( $\text{CO}_2^{\text{ant}}$ ) are land use change (mainly deforestation) and, to lesser extent, cement production. After emission, the anthropogenic  $\text{CO}_2$  takes part in the natural carbon cycle and will thereby divide itself over its various reservoirs (atmosphere, land, ocean).

### *Current and hypothesized consequences of the anthropogenic perturbation*

Approximately about half of the anthropogenic emissions are taken up from the atmosphere by the land and ocean sinks (54% for the decade 2000-2010; [www.globalcarbonproject.org](http://www.globalcarbonproject.org)). The  $\text{CO}_2$  that remains in the atmosphere (thus, 46%) is understood to change the character of the atmosphere in ways that may prove distinctly unfavorable to the welfare of human societies (Field et al., 2012). The heat trapping potential of  $\text{CO}_2$  will reduce that rate at which the planet may radiate heat into space (Arrhenius, 1896). As a consequence of this, the planet is expected

#### **Panel 1.1 – Some useful units**

This thesis uses a variety of units to denote amounts and concentrations of carbon, dissolved carbon. To aid the reader in interpreting these, some scaling factors are listed here.

1 mole of carbon (C) has a mass of ~12 grams

1 mole of  $\text{CO}_2$  has a mass of ~44 grams

1 gram of  $\text{CO}_2$  contains 0.273 grams of carbon

1 PgC = 1 petagram of carbon =  $10^{15}$  grams of carbon = 1 gigaton of carbon = 1 GtC

1 TgC = 1 teragram of carbon =  $10^{12}$  grams of carbon = 1 megaton of carbon = 1 MtC

1  $\mu\text{mol kg}^{-1}$  = 1 micromole (=  $10^{-6}$  mol) per kilogram of seawater

to experience a warming of several degrees above pre-industrial temperatures in coming decades (Solomon et al., 2007). Indeed, this progressing warming has already been unambiguously observed in data sets of land surface temperatures, ocean surface temperatures and ocean interior temperatures. Associated changes are documented in, among others, atmospheric water vapor content, outgoing planetary radiation, stratospheric temperature, sea surface height, sea ice extent, sea ice volume, and glacier and ice sheet mass (Solomon et al., 2007). Other consequences of the rise in CO<sub>2</sub> are as of yet somewhat less well documented, but are commonly considered to be very likely to occur in the near future. Among these are regional increases in the incidence of extreme weather events like storms, flooding, and droughts (Field et al., 2012).

Additionally, the continuous uptake of CO<sub>2</sub> by the ocean leads to the gradual 'acidification' of its surface waters (Feely et al., 2009). A hypothesized societally relevant effect of this is the increase with time of the solubility of certain shells and corals (Feely et al., 2004). The process is presumed to have potentially severe future consequences for the health of coastal and open ocean ecosystems, and the societies that depend on them (Orr et al., 2005, Doney et al., 2009). On the other hand, these ecosystems may display some resilience to these changes due the ability of species to adapt and evolve in the face of changing environmental conditions (e.g., Lohbeck et al., 2012).

Given the low predictability of the medium- and long term effects on society, the current anthropogenic emissions have been likened to an one-off experiment (Revelle and Suess, 1957):

*[...] human beings are now carrying out a large scale geophysical experiment of a kind that could not have happened in the past nor be reproduced in the future. Within a few centuries we are returning to the atmosphere and oceans the concentrated organic carbon stored in sedimentary rocks over hundreds of millions of years. This experiment, if adequately documented, may yield a far-reaching insight into the processes determining weather and climate. It therefore becomes of prime importance to attempt to determine the way in which carbon dioxide is partitioned between the atmosphere, the oceans, the biosphere and the lithosphere.*

Indeed, the momentous opportunity to track the planetary response to a unique perturbation of the global climate system, and the societal concern about its potential outcomes, have triggered the meticulous study of all aspects of the perturbed global carbon cycle.

#### *The current state of global carbon cycle research*

The current best estimates of the time histories of important sources and sinks of anthropogenic CO<sub>2</sub> are shown in Figure 1.2 (reproduced from Le Quééré et al., 2009; [www.globalcarbonproject.org](http://www.globalcarbonproject.org)). An overview of the corresponding mean rates of emissions over the past decade is provided in Table 1. The following section will outline how these time histories have been obtained. For a brief explanation of the used units, please refer to Panel 1.1.

**Emissions to the atmosphere.** Time histories of anthropogenic emissions have been inferred from historic and modern production records of fossil fuel extraction and logging industries (Boden et al., 2011 and Houghton, 2008, respectively). Although the uncertainty of emissions from land use change is considered to be substantial ( $\pm 0.5 \text{ PgC a}^{-1}$ , i.e.,  $\pm 25\text{-}50\%$ ; Canadell et al., 2007) the much larger emissions from combustion of fossil fuels and production

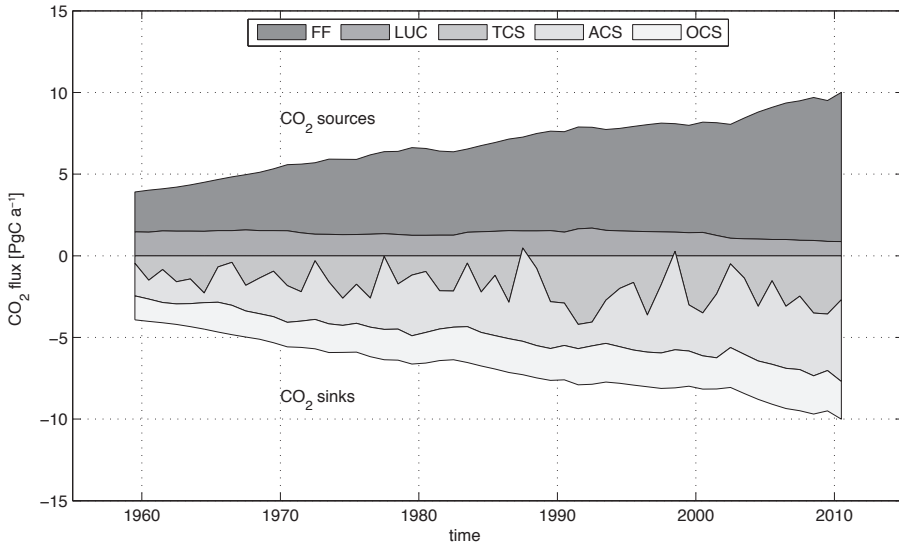


**Figure 1.2.** Current best estimates of the times histories of the source or sink rates of five components of the perturbed global carbon cycle. Sources of anthropogenic CO<sub>2</sub> emissions are the combustion of fossil fuels and cement production (together comprising FFC) and land use change (LUC). Emitted CO<sub>2</sub> is stored as living and dead biomass on land in the terrestrial carbon sink (TCS), as CO<sub>2</sub> in the atmospheric carbon sink (ACS) and as dissolved inorganic carbon in the oceanic carbon sink (OCS). Source terms are obtained from Boden et al. (2011) and Houghton (2008), respectively. The rate of accumulation of CO<sub>2</sub><sup>ant</sup> in the atmosphere is determined from the measured atmospheric concentration of CO<sub>2</sub> (Keeling et al., 2001; Etheridge et al., 1996). The oceanic sink rate is obtained as the mean rate of a suite of computer models (Le Quéré et al., 2009). Each model was calibrated to reproduce the best estimate of the total oceanic inventory of C<sub>ant</sub> in 1994 that was determined by Solomon et al., 2007 on the basis of 7 data-based estimates. The land sink rate is defined as the residual of the emissions and the atmospheric and oceanic sinks (i.e. land sink = (sum of sources) – oceanic sink – atmospheric sink). Source: [www.globalcarbonproject.org](http://www.globalcarbonproject.org).

of cement are accurately known ( $\pm 5\%$ ; Boden et al., 2011). The total emissions accumulated since  $\sim 1750$  are therefore well established to be  $\sim 344$  PgC in the year 2008.

**The atmospheric sink.** A time history of the atmospheric sink of CO<sub>2</sub><sup>ant</sup> (i.e., of the amount of emitted CO<sub>2</sub><sup>ant</sup> that remains in the atmosphere rather than being taken up by ocean or land sink) may be calculated by multiplying the atmospheric time history of the concentration of CO<sub>2</sub><sup>ant</sup> with the volume of the atmosphere. This simple approach is feasible due to the fact that the atmospheric concentrations are virtually uniform due to short mixing timescale of the atmosphere. The concentration history of CO<sub>2</sub><sup>ant</sup> has been reconstructed from atmospheric measurements (since 1959; Keeling et al., 2001) and the analysis of air bubbles trapped in the snow (that is gradually converted to ice) of the ice caps of Antarctica and Greenland (Etheridge et al., 1996). From these ice core records, the pre-industrial concentration is known to have been  $\sim 280$  ppm. Presently (2012), the atmospheric concentration of CO<sub>2</sub> already is  $\sim 393$  ppm and is rising with  $\sim 2$  ppm per year.

**The land sink.** The time history of the land sink of CO<sub>2</sub><sup>ant</sup> is complicated to establish due to involvement of many large- and small-scale processes such as enhanced carbon and nitrogen fertilization, changing agricultural practice, afforestation, fire risk mitigation and graz-

**Table 1.1.** Current best estimates of the source or sink rates of five components of the perturbed global carbon cycle, as determined for the decades 1961-1970 and 2001-2010. For additional details please refer to the caption of Figure 1.2. Uncertainties in totals are the quadratic sums of the uncertainties of constituent fractions. Source: [www.globalcarbonproject.org](http://www.globalcarbonproject.org).

Sources / sinks	Data source	Source / sink rate 1961-1970 (PgC a <sup>-1</sup> )	Source / sink rate 2001-2010 (PgC a <sup>-1</sup> )
<b>Sources</b>			
Fossil fuel & cement	Bookkeeping	3.1±0.2	7.9±0.5
Land use change	Bookkeeping	1.5±0.7	1.0±0.7
<b>Total</b>		<b>4.6±0.7</b>	<b>8.9±0.9</b>
<b>Sinks</b>			
Atmosphere	Measurements	1.8±0.1 (39± 7%)	4.1±0.2 (46±4%)
Ocean	Models & Measurements	1.5±0.4 (33±10%)	2.3±0.5 (26±5%)
Land	Residual	1.2±0.9 (28±12%)	2.5±1.0 (28±6%)
<b>Total</b>		<b>4.5±1.0</b>	<b>8.9±1.1</b>

ing management (Solomon et al., 2007). Although this terrestrial carbon sink has previously been defined as the residual of (i) the emissions and (ii) the atmospheric and oceanic sinks (e.g., Canadell et al., 2007; Solomon et al., 2007), direct estimates may be obtained from global vegetation cover models (Sitch et al., 2008).

**The oceanic sink.** The time history of the oceanic sink is commonly determined from modeling work. Although no validation of the accuracy of the models is possible due to absence of historic data, several estimates of the total inventory of CO<sub>2</sub><sup>ant</sup> are available for the mid 1990s (e.g., Sabine et al., 2004; Waugh et al., 2006). The models may be tuned to reproduce these estimates, thereby optimizing their value. Additionally, measurement-based global estimates of the net air-sea flux are available (e.g., Takahashi et al., 2009), but have a significant uncertainty due to the very high variability of the air-sea fluxes of CO<sub>2</sub> in space and time which is not easily captured by the still relatively sparse measurements. An accurate assessment of the rate of storage of CO<sub>2</sub><sup>ant</sup> in the ocean interior would thus be of high value for the corroboration of the strength of the oceanic sink. Performing this quantification is the objective of this thesis, for case studies focusing on the South Atlantic Ocean.

## 1.2. The ocean carbon cycle

The ocean plays a pivotal role in the global carbon cycle. Due to the large quantities of dissolved CO<sub>2</sub> it contains, and its capacity for rapid gas exchange, the ocean has a strong influence on the atmospheric CO<sub>2</sub> concentration and thereby on global climate (Broecker and Peng, 1982). Clearly then, a thorough understanding of the functioning of the *ocean* carbon cycle is essential for projections of how the *global* carbon cycle may be affected by human activities.

The many fluxes and reservoirs of carbon that are found within the ocean are of diverse nature and scale, and are variable over space and time. The remainder of the present section contains a qualitative description of the processes that govern the dynamics of dissolved CO<sub>2</sub> in sea water. A more technical treatment of these concepts and processes is provided in Chapter 2 of this thesis.

## Chapter 1

### *Origin of CO<sub>2</sub> in the oceans.*

The erosion of terrestrial sedimentary and igneous rock ('weathering') has provided a river-borne flow of dissolved substances to the oceans. Among these substances are all the constituents of sea salt including dissolved inorganic carbon (DIC or C<sub>T</sub>, see Panel 1.2) and calcium (Ca), these latter largely due to dissolution by rain and rivers of limestone deposits (CaCO<sub>3</sub>) on land. The observed concentrations of these compounds in the ocean is determined by the relative rates of **a)** the riverine input and **b)** the removal to the sediment and burial in thick sediment deposits of the ocean floor (Broecker, 1971). The balance between these source and sink terms, and the continuous 'stirring' of the ocean by its currents result in a fairly homogenous average composition of the dissolved substances in sea water that contains approximately 2 moles of dissolved inorganic carbon per cubic meter (~25 grams of inorganic carbon per 1000 liters). However, several processes contribute to significant alterations to this uniform distribution (see below).

### *Air-sea gas exchange.*

The solubility of CO<sub>2</sub> in seawater is negatively related to the water temperature. That is, when surface waters cool, more CO<sub>2</sub> may dissolve in it, causing *undersaturation* with respect to the atmosphere, upon which a net flux of CO<sub>2</sub> from the atmosphere may take place. Reversely, warming of sea water may lead to *oversaturation* and an efflux of CO<sub>2</sub> to the atmosphere.

Surface ocean currents, flowing from equatorial regions towards the poles will, during their journey, experience strong cooling and will thus become strongly enriched in C<sub>T</sub>. When these waters are cooled to near-freezing temperatures, the dense water may sink to depth, filling the abyssal ocean. These deep, cold ocean waters are therefore high in C<sub>T</sub> compared to the more shallow and warm, temperate or equatorial waters. This process of C<sub>T</sub>-enrichment of the deep layers of the ocean by strictly physical processes, is commonly referred to as the *solubility pump*, the *physical pump* or the *gas-exchange pump* (Volk and Hoffert, 1985; subtle differences between these terms exist, see Chapter 8 of Gruber and Sarmiento, 2007). Note that the word

### **Panel 1.2 – Some useful definitions**

*Dissolved inorganic carbon (DIC).* The total amount of dissolved inorganic carbon (TCO<sub>2</sub>, ΣCO<sub>2</sub> or, in this work, C<sub>T</sub>) is defined as the sum of the concentrations of aqueous CO<sub>2</sub>, carbonic acid, bicarbonate ion and carbonate ion. In this thesis, the abbreviation DIC is used as a qualitative term, whereas C<sub>T</sub> refers to the sum of concentrations of the constituents of DIC. Please note that in other literature the term DIC often serves both purposes.

$$C_T = [\text{CO}_{2(\text{aq})}] + [\text{H}_2\text{CO}_{3(\text{aq})}] + [\text{HCO}_3^-(\text{aq})] + [\text{CO}_3^{2-}(\text{aq})] \quad (1-1)$$

In equation (1-1), the brackets represent the concentrations of the molecule enclosed. The exact partitioning of a given amount of C<sub>T</sub> between these three species of dissolved inorganic carbon (HCO<sub>3</sub><sup>-</sup>, CO<sub>3</sub><sup>2-</sup> and CO<sub>2</sub>) at certain location in the ocean is governed by the local temperature, salinity, pressure and *alkalinity* (see below). In all natural seawater, DIC is predominantly present in

‘pump’ here does not have the same meaning as with the biological pumps discussed later, in that the process does not physically transport CO<sub>2</sub> along the water column, but rather acts only at the surface. It is the above process of *deep water formation* that causes the imprint of this ‘pump’ on vertical profiles of C<sub>T</sub>.

The exact degree of the enrichment (the CO<sub>2</sub>-saturation) of the deep layers depends on the duration and vigorousness of contact between surface water with the atmosphere during the cooling phase. This CO<sub>2</sub>-saturation is variable in space and time (e.g., Gruber et al., 1996), and is generally observed to be less than 100% (Murnane, 1999; Toggweiler, 2003).

With the increasing concentration of CO<sub>2</sub> in the atmosphere, the net flux of CO<sub>2</sub> into the surface oceans is gradually becoming larger, while the regions of efflux become more restricted in space and time (Postma, 1964; Takahashi et al., 2009).

#### *Primary production.*

All photosynthetic life forms in the ocean consume dissolved inorganic carbon for the production of their biomass, using sunlight as an energy source. This process locally reduces C<sub>T</sub>. Reversely, when and where this biomass decomposes (due to bacterial activity and/or animal consumption and respiration), C<sub>T</sub> will increase. While the production process occurs exclusively in the euphotic (‘sunlit’) zone, the decomposition process may occur throughout the water column (e.g., Schneider et al., 2003). The tendency of dead organic matter to gradually sink down through the water column, in combination with decomposition by bacteria and animals, leads to elevated C<sub>T</sub> at depth, and tends to reduce concentrations in the shallow layer which, however, are stabilized by replenishment from the atmosphere.

The overall process of biophysically mediated downward displacement of C<sub>T</sub> within the water column is generally referred to as the *soft tissue pump* (Volk and Hoffert, 1985). While the enhancement of the functioning of this pump due to increasing levels of anthropogenic CO<sub>2</sub> was considered unlikely by earlier studies, recent mesocosm experiments suggest that enhanced

the form of bicarbonate ion (~90%) and carbonate ion (~9%). Approximately 1% is present as dissolved CO<sub>2(aq)</sub>, which at the sea surface may rapidly exchange with the gaseous CO<sub>2</sub> in the overlying atmosphere.



Due to uptake of anthropogenic CO<sub>2</sub>(CO<sub>2</sub><sup>ant</sup>) from the atmosphere, the measured C<sub>T</sub> of a sea water sample is the sum of the ‘natural’ amount (C<sub>nat</sub>) that would be present irrespective of human emissions, and the anthropogenic amount (C<sub>ant</sub>) that entered the ocean through gas exchange with the atmosphere. Within C<sub>T</sub>, the fraction C<sub>ant</sub> cannot be analytically distinguished from C<sub>nat</sub>.

$$C_T = C_{\text{nat}} + C_{\text{ant}} \quad (1-3)$$



## Chapter 1

export of carbon to deeper layers may occur under future high-CO<sub>2</sub> scenarios (Riebesell et al., 2007).

### *Calcification and sediment interaction.*

In addition to producing 'soft' biomass (above), various organisms utilize inorganic carbon and calcium ions (Ca<sup>2+</sup>) for the production of calcium carbonate (CaCO<sub>3</sub>) for certain hard tissues (shells, frustules). Upon death of these organisms, the particles may settle down through the water column (often together with the soft tissue) and will often redissolve at depth. This *carbonate pump* (Volk and Hoffert, 1985) thus complements the functioning of the soft-tissue pump. Moreover, the carbonate pump gradually displaces *alkalinity* from the euphotic zone to the deep ocean (alkalinity is the property that represents the 'buffer capacity' of sea water, and is of major importance to the solution chemistry of dissolved inorganic carbon and calcareous sediments; see Chapter 2.1).

Part of the CaCO<sub>3</sub> settles to ocean floor, contributing to the sediments. This latter process removes both dissolved inorganic carbon and alkalinity from the water column. As mentioned, in a steady-state ocean, the net rate of production of calcareous sediments is commonly considered to equal the rate at which freshly eroded terrestrial calcareous material is delivered (in dissolved state) to the oceans by rivers.

The long-term conservation of calcareous sediment is sensitive to the local solubility of calcium carbonate. Intriguingly, that solubility is *positively* related to C<sub>T</sub>. It is therefore commonly expected that, due to gradual increase in C<sub>T</sub> due to accumulation of anthropogenic CO<sub>2</sub> in the deep ocean, calcareous sediments will increasingly dissolve. This dissolution will gradually increase the alkalinity and thereby the 'buffer capacity' of the ocean, allowing more CO<sub>2</sub> to be taken up. Eventually, this will lead to a high-C<sub>T</sub>, high-alkalinity ocean, that is expected to have taken up most of the CO<sub>2</sub> that is currently being emitted by human societies, albeit on a long timescale in the order of ten thousand to one hundred thousand years (Archer and Brovkin, 2005).

### *Circulation and outgassing.*

The processes outlined above overall act to increase C<sub>T</sub> (and alkalinity) at depth. The continuous, gradual circulation of the oceans balances this increase in the deep ocean by upward transport to shallower layers (upwelling). Indeed, in regions of strong upwelling (notably in the eastern equatorial zones of the Atlantic and Pacific oceans, and in the Southern Ocean), the upwelling of highly CO<sub>2</sub>-enriched water results in substantial effluxes of CO<sub>2</sub> to the atmosphere (Takahashi et al., 2009). The rate of the overturning deep circulation thus has a direct influence on the amount of CO<sub>2</sub> that may accumulate in the deep oceans, and thereby also on atmospheric and terrestrial inventories (Broecker and Peng, 1982). Recently, evidence is mounting for the hypothesis that long-term variations in the rate of overturning circulation have been of pivotal importance to the alternation of global climate between glacial and interglacial conditions (e.g., Schmitt et al., 2012).



### 1.3. A brief history of the investigation of anthropogenic CO<sub>2</sub> in the ocean

Due to uptake of anthropogenic CO<sub>2</sub> (CO<sub>2</sub><sup>ant</sup>) from the atmosphere, the measured C<sub>T</sub> of a sea water sample is the sum of the ‘natural’ amount (C<sub>nat</sub>) that would be present irrespective of human emissions, and the anthropogenic amount (C<sub>ant</sub>) that entered the ocean through gas exchange with the atmosphere (Eq. 1-3). Within C<sub>T</sub>, the fraction C<sub>ant</sub> cannot be analytically distinguished from C<sub>nat</sub>. Moreover, as illustrated by the overview of the ocean carbon cycle sketched above, C<sub>T</sub> may be variable over space and time as a function of the natural variability of circulation rates, biological activity and processes affecting air-sea gas exchange (for example wind speed and ice cover).

Despite the above complications, already almost 50 years ago Postma (1964) presented a data-based estimate of an increase of C<sub>T</sub> in ocean surface waters of 0.5 ml l<sup>-1</sup> compared to pre-industrial levels presumably as a result of the accumulation of anthropogenic CO<sub>2</sub> (in present-day units, this is equivalent to approximately 20 μmol kg<sup>-1</sup>; this compared with a natural background concentration of ~2000 μmol kg<sup>-1</sup>). Although the estimate of Postma would later prove remarkably accurate, the used methodology could not be used to infer accurate spatial or temporal patterns of this storage.

In 1978, using the high-accuracy measurements of C<sub>T</sub> and alkalinity made during the GEOSECS expeditions, combined with newly conceived approaches to compensate for biogeochemically induced variability of C<sub>T</sub>, Brewer showed the concentrations of C<sub>T</sub> in a water mass of Antarctic origin to be elevated (by circa 33±15 μmol kg<sup>-1</sup>) at the surface compared to its older, ocean interior extension. This observation strongly suggested the accumulation of that amount of C<sub>ant</sub> in the surface waters. Almost concurrently, Chen and Millero (1979) used a conceptually similar approach to calculate an accumulation of C<sub>ant</sub> in these same waters over industrial times of circa 40±15 μmol kg<sup>-1</sup>. As before, although remarkably accurate in hindsight, the validity of these methods and their results were suggested to be compromised by the assumptions that were required, and by the general lack of high-accuracy data at the time.

In the early 1990s, several advances in the analytical realm were made. The first was the development of coulometry as a new analytical method for the high-accuracy determination of C<sub>T</sub> (Johnson et al., 1993). A second was the introduction and use of *certified reference material* (CRM; Dickson, 2001), which allowed CO<sub>2</sub>-laboratories around the world to set, control and verify their accuracy. Lastly, a set of *standard operation procedures* was published that rigorously harmonized laboratory practice between groups (Dickson and Goyet, 1994; updated as Dickson et al., 2007). These conceptual and technical developments came together in the World Ocean Circulation Experiment (WOCE), which generated in the mid 1990s a nearly synoptic, global, high-accuracy dataset of ocean interior C<sub>T</sub> and related properties.

As another major improvement to the field, Gruber and co-workers in 1996 introduced a refinement of earlier conceptual methods that allowed the explicit quantification of C<sub>ant</sub>. This ΔC\* method allows the user an objective way of quantifying the pre-industrial C<sub>T</sub> content of a water mass, after which the difference with modern measurements yields C<sub>ant</sub>. The method gained considerable recognition in the research community, and was applied to almost every major ocean basin (e.g., Atlantic ocean: Gruber et al., 1998; Indian Ocean: Sabine et al., 1999; Pacific Ocean: Sabine et al., 2002).

The WOCE-era data and results were used by Sabine and co-workers to synthesize, in 2004, for the first time, an estimate of the global ocean inventory of  $C_{\text{ant}}$  (valid for 1994) of  $120 \pm 18$  PgC. Although the study constituted a major milestone in the field of carbon cycle research, the employed  $\Delta C^*$ -technique has subsequently been suggested (Matsumoto and Gruber, 2005) to suffer from conceptual drawbacks, particularly regarding its application to the Southern Ocean. In the Southern Ocean south of  $50^\circ\text{S}$ , Sabine et al. (2004), report negligible  $C_{\text{ant}}$ . However, later studies suggested moderate (Waugh et al., 2006) to high (Lo Monaco, 2005a,b) concentrations of  $C_{\text{ant}}$  and correspondingly higher inventories. Further exemplifying this uncertainty, specific to the Southern Ocean, are the mutually discordant results from sea surface  $\text{CO}_2$  flux studies (Takahashi et al., 2009), ocean carbon cycle models (Doney et al., 2009a), and oceanic and atmospheric inversion studies (Gruber et al., 2009, and references therein).

Additional uncertainty about the oceanic uptake and storage of  $\text{CO}_2^{\text{ant}}$  is presented by the suggestion, based on recent sea surface observations (e.g., Schuster and Watson, 2007; Metzl et al., 2010; McKinley et al., 2011) and atmospheric inversion models (Le Quéré et al., 2007), that the percentage of emitted  $\text{CO}_2^{\text{ant}}$  taken up by the oceans has been decreasing over recent years. This would leave an increasing part of the emitted  $\text{CO}_2^{\text{ant}}$  in the atmosphere, thereby further accelerating global climate change. Several mechanisms are hypothesized to be involved in this process (although not all are pertinent to the above-mentioned observations in the North Atlantic Ocean). Among the proposed mechanisms are changes in ocean circulation, driven by changing atmospheric wind patterns (Le Quéré et al., 2007, Lovenduski et al., 2009; but see Böning 2008). Others propose that a global warming-induced reduction of the solubility of  $\text{CO}_2$  may play a role (McKinley et al., 2011). On the other hand, the more straightforward increase in the *Revelle factor* (see chapter 2 of this thesis) with increasing  $C_T$  (Sarmiento et al., 1995, Thomas et al., 2007) is alternatively considered to be a sufficient explanation.

Conspicuously absent from the above discussion are actual, ocean interior data-based estimates of the rate of storage of anthropogenic  $\text{CO}_2$  by the oceans. Only very few such estimates are currently available, for just a few locations around the world (Sabine and Tanhua, 2010, and references therein). Obtaining additional such estimates, preferably on basin-wide scale, would be of significant value to help elucidate these recent developments within the global carbon cycle.

### 1.4. CarboOcean and the next steps forward

This thesis work was performed in the context of the European Union-funded *CarboOcean Integrated Project*. Among the major aims of the larger program were the assessment of the capacity of the ocean for continued uptake and storage of  $C_{\text{ant}}$ , as was stated as one of its *primary objectives* (CarboOcean Scientific Steering Committee, 2004):

***Objective 2.1:** Quantify the Atlantic and Southern Ocean carbon sink, and its decadal change, through highest accuracy measurement of the changing inventories of inorganic carbon and carbon-related tracers.*

Of the 15 work packages defined within the CarboOcean project, two are of specific relevance to both Objective 2.1 and this thesis:

*Work Package 8: Assemble and report an observational database of measurements of carbon and carbon related properties in the ocean interior through collection, merging and reporting of new and historical data.* Elements of this work package were stated to be the carrying out of new research expeditions and the merging and processing (for optimal internal consistency) of all available new and historical high-quality datasets of ocean interior, carbon-relevant measurements.

*Work Package 9: Anthropogenic carbon and decadal changes in carbon inventory.* Elements of this work package that are relevant to this thesis work are the aim to provide a comparison of the various methods that were available at the time for the assessment of concentration of  $C_{\text{ant}}$  in the oceans, and the selection of one or more best-in-class methods to be applied to new and available datasets.

## 1.5. Organization of this thesis

This thesis contains chapters that pertain to each of the two above mentioned Work Packages involved in the assessment of the accumulation of  $C_{\text{ant}}$  in the oceans. The tasks performed for this thesis are the collection of new ocean interior datasets, their merging with existing data, and the application of novel calculations to extract from these databases the relatively small signal of increasing  $C_{\text{ant}}$ .

A brief historical account of attempts to quantify the invasion of  $C_{\text{ant}}$  into the global ocean has been presented in this introduction. **Chapter 2** presents the complex, but well-understood, solution chemistry of  $\text{CO}_2$  in seawater.

The subsequent **Chapter 3** presents the methods used for the collection of data of  $C_T$  and alkalinity during several of the open ocean cruises in which the author participated. The commercially available instrument used for this thesis research has revealed various minor shortcomings. Modifications to alleviate these are discussed, and recommendations are made to further improve the analytical capability. Furthermore, the results of these expeditions are summarized, in a strictly technical manner (i.e., without a scientific assessment). Various metrics of quality and relevant descriptions (metadata) are accompanied by ocean section plots which illustrate the distribution of  $C_T$  along various cruise transects. These transects cover the northern Atlantic Ocean between Greenland and Scotland (occupations by *RV Pelagia* in 2005 and 2007), the western Atlantic Ocean between 60 °N and the equator (2010, again on *RV Pelagia*), and between 40 °S and the Antarctic continent (on *PFS Polarstern*, 2008). In later chapters, some of these data (notably the *Polarstern* data from 2008) are used in local and basin scale assessments of  $C_{\text{ant}}$  accumulation.

In **Chapter 4**, the CARINA (*Carbon in the North Atlantic*) effort is introduced. Due to the often *ad hoc* nature of European ocean carbon research efforts in the 1990s and early 2000s, many valuable datasets had never been made available in a convenient way to the international research community. The CARINA effort (Chapter 4, i.e., Key et al., 2010) succeeded in the ‘salvaging’, quality control and merging of these historical and recent ocean interior data. Although initiated with a focus on the North Atlantic, the final synthesized product also includes cruises

## Chapter 1

from the South Atlantic, Indian, Pacific and Southern Oceans. Details are provided on data origin, initial quality control, processing for internal consistency, and the final published format.

**Chapter 5** constitutes a more technical description of the CARINA effort. It details the considerations for, and implementation of, the methods that were devised to optimally control the quality of the resultant database (Chapter 5, i.e., Tanhua et al., 2010). Briefly, every measurement effort suffers some degree of uncertainty. That uncertainty may consist of random noise and systematic errors of calibration ('biases'). Whereas noise cannot be improved after measurements have been completed (except by averaging, which however generally reduces the spatial or temporal resolution of the dataset), CARINA went to great lengths to identify and correct the biases in cruises datasets. Firstly, individual datasets were critically examined for general quality (e.g., lack of measurement drift, proper documentation of analytical methods, use of calibration standards), and clearly outlying datapoints were removed. In a second step, approximately 1500 *crossover* locations were determined, that is, those exact locations where two cruises sampled the same deep water column. At each of these locations, where the deep-ocean characteristics are expected not to show variability on timescales of years to decades, the offsets in the measurements between the two cruises were determined, for each parameter of interest ( $C_T$ , alkalinity, dissolved nutrients, etcetera). Note that the offset does not represent the *absolute* bias of either cruise with respect to the 'true' values in the ocean, but only the *relative* bias between the two cruises. After determining a sufficient amount of such offsets, an inverse technique was employed that yielded the adjustments that had to be made to individual cruise datasets in order to minimize the mean offset of the whole dataset. Since the biases of all the cruises are considered to be neutral on average (i.e., some too high, some too low), the resultant dataset is deemed to be significantly more accurate than the original data of the individual cruises were, and therefore highly suitable for large-scale and multi-year investigations of, among other subjects, the accumulation of  $C_{ant}$  into the oceans.

**Chapter 6** describes the detection of the increase of  $C_T$  (due to accumulation of  $C_{ant}$ ) in the bottom waters of the Weddell Gyre, a major region of deep water formation in the Atlantic sector of the Southern Ocean where uncertainty about this accumulation has historically been large, in part due to the questionable assumptions required by earlier employed techniques. The study uses a subset of cruises from CARINA and the preceding (but similar) GLODAP effort, together with new data obtained during this thesis research. Additional, objective adjustments of the data are performed to minimize dataset variability in the least well ventilated part of the local water column. Subsequently, the trend in  $C_T$  is unambiguously shown to resemble the well-constrained pattern of accumulation observed for the anthropogenic refrigerant CFC-12, absorbed by the ocean from the atmosphere since the 1950s. Moreover, a statistical technique is developed that is expected to be able to attribute the rise in  $C_T$  to the invasion of  $C_{ant}$ .

In **Chapter 7**, the Time Series Residuals technique (chapter 6) is applied to a database consisting of as many as 53 cruises spanning 1973 to 2008, covering the whole of the South Atlantic Ocean between the equator and the Antarctic continent. These data are obtained largely from the CARINA database (chapter 3 and 4), or are contributed by the authors (chapter 3). The method is shown to be very well able to discern the gradual rise of  $C_{ant}$  in this large ocean ba-

sin. Briefly, for samples from each of seven distinguished water masses in the South Atlantic Ocean, the TSR technique quantifies the dependence of the time rate of change of  $C_{\text{ant}}$  on the distance from the ventilation region. The accumulation is shown to be fastest at the ventilation region, whereas deeper into the ocean interior,  $C_{\text{ant}}$  increases at a lower rate. This is to be expected, because these latter samples were at the surface at times of a lower rate of increase of atmospheric  $\text{CO}_2^{\text{ant}}$ . The determined relationships are used to project accumulation rates onto a high resolution climatology of ocean properties, which allows for convenient integration of basin scale estimates. For the mid-1990s the rate of increase of  $C_{\text{ant}}$  in the South Atlantic Ocean is determined to be  $0.389 \pm 0.080$  PgC per year, circa 20% of the global rate of oceanic storage of  $C_{\text{ant}}$ . Most of the  $C_{\text{ant}}$  is shown to be stored in the water layers at intermediate depth, around  $40^\circ\text{S}$ , that is, slightly north of where these waters form at the surface. The results compare favorably to conceptually independent tracer-based studies.

**Chapter 8** presents a synthesis of this thesis research, including recommendations for future work. Mainly, it is concluded that the TSR approach (introduced in chapters 6 and 7) may have significant value for the determination of large-scale accumulation of  $C_{\text{ant}}$  in the other ocean basins. Being partly or wholly conceptually independent from other employed techniques, it is expected to contribute novel information to the much desired understanding of this important process in the perturbed global carbon cycle.

The remaining **Chapter 9** is formed by a summary of the presented work in English. This is followed by a summary in Dutch, the full list of references, acknowledgements and the author's curriculum vitae.



# Chapter 2

## Background





Performing and interpreting CO<sub>2</sub>-related measurements in seawater were fundamental elements of this thesis work. This chapter provides, in section 2.1, a brief outline of the principles of the inorganic carbonate chemistry of seawater, followed in section 2.2 by an outline of the methods used to assess this carbonate system, and lastly in section 2.3, it describes those biogeochemical processes that lead to changes in the carbonate chemistry of seawater. An understanding of the carbonate chemistry, its measurement and the relevant biogeochemistry is essential for the analytical and scientific work presented in subsequent Chapters 3-8.

This chapter provides a brief description that is largely based on the various existing excellent publications in the literature, notably the *Guide to best practices for ocean CO<sub>2</sub> measurements* (Dickson, Sabine and Christian, 2007) and the textbook *Ocean Biogeochemical Dynamics* (Sarmiento and Gruber, 2006).

## 2.1. Carbonate system chemistry.

When gaseous CO<sub>2</sub> equilibrates with the large pool of dissolved CO<sub>2</sub> in seawater (or freshwater), it becomes a part of the system of four equilibrium reactions (the *carbonate system*) shown below.



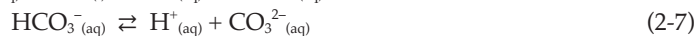
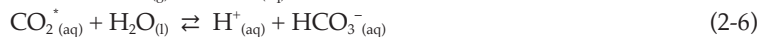
As already shown in Panel 1.2 (Chapter 1), the sum of the concentrations of the four species of dissolved inorganic carbon (DIC) is abbreviated as C<sub>T</sub>. In this thesis, the abbreviation DIC is used as a qualitative term, whereas C<sub>T</sub> refers to the sum of concentrations of the constituents of DIC. Please note that in other literature the term DIC often serves both purposes.

$$\text{C}_T = [\text{CO}_{2(\text{aq})}] + [\text{H}_2\text{CO}_{3(\text{aq})}] + [\text{HCO}_3^-_{(\text{aq})}] + [\text{CO}_3^{2-}_{(\text{aq})}] \quad (1-1)$$

In equation (1-1) the brackets represent the concentrations of the molecule enclosed. In seawater the equilibria are such that the bicarbonate ion (HCO<sub>3</sub><sup>-</sup>) is the dominant species at ~90% of the total pool of DIC, followed by the carbonate ion (CO<sub>3</sub><sup>2-</sup>; ~9%), dissolved CO<sub>2(aq)</sub> at ~1% and a very small amount (~0.002%) of carbonic acid (H<sub>2</sub>CO<sub>3(aq)</sub>).

$$[\text{HCO}_3^-_{(\text{aq})}] : [\text{CO}_3^{2-}_{(\text{aq})}] : [\text{CO}_{2(\text{aq})}] : [\text{H}_2\text{CO}_{3(\text{aq})}] \approx 90 : 9 : 1 : 0.002 \quad (1-2)$$

The carbonic acid (H<sub>2</sub>CO<sub>3(aq)</sub>) cannot be analytically distinguished from the dissolved CO<sub>2(aq)</sub> (Weiss, 1974). In order to simplify the equations of the above carbonate system, it is customary to combine the concentrations of CO<sub>2(aq)</sub> and H<sub>2</sub>CO<sub>3(aq)</sub> into the hypothetical species CO<sub>2\*</sub><sub>(aq)</sub>. That gives the following set of simplified equilibrium reactions:



## Chapter 2

The definition of the total amount of dissolved inorganic carbon ( $C_T$ ; Eq. 1-1) is accordingly simplified to become:

$$C_T = [\text{HCO}_3^-] + [\text{CO}_3^{2-}] + [\text{CO}_2^*] \quad (2-8)$$

In a given sea water sample, these dissolved substances (often called 'carbonate species') will be present in relative concentrations that are described by the *conditional equilibrium constants*  $K'$  (Panel 2.1).

$$K'_0 = [\text{CO}_2^*] / f\text{CO}_2 \quad (2-9)$$

$$K'_1 = [\text{H}^+][\text{HCO}_3^-] / [\text{CO}_2^*] \quad (2-10)$$

$$K'_2 = [\text{H}^+][\text{CO}_3^{2-}] / [\text{HCO}_3^-] \quad (2-11)$$

In Eq. (2-9), the term  $f\text{CO}_2$  represents the fugacity of  $\text{CO}_2$  gas in equilibrium with the concentration of dissolved  $\text{CO}_2^*_{(\text{aq})}$  in the seawater. The fugacity approximately corresponds to the idealized *partial pressure* of the gas (defined as the product of mixing ratio and total pressure:  $p_{\text{Gas}} = x_{\text{Gas}}P$ ), with a minor correction factor to account for non-ideal behavior of the gas mixture. In equations (2-10) and (2-11) the proton concentration  $[\text{H}^+]$ . The proton concentration in a sample is usually reported as the pH:

$$\text{pH} = -\log([\text{H}^+]) \quad (2-12)$$

In Eq. (2-12), as before, for simplicity the *concentration* notation is used instead of the thermodynamically correct *activity* notation (see Panel 2.1). Most important for the  $[\text{H}^+]$  concentration (and the associated pH) is Eq. (2-11), where the bicarbonate ion and carbonate ion comprise the natural pH buffer of seawater. Briefly, the very abundant  $\text{HCO}_3^-$  ion and the moderately abundant  $\text{CO}_3^{2-}$  ion control the concentration of free proton,  $[\text{H}^+]$ . In modern ocean surface waters the concentration of free protons is approximately  $10^{-8} \text{ mol l}^{-1}$  (i.e.,  $\text{pH} \approx 8$ ). The conditional equilibrium constant  $K'_w$  (Eq. 2-13) directly relates the concentration of  $\text{H}^+$  to the concentration of hydroxide ion ( $\text{OH}^-$ ) in seawater.

$$K'_w = [\text{H}^+][\text{OH}^-] \quad (2-13)$$

Eq. (2-13) shows that in the modern, slightly basic surface ocean of  $\text{pH} \approx 8$ , hydroxide ion is about 100-fold more abundant than free protons ( $10^{-6}$  versus  $10^{-8} \text{ mol l}^{-1}$ , respectively).

The values of the conditional equilibrium constants  $K'_0$ ,  $K'_1$ ,  $K'_2$  and  $K'_w$  are a function of salinity, pressure and temperature (S, P and T). As a consequence of that, when the temperature or pressure of a seawater sample (with given, measured  $C_T$  and alkalinity; see Panel 2.2) is changed, shifts will take place in the concentrations of the individual species of dissolved inorganic carbon and of  $\text{OH}^-$  and  $\text{H}^+$ . The relationships between the conditional equilibrium constants and S, P and T have been very accurately described in the literature (Millero et al., 2006 and references therein).

The various equilibrium reactions above (Eqs. 2-5 to 2-7, 2-13) do not only observe *mass balance* (Eq. 2-8), but additionally must respect *charge balance*. That is, sum of charges of the ions involved

in these reactions may not change. This sum of charges of the species involved in these reactions is often denoted as the alkalinity, of which a simple definition (“ $A_{\text{simple}}$ ”) is presented here:

$$A_{\text{simple}} = [\text{HCO}_3^-] + 2[\text{CO}_3^{2-}] + [\text{OH}^-] - [\text{H}^+] \quad (2-14)$$

The value of  $A_{\text{simple}}$  (Eq. 2-14) is nearly identical to the sum of charges of all strong cations and anions (positively and negatively charged ions, respectively) that are encountered in seawater, as prescribed by the electric neutrality of seawater. The small residual difference between the two is accounted for by the presence of several other minor dissolved substances. Panel 2.2 presents the more formal definition of total alkalinity ( $A_T$ ) that does include all relevant contributing dissolved substances, and is the property that may be measured in seawater.

These above-mentioned constraints of *mass balance* (Eq. 2-8) and *charge balance* (Eq. 2-14, or Eq. 2-23 in Panel 2.2) do not only apply to reactions in a *closed* carbonate system in a sample or volume (parcel) of seawater, but also must be obeyed when ‘external’ changes are imposed on the seawater. Such external changes that may affect  $C_T$  and/or  $A_T$  are the biogeochemical processes (air-sea gas exchange; biological production and remineralization; calcification and dissolution of  $\text{CaCO}_3$ ) that are discussed in section 2.3, below.

### Panel 2.1 – Activity vs. concentration.

The activity  $a_i$  of a solute  $i$  may differ from its concentration  $c_i$  due to electrostatic interactions between molecules in solution. The deviation between  $a_i$  and  $c_i$  is represented by the dimensionless activity coefficient  $\gamma_i$ :  $a_i = c_i \gamma_i$ . The value of  $\gamma$  equals 1 in infinitely dilute mixtures and decreases with increasing overall concentration of dissolved substances in the solution (i.e., with increasing *ionic strength of the medium*). For solutes in media of high ionic strength (such as seawater), the activity coefficients  $\gamma$  may differ strongly from unity.

*Chemical thermodynamics* allows the calculation of the relative activities of solutes at chemical equilibrium in an infinitely dilute solution (in which  $\gamma=1$ ). This equilibrium state is described by the equilibrium constant  $K$ . However, in high ionic media such as seawater, the thermodynamic equilibrium constants  $K$  of solution reactions do not apply. What is used instead is the *apparent* (or *stoichiometric*) equilibrium constant  $K'$  of a solution, which is not calculated, but inferred from observations. The value of  $K'$  varies with salinity, temperature and pressure ( $S$ ,  $T$  and  $P$ ).

The extensive laboratory work that is required to adequately describe  $K'$  for the natural ranges of  $S$ ,  $T$  and  $P$  has been performed for both seawater and fresh water (Millero et al., 2006 and references therein).

The apparent (or stoichiometric) equilibrium constant may alternatively be referred to as the *conditional stability constant*, and are then often denoted as  $K^*$  instead of  $K'$ .

## Chapter 2

At this point, we have a set of 6 equations (Eqs. 2-8, 2-9, 2-10, 2-11, 2-13 and 2-14) that together constrain the carbonate system, which has 8 variables ( $C_T$ ,  $A_T$ ,  $fCO_2$ ,  $[H^+]$ ,  $[OH^-]$ ,  $[CO_2^*]$ ,  $[HCO_3^-]$  and  $[CO_3^{2-}]$ ). Thus, additional knowledge of only 2 variables is sufficient to fully constrain the system and allow us to calculate the values of the remaining 6 variables (Park, 1969; Lewis and Wallace, 1998 – updated as Van Heuven et al., 2009, 2011).

Conveniently, of the seven unknown variables, common measurement techniques exist for no less than four ( $C_T$ , alkalinity,  $fCO_2$  and  $[H^+]$ ). These four measurements are briefly described in section 2.2 below, with reference to the literature for commonly employed analytical techniques. Novel spectrophotometric assessment of  $[CO_3^{2-}]$  is currently being developed (Byrne and Yao, 2008; Martz et al., 2009) but is not yet commonly used. The shipboard methods employed for obtaining the measurements of  $C_T$  and  $A_T$  reported in this thesis work are described in detail in Chapter 3.

## 2.2. Measurements of the carbonate system in seawater

### 2.2.1. The total concentration of dissolved inorganic carbon: $C_T$ .

The  $C_T$  of a water sample is defined as the sum of carbonate species (Eqs. 1-1 and 2-8) and is generally expressed in units of micromoles per kilogram of seawater ( $\mu\text{mol kgSW}^{-1}$ , or simply  $\mu\text{mol kg}^{-1}$ ).

Measurement of  $C_T$  generally involves the acidification of a seawater sample, which converts all species of DIC into  $CO_{2(aq)}$ , which is easily removed from solution either under vacuum or by sparging the solution with nitrogen or helium gas. The evolved  $CO_2$  is quantified by one of several means (*coulometry*: Johnson et al., 1993; *manometry*: Dickson, 2010, or *infrared gas analysis*; e.g., the AIRICA instrument, Marianda, Kiel, Germany). Additionally, progress is being made in the development of continuous-flow analytical systems (Kaltin et al., 2005; Bandstra et al., 2006). The method of sparging with  $N_2$  with subsequent coulometric quantification of  $CO_2$  has been used extensively in the course of this thesis. Details of this method are presented in Chapter 3.

### 2.2.2. Total alkalinity: $A_T$

The measurement of  $A_T$  (Panel 2.2) commonly involves the gradual, stepwise addition of small increments of dilute acid to a sample, and observing the consequent change in the electromotive force (e.m.f.) of free protons, as measured by an electrochemical cell (a 'pH-electrode').

Stated slightly simplified, during the addition of the initial aliquots of acid, almost all of the added protons (i.e.,  $H^+$ -ions) are neutralized by the conversion of the original  $CO_3^{2-}$  to  $HCO_3^-$  and as a result the measured decrease of pH (i.e., increase of  $[H^+]$ ) as inferred from the measured e.m.f. is much less than the actually added amount of  $H^+$ . However, at some point all the original  $CO_3^{2-}$  has been converted to  $HCO_3^-$  and a rapid drop of pH is observed: the first conversion point. The pool of  $HCO_3^-$  has now increased with exactly the same amount as the now disappeared pool of  $CO_3^{2-}$  ions. Next, upon further additions, the added protons are neutralized by the conversion of  $HCO_3^-$  ions to  $CO_{2(aq)}^*$  until all  $HCO_3^-$  is converted, at which

point the pH again drops rapidly: the second conversion point. The total amount of added  $H^+$  now is equal to  $[HCO_3^-] + 2 [CO_3^{2-}]$  as initially present.

However, matters are complicated by the fact that some of the added  $H^+$  is neutralized also by the small amount of original  $OH^-$  (Eq. 2-13) and some of the other constituents of real seawater (see Eq. 2-23 in Panel 2.2). A curve fitting routine is used to accurately determine the total alkalinity of the sample from the titration results.

Many variations of the titration technique exist, with varying strengths and drawbacks related to the attainable degree of precision, accuracy, throughput, automation or to sample size requirements (e.g., Perez and Fraga, 1987; Haraldsson et al., 1997; Roche and Millero, 1998; Dickson et al., 2003; Watanabe et al., 2004). Finally, sometimes in the literature the  $A_T$  is defined as ‘titration alkalinity’ which for all practical purposes is identical to ‘total alkalinity’ as used in this thesis.

### 2.2.3. The total concentration in $H^+$ : pH

Measurement of pH (Eq. 2-12) is generally performed either by potentiometric or spectrophotometric methods (Dickson, 1993 and references therein). Especially the latter, spectrophotometric method has seen considerable use in recent years due to high precision and accuracy, its low drift (Friis et al., 2004) and other characteristics that make it highly suitable for shipboard work (Clayton and Byrne, 1993) or in-situ deployment (Seidel et al., 2008).

### 2.2.4. The fugacity of $CO_2$ : $fCO_2$

Measurement of  $fCO_2$  is nowadays not commonly performed on discrete sea water samples (but see Wanninkhof and Thoning, 1993). Continuous surface sea water analysis for  $fCO_2$ , on the other hand, is performed on a very large scale (e.g., [www.socat.info](http://www.socat.info)) using equilibrator instruments in which a constant stream of seawater is allowed to exchange  $CO_2$  with a relatively small amount of recirculated air in a gas headspace. An infrared gas analyzer is used to determine the mixing ratio of  $CO_2$  in the air stream, which is proportional to the  $fCO_2$  of the seawater when the proper corrections for air pressure, moisture content and temperature and taken into account (Pierrot et al., 2009).

## 2.3. Processes affecting the carbonate system.

### 2.3.1. Air-sea gas exchange

The rate of exchange of  $CO_2$  across the sea surface is governed by the concentration difference of  $CO_2$  between the ocean and the atmosphere (the *gradient*), and the rate at which gas transfer is made possible by wind and wave action. The flux of  $CO_2$  ( $F$ , in  $mol\ m^{-2}\ s^{-1}$ ) is commonly expressed as the product of the gas transfer velocity ( $k$ , in  $m\ s^{-1}$ ), the aqueous phase solubility of  $CO_2$  ( $K'_0$ , in  $mol\ m^{-3}\ atm^{-1}$ ) and the difference of the fugacity of  $CO_2$  between ocean and atmosphere ( $fCO_2$ , both in  $\mu atm$ ):

$$F = k \cdot K'_0 \cdot (fCO_2^{ocean} - fCO_2^{atmosphere}) \quad (2-15)$$

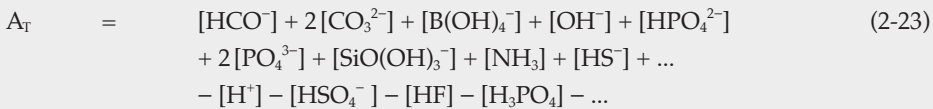
## Chapter 2

Here,  $f\text{CO}_2^{\text{ocean}}$  is the fugacity in a gas headspace in equilibrium with the concentration of  $\text{CO}_2^*_{(\text{aq})}$  in the seawater. Fluxes from the atmosphere into the ocean are thus defined as negative numbers, while effluxes to the atmosphere have positive values. The value of  $K'_0$  is governed by temperature and salinity (Weiss, 1974). The  $f\text{CO}_2^{\text{ocean}}$  is a property of the carbonate system and may either be measured directly or may be calculated from measurements of two other properties of the carbonate system. The gas transfer velocity  $k$  is best approximated as a function of wind speed, with stronger winds facilitating higher gas exchange due to enhanced turbulence, swell, bubble formation and dispersion of surfactants. Various empirical parameterization of  $k$  on the basis of wind speed are available, which generally differ slightly at high wind speeds (Wanninkhof et al., 2009 and references therein). This as yet unresolved variation in definitions leads to substantial uncertainty in the estimation of  $\text{CO}_2$ -fluxes (Takahashi et al., 2009; Sweeney et al., 2007). In polar regions, the gas transfer velocity  $k$  may be strongly reduced by the variable presence of sea-ice (Ito et al., 2004), which impedes also the exchange of other gases such as oxygen and the anthropogenic chlorofluorocarbons (CFCs).

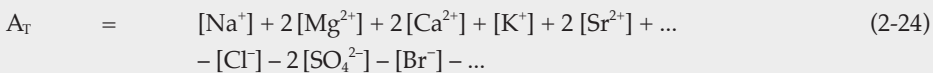
The increase of the atmospheric  $f\text{CO}_2$  due to emissions of anthropogenic  $\text{CO}_2$  leads to an increased net flux of  $\text{CO}_2$  from the atmosphere into the ocean. A limitation to continuous oceanic uptake of  $\text{CO}_2$  from the atmosphere is presented by the fundamental chemistry of the carbon-

### Panel 2.2 – A rigorous definition of total alkalinity

*Alkalinity* is the property that may be understood to represent the ‘buffer capacity’ or ‘charge balance’ of sea water, and is of importance to the solution chemistry of dissolved inorganic carbon and calcareous sediments. The rigorous definition is that of Dickson, (1981): *The total alkalinity of a natural water is defined as the number of moles of hydrogen ion equivalent to the excess of proton acceptors (bases formed from weak acids with a dissociation constant  $K \leq 10^{-4.5}$  at 25 °C and zero ionic strength) over proton donors (acids with  $K > 10^{-4.5}$ ) in 1 kilogram of sample.* Thus:



In this definition, the ellipses represent unidentified or negligibly dilute weak acids and bases. The unit of  $A_T$  is micromoles per kilogram of seawater ( $\mu\text{mol kg}^{-1}$ ). Because the oceans are electrically neutral, the value of  $A_T$  defined above must be identical to the balance of the charges of the strong cations minus the charges of the strong anions. Therefore, one may encounter  $A_T$  to be alternatively defined in the following manner:



ate system: the uptake of CO<sub>2</sub> will gradually deplete the carbonate ion (CO<sub>3</sub><sup>2-</sup>) that is naturally present in seawater (as a result of aforementioned weathering processes). This depletion process may be qualitatively summarized by the following overall reaction.



A direct consequence of the depletion of CO<sub>3</sub><sup>2-</sup> by addition of CO<sub>2</sub> is that the capacity for uptake of additional CO<sub>2</sub> progressively decreases (see Panel 2.3). This process may be expected to become the primary cause of the gradual decrease of the oceanic sink strength (together with second-order effects of carbon emissions such as surface ocean warming and ecosystemic feedbacks). However, continuous ocean circulation (i.e., supply of ‘uncontaminated’ water from the deep ocean) will likely maintain a moderate sink strength on timescales shorter than the circulation timescale of the ocean.

### 2.3.2. Photosynthesis and respiration of organic matter

All oceanic photosynthetic life consumes dissolved inorganic carbon for the production of biomass, using sunlight as the energy source. Moreover, these organisms take up from the seawater nutrients that are essential to cell physiology. These nutrients provide the organism

The *explicit conservative equation for total alkalinity* ( $A_T^{\text{EC}}$ ; Eq. 2-25) presented by Wolf-Gladrow et al. (2007) recasts the two above definitions using only conservative terms, i.e., terms that are not affected by variability of temperature, pressure or mixing processes. As noted by Wolf-Gladrow et al. (2007), this is not a new definition of total alkalinity, but rather an expression that is different from but equivalent to expressions (2-23 and 2-24).

$$\begin{aligned} A_T^{\text{EC}} = & \quad [\text{Na}^+] + 2[\text{Mg}^{2+}] + 2[\text{Ca}^{2+}] + [\text{K}^+] + 2[\text{Sr}^{2+}] + \dots & (2-25) \\ & - [\text{Cl}^-] - [\text{Br}^-] - [\text{NO}_3^-] - \dots \\ & - \text{TPO}_4 + \text{TNH}_3 - 2\text{TSO}_4 - \text{THF} - \text{THNO}_2 \end{aligned}$$

in which,

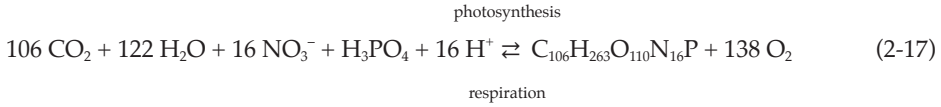
$$\begin{aligned} \text{TPO}_4 &= [\text{H}_3\text{PO}_4] + [\text{H}_2\text{PO}_4^-] + [\text{HPO}_4^{2-}] + [\text{PO}_4^{3-}] \\ \text{TNH}_3 &= [\text{NH}_3] + [\text{NH}_4^+] \\ \text{TSO}_4 &= [\text{SO}_4^{2-}] + [\text{HSO}_4^-] \\ \text{THF} &= [\text{F}^-] + [\text{HF}] \\ \text{THNO}_2 &= [\text{NO}_2^-] + [\text{HNO}_2] \end{aligned}$$

This expression  $A_T^{\text{EC}}$  is useful for the interpretation of the effects of biogeochemical processes on alkalinity. For example, from (2-25) it may be easily observed that the biological removal of 1  $\mu\text{mol kg}^{-1}$  of the nutrient phosphate from seawater – irrespective of the exact dissolved form taken up – will increase  $A_T$  with exactly 1  $\mu\text{mol kg}^{-1}$ . This is not evident from either expression (2-23) or (2-24). Likewise, formation of 1 mole of CaCO<sub>3</sub> is easily seen to decrease alkalinity by 2  $\mu\text{mol kg}^{-1}$ , which is evident from (2-24) but not from (2-23).



## Chapter 2

with the elements nitrogen (N), phosphorous (P) and silicon (Si). The uptake of carbon and nutrients occurs in approximately constant proportions:



Equation (2-17) denotes the chemical stoichiometry of photosynthetic production (or, reversely, bacterial remineralization) of organic matter originally provided by Redfield et al., (1963). The shown ratios (C:N:P:O = 106:16:1:-138; in moles) have regularly seen minor revisions over the last 30 years (e.g., Anderson and Sarmiento, 1994; Körtzinger et al., 2001; Thomas, 2002), but the concept of proportionality has proved remarkably valid.

Given the substantial rigidity of these ‘Redfield Ratios’ it is possible, in principle, to quantify the strength of the soft-tissue pump by using the concept of Apparent Oxygen Utilization (AOU). The very rapid exchange of oxygen between sea water and the atmosphere approximately saturates surface waters with oxygen before they are subducted into the deep ocean. This ‘preformed’ saturation concentration ( $\text{O}_2^{\text{sat}}$ ) of a water sample, located anywhere in the deep ocean, may be calculated on the basis of salinity and temperature (Weiss, 1970) of the sample, which have not changed since subduction. The difference between  $\text{O}_2^{\text{sat}}$  and measured  $\text{O}_2$  ( $\text{O}_2^{\text{meas}}$ ) is considered to equal the amount of oxygen that has apparently been consumed by bacterial remineralization of organic matter:

$$\text{AOU} = \text{O}_2^{\text{sat}} - \text{O}_2^{\text{meas}} \quad (2-18)$$

### Panel 2.3 – The Revelle Factor

Before 1957, consensus thinking was that emissions from human activities would not be able to significantly increase the atmospheric concentration of  $\text{CO}_2$ , because these emissions would efficiently be absorbed by the oceans. The seminal paper of Revelle and Suess (1957) pointed out that, opposed to what was commonly believed,  $\text{CO}_2$  in the atmosphere does not equilibrate with the concentration of dissolved inorganic carbon ( $C_T$ ) in the seawater (which would hardly be increased by the addition of the anthropogenic  $\text{CO}_2$ ), but rather that it equilibrates with the concentration of  $\text{CO}_{2\text{aq}}$ . Due to the fundamental chemistry of the carbonate system (Eqs. 2-5 to 2-14), that property increases 10 times more rapidly upon absorption of additional  $\text{CO}_2$  than  $C_T$  does. The consequence is that the oceanic sink for anthropogenic  $\text{CO}_2$  is approximately 10 times smaller than was believed at the time. This ‘factor of 10’ is nowadays referred to as the ‘Revelle Factor’, defined more rigorously as the fractional increase in  $p\text{CO}_2$  (or  $[\text{CO}_{2\text{aq}}]$ , see Eq. 2-15) that is associated with a fractional increase in  $C_T$ .

$$\text{Revelle Factor} = (dp\text{CO}_2/p\text{CO}_2) / (dC_T/C_T) \quad (2-26)$$

For typical surface waters of the pre-industrial ocean, the Revelle Factor was between 8 and 12 (depending on salinity, temperature and other characteristics), meaning that upon an increase of  $C_T$  of 1%, the surface ocean  $p\text{CO}_2$  would increase by 8% to 12%. The Revelle



The amount of dissolved CO<sub>2</sub> released by remineralization of organic matter ( $\Delta C_T^{\text{bio}}$ ) may thus be calculated as:

$$\Delta C_T^{\text{bio}} = 138/106 \cdot \text{AOU} \quad (2-19)$$

### 2.3.3. Formation and dissolution of calcium carbonate

In addition to producing soft tissue (2.3.2, above), many organisms additionally utilize CO<sub>2</sub> for the production of certain hard tissues made of calcium carbonate (CaCO<sub>3</sub>; Eq. 2-20), in one of two general crystalline forms. Coccolithophores (unicellular algae) and foraminifera (free-floating and benthic amoebas) produce *calcite*. Pteropods (minute free floating snail-like animals) and various calcareous algae (e.g., coral reef builders) synthesize the slightly more readily soluble *aragonite*.



For each of these crystal structures (which below will not be further distinguished), the *apparent solubility product*  $K'_{\text{sp}}^{\text{CaCO}_3}$  is defined as the product of the concentrations of the ionic constituents of CaCO<sub>3</sub> (i.e., the solutes Ca<sup>2+</sup> and CO<sub>3</sub><sup>2-</sup>) in a saturated solution of CaCO<sub>3</sub>.

$$K'_{\text{sp}}^{\text{CaCO}_3} = [\text{CO}_3^{2-}]^{\text{sat}} \cdot [\text{Ca}^{2+}]^{\text{sat}} \quad (2-21)$$

Factor may be calculated to increase to values of 14 to 18 during the conceivable increase of atmospheric *p*CO<sub>2</sub> over the 21<sup>st</sup> century (up to ~850 μatm in year 2100; Solomon et al., 2007). The relative constancy of the Revelle Factor (within a factor of ~1.5) may be misunderstood to indicate that the fraction of anthropogenic emissions that the ocean will take up from the atmosphere will not decrease by more than a factor of ~1.5.

However, an underappreciated consequence of ocean carbonate chemistry is that the fractional uptake of anthropogenic CO<sub>2</sub> (i.e., the amount of CO<sub>2</sub> taken up per amount of CO<sub>2</sub> emitted) will decrease significantly under high-*p*CO<sub>2</sub> scenarios. Underlying this phenomenon is the characteristic of the oceanic carbonate system to exhibit a much stronger rise in *p*CO<sub>2</sub> for a given addition of CO<sub>2</sub> when C<sub>T</sub> is already high (i.e., towards the year 2100), than when C<sub>T</sub> is still close to natural, pre-industrial levels. This means, for example, that a 'preindustrial' liter of seawater that is in *p*CO<sub>2</sub>-equilibrium with an overlying atmosphere of 280 μatm will be able to take up ~0.7 μmol of CO<sub>2</sub> when the *p*CO<sub>2</sub> of the atmosphere is increased with 1 μatm (i.e., from 280 to 281 μatm). At the present (year 2012) level of *p*CO<sub>2</sub> of ~395 μatm, the fractional rate of uptake by an equilibrated liter of seawater has already dropped by ~35% from pre-industrial times to ~0.45 μmol per μatm. At the foreseen atmospheric *p*CO<sub>2</sub> of 780 μatm of the year 2100, that same liter of seawater will take up only ~0.2 μmol of CO<sub>2</sub> upon the same increase of the atmospheric *p*CO<sub>2</sub> of 1 μatm – a reduction of more than 70% from pre-industrial conditions.

## Chapter 2

The *degree of saturation*  $\Omega$  of a parcel of seawater is defined as the ratio between the *in situ* product of solutes and the apparent solubility product:

$$\Omega = ([\text{CO}_3^{2-}]_{\text{in situ}} [\text{Ca}^{2+}]_{\text{in situ}}) / K'_{\text{sp}}^{\text{CaCO}_3} \quad (2-21)$$

Undersaturation of the seawater with respect to  $\text{CaCO}_3$  is thus defined by values of  $\Omega$  below 1. Under such conditions  $\text{CaCO}_3$  will slowly dissolve. Note that even in conditions of  $\Omega < 1$ , biological (enzymatic) production of  $\text{CaCO}_3$  (for instance in a living organism) may compensate for the abiotic (physicochemical) dissolution. Whenever  $\Omega$  is above 1, this signifies conditions in which  $\text{CaCO}_3$  is preserved. Spontaneous precipitation of  $\text{CaCO}_3$  from dissolved  $\text{CO}_3^{2-}$  and  $\text{Ca}^{2+}$  will not take place unless  $\Omega$  is well above 10 (e.g., Jimenez-Lopez, 2001) – a condition that is not reached anywhere in the modern ocean.

The concentration of  $\text{Ca}^{2+}$  is directly proportional to salinity ( $\sim 10.3 \text{ mmol kg}^{-1}$  at  $S=35$ ) and is some three orders of magnitude higher than that of  $\text{CO}_3^{2-}$  ( $20\text{--}200 \text{ } \mu\text{mol kg}^{-1}$  at  $S=35$ ). It is therefore not noticeably affected by the formation or dissolution of  $\text{CaCO}_3$ , and is commonly considered to be constant (for a given salinity). Solubility of  $\text{CaCO}_3$  thus mainly depends on the concentration of  $\text{CO}_3^{2-}$ .

The concentration of  $\text{CO}_3^{2-}$  is strongly dependent on the ratio of  $C_T$  and  $A_T$ , on pressure, temperature and salinity. All else being equal,  $[\text{CO}_3^{2-}]$  decreases with increasing pressure. Moreover, an increase of seawater  $C_T$  – either by remineralization of organic material or due to accumulation of anthropogenic  $\text{CO}_2$  – leads to the depletion of  $\text{CO}_3^{2-}$ . Although the complexity of the carbonate system precludes a straightforward explanation of this counterintuitive process, it may well be illustrated by the following overall reaction:



The value of  $K'_{\text{sp}}^{\text{CaCO}_3}$  itself is also dependent on temperature, salinity and, most importantly, pressure (Mucci, 1983). For example, at 5 kilometers depth,  $K'_{\text{sp}}^{\text{CaCO}_3}$  is about twice as high as that of surface water of comparable properties. The preservation of  $\text{CaCO}_3$  at depth thus requires the product of solutes to be about twice as high as at the surface. Given the constancy of  $[\text{Ca}^{2+}]$  with depth, and the decrease of  $[\text{CO}_3^{2-}]$  with depth, this condition is not generally met. As a result hereof, the deep ocean floor is largely devoid of  $\text{CaCO}_3$  sediments. Such sediment layers are, on the other hand, found ubiquitously in shallower basins ( $< \sim 2500 \text{ m}$ ) and as ‘snow’ on the tops of deep ocean seamounts (Broecker and Peng, 1982).

A major purpose of the measurement of alkalinity (section 2.2.2, above) is the quantification of the amount of formation and dissolution of  $\text{CaCO}_3$  that has taken place in a water sample. For each mole of  $\text{CaCO}_3$  that dissolves in the deep ocean, the local alkalinity will increase by 2 moles (Panel 2.2).

The interpretation of alkalinity measurements requires that the effect of photosynthesis (or its reverse: respiration) on alkalinity is additionally accounted for. For photosynthesizing organisms, the consumption of nitrate ion (for production of amino acids) must be balanced by the co-uptake of  $\text{H}^+$  in order to maintain the charge neutrality. This also applies to the uptake of phosphorous from the seawater. From Eqs. 2-17 and 2-25, it may be seen that alkalinity thus increases with 17 moles for every 106 moles of carbon integrated into organic matter (Brewer and Goldman, 1976).





# Chapter 3

## Shipboard methods and results



Highly precise and accurate determination of the total concentration of dissolved inorganic carbon ( $C_T$ ) is required for the detection of the increasing ocean inventory of anthropogenic  $CO_2$  over the large natural background concentration of  $C_T$ . Moreover, in order to compensate for the complex effects of biogeochemically induced variability of  $C_T$ , as outlined in section 2.3, high-quality measurements of additional parameters need to be made. Among these are total alkalinity ( $A_T$ ), the major dissolved nutrients nitrate, phosphate and silicate ( $NO_3$ ,  $PO_4$  and Si, respectively), dissolved oxygen ( $O_2$ ), pressure (P), temperature (T) and salinity (S).

Between 2005 and 2010, I participated in seven research expeditions dedicated to, among other goals, performing such analyses, often on a basin-wide scale (see Table 3.1 at the end of this section). During these cruises, a grand total of more than 8000 seawater analyses for  $C_T$  and  $A_T$  were performed. Standard operating procedures and quality control strategies for the measurement of  $C_T$  and  $A_T$  in seawater samples are concisely provided by Dickson et al. (2007). In the current section details are provided of the analytical techniques for the determination of  $C_T$  and  $A_T$  as implemented during this thesis research. Although the used methodology and instrumentation did not significantly change over the several cruises performed during this thesis research, a brief selection of relevant cruise-specific details is additionally provided for future reference in Table 3.1, together with statistical measures of attained quality. Maps depicting the relevant cruise tracks are shown in Figure 3.1.

### 3.1. Deep-ocean sample collection.

A CTD system is an sensor package with the capability of performing *in-situ* measurements of Conductivity (from which salinity is derived), Temperature and hydrostatic pressure (from which depth is derived). Most often, dissolved oxygen is measured by a fourth sensor. This instrument package provides ship-board scientists real-time visualization of these deep ocean properties during lowering to (and retrieval from) the depths of the ocean. Analysis for  $C_T$ ,  $A_T$  and dissolved nutrients, on the other hand, cannot be performed *in-situ* due to lack of suitable sensor technology. Because, additionally, the *in-situ* sensors for dissolved oxygen and salinity require careful calibration against ship-board analyses of superior accuracy, there exists the need to retrieve water samples from the ocean interior.

The primary instrument for this purpose is referred to as the Rosette, and consists of an array of (generally) 24 sampling bottles of 12 liters, mounted around the CTD instrument. These are in opened position when lowered, and are closed on demand by the operator during retrieval. The bottles may be closed by choice either at pre-selected depths or *ad hoc*, based on the observed hydrographical properties (S, T,  $O_2$  and conceivably other properties not discussed in this text).

Once back on deck, sub-samples are tapped from the Rosette bottles by the various research teams on board. The order of tapping is generally dictated by the speed of contamination of the seawater with respect to the various properties of interest. Thus, samples intended for analysis for dissolved gases are generally the first to be withdrawn from the volume, while samples for dissolved nutrients, salinity and total alkalinity may safely be collected at a later

stage. Generally, all groups collect samples within the first hour after the return on deck of the CTD-rosette.

### 3.2. Sub-sample collection

Water samples of 0.5 liter for combined determination of  $C_T$  and  $A_T$  were collected into borosilicate glass sample bottles (Duran, Schott AG, Mainz, Germany) using flexible sampling tube. Generally, samples were collected from all available depths. Additionally, from each profile several duplicate samples were collected. Glassware and stoppers were carefully rinsed with seawater before sampling. Bottles were allowed to smoothly overflow approximately a full volume in order to flush out the first half of the sample, which may have exchanged  $CO_2$  with the headspace of the bottle. A small headspace was created by removal of the closed-off sampling tube, after which the bottle was closed with a plastic (polypropylene) stopper, which was subsequently secured in place in order to reliably maintain closure.

After collection, samples were stored in Styrofoam-lined boxes. This kept the samples dark and additionally kept the (deep-ocean) samples cold for several hours (collection temperature of such samples is often around  $0\text{ }^\circ\text{C}$ ). When analysis was expected not to commence within 12 hours, samples were placed in cool storage ( $\sim 4\text{ }^\circ\text{C}$ ) until analysis. Samples were generally analyzed within 12 hours, and always within 36 hours. This rapid processing eliminated the requirement of poisoning of the samples (intended to prevent bacterial remineralization of organic material) and of the use of more gas-tight ground-glass stoppers (to permanently prevent exchange of  $CO_2$  between sample headspace and atmosphere).

### 3.3. Measurement of $C_T$ and $A_T$

Quantification of  $C_T$  and  $A_T$  in seawater was performed using a VINDTA 3C (Versatile INSTRUMENT for the Determination of Total Alkalinity, designed and built by Dr. L. Mintrop, MARIANDA, Kiel, Germany), which incorporates an elaborate front end for water sample handling, a  $CO_2$  coulometer (Model 5011 or 5012, UIC Inc., Joliet, IL, US) and an automated burette (Titrimo 702 or 719, Metrohm AG, Herisau, Switzerland.). The instrument performs concurrent quantification of  $C_T$  and  $A_T$ , and is controlled by a single PC running LabView software (National Instruments Inc., Austin, TX., US). Several minor modifications were made to the standard VINDTA instrument to improve capacity and ease-of-use, see section 3.4, below.

During each cruise, two VINDTAs were available, referred to as A and B. Because NIOZ owns four such instruments and a variable two of these would be taken to sea, the instrument serial numbers associated with 'A' and 'B' differed from cruise to cruise (Table 3.1). Total sample volume required by a VINDTA for the measurement of  $C_T$  and  $A_T$  is  $\sim 200\text{ ml}$ . The collected 500 ml samples are thus sufficiently large to allow both instruments to analyze the same sample. Such instrument-replicates would be made only when analysis capacity was sufficient. Whenever too many samples were queued for analysis, instruments would be dedicated to individual ocean profiles. Profiles would always be analyzed by one instrument, i.e. not be split over the two instruments.

Sample bottle stoppers were removed immediately prior to insertion of the sample line to the instrument. Samples were 'injected' into the VINDTA through the counter-flow heat exchange system by creating an overpressure of  $\pm 0.5\text{ bar}$  in a sample headspace using air from



the ship's central compressed air circuit (see below). Samples were manually separated by a small volume of air in order to avoid carryover. Sample was used to rinse the instrument lines before filling the pipettes of the  $C_T$  and  $A_T$  subsystems (detailed descriptions of these procedures follow below).

Measurements were generally performed 24 hours per day as permitted by 8 hour on/off shifts of 2 analysts with only minimal downtime during coulometric cell replacement and restart (circa once a day, two hours per instrument).

#### Quantification of $C_T$

Quantification of  $C_T$  is performed by coulometric titration according to the method described by Johnson et al. (1985, 1993). An accurately known volume of sample (~20 ml) is dispensed from a thermostated glass pipette into a glass sparging volume, which already contains ~1 ml of ~10% phosphoric acid ( $H_3PO_4$ ). The acidified sample is quantitatively purged of  $CO_2$  by  $N_2$  gas (flow rate ~150 ml  $min^{-1}$ ). The flow of nitrogen carries the  $CO_2$  gas through a condenser (~2 °C) to remove water vapor. The  $N_2/CO_2$  gas stream is subsequently introduced into the primary compartment of a coulometric titration cell, containing circa 100 ml of *cathode solution* (a proprietary solution containing, among others, dimethylsulfoxide, ethanolamine and thymolphthalein indicator). The  $CO_2$  reacts quantitatively with the ethanolamine to form hydroxyethylcarbamic acid:



The weak acid formed in (3-1) partly dissociates, effectively decreasing the pH of the solution:



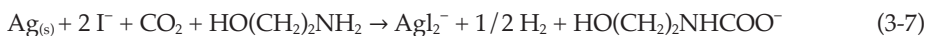
The resultant fading of the deep blue color of a thymolphthalein indicator is detected by the coulometric setup, which photometrically monitors the transmittance of the solution at approximately 610 nm. Subsequently, an electrical current is forced through the solution, and the resultant electrolysis reaction (3-3) at a platinum cathode produces hydroxide ions ( $OH^-$ ) that gradually restore the pH (3-4).



Circuit closure is maintained by the dissolution of silver ions at the anode (3-5), which subsequently complexate with the iodide ions of a saturated potassium iodide (KI) solution (3-6):



The following equations describes the overall reaction (Johnson et al., 1985):



The titration current is integrated over the time required to restore the pre-measurement transmission of the solution. This integral of the current (that is, the *charge*, in coulombs) is – after subtraction of the integrated background current of the coulometer (the 'blank' or 'baseline')

– linearly related to the amount of CO<sub>2</sub> absorbed by the coulometric solution. After the titration is completed, the stripper and condenser are automatically emptied. From volume and salinity, the mass (in kg) of sample may be calculated, which allows the determined C<sub>T</sub> to be expressed in μmol kg<sup>-1</sup>. Exact calibration of the coulometer may conveniently be performed by use of a gas-loop calibration system (GLCS; see section 3.6 below) that feeds accurately known quantities of pure CO<sub>2</sub> to the coulometer (Wilke et al., 1993).

#### *Quantification of A<sub>T</sub>*

Quantification of A<sub>T</sub> is performed by a potentiometric titration of a seawater sample with dilute hydrochloric acid (Mintrop et al., 2000). An accurately known volume of seawater (circa 100 ml) is dispensed from a thermostated pipette into an open, acrylic titration cell, after which it is constantly stirred. Over the course of circa 15 minutes, 28 small (0.15 ml) additions of dilute HCl are made with the automated burette. This titration acid is of accurately known strength (approximately 0.1 mol l<sup>-1</sup>) and is prepared as a 35 g l<sup>-1</sup> NaCl solution in order to maintain uniform ionic activity of the titrated sample during analysis. During titration, the electromotive force (e.m.f.) of free protons is measured by an electrochemical cell consisting of a glass measurement electrode (Orion ROSS 8101BNWP, Thermo Fisher Scientific, Waltham, MA, USA) and a double junction Ag/AgCl reference electrode (Metrohm, model 6.0729.100), both connected to the Titrino. Solution temperature is recorded by a probe inserted into the titration cell, and is maintained close to 25.0 °C by a water jacket. The titration is considered complete when 4.2 ml of acid have been added. Before the next sample is analysed, the titration cell is automatically rinsed twice. Rinsing solution consists of distilled (i.e., alkalinity-free) water with 35 g l<sup>-1</sup> NaCl added to approximately match the ionic strength of the samples.

Total alkalinity (in μmol kg<sup>-1</sup>) is accurately inferred from the recorded e.m.f. response by a non-linear least squares fitting routine, based on the routine described in Millero et al. (1993). Although the routine was developed for variable-volume closed cell titrations (where gaseous CO<sub>2</sub> is not allowed to escape the titrated sample), it is used here under the assumption that CO<sub>2</sub> loss due to acidification is minimal. Although this assumption is known not to be accurate, the calculated value of A<sub>T</sub> is not affected by this approximation. The approximation *does* invalidate the additionally calculated values of C<sub>T</sub> and carbonate alkalinity. However, the former of these parameters is additionally, and with superior accuracy, obtained by coulometry (see above) and the latter may be calculated from A<sub>T</sub> and (coulometric) C<sub>T</sub>. The use of the calculation routine for the purpose of calculation of A<sub>T</sub> is thus appropriate.

### 3.4. Analytical accuracy

In order to set the measurement accuracy, *certified reference material* (CRM; made available by prof. A. Dickson, Scripps Institute of Oceanography, San Diego, USA) was regularly analyzed. Generally this occurred three times per day (during days of continuous analysis), but never before both coulometric cells were successfully started (i.e., after a suitable number of dummy runs (using surface sea water) were performed and coulometer blank level was stable). Comparison of the results of these analyses (both for C<sub>T</sub> and A<sub>T</sub>) with the certified values allows the determination of a correction factor to be applied to the oceanographic samples.

Formally, however, CRM is not intended for *setting* the accuracy of the measurement setup but rather to *verify* the independently attained accuracy. Nonetheless, it is often reported

that many labs do use CRM for calibration purposes, and we did this too. In the presence of *non-linear sources of error*, this approach may have unintended consequences, mostly for analyses for  $A_T$ , as will be illustrated below,

For  $C_T$ , correction of results to CRM may be argued to be a valid procedure because the conceivable errors that are to be corrected are all linear in nature. For example, a calibration error of, say,  $-0.1\%$  of the volume of the dispensing pipette would lead to an error of  $-0.1\%$  in results of measurement of CRM and samples alike. Sample results may therefore be corrected by simply adjusting them upwards by  $0.1\%$ . A similar reasoning may be followed for biases in coulometer electronics, temperature measurements et cetera.

For  $A_T$ , on the other hand, errors related to  $A_T$  electrode response may be non-linear in nature (so called ‘non-Nernstian behavior’, see section 3.6). These errors are thus not corrigible by a correction to CRM, constituting, as it does, only a one-point calibration. To make matters worse, the incorrigible biases resulting for electrode malfunctioning are not easily detectable by the operator (if they are not exceedingly severe), which is one of the reasons why such ‘primary calibration’ use of CRM is considered improper, and advised against.

The concern about non-linear biases is not merely of academic nature. During the 2008 expedition of Polarstern (ANT-XXIV/3, Table 3.1), the two VINDTAs yielded datasets for  $A_T$  that showed - after individual calibration and correction to CRM of the two datasets - a mean difference between instrument-replicates of  $6.9 \pm 4.7 \mu\text{mol kg}^{-1}$  ( $n=350$ ). Regrettably, this discrepancy was dismissed during the cruise as likely resulting from an error in data processing. Its veracity was only corroborated in the home laboratory, when it was too late to locate with confidence the cause of the bias. This error is most likely due to the use of a faulty electrode on one of the instruments. We have discarded the  $A_T$  results of that instrument and note that, if we had used only a single (faulty) instrument, this error would have gone unnoticed.

#### *Lab standards.*

Occasionally the measurements of CRM made over the course of a day might appear to exhibit a trend, conceivably caused by environmental conditions (such as laboratory temperature). Without additional data to corroborate the veracity of this analyzer response, no correction for such apparent drift is warranted. Doubling the amount of CRM analyses in order to better constrain such potential variability is prohibitively expensive. As an alternative, starting with the cruises in 2007, laboratory standards were analyzed approximately every two hours. These standards were prepared on board in batches of  $\sim 60$  l, using water from deeper than 1500 m which was filtered, poisoned with  $\text{HgCl}_2$  and brought to analysis temperature ( $25.0^\circ\text{C}$ ). The vessel of lab standard was placed under continuous overpressure of  $\sim 0.5$  bar. Before pressurization, the lab standard was sparged with lab-air to attain the  $p\text{CO}_2$  that was expected to approximate that of the pressurized headspace (i.e., 1.5 times the ship’s compressed air  $p\text{CO}_2$ ), in order to limit outgassing after the vessel would be pressurized. A manifold (placed before the heat-exchanger) allowed the analyst to easily switch from analyzing glass bottle samples to lab standards and back. Although gradual drifts in standards were observed (affecting  $C_T$  more than  $A_T$ ), the deviations in de-trended measurements have occasionally been informative of, and beneficial to, VINDTA instrument precision and accuracy.

### *Assessment of precision and accuracy*

For analyses performed on a single instrument, analytical precision and accuracy are generally reported based on an assessment of the differences between replicates. These replicates are either run back-to-back (yielding the generally favorable ‘short term precision’) or with some other samples (i.e., time) in between them (yielding the often more sobering ‘medium term precision’). The mean and standard deviation of replicates analyzed over very long times (generally in the form of CRM) provide the ‘long term precision’ of the analysis. This medium-term and, especially, the long-term precision may be improved by applying corrections based on the results of the CRM itself. However, that method in a sense constitutes circular reasoning and although data quality may be improved by applying such corrections, one loses the estimates of medium and long term precision. Moreover, after such correction, no independent estimate of accuracy can be provided anymore.

The concurrent use of two (or more) analytical instruments provides a significant benefit with regard to quality assessment, provided that a significant amount of samples is analyzed on both instruments (providing ‘instrument replicates’). The datasets obtained by both instruments are individually processed for outliers, biases, drift, et cetera. The difference between the results yielded by each instrument should ideally be zero. In practice, the *average* of these differences constitutes a lower bound to the accuracy of the individual instruments (no upper limit can be given, since both instruments may be biased to the same degree). In absence of a significantly non-zero mean, the standard deviation of the differences is an indication (but no more than that) of the precision of the two instruments. For example, if both instruments, after all quality control steps have been taken, yield almost exactly the same results (say, a mean difference of determined  $A_T$  of  $0.04 \pm 1.15 \mu\text{mol kg}^{-1}$ , determined over 200 samples), that means that the two instruments are very precise, although it cannot be ruled out that they suffer from (unknown) biases to the same degree. Conversely, if the difference between the instrument replicates is  $6.15 \pm 2.45$  ( $n=200$ ), that means that, although precision of both instruments may be acceptable, the data from one or both instruments are inaccurate to a significant degree.

### **3.5. Analyzer modifications**

The following modifications have been made to the VINDTA instruments to increase analytical capacity and usability.

#### *Sample loading*

The peristaltic pump for sample intake was replaced with a sample headspace overpressure system. The notable benefit of this setup is the ability to deliver the sample into the  $C_T$  and  $A_T$  pipettes without formation of air bubbles in the instrument lines. Volumetric control and the  $C_T$  of samples may in this way be better maintained. Overpressure is maintained at  $\sim 0.5$  atm using dry, clean compressed air.

#### *Temperature control*

A second adaptation is the use of a custom made counter-flow heat exchanger in the sample line towards the VINDTA. The heat exchanger is made of circa 2 meters of 1/8 inch OD stainless steel or copper tubing, contained in 2 meters of PVC tubing. The concentric tubing is coiled up and positioned directly downstream of the sample bottle. Thermostating of the inner tube, and the sample flowing therein is performed by the return flow of the VINDTA stable temperature

circulation system (25.0-25.2 °C). The heat exchanger has the ability to bring a sample to within 0.2 °C of the desired 25.0 °C analysis temperature, irrespective of initial sample temperature. Notable benefits are that messy sample pre-heating in water baths is no longer required and that sample temperature is better controlled to be exactly 25.0 °C. Without the overpressure system the use of the heat exchanger would lead to unacceptable amounts of bubble formation in the sample lines, due to its resistance to sample flow.

To further assure sample analysis temperature, a delay of 30 seconds was observed between the filling and draining of the pipettes into the measurement vessel ( $A_T$ : titration cell,  $C_T$ : stripper). This pause allows the sample to further approach the exact 25.0 °C of the incoming circulation batch water in the outer jacket of the pipettes.

The adaptations mentioned above virtually guaranteed the desired 25.0 °C of the samples to be reached. This allowed all four factory-standard temperature probes to be removed. These were **a**) the PRT (platinum resistance thermometer) probe inserted into the  $A_T$  titration cell (intended for allowing optimal calculation of dissociation constants for  $A_T$  determination; Chapter 2); **b**) the thermocouple probe downstream of the top of the  $C_T$  pipette (intended for allowing optimal determination of temperature dependent  $C_T$  pipette volume); **c**) the two PRT-probes intended for measuring sample temperature and thereby to allow the software to avoid running a sample that is still too cold for proper analysis.

All of these temperature probes were considered to be prone to failure and inaccuracies. Especially the probe at the  $C_T$  pipette which, due to its minimal extension into the sample and its substantial mass, appeared biased towards laboratory temperature. For each of the removed probes, the software was made to assume a temperature of 25.0 °C. The temperatures of circulation water and dispensed sample (in the alkalinity titration cell) were checked regularly to indeed be 25.0 °C, in order to assure the continued proper functioning of the sample heat exchanger.

#### *Instrument reliability*

Due to repeated breakdowns of two of the instruments' sample level sensors (located in the  $A_T$  titration cell and pipette overflow vessel), these were removed and analysis execution was switched from sensor-based to timing-based. This would require occasional re-timing of the  $A_T$  rinsing procedure, but overall provided for a less complicated operation.

Minor changes were made to the flow of  $N_2$  through the system, with the aim of maintaining, at all times, a flow of  $N_2$  through the coulometer cell. In the default configuration of the instrument, this flow is cut off while the of the stripper is emptied of the previous sample. The sudden recommencement of the  $N_2$  stream after this purging occasionally had the effect of generating a titration burst of the coulometer, which could take up to 5 minutes to recover. Not waiting for this recovery (as evidenced by the continuation of coulometer background counting), would result in an underdetermination of the  $C_T$  of the next sample. This problem was fully alleviated by making the mentioned adjustment.

Additionally, the  $N_2$  mass flow controller was removed. No dependence of determined  $C_T$  on gradual, minor deviations ( $\pm 25\%$ ) of the  $N_2$  flow rate (target value:  $150 \text{ ml min}^{-1}$ ) were observed. The  $N_2$  mass flow controller, which is intended to precisely maintain that target value, occasionally proved troublesome in operation (e.g., would remain in closed position after instrument startup), and was removed in order to further simplify operation.

### *Blank determination*

The control software was adapted so as to allow the coulometric titration of  $C_T$  to continue throughout the duration of the concurrently performed potentiometric  $A_T$  titration, i.e., for a total of circa 18 minutes. The titration current throughout the last circa 8 minutes is no longer due to the (earlier) peak of sample  $CO_2$ , but rather reflects the background current ('baseline' or 'blank') of the instrument. Performing this extended titration allows obtaining a meaningful estimate of the coulometer blank *during* runs and thus eliminates the requirement to perform occasional determination of the blank between runs. Furthermore, the coulometer blank is in this way made traceable over time, which conceivably allows for early detection of cell 'aging'.

### *Coulometer light source*

Before cruise ANT-XXIV/3 (February-April 2008; Table 3.1), the coulometers were adapted to use LED light sources in stead of incandescent bulbs for the detection of the transmission of the coulometric cell solution. Factory-standard coulometers are equipped with a regular wide bandwidth incandescent bulb and a wide bandwidth photodiode. In order to minimize sensitivity to undesired wavelengths, they are supplied with a spectral filter (band gap around 610 nm, coinciding with the maximal absorbance of the thymolphthalein dye in the solution) located in front of the photodiode. Because the spectral filter is not perfectly opaque to non-desired wavelengths, some sensitivity remains to **a**) the light from the incandescent bulb and **b**) ambient light. The use of the LED light source can address the former influence, allowing the photodiode to observe the transmission with a higher signal to noise ratio, which theoretically allows measurements to be made more precisely. Influence (b) may be shown to be small by varying the amount of ambient light, and observing that this does not evoke a response from the coulometer. Additionally, and perhaps more relevantly, LEDs have a much longer life than incandescent light, and due to their solid state nature exhibit less variability due to ship motion. This sensitivity to motion is commonly observed in shipboard spectrophotometric setups that use incandescent bulbs, and is highly detrimental to measurement precision (Karel Bakker (NIOZ), pers.comm., and personal experience). The LED-update was conceived and skillfully performed by Ruud Groenewegen of the Electronics Department of NIOZ.

### *Titration acid stability*

The  $\sim 0.1$  mol  $l^{-1}$  HCl acid for  $A_T$  titrations is, for use on longer cruises, generally prepared beforehand as a single, large batch, which is subsequently subdivided into individual bottles of 1 liter, to be properly capped and stored for later use. Although this method is convenient for use during long cruises, the conceivably variable strength of the acid in each bottle may lead to slight discrepancies in results of measurements of reference material between bottles and between instruments (which normally each use a dedicated bottle).

Attribution of variability or trends in results of measurements of reference material (lab standards or CRM) to environmental factors is aided by removing the variability in acid strength between bottles and (thus) between instruments. Therefore, starting with the cruises in 2007 (Table 3.1), we prepared a single, very large ( $\sim 20$  l) batch of acid, and had both instruments tap straight from this vessel. Acid was diluted from a carefully determined amount of 6 mol  $l^{-1}$  HCl to 20 l with de-ionized water (Milli-Q), while gradually adding 700 grams of NaCl in order to match the ionic activity of seawater. During research cruises, subsequent stirring of the acid was provided by ship motion. On calm days or during in-ice sailing, stirring was



performed manually every few days. The acid batch was kept well-insulated, so as to maintain a very constant 25.0 °C temperature of the acid (i.e., the mean laboratory temperature). Lines from the acid vessel to the automated burettes (internal volume of lines is smaller than 2 ml) were thermally insulated to maintain temperature of the acid during its transfer.

### 3.6. Recommendations for future work.

Although several improvements (or at least alterations) have been made to the VINDTAs, the coulometers and the analytical setup in general, the following section will suggest several additional alterations to instruments or procedures that may be expected to improve analytical accuracy and precision, or improve general usability.

#### *Coulometer calibration*

The accuracy of the coulometer electronics (i.e., the degree to which the reported electrical charge matches the charge that was actually delivered to the titration cell) may be conveniently determined by connecting a second current integrator (i.e., a coulometer) in series with (or in place of) the coulometric cell, and simply comparing the output of both coulometers. Such a second, superior quality current integrator has been designed and built at NIOZ, but has yet to be used to rigorously intercompare and calibrate the UIC coulometers. During expeditions 64PE319 and 64PE321, both in 2010, such comparisons have been made on an experimental basis, indicating minor offsets in individual coulometer calibrations, although these offsets appeared invariable over time.

#### *Gas loop calibration system (GLCS)*

Although the electrical charge, delivered to the coulometric cell, may be calibrated accurately using an electronic calibration (see above), the titration efficiency (the fraction of electrons that contribute to the desired electrochemical reactions) may not be equal to 100%, for instance if part of the delivered charge is used for electrolysis of water into oxygen and water. This coulombic efficiency may be expected to vary during long runs due to the slowly shifting composition of the coulometric solution. Thus, for optimal accuracy of the determination of  $C_T$ , the regular calibration of the coulombic efficiency is required. Use of a GLCS offers a conceptually straightforward method of accomplishing this, as follows.

One may calculate to a high degree of accuracy the number of moles of  $CO_2$ , contained in a steel loop connected to a multi-port valve, from the known volume of the loop and the measured temperature and pressure of the  $CO_2$  (Wilke 1993; SOP13 of Dickson et al., 2007.). A relative accuracy of 1 in 5000 may be obtained if proper calibration procedures are observed. This known amount of  $CO_2$  is subsequently fed to a coulometer, allowing for convenient and rapid assessment of the coulombic efficiency. The near-zero cost-of-use of a GLCS allows the operator to closely track the performance of the coulometer during the day without having to rely on tedious extractions of  $CO_2$  from laboratory standards or CRM.

The construction and, especially, the calibration of such gas loops is no trivial task. Nonetheless, we have at NIOZ been able to produce and calibrate two such GLCSs (one for each VINDTA used on board). Both systems have been used on a trial basis during the two 2010 cruises (Table 3.1) but their results have not been used as part of the measurement or calibration routine. Such use is highly recommended in order to minimize the influence of unnoticed drift of the coulometric system during extended measurement days. If use of GLCS proves

beneficial to results, this may obviate the regular use of lab standards, saving significant time, as well as the inconvenience associated with preparing these standards.

### *Optimizing the use of CRM.*

CRM currently is available only in 500 ml glass bottles. This allows for only a single measurement of  $C_T$  to be performed, before exchange of  $CO_2$  between CRM and its headspace conceivably alters the  $C_T$  of the material, rendering the material useless for its purpose (although it remains of use for  $A_T$  analysis). Use of CRM may be made more economical by repackaging CRM into large (2-5 l) gas-tight bags (e.g., a multilayer Mylar/aluminium composite). Because no headspace would be formed during tapping of a subsample from such a bag, the  $C_T$  value of the CRM would be maintained between analyses. However, the degree to which the certified  $C_T$  of the CRM is maintained during *filling* of such bags must be carefully established before such a deviation from regular practice is implemented.

### *Characterization of $A_T$ electrodes.*

As briefly mentioned in section 3.4, for analytical accuracy it is of utmost importance to use an  $A_T$  measurement electrode with an 'ideal' or 'Nernstian' response. That is, the increase in the electromotive force (e.m.f.) should increase with a dictated decrease in pH exactly according to Nernst equation (Millero, 1993). For example, at a titration temperature of 25 °C, for each exact one-unit decrease of pH, the e.m.f. should increase by 59.16 mV. However, many electrodes are reported to exhibit responses well below this ideal rate (despite what may be written on the packaging). To make matters worse, responsiveness may vary with the pH. For example, an electrode may exhibit proper Nernstian response around pH=7, but below-Nernstian response around pH=4. This may severely impact the ability of the curve-fitting routine (section 3.3) to accurately infer  $A_T$  from the titration results.

To avoid such complications, the response of to-be-used electrodes should be verified across the entire pH range from 3 to 8, and non-conforming electrodes should be rejected. However, the commonly used titration with HCl of an NaCl solution is not suitable for this test (see section 8.3 of SOP3a of Dickson et al., 2007), and no accurate seawater buffers have been described for the lower pH range. As a compromise then, one may prepare two buffer solutions ('AMP': 2-aminopyridine, and 'TRIS': 2-amino-2-hydroxymethyl-1,3-propanediol; Dickson et al., 1993) with highly accurately known pH values (around 6.8 and 8.1, depending on exact makeup and temperature). From the observed step changes in e.m.f. when testing electrodes in these buffers and their accurately known pH values, the e.m.f. response may be calculated for the region around pH=7. We have prepared such solutions before the 2010 expeditions (Table 3.1), and have used these for (among others purposes) an informal assessment of the circa 10 electrodes available at the laboratory. I highly recommend making this electrode assessment a routine procedure at the NIOZ  $CO_2$  laboratory, in order to maintain analytical capabilities for  $A_T$  of the highest possible level.

### *Rinsing of the $A_T$ cell*

Currently, before an  $A_T$  sample is loaded into the  $A_T$  titration cell, the cell is drained and rinsed (twice) with an alkalinity-free solution of NaCl. This rinsing solution (distilled water to which 40 g/l NaCl has been added) is prepared and stored in 25 liter plastic vessels. The required frequent transportation of these vessels provides significant discomfort to the VINDTA operators.



Additionally, on several occasions did a vessel accidentally run dry, and did a measurement subsequently fail. To eliminate the requirement of having to regularly fetch large volumes of distilled water from outside the laboratory, during the 2010 cruises (Table 3.1), we made our own inside the laboratory, used a distilled water generation cartridge, connected to the local faucet. Use of the 25 l vessels and NaCl was maintained during these cruises. However, it may be questioned whether the use of NaCl (and hence the vessels) is at all required. Several investigators mention rinsing the  $A_T$  cell and electrode with simple distilled water (e.g., SOP3b of Dickson et al., 2007). If this indeed is confirmed to be feasible, one may opt to simplify VINDTA operation by constructing a 'distilled water shower head' or something to that effect at the top of the  $A_T$  cell, connected to the de-ionization cartridge. This system would speed up run preparation, save operator time and effort, reduce cost and improve consistency. Additional simplifications could subsequently be made to the titration cell drainage system. In this regard I propose to remove the (highly failure-prone) servo motor, currently in use for opening and closing the  $A_T$  drainage valve. In the proposed setup, a small check valve would maintain cell closure during titration. Subsequent cell drainage would be accomplished by pumping the sample away through the check valve. Ideally, this pumping would be performed by a small membrane-based liquid pump, replacing the current peristaltic ('roller') pump, the tubing of which is failure-prone and requires regular replacement.

#### *Replacing the air pump with an $N_2$ -line*

The currently used method of emptying the  $A_T$  pipette is by using a small air pump to blow out the sample. As a means of regulating the blowout pressure, an open ended air line (tee'd off from the line between pump and pipette top), may be partly squeezed. However, this method is imprecise, and prone to variations if the clamp is accidentally touched. Moreover, the used pump is expensive, noisy and requires maintenance. The simple replacement of the pump with an  $N_2$ -line (tee'd off from the main supply), equipped with a needle valve for precise and permanent flow regulation, would suffice to remedy this.

#### *Thermostating $A_T$ titration acid*

Uncontrolled variation in the temperature of the  $A_T$  titration acid may lead to a significant uncertainty of about  $0.5 \mu\text{mol kg}^{-1} \text{ } ^\circ\text{C}^{-1}$ , due to covariation of the density (and thus the mass) of acid contained in the titration burette. In order to maintain a highest level of accuracy, acid temperature must be carefully controlled, preferably at the calibration temperature of the titration burette ( $25.0 \text{ } ^\circ\text{C}$ ). Although temperature swings of the acid vessel are currently largely eliminated due to thermal insulation from the (more variable) laboratory, the mean temperature maintained in the vessel is currently unknown, and may well be variable on a timescale of days to weeks. Moreover, the temperature of the burette itself and the lines leading to it are susceptible to the variability of the laboratory temperature variation. Connection of the burette jacket to the VINDTA's central thermostating system is highly recommended. Additionally, acid vessel thermostating may be accomplished by wrapping it with a length of small diameter circulation line as well. Temperature monitoring of the burette jacket may be required for corroboration of effective thermostating.

### *Laboratory thermostating*

Strongly related to the above, the analytical results have been negatively impacted by temperature variations of the laboratory containers in which analyses were carried out. Especially during the pre-2010 cruises (Table 3.1), sudden air temperature drops of up to 10 °C were observed during the regular periods of air cooling. Although the mean temperature of the container and the equipment in it did not vary much over the length of a cruise, the short term variability has demonstrably affected measurements. In response to earlier requests, the NIOZ currently uses a newly built container, designed specifically with accurate temperature control in mind, thereby to large extent allaying fears of temperature-driven variation of measurements. It is recommended to additionally monitor and log the temperatures of the laboratory container and the relevant parts of the analytical setup over the length of future research cruises.

### *Coulometric cell thermostating*

The transmission of the coulometric solution has a slight dependence on temperature, mostly through the temperature sensitivity of the pH of the solution. The increase in temperature results from two processes: a) heat radiating from the coulometer hardware and b) current flow during the early minutes of a titration. Heating of the cell solution results in minor fading of the color, without the involvement of CO<sub>2</sub>. This leads a coulometer to titrate approximately 250 counts per degree of temperature rise, falsely adding 2.5 μmol kg<sup>-1</sup> °C<sup>-1</sup> to the later calculated C<sub>T</sub> of the sample. Although the warming experienced from the radiation from the coulometer hardware is constant, the heating from the electrical titrations is a ‘pulsed’ process. After allowing the cell to come to thermal equilibrium with the coulometer, the ‘pulsed’ addition of heat may be clearly observed during the initial ~7 titrations in a newly prepared cell. The first run results in a temperature rise of +0.5 °C, decreasing to +0.1 °C during the seventh run). Hereafter, a dynamic temperature equilibrium with the environment sets in. That is, the heat gained during the early minutes of the titration equals the heat lost during the later minutes, thus producing no net effect. However, if titrations are halted for an extended amount of time, cooling continues, and an erroneous elevation of counts may again be expected during titration of the next sample.

To counter these effects, it is desirable to rapidly approach a stable temperature of the coulometric solution (so that measurements may commence as soon as possible) and to subsequently maintain that temperature carefully in order to minimize variability. To these ends, the coulometer cells cap may be outfitted with a 9 mm OD U-shaped glass tube, hanging down to the bottom of the cell, to the side of the light path. Through this tube, water of 25 °C may be circulated in order to maintain coulometric solution temperature slightly above that level. The additional monitoring of solution temperature is realized straightforwardly by insertion of a stainless steel temperature probe through the cell cap. So equipped, coulometric titrations increase the temperature only slightly during the early minutes of a run. Subsequent cooling back to ~25 °C is accomplished well within the same run, thereby resulting in no net temperature change during the run. Moreover, extended periods of inactivity will not influence subsequent runs.

This arrangement has been tested for brief periods at the NIOZ laboratory. No adverse effects were noted, but neither was a significant improvement in results. Nonetheless, given

its conceivable benefit to analytical precision, a formal evaluation of the proposed setup for efficacy and suitability during research expeditions is recommended.

#### *Autosampling*

Above modifications would, taken together, do away with both peristaltic pumps, with several valves, sensors, a mass flow controller and other components, thereby substantially simplifying operation and potentially improving mechanical reliability. But even without the alterations suggested above, the VINDTA has already proven to be capable of performing dozens of consecutive analyses with consistently high accuracy, during which the single task of the operator is to transfer the sample intake line from one bottle to the next between runs.

These observations suggests that the VINDTA instrument may be equipped with an autosampler and put to unattended operation with minimal risk. Especially if operators would remain near the instrument during automated runs (due to involvement in other analysis or sampling activities), the unnoticed loss of samples would likely be minimal, and the gain in throughput substantial. Additionally, automated and standardized intake of samples would likely be beneficial to precision and accuracy. Mechanically, the autosampler would consist straightforwardly of (for example) eight sample bottles (or CRM or laboratory standards) under slight headspace overpressure, connected to a multiport manifold, which selects the sample to be fed to the instrument.

Use of an autosampler would likely require moderately large changes to the control software. However, performing these changes concurrently with a larger rewriting of the software, mentioned below, would yield a highly integrated, automated and reliable instrument for high-throughput analysis for  $C_T$  and  $A_T$ .

#### *New control software*

I consider the currently used control software of the VINDTA to be somewhat unwieldy and erratic. Its spottiness renders advanced operations (notably the re-processing of  $A_T$  titration results) challenging even to long-term users. At least one laboratory using VINDTA instruments (that of Dr. Dorothee Bakker at UEA, Norwich, UK) has had new control software programmed on a non-LabView platform, and use that to their decided satisfaction. I would recommend to either attempt to acquire a (trial-) copy the UEA software, or to develop such software anew.

Various software routines for various software platforms (Matlab, S, R, Python et cetera), have become available for the calculation of  $A_T$  from titration data. The re-writing of the control software additionally may be used to enhance the co-operability of the control software with these various post-processing routines. Currently, such interoperability is near-absent, and extracting from the control software all raw data relevant to post-processing requires significant skill of the VINDTA operator.

#### *Post-cruise data processing.*

As a last point, albeit one with high priority and relevance, I recommend to attempt to rigorously formalize the post-cruise data processing. Currently, the determination of coulometer blank levels, determination of outliers, corrections against CRM et cetera, in essence is a subjective enterprise. Although always performed in good faith, these decisions should be based on a formalized set of criteria, in the interest of usability of the final data to investigators not involved in their collection.

**Table 3.1.** Cruise metadata and analytical performance.

		64PE239	64PE240	ANT-XXIII/7
Vessel		RV Pelagia	RV Pelagia	PFS Polarstern
Start port		Texel, Netherlands	Peterhead, Scotland	Cape Town, S. Africa
End port		Peterhead, Scotland	Texel, Netherlands	Cape Town, S. Africa
Start date		Aug. 17, 2005	Sep. 7, 2005	Aug. 25, 2006
End date		Sep. 6, 2005	Oct. 5, 2005	Oct. 29, 2006
Chief scientist(s)		Helmuth Thomas Dalhousie University Canada	Cees Veth NIOZ, Texel Netherlands	Peter Lemke AWI, Bremerhaven Germany
CO <sub>2</sub> analyses		Steven van Heuven Friederike Prowe	Steven van Heuven Henk Zemmeling	Steven van Heuven
CO <sub>2</sub> parameters measured		C <sub>T</sub> , A <sub>T</sub> (pCO <sub>2</sub> )		C <sub>T</sub> , A <sub>T</sub> (pCO <sub>2</sub> )
VINDTA instruments used		A: VINDTA 9 (Dalhousie) B: VINDTA 10		A: VINDTA 15 B: VINDTA 14
unique ocean samples for C <sub>T</sub> /A <sub>T</sub>	#	circa 750	circa 725	circa 525
CRM for C <sub>T</sub> /A <sub>T</sub>	#	circa 60	circa 85	circa 80
Samples poisoned?		no, immediate analysis		yes, analysis within 2 months
<b>C<sub>T</sub></b>				
Coulometer light source <sup>(a)</sup>		incandescent		incandescent
Coulometer electronic calibration <sup>(b)</sup>		no		no
Startup junks volume <sup>(c)</sup>	mISW	ca. 80		ca. 160
CRM deviation from cert. value <sup>(d)</sup>	μmol kg <sup>-1</sup>	A: -8.1±2.5 B: -3.6±7.3	A: -8.1±1.4 B: -4.9±1.7	A: -6.3±4.4 B: -4.3±3.3
Short term precision <sup>(e)</sup>	μmol kg <sup>-1</sup>	A: not enough data B: not enough data	A: ±1.2 B: ±0.8	A: ±1.4 B: ±1.0
VINDTA A-B (corrected data) <sup>(f)</sup>	μmol kg <sup>-1</sup>	not enough data		+0.7±2.8
Estimate of final accuracy <sup>(g)</sup>	μmol kg <sup>-1</sup>	±4		±2
Estimate of final precision <sup>(g)</sup>	μmol kg <sup>-1</sup>	±3		±3
<b>A<sub>T</sub></b>				
Acid batch size		1		1
Acid strength calibrated?		no		no
Acid strength(s)	mol l <sup>-1</sup>	approx. 0.1		approx. 0.1
CRM deviation from cert. value <sup>(d)</sup>	μmol kg <sup>-1</sup>	A: +51.9±2.4 B: +54.5±3.5	A: +48.8±2.2 B: +52.2±2.0	A: -8.0±4.9 B: -14.0±3.4
Short term precision <sup>(e)</sup>	μmol kg <sup>-1</sup>	A: not enough data B: not enough data	A: ±0.6 B: ±1.2	A: ±1.1 B: ±1.0
VINDTA A-B (corrected data) <sup>(f)</sup>	μmol kg <sup>-1</sup>	not enough data		+0.9±1.6
Estimate of final accuracy <sup>(g)</sup>	μmol kg <sup>-1</sup>	±6		±3
Estimate of final precision <sup>(g)</sup>	μmol kg <sup>-1</sup>	±3		±2

(a) Refers to section 3.5

(b) Refers to section 3.6

(c) Larger amounts of 'startup junk analyses' improve cell stability over the initial several runs

(d) Mean and standard deviation of differences between measured and certified values of CRM. Large values here may indicate noisy measurements and/or instrument drift over the course of a cruise.

(e) Mean and standard deviation of replicate measurements performed within a short time span. In all cases, n>>20

(f) Mean and standard deviation of samples analyzed on both instruments. In all cases, n>>50

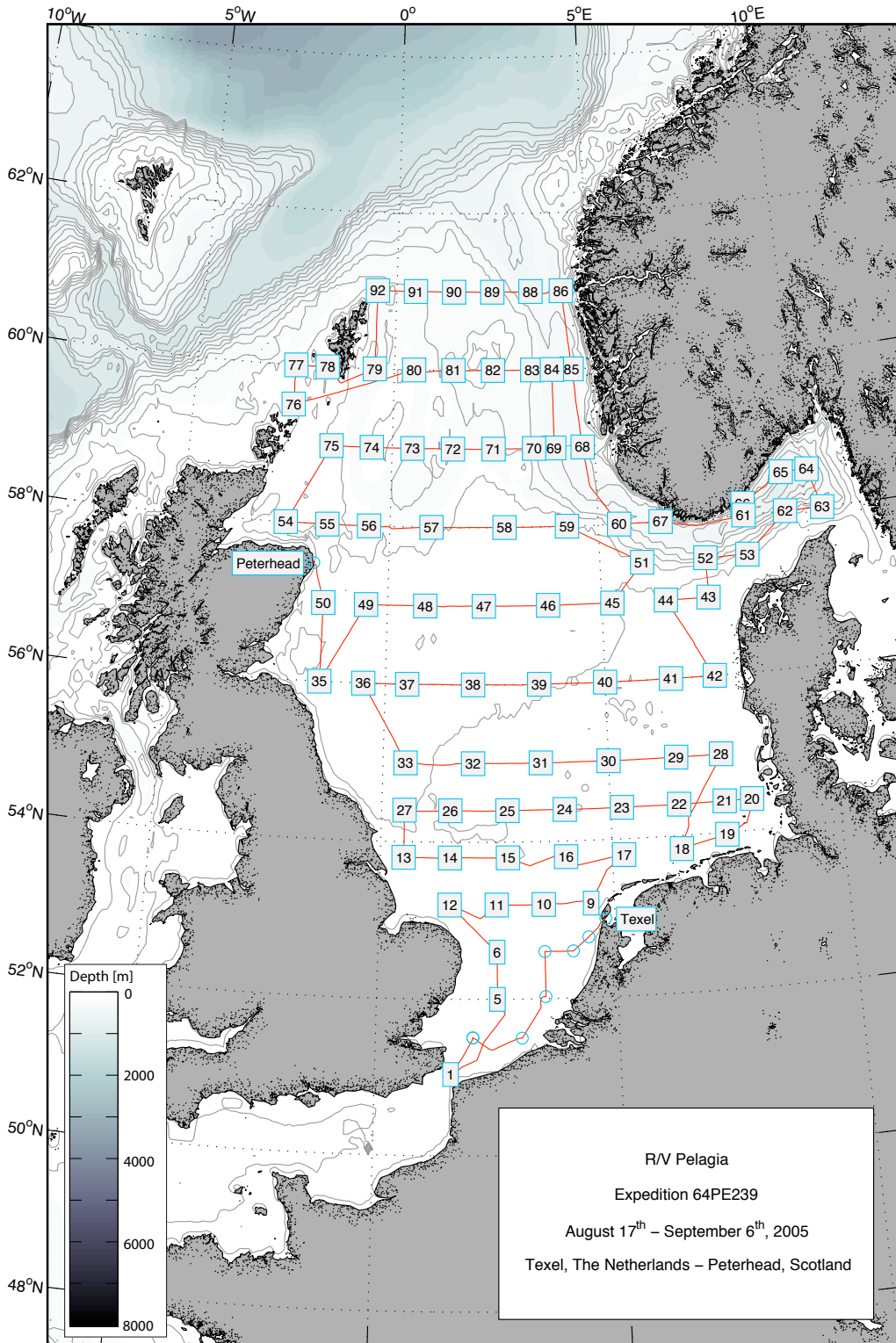
(g) Subjective estimate

(h) A gradual drift in results was observed

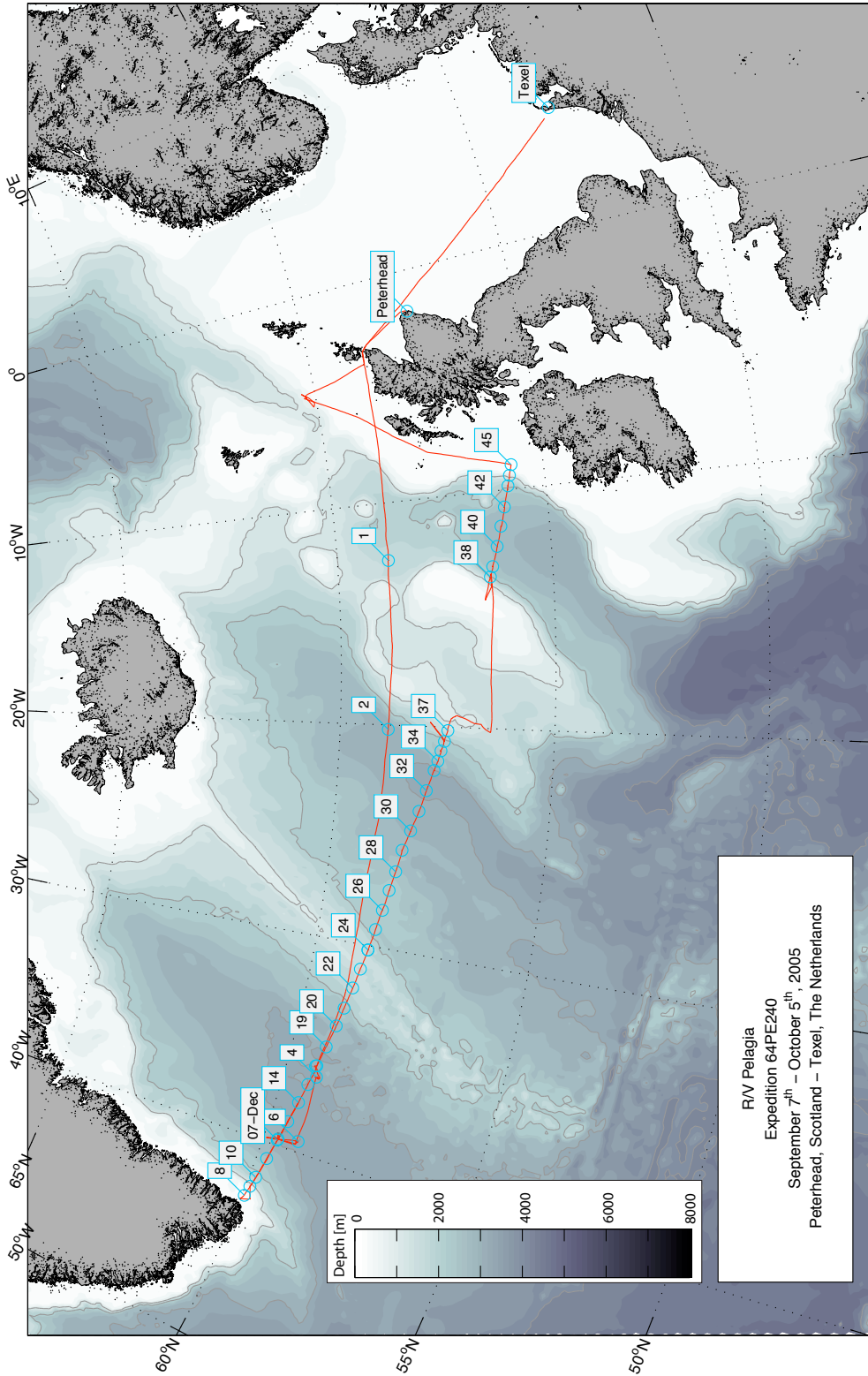
ARK-XXII/2	64PE275	64PE278	ANT-XXIV/3	64PE319	64PE321
PFS Polarstern	RV Pelagia RV Pelagia		PFS Polarstern	RV Pelagia RV Pelagia	
Tromsø, Norway	Texel, Netherlands	Galway, Ireland	Cape Town, S. Africa	Scrabster, Scotland	St. George, Bermuda
Bremerhaven, Ger.	Galway, Ireland	Canical, Madeira	Punta Arenas, Chile	St. George, Bermuda	Fortaleza, Brasil
Jul. 28, 2007	Aug. 30, 2007	Oct. 26, 2007	Feb. 10, 2008	Apr. 28, 2010	Jun. 11, 2010
Oct. 10, 2007	Sep. 27, 2007	Nov. 17, 2007	Apr. 16, 2008	May 25, 2010	Jul. 8, 2010
Ursula Schauer AWI, Bremerhaven Germany	Geert-Jan Brummer NIOZ, Texel Netherlands	Dagmar Kieke IUP, Bremen Germany	Eberhard Fahrbach AWI, Germany Hein de Baar NIOZ, Netherlands	Loes Gerringa NIOZ, Texel Netherlands	Micha Rijkenberg NIOZ, Texel Netherlands
Sven Ober	Steven van Heuven Astrid Hoogstraten Henk Zemmeling	Steven van Heuven Maaïke Claus	Steven van Heuven Hans Slagter	Steven van Heuven Lesley Salt	
$C_T, A_T$	$C_T, A_T$		$C_T, A_T, (pCO_2)$	$C_T, A_T$	
A: VINDTA 14	A: VINDTA 15 B: VINDTA 17		A: VINDTA 17 B: VINDTA 15	A: VINDTA 14 B: VINDTA 17	
circa 450	circa 725	circa 850	circa 2850	circa 400	circa 500
circa 70	circa 40	circa 80	circa 200	circa 50	circa 50
no, immediate analysis	no, immediate analysis	no, immediate analysis	no, immediate analysis	no, immediate analysis	no, immediate analysis
incandescent	incandescent	incandescent	LED	LED	
no	no	no	no	yes	
ca. 80	ca. 160	ca. 160	ca. 160	ca. 160	
A: +5.0±1.5	A: -9.4±4.7 B: -11.2±3.4	A: +7.6±3.7 B: +2.5±3.1	A: -2.2±5.3 B: -12.5±3.3	A: +1.9±2.0 B: -6.1±9.3 (h)	
A: ±1.5	A: ±1.4 B: ±1.3	A: ±0.9 B: ±1.0	A: ±1.3 B: ±1.5	A: ±1.6 B: ±0.9	
--	+0.1±2.6	-0.9±3.1	+0.1±2.1	-0.6±1.9	
±3	±3	±2	±2	±2	
±2	±3	±3	±2	±2	
1	10	10	10	20	
no	no	no	yes	no	
approx. 0.1	approx. 0.1	approx. 0.1	0.125 / 0.093 / 0.123	approx. 0.1	
A: 0.5±4.5	A: +6.0±8.0 (h) B: +6.7±2.8	A: +21.4±2.9 B: +82.4±1.9	A: -11.9±4.2 B: -6.8±9.8 (h)	A: +21.1±6.1 (h) B: +17.4±2.3	
A: ±1.5	A: ±1.4 B: ±1.8	A: ±1.0 B: ±1.2	A: ±1.9 B: ±2.5	A: ±1.5 B: ±1.1	
--	+1.0±1.4	+2.9±2.1	-6.9±4.7	+0.7±3.7	
±4	±3	±4	±4	±2	
±2	±2	±2	±2	±3	

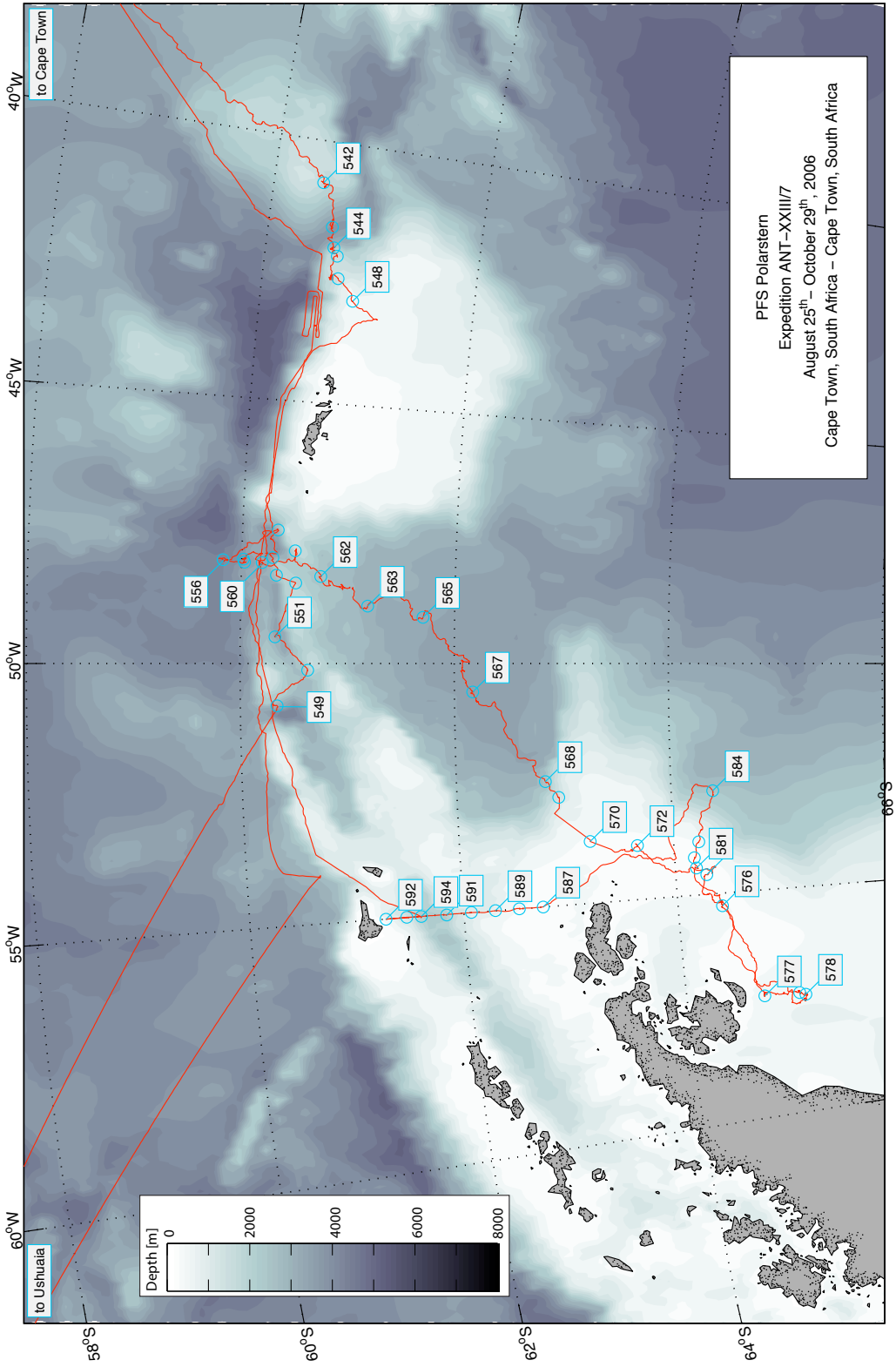
**On the following pages:** Maps depicting the cruise tracks of the 9 research cruises in which the author was, to greater or lesser extent, involved. Research cruises 64PE319 and 64PE321 are shown on a single map.

Chapter 3

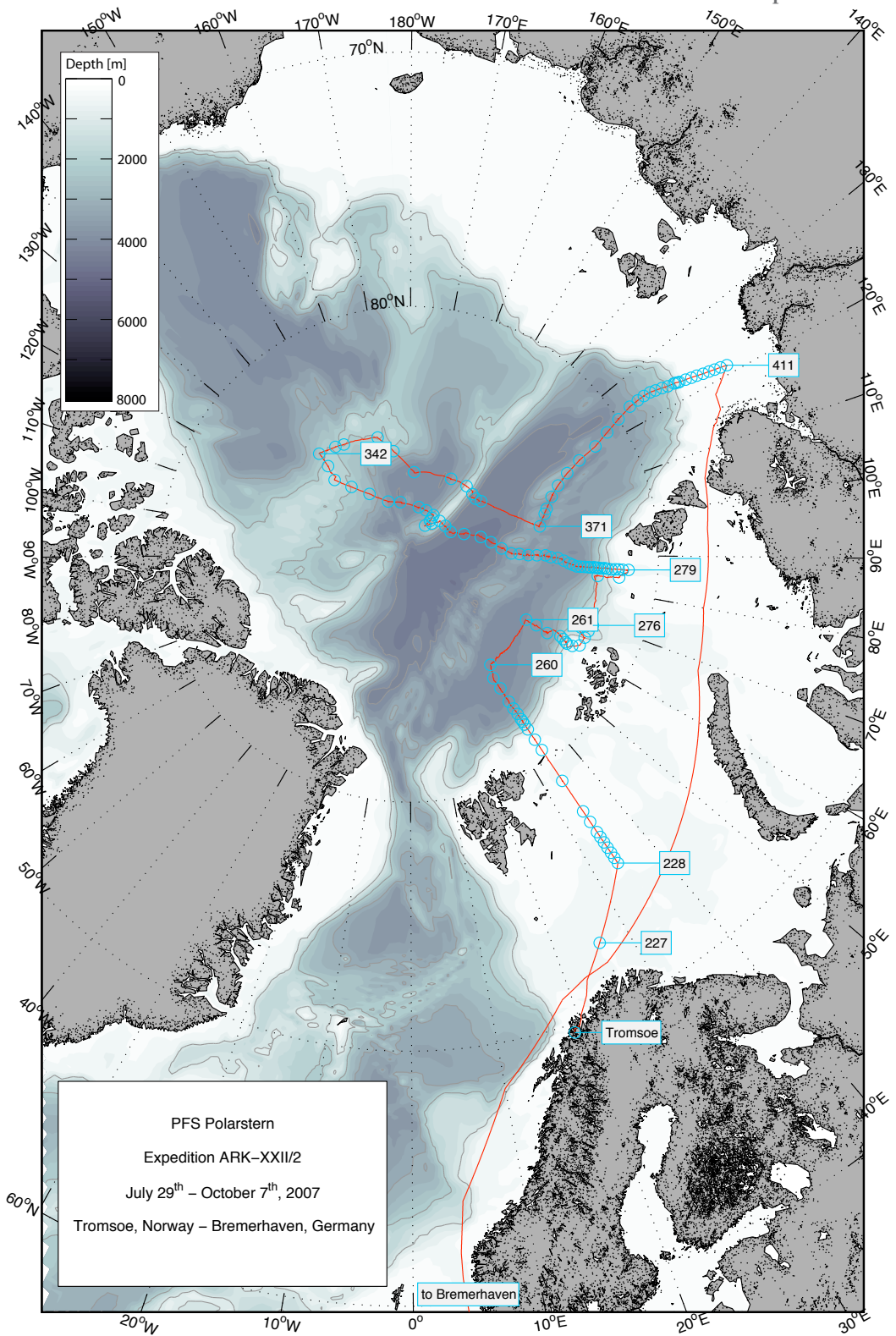


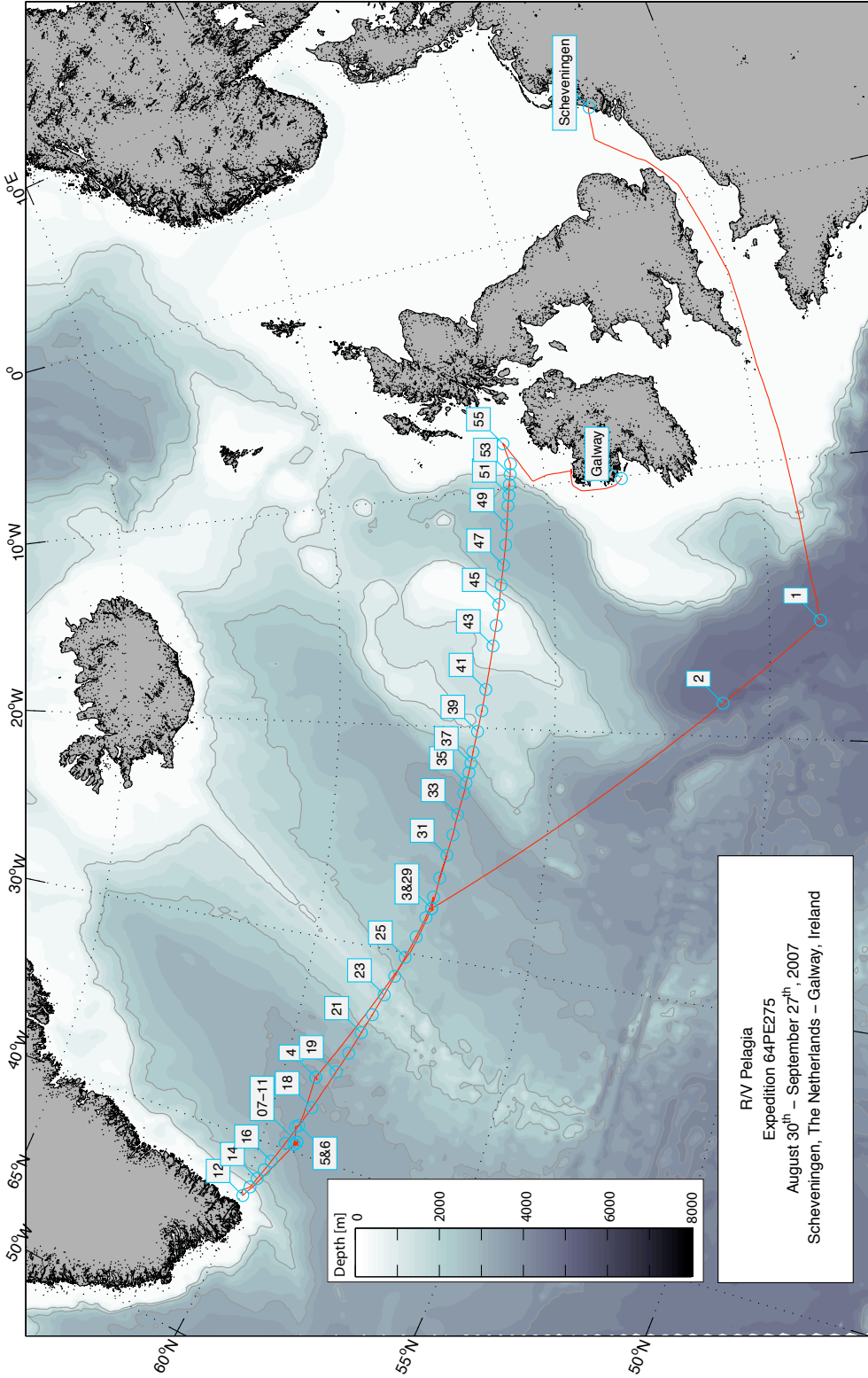


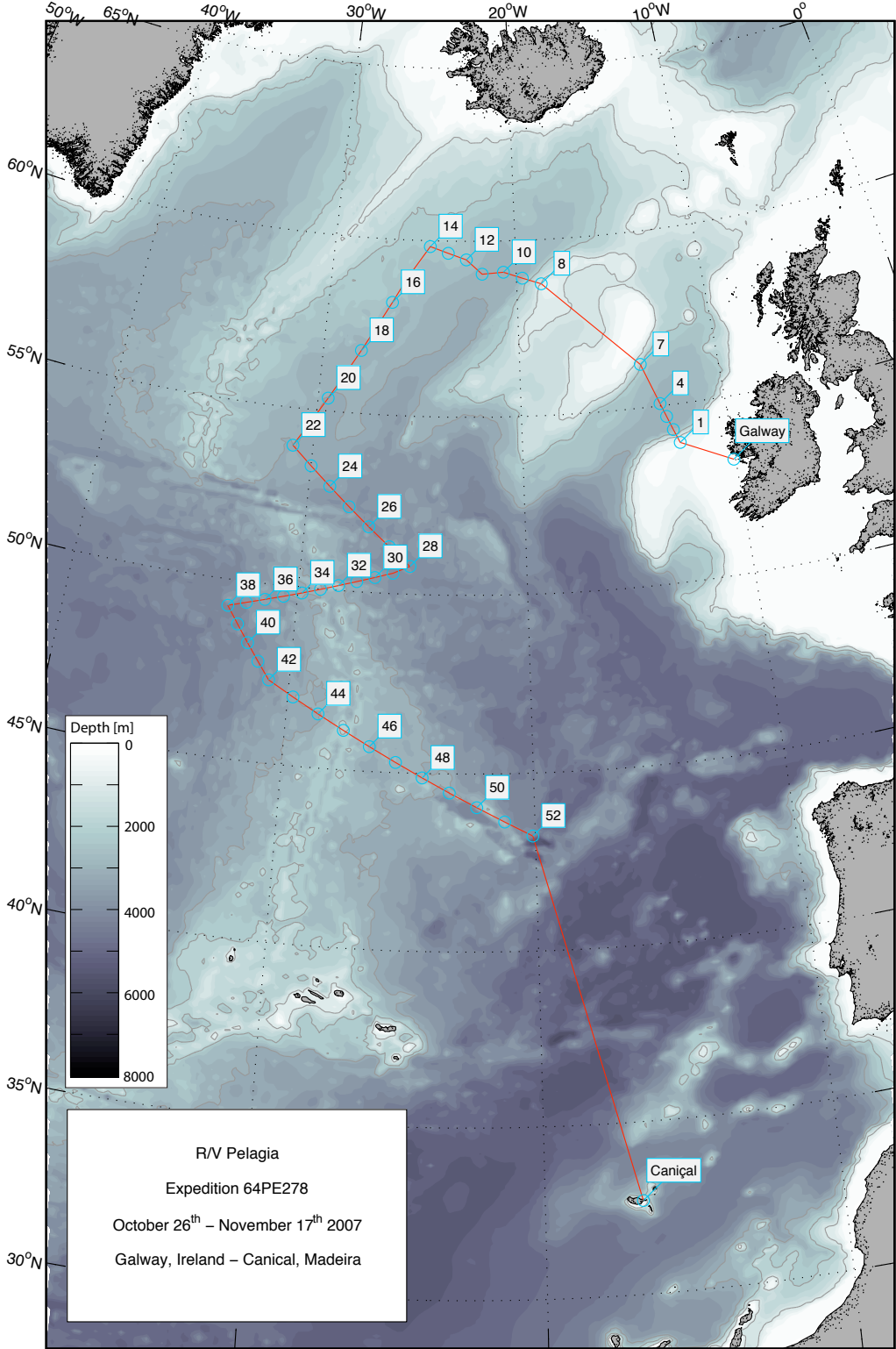


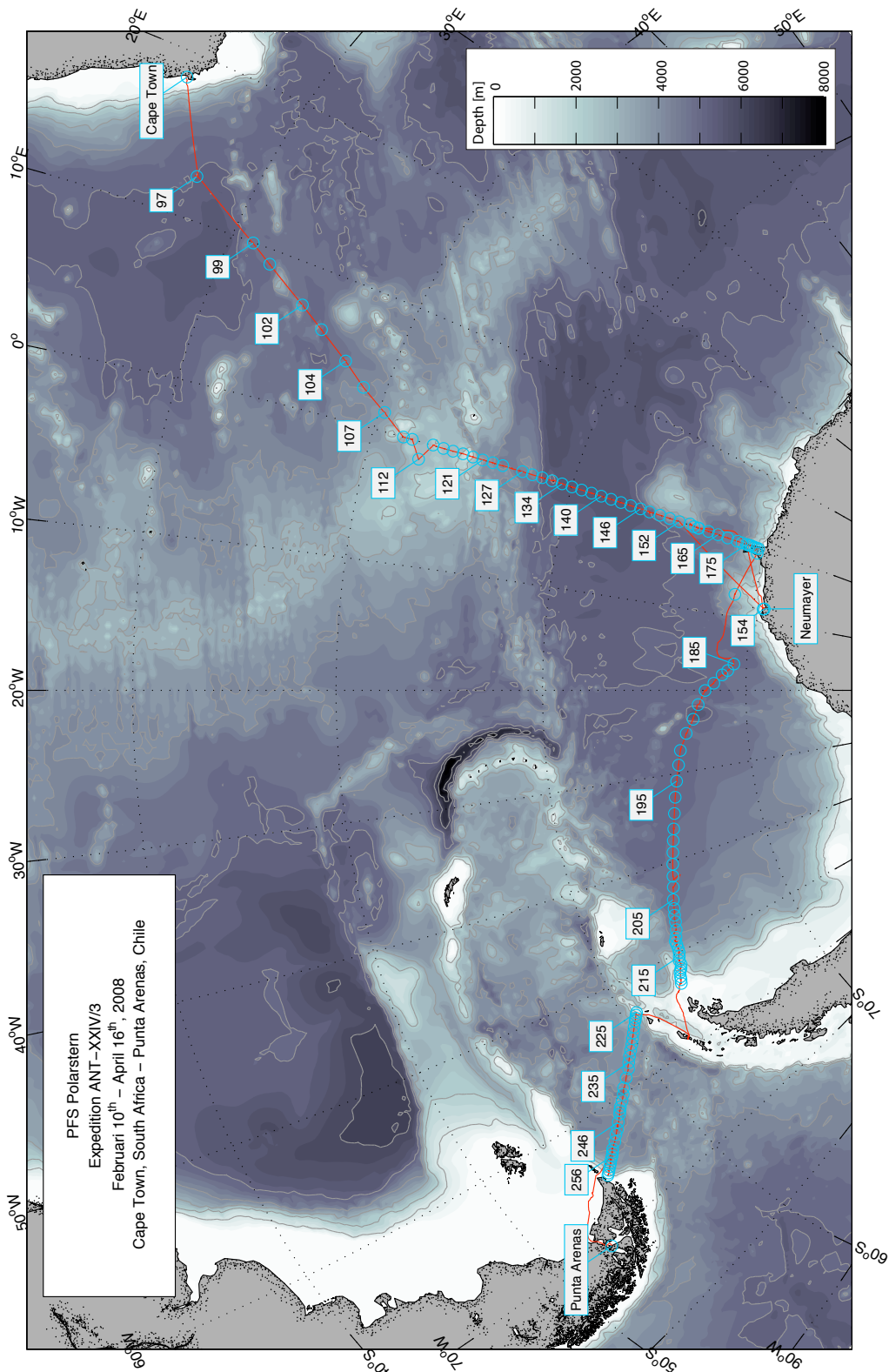




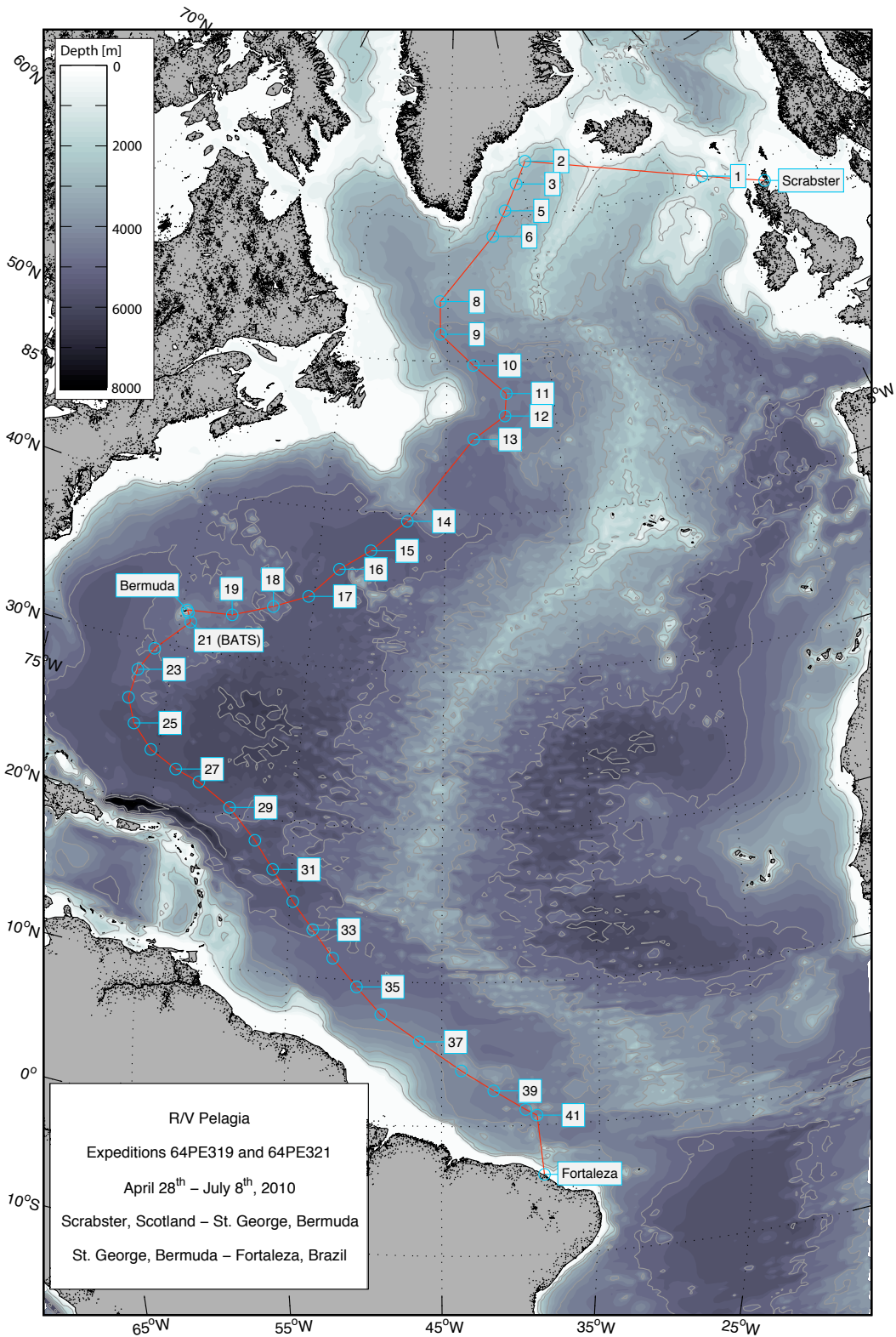














# Chapter 4

## **The CARINA data synthesis project: introduction and overview**

Slightly adapted from the publication  
*Key, R.M., T. Tanhua, A. Olsen, M. Hoppema, S. Jutterström, C. Schirnick,  
S. van Heuven, A. Kozyr, X. Lin, A. Velo, D.W.R Wallace and L. Mintrop  
(2010). The CARINA data synthesis project: introduction and overview.  
Earth System Science Data, 2, 105–121.*





## Abstract

The original goal of the CARINA (Carbon in Atlantic Ocean) data synthesis project was to create a merged calibrated data set from open ocean subsurface measurements by European scientists that would be generally useful for biogeochemical investigations in the North Atlantic and in particular, studies involving the carbon system. Over time the geographic extent expanded to include the entire Atlantic, the Arctic and the Southern Ocean and the international collaboration broadened significantly. In this paper we give a brief history of the project, a general overview of data included and an outline of the procedures used during the synthesis.

The end result of this project was a set of 3 data products, one for each of the listed ocean regions. It is critical that anyone who uses any of the CARINA data products recognize that the data products are not simply concatenations of the originally measured values. Rather, the data have been through an extensive calibration procedure designed to remove measurement bias and bad data. Also a significant fraction of the individual values in the data products were derived either by direct calculation or some means of approximation. These data products were constructed for basin scale biogeochemical investigations and may be inappropriate for investigations involving small areal extent or similar detailed analyses. More information on specific parts of this project can be found in companion articles in this issue. In particular, Tanhua et al. (2009) and Tanhua (2010b; Chapter 5 of this thesis) describe the procedures and software used to remove measurement bias from the original data.

The three data products and a significant volume of supporting information are available from the CARINA web site hosted by the Carbon Dioxide Information Analysis Center (CDIAC; [http://cdiac.esd.ornl.gov/oceans/CARINA/Carina\\_inv.html](http://cdiac.esd.ornl.gov/oceans/CARINA/Carina_inv.html)). Anyone wanting to use the data is advised to get the highest version number of each data product. Incremental versions represent either corrections or additions. The web site documents specifics of the changes.

### 4.1. Background

Historically, the vast majority of chemical oceanographic investigations have focused on problems that had the scale of an ocean basin or smaller. There were multiple reasons for this restricted view that included lack of financial resources, lack of manpower, and the fact that very limited data sharing occurred between individual researchers. Some data sets were submitted to national data centers, however, many were not, and the level of quality control possible at the national data repositories is limited. The end result was that no really high quality biogeochemical ocean data set with global scope existed.

The GEOSECS program (Geochemical Ocean Sections) was conceived in 1967 and carried out during the 1970s. GEOSECS sampling consisted of 312 stations distributed approximately along the center of each major ocean basin. Many parameters were analyzed in addition to the common hydrographic measurements, i.e. pressure, temperature, salinity, oxygen, and the macro nutrients nitrate, silicate and phosphate. Most remarkable about GEOSECS was the extremely high quality of the measurements – in some cases equivalent to the best data being generated today. Also revolutionary was the fact the entire data set was available to the pub-

lic in a reasonably short time. It is not an overstatement to say that GEOSECS revolutionized chemical oceanography. The greatest limitation of GEOSECS is that fact that it only provided a two dimensional picture of chemical distributions in the global ocean. The data were not sufficient to generate property distributions on horizontal surfaces. Global property integrals computed from the data had significant errors (Peacock, 2004; Key et al., 2004).

During the 1980s the TTO (Transient Tracers in the Ocean) and SAVE (South Atlantic Ventilation Experiment) programs extended the GEOSECS view to three dimensions for the Atlantic. Station spacing was still sparse, however the individual station locations were chosen so that the combined data could be used to produce property maps on potential density surfaces with reasonable interpolation error (e.g. Kawase and Sarmiento, 1985). The number of measured parameters was significantly smaller than for GEOSECS, but the data quality was again remarkably high, and the data were made public.

Two other transitions resulted from these programs. The first was that nutrient and oxygen data were reported in micromoles per kilogram rather than in micromoles or milliliters per liter. This change was based on chemical arguments and has been adopted by subsequent large-scale programs. Unfortunately, this transition has not been universal. Second, the data were presented in a format designed for computer access. By today's standards, the formats were far from ideal, but they were carefully thought out and the format "flaws" were largely a result of computer limitations.

TTO and SAVE organizers had planned to extend the programs to the other oceans, however, this never materialized. In the late 1980s WOCE (World Ocean Circulation Experiment) and JGOFS (Joint Global Ocean Flux Study) began. Unlike the previous studies, both of these had international organization and participation. Both programs had accuracy goals for every measured parameter, both required that the data be released quickly for public use in uniform-format computer-accessible files, and both had standard reporting units for every measurement. WOCE protocol had the additional requirement that each measurement in a bottle data set (except CTD derived temperature and pressure) be assigned an integer quality flag. The flag values were determined either by first hand knowledge of the analysis, or by "data experts" after a data set was submitted. This data flagging procedure has come to be called "primary quality control" or simply "QC1". Primary quality control is largely a measure of the precision of a particular measurement rather than accuracy. The WOCE data flags have been used by many subsequent programs.

WOCE originated as a physical oceanographic program with sampling designed to optimize global transport calculations. The occupied sections were either meridional or zonal and had dense sampling along the sections relative to previous studies (~30 nm station spacing; 24 to 36 bottle samples per station; high accuracy CTD records). In addition to the common hydrographic measurements a subset of the samples were analyzed for transient tracers ( $^3\text{H}$ ,  $^3\text{He}$ ,  $^{13}\text{C}$ ,  $^{14}\text{C}$ , CFC-11 and CFC-12).

JGOFS was a process oriented investigation and included repeated sampling at a few locations. The JGOFS locations were chosen for specific hydrographic and biogeochemical conditions. JGOFS measurements included the common hydrographic parameters, but focused on less common biogeochemical measurements. Critical to the CARINA project, JGOFS also funded the analysis of carbon system parameters (total dissolved inorganic carbon, DIC

or  $\text{TCO}_2$  or  $C_T$ ; total alkalinity, ALK or  $A_T$ ; pH; the partial pressure (or fugacity) of dissolved carbon dioxide,  $p\text{CO}_2$  or  $f\text{CO}_2$ ) on WOCE cruises.

Many of the papers in this special issue discuss  $C_T$  and/or  $A_T$  data. In these papers as well as within the chemical oceanographic community there is no standard abbreviation for these two parameters. Total dissolved inorganic carbon is abbreviated by DIC,  $\text{TCO}_2$ ,  $C_T$  etc. Total alkalinity is abbreviated with Alk, ALK,  $A_T$ , TA, etc. Regardless of the abbreviation used, in the CARINA literature all are talking about the exact same thing. Efforts to standardize these abbreviations have failed.

Concurrent with WOCE sampling came the general acceptance that human activities – most importantly the release of  $\text{CO}_2$  into the atmosphere by burning fossil fuels had the potential to alter global climate. By the end of WOCE one of the largest uncertainties in global climate change studies was the inventory of anthropogenic  $\text{CO}_2$  stored in the ocean. Accurate quantification of this inventory was the primary motivation for GLODAP (Global Ocean Data Analysis Project). GLODAP was a formally organized and funded collaboration. Most of the GLODAP team members were US scientists, but the project included participation by scientists from Australia, Japan, Korea and Europe. To achieve the stated goal, the first requirement was a high quality, uniformly calibrated global data set that included carbon system measurements and ancillary data. The core data for GLODAP were provided by WOCE and JGOFS. The uniform calibration requirement led to the development (or adoption) of various techniques designed to quantify (and subsequently correct) measurement bias that existed between various cruise data sets. The data bias existed because there were no universal standards for most of the needed measurements (e.g. nutrients, oxygen, carbon system measurements). The quantification of measurement bias has come to be known as secondary quality control or simply “QC2”. Details of the GLODAP QC2 procedures can be found in the literature (Key et al., 2004; Sabine et al., 2005) and at the CDIAC web site ([http://cdiac.esd.ornl.gov/oceans/glodap/Glodap\\_home.htm](http://cdiac.esd.ornl.gov/oceans/glodap/Glodap_home.htm)). For the carbon system, most of the data bias was eliminated by the availability, part way through the WOCE sampling, of CRMs (Certified Reference Material) which were devised, prepared and distributed by A. Dickson (Dickson, 1990; Dickson et al., 2003; Dickson, <http://andrew.ucsd.edu/co2qc/index.html>). The GLODAP team did not have the manpower to do complete QC2 on all of the parameters included in the data products, but rather adopted results from previous studies where available (Gouretski and Jancke, 2001; Johnson et al., 2001; C. Mordy and L. Gordon, personal communication to R. Key, 2003).

Once the GLODAP team had completed the QC2 work, they produced two data products (Key et al., 2004). The first was a set of three merged calibrated data sets, one each for the Atlantic, Indian and Pacific Oceans. These compilations used a simplified set of quality flags (subset of the WOCE flags), had all questionable/bad data removed, included interpolated values for missing salinity, oxygen and nutrient data and reduced the carbon measurements to  $A_T$  and  $C_T$  (by calculation from whatever carbon-pair was measured). The second product was a series of objectively mapped property distributions. The maps used the same grid spacing and depth levels as previous work (e.g. Levitus, 1982 and subsequent revisions) for compatibility. The maps were then integrated to provide inventories (for the region covered by the data) for  $C_T$ ,  $A_T$ , natural  $^{14}\text{C}$ , bomb-produced  $^{14}\text{C}$ , anthropogenic  $\text{CO}_2$ , CFC-11 and CFC-12 (Table 1 in Key et al., 2004). These inventories were not quite global since GLODAP included very little data from the Arctic Mediterranean Seas. Sabine et al. (2004) made reasonable extrapolations

to extend the data to the remainder of the global ocean and produced the first data-based anthropogenic CO<sub>2</sub> global ocean inventory using the method of Gruber (1998). The same data have been used with different methods to calculate alternate anthropogenic CO<sub>2</sub> inventory estimates (McNeil et al., 2003; Waugh et al., 2006). The GLODAP data products were released to the scientific community immediately, and have subsequently been very widely used for varied biogeochemical and physical investigations by modelers and data analysts (Orr et al., 2001, 2005; Feely et al., 2002, 2004; Gnanadesikan et al., 2004; Lee et al., 2006; Matsumoto et al., 2004; Matsumoto, 2007; McNeil et al., 2007; Mikaloff-Fletcher et al., 2006, 2007; Roussenov et al., 2004; Sarmiento et al., 2007; Sweeney et al., 2007; Vazquez et al., 2009; and many others).

While quite successful, GLODAP did not cover all ocean areas. The only data in the collection from latitudes north of approximately 60 °N were a few GEOSECS and TTO stations in the Nordic Seas. GLODAP included no data from the Arctic Ocean or the Gulf of Mexico, only a couple of stations in the Caribbean Sea, one GEOSECS station from the Mediterranean Sea, etc. Some of the research referenced above also demonstrated that the data density in the North Atlantic was exceptionally sparse relative to the concentration gradients and complicated physics encountered there. These deficiencies were partially responsibility for the CARINA project.

### 4.2. History of the CARINA project

Unlike GLODAP, the CARINA project began as an informal collaboration with very limited funding. The project was started by D. Wallace and L. Mintrop, and had an organizational meeting at Delmenhorst, Germany in 1999. Subsequently, funding was obtained from German JGOFS to support Mintrop who acted as data collector. Participation was voluntary and consisted mostly of European scientists. Participating scientists were required to submit their historical data sets that included either subsurface carbon system measurements or underway surface *p*CO<sub>2</sub> data. The last meeting of this group was held in 2002. By that time the group had accumulated subsurface data from approximately 30 cruises (excluding those that were in GLODAP) and twice that number of underway data sets. The funding ended in March 2003 and, unfortunately, the support level was insufficient to do much more than amass and catalog the submitted data.

In 2004 the original CARINA data collection was transferred to CDIAC. This was about the same time that the North Atlantic GLODAP data deficiencies were recognized. Consequently, a copy of the CARINA bottle data was transferred to Princeton for data assessment and quality control.

In January 2005 the EU funded CarboOcean program began. This consortium consists of more than 40 research groups and includes the most of original CARINA scientists. CarboOcean is an integrated program with the aim of making an accurate assessment of oceanic sources and sinks of carbon over space and time. It has focus on the Atlantic and Southern Ocean and a time interval of -200 to +200 years from the present. All funded CarboOcean partners are required to make public all historical data and new data after a two year proprietary period. During workshops held in the first two years of CarboOcean, the CARINA project was reactivated and additional data sets collected.

In June 2007 the CarboOcean/CARINA scientists met in Laugarvatn, Iceland to discuss methods and responsibilities for the CARINA data synthesis. By that time, the CARINA collection had grown to approximately 80 cruises. During this meeting the group decided to extend the original scope of CARINA to include the entire Atlantic, the Arctic and the Southern Ocean. Various team and project leader assignments were:

- Data collection, primary QC and production of final data products: R. Key and X. Lin
- Atlantic Ocean: T. Tanhua
- Arctic Ocean: S. Jutterström
- Nordic Seas: A. Olsen
- Southern Ocean: M. Hoppema
- QC2 code development: S. van Heuven
- Web site development and maintenance: C. Schirnick
- Carbon calculation software: A. Velo
- Data archive: A. Kozyr / CDIAC

The team also decided to include data from CLIVAR (Climate Variability and Predictability) repeat hydrography cruises ([http://www.clivar.org/carbon\\_hydro/hydrotable.php](http://www.clivar.org/carbon_hydro/hydrotable.php)) that were final and that were in one of the focus regions. Since the new CLIVAR data were known to be high quality, those data, along with WOCE results would serve as “master cruises” for the data calibration (i.e., QC2) phase of the synthesis. The areal expansion of the project led to a flood of new data and a final total of 188 cruises. The CARINA station locations are shown in Fig. 4.1. The CARINA web site ([http://cdiac.esd.ornl.gov/oceans/CARINA/Carina\\_inv.html](http://cdiac.esd.ornl.gov/oceans/CARINA/Carina_inv.html)) includes links to the original cruise data files (via the Cruise Summary Table), the resulting data products and publications, and detailed information on the quality control procedures used.

### 4.3. Instrumentation

Data included in the CARINA data products span almost 30 years of measurements. Rather than attempt to summarize the specific methods and instruments in this document, we have included this information in the individual cruise file headers. For many cruises additional information can be found in the individual final cruise reports and other documentation provided with the cruise data. In many instances, a full description of the methods and instruments can be found in the footnotes to the Cruise Summary Table at the CARINA web site that refer to specific publications. Certainly the most important changes in methods and instrumentation are the adoption of CRM for standardization of  $A_T$  and  $C_T$  measurements, the development of the SOMMA-type analyzer (Johnson et al., 1998 and references cited therein) for  $C_T$  and the shift from electrode based to spectrophotometric pH determination (Clayton and Byrne, 1993). All three began to be used in the early 1990s.

### 4.4. CARINA data assembly and synthesis

Here we describe the data collection and synthesis steps used for this project. Many of the procedures used during CARINA were adopted from GLODAP, however, the number of cruises included in CARINA combined with the additional manpower and funding available from



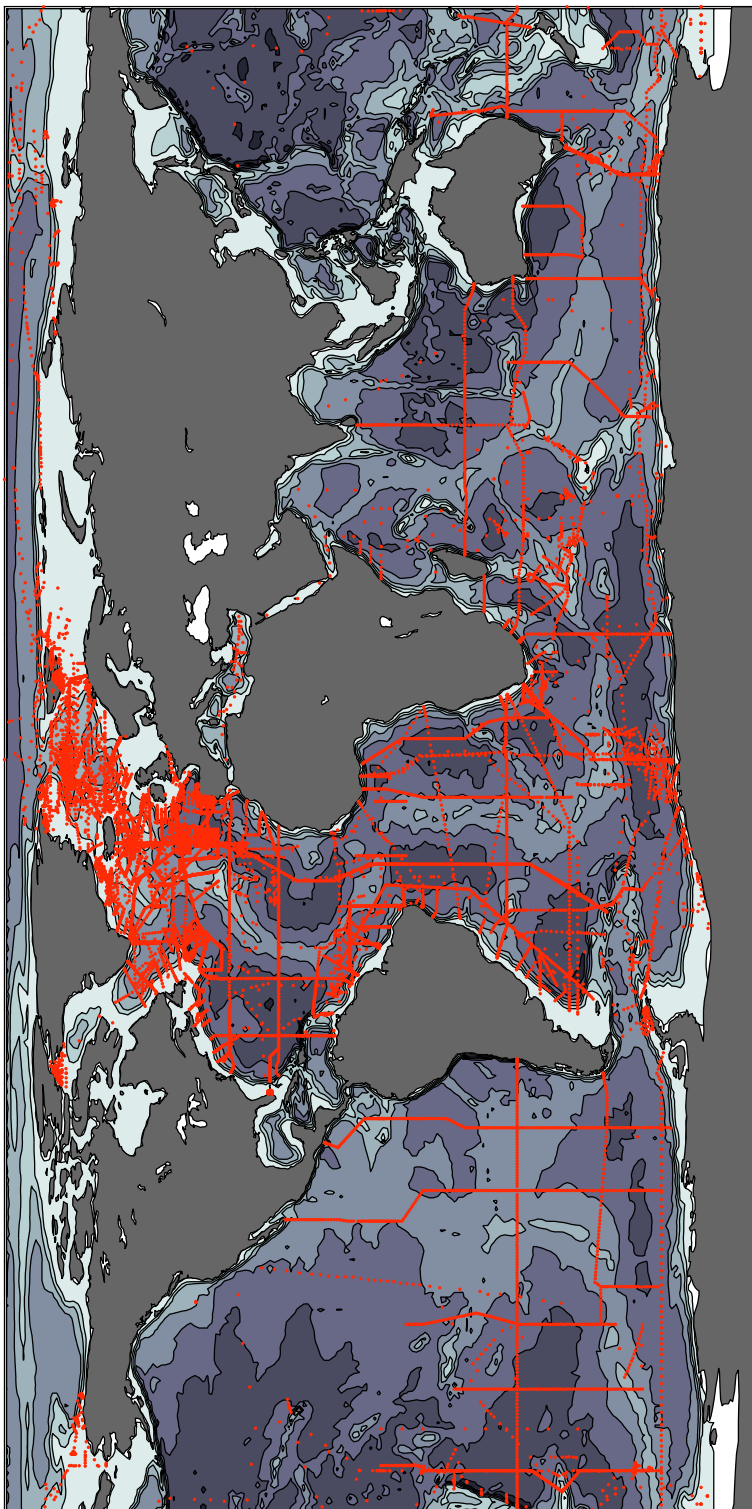


**Figure 4.1.** Station locations for cruises included in the three CARINA data products. The division between the Southern Ocean collection and the Atlantic collection was approximately 30°S and between the Atlantic and Arctic approximately 60°N (the Greenland-Scotland Ridge). Several cruises that cross one of the boundaries are included in both collections. Regional maps are available at [http://cdiac.esd.ornl.gov/oceans/CARINA/Carina\\_inv.html](http://cdiac.esd.ornl.gov/oceans/CARINA/Carina_inv.html) and a cruise map and data file for each cruise at [http://cdiac.esd.ornl.gov/oceans/CARINA/Carina\\_table.html](http://cdiac.esd.ornl.gov/oceans/CARINA/Carina_table.html).

the CarboOcean contract allowed improvements. The most significant changes were: **(a)** more parameters were subjected to QC2 by the project participants; **(b)** software was designed to automate portions of the QC2 procedures; **(c)** work was coordinated among the different groups and within groups by means of a web site; **(d)** pH was included in the final data products along with  $A_T$  and  $C_T$ ; **(e)** fully formatted versions of all the individual cruise files were submitted to both CCHDO (CLIVAR & Carbon Hydrographic Data Office: <http://whpo.ucsd.edu/>) and CDIAC for archive and distribution; and **(f)** a significant collection of references to literature describing the individual cruise results was compiled.

This effort led to two distinct results. The first is a set of individual cruise files with the measured data converted to common units, having quality flags added for all parameters, and accompanied by metadata. All of the individual cruise files are in “WHP-Exchange” format (Swift, 2008). This format is a standard that developed during the 1990s and has since become widely accepted. It is a comma separated data file with formal column header names and units and that can include metadata within the header. The second is a set of 3 data products (Arctic Mediterranean Seas-AMS, Atlantic Ocean-ATL and Southern Ocean-SO) that have been fully calibrated (i.e. measurement bias removed via QC2) and include some calculated values. For CARINA we defined Arctic Mediterranean Sea(s) to include the main Arctic basin and all adjacent seas southward to approximately 60 °N. Thus the AMS region includes the Nordic Seas (down to the Greenland-Iceland-Scotland Ridge) on the Atlantic side and the Bering Sea on the Pacific side. The format for the data products is simple comma separated records with a single header record defining the included values. The header does not include units since everything is standard (as defined for the Exchange format). Additionally, the data products are purely numeric other than the single header record.

The CARINA data products are compatible with the three GLODAP data products, but they are not identical, differing somewhat in column order and included parameters. We plan to merge CARINA and GLODAP once the initial scientific analysis of CARINA is completed.

#### 4.4.1. Collection and primary quality control (QC1)

The most time consuming portion of the CARINA synthesis was data assembly. Investigators who had participated in data collection and/or made the measurements, submitted most of the data sets. Along with the data file, submitters were asked to supply references to any publication(s) that had resulted from the data. Whenever they existed, final cruise reports were obtained. The remaining data sets were obtained by “discovery” which amounted to scanning publications for mention of other cruises, data discussed at CarboOcean and other meetings and similar. Once discovered, either the chief scientist or another cruise participant was contacted for a copy of the data and any existing documentation. In most cases, a complete copy of the cruise data set was not available. In these instances the missing data were sought from the principal investigator(s) (PI) responsible for that data. Though the effort was not completely successful, we tried to obtain all of the bottle measurements from each cruise. As the data were collected, we also obtained permission from each PI to release his/her data to the public. In a few cases electronic versions of the data did not exist and the results were manually entered into the existing files.

For all of the CARINA cruises the following conventions were used for station information. Only one location was recorded for each station of each cruise. When multiple casts were collected, the location and date of the first cast was used for the entire station. Locations were stored as decimal degrees with negative values for west longitude and south latitude. For many of the cruises bottom depth was not recorded for each station. In these cases bottom depth was first approximated from a global (0.25 degree resolution) topography. This depth was then compared to the deepest sample pressure at the station. Whichever was greater, the topographic depth or the deepest sample pressure +10 was recorded for the water depth. These bottom “depths” are not meant for research purposes, but rather to enable drawing approximate bottom topography for section plots.

For most cruises multiple files with different subsets of the data were collected. The first synthesis task, and the most error prone, was merging data from these subsets. File merging is a quick and easy computer matching procedure whenever adequate sample identification is given. However, for most of the CARINA cruises the identification information was either incomplete or totally missing. In these instances the data files were manually merged based on available information. The manual merges, which consist of multiple cut and paste operations were made especially tedious by the fact that “intended bottle depth”, “bottle pressure” and “bottle depth” were often used synonymously. In the many instances where the cast and bottle information was missing, values were fabricated to ease subsequent discussion of specific results among various project participants and to make the files more format consistent with modern oceanographic records. Such fabrication is noted in the metadata header of the final format files submitted to the data centers. Alphabetic station names were converted to numeric and unnecessarily complex station numbers were simplified. These alterations were documented in the file header information.

Immediately after merging, cruise data were read into the same data system used for the GLODAP collection. There, units were converted to match those used during the WOCE program. Most commonly, this amounted to converting oxygen and nutrient data from milliliter per liter and micromole per liter into micromole per kilogram ( $\mu\text{mol kg}^{-1}$ ). Unfortunately, there is no standard method for this conversion. For this work the most common method was to use density calculated from measured salinity for each sample with an assumed lab temperature (default of 22 °C) and pressure (1 atmosphere). In cases where the concentration was reported in standard units ( $\mu\text{mol kg}^{-1}$ ) the conversion method is unknown, but simple division by a constant assumed density (often 1.025) is common. Regardless of method, this conversion error is less than the measurement errors, so we consider this inconsistency to be bothersome, but minor. Another source of error that we were not able to completely eliminate is the possibility of erroneous units for the nutrients, i.e. that data were given in volumetric units instead of the stated gravimetric units, or the vice versa. Both cases would cause an offset of 2–3%.

Another complication arose with nitrate data. In ideal cases nitrate and nitrite measurements were reported separately. In others only nitrate was reported or only the combination of nitrate plus nitrite. Finally, in a few instances nitrate plus nitrite was reported along with values for nitrite. For the last example the nitrite values were simply subtracted from the reported nitrate plus nitrite values. For cases where only nitrate plus nitrite was reported we had a choice: carry an additional parameter (i.e.  $\text{NO}_3 + \text{NO}_2$  in addition to nitrate) or simply rename the data nitrate (ignoring the nitrite contribution in the upper water column). Both



choices are problematic. We chose the latter for CARINA cruises (both original cruise files and final data products).

Chlorofluorocarbon data in the CARINA collection cover the time span from 1982 to 2005 and were originally reported on either the SIO-93 or SIO-98 scale. All of these (CFC-11, CFC-12, CFC-113, CCl<sub>4</sub>) were converted to the SIO-98 scale (Prinn et al., 2000). SF<sub>6</sub> data are reported on the NOAA/GMD 2000 calibration scale.

Reported pH data were also converted to uniform scale and temperature. The CARINA data span 1977–2005. Over that time pH measurements have been made with radically different techniques and the results reported on three different pH scales: National Bureau of Standards scale (NBS), seawater scale (SWS) and total hydrogen scale (TOT). Values are also reported at various temperatures (measurement temperature, some arbitrarily chosen temperature or in situ temperature). The difference between these scales isn't too large, but it is significantly larger than the precision/accuracy of modern spectrophotometric techniques. All of the measured pH data were converted to SWS at 25 °C in both the individual cruise files and in the final products. While we were producing the data products, a new version of the handbook of best practices for ocean carbon measurements was published (Dickson et al., 2007). This handbook suggests that the preferred pH scale is the total hydrogen, however, at that point it was already too late for our project. Velo et al. (2009) give the conversion functions and additional details for this work.

Historically, salinity has been analyzed on every bottle sample from a CTD/Rosette cast. The bottle salinity results were calibrated by analyzing seawater standards. The calibrated bottle salinity values were subsequently used to calibrate the CTD conductivity probe. Also, because bottle salinity can routinely be measured with high precision, the bottle salinity data provide the best check that a sample bottle closed properly and at the desired depth (for most ocean regions). That is, bottle salinity is the best way to identify mis-trips and leaking sample bottles for most of the global ocean. On many of the CARINA cruises, bottle salinity was only analyzed with sufficient frequency to calibrate the CTD. Without bottle salinity, identification of mis-trips and leaking sample bottles is reduced to an educated guess, at best. An additional problem with many of these data sets was that bottle salinity and CTD salinity values were not discriminated. That is, it was impossible to determine which of the two was included in a data file. When we could not determine if a set of values was CTD or bottle salinity, we assumed that it was bottle salinity. Therefore it is virtually certain that some of the bottle salinity data is actually CTD salinity. See also the discussion below on special steps taken with salinity data during production of the final data products. In general, the treatment of salinity data in CARINA could be labeled sloppy. We wouldn't argue with that, however, this wasn't due to lack of effort – we did the best we could. We also believe that the salinity data in CARINA are adequate for “normal” chemical oceanographic applications. We do not know whether or not the salinity data will be of sufficient quality for detailed physical oceanographic applications.

The next step in the synthesis was primary QC – the assigning of a data quality flag to each measured value. This is a process by which individual data points are closely scrutinized. It is a method of improving precision and removing spurious data. Details of this procedure are in Tanhua et al. (2010b).

The QC2 procedures (discussed in Tanhua et al., 2010b) critically examine data using different techniques than QC1. The goal of QC2 is to quantify measurement bias. In some cases

additional spurious data points were identified during QC2, and the initial flag values altered appropriately. Once all of the flag values are final, each cruise file was submitted to national data centers (CCHDO and CDIAC). Data bias identified during QC2 was corrected in the final data products, but these adjustments were not applied to the individual cruise data sets.

The CARINA data product incorporates one additional flag with value zero (0). This flag was also used in GLODAP. The zero flag indicates a datum that “could have been measured”, but was approximated in some manner. There are three different uses for the zero flag in the data products:

- Instances where bottle salinity was missing or bad and consequently was replaced with CTD salinity.
- Interpolated values for salinity, oxygen or nutrients.
- Calculated carbon parameters.

### 4.4.2. Secondary quality control (QC2)

While QC1 is designed to improve the overall precision of a data set, QC2 procedures are designed to quantify measurement bias. That is, the goal of QC2 is to improve the accuracy of a data set. Measurement bias is rather common with nutrient and oxygen measurements because certified standards are not routinely used. The very best nutrient measurements can have precision better than 1%, but the accuracy is seldom better than 2%. The same condition existed for  $A_T$  and  $C_T$  measurements until the early 1990s when CRM were developed. From GEOSECS to WOCE,  $A_T$  and  $C_T$  measurement precision improved from 5–10 to 4–5  $\mu\text{mol kg}^{-1}$ . The best CLIVAR data now have precision of  $<2 \mu\text{mol kg}^{-1}$ . Prior to CRM development, however, it wasn't uncommon for these measurements to have a bias of  $>20 \mu\text{mol kg}^{-1}$ . The use of CRMs has lowered that to  $<5 \mu\text{mol kg}^{-1}$ .

The QC2 is based on the initial assumption that abyssal waters are at steady-state. That is, deep water concentrations are invariant over time for a given location. This assumption was reasonable for the WOCE cruises included in GLODAP since the collection period only spanned a few years and few of the cruise track intersections occurred in regions with strong horizontal abyssal concentration gradients. This is not the case for CARINA. Many publications have clearly demonstrated that the abyssal steady state assumption is false over the time interval spanned by CARINA data and especially for some of the regions sampled by CARINA cruises (i.e. the far North Atlantic, the Labrador Sea and the Nordic Seas). Decadal change due to anthropogenic and natural forcing was one of the CarboOcean/CARINA focus areas, so all of the scientists involved in QC2 were aware of the potential to erase real changes when attempting to correct measurement bias.

The QC2 normally consisted of two steps: quantification of the relative measurement offsets between different cruises and assignment of an adjustment factor to data deemed to have a measurement bias that exceeded a predetermined limit. The first step was objective, the second subjective and influenced by the experience of the scientists involved and the knowledge that real temporal changes were expected for some regions. Offset was determined using variants of the crossover technique developed for GLODAP (Key et al., 2004; Sabine et al., 2005) and different forms of the inversion methods derived by Gouretski and Jancke (2001) and Johnson

et al. (2001). The QC2 methods are discussed in detail by Tanhua et al. (2010b). QC2 tests were run for salinity, oxygen, nutrients,  $C_T$ ,  $A_T$ , pH, CFC-11, CFC-12, CFC-113 and  $CCl_4$ .

For the carbon system parameters, additional tests were possible using calculated values. For example, if  $C_T$  and  $A_T$  were measured, calculated pH could be compared to measured pH from another cruise. To demonstrate the validity of this comparison, we compared calculated to measured parameters for one Atlantic cruise that had very high quality measurements for three carbon system parameters (Cruise #86; 33RO20030604; Fig. 4.2). Regardless of the pair used for the calculation, the mean difference between the measured and calculated values was statistically indistinguishable from zero and the standard deviation of the differ-

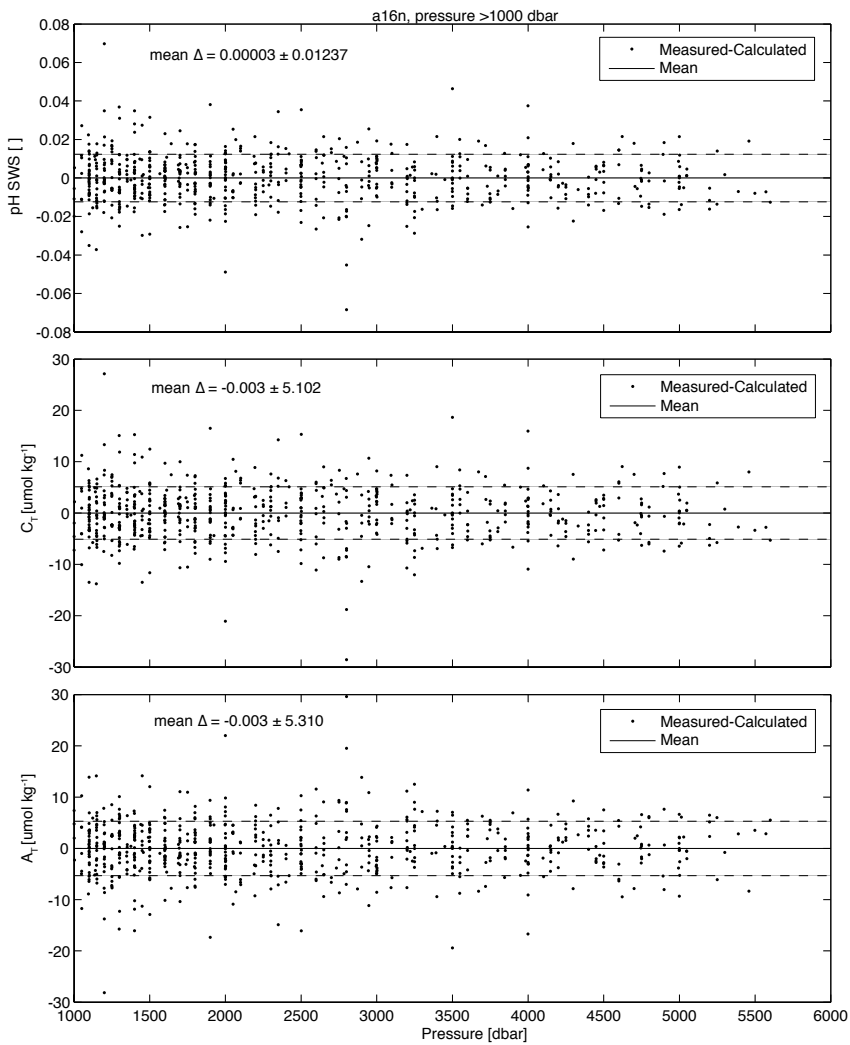


**Figure 4.2.** Comparison of measured and calculated carbon system values from Cruise #86; 33RO20030604. Regardless of which pair was used to calculate the third, the mean difference is statistically indistinguishable from zero. The standard deviation of the difference is only marginally larger than the precision estimate based on replicate analyses.

ence was not much larger than the measurement precision. This comparison provides strong evidence that the calculation error is insignificant and that calculated carbon parameters can be used for QC2 investigations. If a calculated carbon parameter is biased, the implication is that one of the input parameters is biased.

The QC2 procedures yield an offset for virtually every cruise. In some previous studies (Gouretski and Jancke, 2001 and Johnson et al., 2001), in order to be as objective as possible, all of the determined offsets were corrected. This will produce a combined data set with the lowest combined variance between cruises. In GLODAP and CARINA a more subjective approach was used. First, only those offsets that exceeded a predetermined minimum value were considered for correction. Second, all offsets that exceeded the threshold were examined by the working groups prior to assigning a final adjustment value. This subjective approach was necessary because the different QC2 procedures often gave different results and because some of the parameters were expected to change with time. This issue is discussed in detail in the accompanying methods paper (Tanhua et al., 2010b) and in each of the regional CARINA papers in this issue. The minimum offsets considered for adjustment are given in Table 4.1. All of the details of the crossover checks, inversion results and final adjustments are available at the CARINA web site. In a few instances QC2 and associated investigations

determined that all of the measurements of some parameter from a cruise could not be adequately adjusted. The reasons varied, but included strongly conflicting QC2 results, extremely noisy data and similar problems. In these cases the entire set of parameter measurements was discarded from the data product. Instances of this are indicated in the on-line version of the adjustment table by the lower case letter “o” in the flag column for each parameter instead of the normal check mark (✓) which indicates acceptable results. If this table is downloaded these two adjustment quality flags are translated into “3” and “2”, respectively. The decision to discard an entire set of measurements was made independently from the individual datum QC1 flags.

#### 4.4.3. Construction of the data products

The CARINA project resulted in three data collections or products: the Arctic Mediterranean Seas (AMS), the Atlantic Ocean and Mediterranean Sea (ATL), and the Southern Ocean (SO). The divisions between the regions were approximately 60 °N (the Greenland-Scotland Ridge in the Atlantic and the Aleutians in the Pacific) and 30 °S. Cruises which spanned a division line were generally included in both collections. Each cruise in the collection was assigned an EXPOCODE (Swift, 2008). These codes provide a unique identifier and are composed of NODC (National Ocean Data Center) platform code for the research vessel (<http://www.nodc.noaa.gov/General/NODC-Archive/platformlist.txt>) followed by the date when the cruise left port. The NODC code is composed of a 2 digit country code and a 2 character (number

**Table 4.1.** Minimum offset values considered for adjustment. Not all cruise-to-cruise differences that exceeded the minima were adjusted. In a very few cases (with very precise data) smaller adjustments were made.

Parameter	Minimum Offset
Salinity (CTD and/or bottle)	0.005
Oxygen	1%
Nitrate	2%
Phosphate	2%
Silicate	2%
A <sub>T</sub>	6 μmol kg <sup>-1</sup>
C <sub>T</sub>	4 μmol kg <sup>-1</sup>
pH	0.005

or letter) ship code. For example a cruise that started on 3 October 1999 aboard the Norwegian vessel Haakon Mosby would have EXPOCODE 58AA19991003. All of the cruises were then sorted by EXPOCODE, numbered sequentially, and a Cruise Summary Table (CST) was created ([http://cdiac.esd.ornl.gov/oceans/CARINA/Carina\\_table.html](http://cdiac.esd.ornl.gov/oceans/CARINA/Carina_table.html)). The last 5 entries in the CST are not single cruises, but cruise collections representing a single investigator (#'s 184 and 185) or a single project (#'s 186–188). Assignment of an EXPOCODE in these 5 cases was inappropriate so they were simply named. The data for these 5 collections were not segregated into individual cruise files because we thought the data more valuable as a collection and because the limited amount of data for each individual cruise did not warrant the increased record keeping that would have been required. The three data products include only the sequential cruise number, not the EXPOCODE so that the data records could remain purely numeric. Lookup tables are provided along with the data products so that the cruise number can be matched to the EXPOCODE.

The Cruise Summary Table (CST) contains a wealth of additional information. Along with the EXPOCODE the second column also lists aliases. Aliases include names used by the original investigators for the cruise or project and in some cases WOCE line designations (e.g. for cruise #4 the “WOCE SR04e”). The third column (Area) refers to the CARINA region (and data product) with: 1 = ATL, 2 = SO, 3=ATL & SO, 4=AMS and 5=AMS & ATL. The numbers under the parameter columns indicate the number of stations that have the particular measurement. Two entries under the parameter columns have a different meaning. Very few cruises in this collection included discrete  $p\text{CO}_2$  sampling. For these few, a numeric entry is the station count. A “U” entry, however, indicates that underway  $p\text{CO}_2$  measurements were made. The CARINA work does not include underway data. Underway  $p\text{CO}_2$  data are being compiled by another team (SOCAT; Surface Ocean  $\text{CO}_2$  Atlas Project; <http://ioc3.unesco.org/iocccp/Synthesis.html#SOCAT>). A “C” entry in the CST under the pH,  $C_T$  or  $A_T$  column indicates that the values in the compiled data product were calculated from other carbon parameters. The calculated values are not included in the individual cruise files submitted to the CDIA and CCHDO. The last column of the CST (Other) lists other measurements made on that cruise. When we were able to obtain these data, they are included in the original cruise files.

The data products do not contain all of the measurements from all of the cruises. Rather we narrowed the total list of different measurements down to those that were commonly measured or would be useful for carbon system calculations using current methods. The list of retained parameters is given in Table 4.2. This table also translates the parameter names in the products to the “official” Exchange format nomenclature and it gives units for the measurements. This naming convention was selected so that the CARINA data products matched the GLODAP data products as closely as possible.

With a few minor changes the CARINA data products were constructed with the same software used for GLODAP. The procedure is semi-automated and execution amounts to manually calling several programs in sequence with the appropriate options set for each program. With the exception of one step, all of the code was developed and runs on the same computer used for archiving the master version of each cruise data file. All of this code is written in S-Plus (Version 3.4 release 1 for Sun SPARC; TIBCO Spotfire, previously Insightful). Below, each step of the procedure is briefly described.

## Chapter 4

**Table 4.2a.** Translation table for parameter names, flags and units.

Data product parameter name	Data product flag name	Exchange file parameter name or full name of parameter	Exchange file flag name	Units
station		STANBR		
nosamp		Number of samples at each station		
day		DATE		
month		DATE		
year		DATE		
latitude		LATITUDE		decimal degrees
longitude		LONGITUDE		decimal degrees
maxdepth		DEPTH		meters
maxsampdepth		Pressure of deepest sample at station		dbar
cruise		CARINA assigned sequential number		
bottle	bf	BTLNBR	BTLNBR_FLAG_W	
cast		CASTNO		
depth		Calculated sample depth		meters
temperature		CTDTMP		°C
salinity	sf	SALNTY	SALNTY_FLAG_W	
ctdsal	ctdsf	CTDSAL	CTDSAL_FLAG_W	
pressure		CTDPRS		decibars
oxygen	of	OXYGEN	OXYGEN_FLAG_W	$\mu\text{mol kg}^{-1}$
nitrate	no3f	NITRAT	NITRAT_FLAG_W	$\mu\text{mol kg}^{-1}$
nitrite	no2f	NITRIT	NITRIT_FLAG_W	$\mu\text{mol kg}^{-1}$
silicate	sif	SILCAT	SILCAT_FLAG_W	$\mu\text{mol kg}^{-1}$
phosphate	po4f	PHSPHT	PHSPHT_FLAG_W	$\mu\text{mol kg}^{-1}$
tco2	tco2f	TCARBN	TCARBN_FLAG_W	$\mu\text{mol kg}^{-1}$
alk	alkf	ALKALI	ALKALI_FLAG_W	$\mu\text{mol kg}^{-1}$
phsws25	phsws25f	PH_SWS PH_TMP	PH_SWS_FLAG_W	
cfc11	cfc11f	CFC-11	CFC-11_FLAG_W	$\text{pmol kg}^{-1}$
cfc12	cfc12f	CFC-12	CFC-12_FLAG_W	$\text{pmol kg}^{-1}$
cfc113	cfc113f	CFC113	CFC113_FLAG_W	$\text{pmol kg}^{-1}$
CCl4	CCl4f	CCl4	CCl4_FLAG_W	$\text{pmol kg}^{-1}$
SF6	SF6f	SF6	SF6_FLAG_W	$\text{fmol kg}^{-1}$
c14	c14f	DEL14	DEL14_FLAG_W	‰
c13	c13f	DEL13	DEL13_FLAG_W	‰
h3	h3f	TRITUM	TRITUM_FLAG_W	TU
he3	he3f	DELHE3	DELHE3_FLAG_W	%
he	hef	HELIUM	HELIUM_FLAG_W	$\text{nmol kg}^{-1}$
c14e		C14ERR		‰
h3e		TRITER		TU
he3e		DELHER		%
hee		HELIER		$\text{nmol kg}^{-1}$

**Table 4.2b.** Calculated values included in the data products. These parameters are not listed in standard exchange format files.

Data Product Pa- parameter name	Flag Name	Full name of parameter	Units
pf11		CFC-11 Partial Pressure	ppt (parts per trillion)
pf12		CFC-12 Partial Pressure	ppt
pf113		CFC-113 Partial Pressure	ppt
pCCl4		CCl <sub>4</sub> Partial Pressure	ppt
pSF6		SF <sub>6</sub> Partial Pressure	ppt
aou	aouf	Apparent Oxygen Utilization	μmol kg <sup>-1</sup>
theta		Potential Temperature	°C
sigma0		Potential Density relative to 0 dbar	kg m <sup>-3</sup>
sigma1		Potential Density relative to 1000 dbar	kg m <sup>-3</sup>
sigma2		Potential Density relative to 2000 dbar	kg m <sup>-3</sup>
sigma3		Potential Density relative to 3000 dbar	kg m <sup>-3</sup>
sigma4		Potential Density relative to 4000 dbar	kg m <sup>-3</sup>

The cruises included in the CARINA data products generally exclude those that were included in GLODAP. This was done primarily to facilitate later merging of these two data products. There are, however, 3 exceptions: 06MT19941012, 06MT19941115 and 74DI19970807 (Cruise Numbers 12, 13 and 171 respectively). These cruises were added to CARINA because additional parameters critical to the CARINA goals became available after GLODAP was published. The CARINA QC2, however, made full use of many of the GLODAP cruises and details are given in many of the accompanying publications in this issue.

#### 4.4.3.1. Concatenation and adjustment

Program makeocean is the main routine for building merged calibrated data products. Input includes: (1) a list of cruise names, (2) a list of parameters to be included in the data product, (3) a list of parameters that were considered for adjustment and (4) the name of the table that contains all of the various parameter adjustment factors. In sequence, each cruise file is first read and then reduced to the list of measured parameters that are included in the output product. Any parameter (and accompanying flag) that is in the include list, but not in the cruise data set is generated and filled with null values (NA; -999 on output). The parameter columns are then sorted into the same order as the input parameter list. Finally, any necessary adjustments (multiplicative or additive) are taken from the adjustment table and applied. The result is two files: one with station information and a second with data.

The two files are checked for missing value numbers (-9, -999, etc.) that may have resulted from other software and these are replaced with NA. Care is required with the station file since -9 is a possible real value for latitude and longitude, consequently, a very few latitude and longitude values that were exactly -9 were changed to -9.00001. This change is scientifically inconsequential.

Finally, the compiled data were subjected to a very coarse primary QC to eliminate any highly anomalous data points that had not previously been discovered. This check was made by plotting all values of each parameter against pressure. For most parameters a few



points were noted. These few anomalous points were removed from the data product. With this procedure, it is far more likely that questionable values were retained than good data eliminated, but the latter is still possible.

#### 4.4.3.2. Flag simplification

Program `flagmod` simplifies the full set of WOCE quality control flag values (Table 4.3) to a minimum subset. The rationale is to make the data products easily usable to the widest audience without losing information that is critical to a large merged data set. The following transformations to the flags (and values) in the merged data file were made:

- flag 0, 2, 9: no change to data or flag
- flag 3, 4, 5 (questionable, bad, not reported): data reset to NA; flags reset to 9
- flag 6: data unchanged; flags reset to 2
- to correct flag errors which occurred at any step, the data are searched for NA and the flag associated with NA is set to 9.

The final result should thus be a file that only has flag values 0, 2, or 9. This procedure is not perfect. It is impossible to predict all the possible typographical errors in files of this size. While it is trivially easy to identify the unique flag values in the combined data set it can be extremely tedious to identify the exact location of the error and know the appropriate correction.

#### 4.4.3.3. Salinity and miscellaneous corrections

For CARINA we decided that a sample must have pressure and temperature to have any value. Basically, we assumed that if either of these values was missing then something had gone critically wrong with that sample. Consequently, if either temperature or pressure was missing, then all data for that sample bottle was set to NA and the flags to 9. Fortunately, there were very few instances.

Salinity data is also critical, however, the circumstances are different. For CARINA we chose bottle salinity in preference to CTD derived salinity. Some original data files contained bottle measurements only, others contained CTD salinity values only, others contained both, and many files had salinity values with the source not identified. When the source was not identified, we assumed that the values were bottle salinity.

Up to this point the two types of salinity data were both retained and stored separately. Here we made two assumptions: first that any CTD salinity was better than nothing and that any existing salinity was

**Table 4.3.** Summary of data quality flags used for CARINA cruise files. For the data products the flag list was reduced to 0, 2 and 9 (see text).

Flag value	Interpretation in CARINA
0	Approximated
1	Not used
2	Good
3	Questionable
4	Clearly bad result
5	Value not reported
6	Average of replicate
7	Not used
8	Not used
9	Not measured



better than what could be interpolated. Both assumptions should usually be true even with uncorrected CTD salinity. Consequently, wherever bottle salinity was missing and a CTD salinity value existed, the CTD salinity (and flag) was copied into the bottle salinity data slot. The rationale for this procedure was to make the data easier to use without incurring errors that would be significant for most applications. This procedure probably added noise to the salinity data, but one might expect the noise to be pseudo-random for the entire data set.

#### 4.4.3.4. Interpolation

Many of the procedures used to interpret biogeochemical data involve various property-property plots or linear least squares fitting procedures. Since the highest priority application for the CARINA data set was oceanic carbon chemistry, we did not want to exclude relatively expensive carbon measurements from such analyses only because the sample was not analyzed for salinity, oxygen or one of the nutrients. Consequently, we made the same decision as was made during the GLODAP effort (Key et al., 2004) and interpolated missing values for salinity, oxygen, nitrate, phosphate and/or silicate where it was reasonable to do so. The GLODAP algorithm was used. That is, a quasi-Hermetian piecewise polynomial was fit to existing data and that fit used to approximate missing values. The distance over which interpolation was allowed varied with pressure in the water column and by region. The zones and limits were determined by experiment and consensus between Princeton and the four area team leaders. Table 4.4 summarizes the pressure zones and the maximum allowable data separation for each zone. Extrapolation was not allowed. These interpolated values were assigned a zero flag value.

While this procedure has proven to be very reliable, it is not perfect. Unusual sample distributions combined with the nature of the fitting function can generate anomalous values. In particular for the CARINA cruises it was not uncommon to have multiple samples at very similar pressures for a given station. This situation was virtually never encountered with GLODAP sampling. The Hermite fitting function is not prone to “ring”, however, when adjacent samples are extremely close together the function can give spurious results. Consequently, the interpolated values generated with the Hermitian scheme were compared to values derived by simple linear interpolation. In cases where the Hermitian approximation differed from the linear

**Table 4.4.** Interpolation zones and limits (all values in meters). Zones and limits were determined by experimentation. For each interpolated value the adjacent measured values (above and below) can be separated by no more than the corresponding limit for the interpolated value to be deemed acceptable.

Arctic Ocean		Atlantic Ocean		Southern Ocean	
<i>depth range</i>	<i>limit</i>	<i>depth range</i>	<i>limit</i>	<i>depth range</i>	<i>limit</i>
0-100	25	0-100	25	0-100	25
101-300	75	101-300	75	101-300	75
301-750	150	301-750	205	301-750	150
751-2000	250	751-1500	405	751-2000	505
2001-bottom	500	1501-2500	605	2001-bottom	500
		2501-bottom	1005		

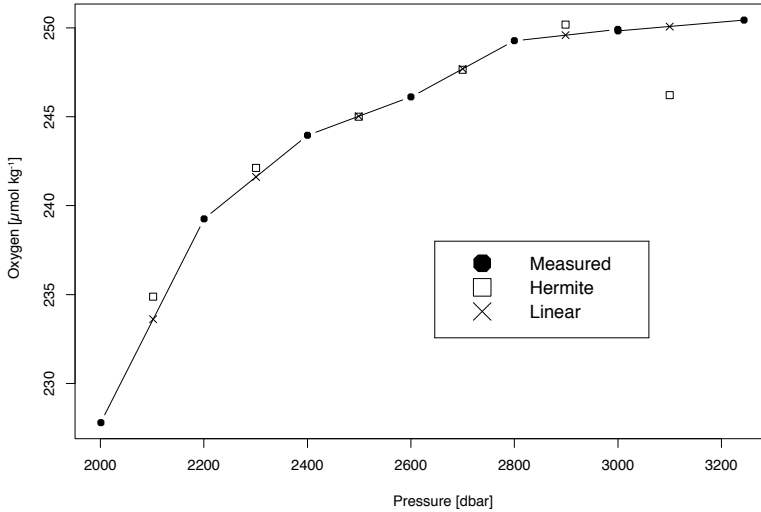


**Figure 4.3.** Illustration of interpolation. The black dots are measured data. The boxes and x's are interpolated values at the indicated pressures using the Hermite and linear fitting functions, respectively. Note that there are two measurements near 3000 dbar and that these measured values are very nearly identical. The close proximity (in pressure) of these two measurements causes the Hermite fitting function to “ring” thus producing the errant interpolated value near 3100 dbar. In cases such as this, when the two fitting functions produce results that differ by more than 1%, the linear interpolation is used. For all the other cases shown the difference is less than 1% and the approximation from the Hermite function is used. All of the interpolated points shown in this example pass the “maximum measured data separation distance” test described in the text and in Table 4.4.

approximation by more than 1%, the linear value was chosen. An example of this is shown in Fig. 4.3. Even these precautions will not cover all questionable interpolations, therefore, after the interpolation step was completed, the combined (measured + interpolated) parameters were checked and the obvious fliers eliminated from the data set. This check was very crude with the result that the final data set undoubtedly contains a few anomalous interpolated values.

As an experiment, the data shown in Fig. 4.3 were also fitted with spline, spline under tension, “csakm” (from the IMSL FORTRAN library; Virtual Numerics, Inc.), and “loess” (from the S-Plus library; see Cleveland and Devlin, 1988) functions. The first 3 showed “ringing” equal to or worse than the Hermite function. The “loess” fit does not ring, but is overly smoothed. For this example an obvious “fix” would be to average the two data points that are so close to each other (near 3000 dbar) and use the average as input to the fitting routine. Such an averaging scheme for data that are nearly co-located would be a good modification to the interpolation software. The problem is that one has to define “close” and that definition will certainly vary with pressure and geographic location. If one only had 10 or 100 interpolations then the interpolation procedure could be visually monitored, however, with more than 84 000 possible interpolations that was not practical. Therefore, the required software development and testing has been left as a future exercise.

We are aware that myriad other interpolation algorithms exist. Only those mentioned were tested and we do not imply that the method used is the “best” (however one might choose

to define best). We do feel that the interpolation is worthwhile and that the method used is both reasonable and adequate. In the end, the limits over which interpolation is allowed tend to be more important than the fitting algorithm.

#### 4.4.3.5. Basic calculations

The existing data were used to calculate values for potential temperature, potential density relative to 0, 1000, 2000, 3000 and 4000 dbar, and apparent oxygen utilization (AOU) using the same algorithms used for GLODAP. Additionally, sample depth was approximated for all samples using a simple function based on pressure and latitude (in cases where only depth was available, pressure was approximated using a similar function). These parameters were added to each data file.

#### 4.4.3.6. Carbon calculations

All of the various carbon calculations in CARINA used the MATLAB translation (van Heuven et al., 2009; <http://cdiac.esd.ornl.gov/oceans/co2rprt.html>) of the code originally developed by Lewis and Wallace (1998). CARINA used the same constants used for GLODAP (most importantly, the Dickson and Millero (1987) refit of Mehrbach et al. (1973)). This decision is supported by significant literature (e.g. Lee et al., 1996; Wanninkhof et al., 1998; McElligot et al., 1998; Millero et al., 2002; Mojica Prieto and Millero, 2002). Others have suggested different constants and given new fits to old data, but these studies were either vetted on a regional scale rather than globally or offered only very minimal improvement. The CARINA team carbon experts decided that the potential for minor improvement was less important than being consistent with values calculated during GLODAP since data from the two collections will undoubtedly be used together.

#### 4.4.3.7. Partial pressure

The partial pressures of CFC-11, CFC-12, CFC-113, CCl<sub>4</sub> and SF<sub>6</sub> were calculated based on the solubility equations given by Warner et al. (1995), Bu and Warner (1995), Bullister and Wisegarver (1998) and Bullister et al. (2002). The partial pressure values and fractional equilibrium relative to the atmosphere at sampling time were extremely useful in the QC2 procedures for these parameters (Steinfeldt et al., 2010). Note that the GLODAP data products included “simple” CFC ages rather than partial pressures.

#### 4.4.3.8. Data product parameter accuracy

Stated simply, it is impossible to determine the general accuracy of the various parameters included in the CARINA data products. Precision estimates could be calculated for various subsets of the data, however those results would have limited, if any, value. In lieu of such numbers, we investigated the “internal consistency” of the data products. Details of these estimates are given in Tanhua et al., 2010b (Chapter 5 of this thesis; table 5.3). This exercise clearly demonstrated that the internal consistency of the data product was significantly better than for the original data. Excluding oxygen and nutrient data (since there are no “standards”) the consistency values could loosely be interpreted as an upper limit of accuracy. This approximation

is an upper limit since some of the variance included in the internal consistency calculation is due to real change. Conversely, if the QC2 procedure removed real change signals rather than measurement bias, then the internal consistency calculation would imply that the data in the products are “better” than they really are.

### 4.5. Lessons learned

Two things are clear. The CARINA project both benefited from and improved upon GLODAP techniques. The most significant improvements include development of software to automate much of the QC2 work and consequently being able to carry out QC2 on a larger subset of the total parameter set. This software also allowed the CARINA team to derive either additive or multiplicative adjustment factors for the various parameters. Experience has shown that multiplicative adjustments are superior to additive adjustments for oxygen and nutrients in particular (the additive nutrient adjustments used in GLODAP occasionally generated negative near surface concentrations!). As with GLODAP, CARINA QC2 demonstrated that different analytical techniques can yield different results with respect to data adjustments. We believe that retaining human control is preferable to fully automated analysis for data such as these.

Certainly the most glaring shortcoming for many of the cruise data sets was that complete records were not retained with the data. Prior to the WOCE program in the 1990s final cruise reports were not produced for many cruises. This was particularly prevalent when the cruise was manned by a single group from one institution. This situation was exacerbated by the fact that the data from most of the CARINA cruises were held exclusively in the collection of individual scientists. By the time the data were released for inclusion in this data product many of the people who had made the measurements were no longer working in the field. Fortunately, these practices are slowly ending. The CarboOcean program requires that all funded projects report data within 2 years after the cruise. For CLIVAR, shipboard measurements are made public immediately and final data are required within 6 months after the cruise (except for shore based measurements). This paradigm shift from “proprietary forever” to rapid public availability carries the risk that another scientist will publish data before the PI responsible for the data has a chance. This occurrence is, however, extremely rare. Rapid public scrutiny of data more commonly results in elimination of data errors and new collaborative research opportunities. Timely data reporting ensures that sufficient metadata can still be obtained if it is not originally provided.

The development of CRM for the calibration of  $A_T$  and  $C_T$  was noted as one of the most important developments with carbon system measurements for GLODAP (Key et al., 2004). The same is true for CARINA. CRM are readily available and reasonably priced. Production of a high quality  $A_T$  and/or  $C_T$  data set requires frequent CRM analysis.

Measurements of pH were rarely made during the WOCE program and the few measurements that were made were not included in GLODAP. Rather in GLODAP, pH and  $C_T$  were used to calculate  $A_T$ . With the CARINA collection pH was frequently measured. Additionally, since GLODAP was completed the issue of ocean acidification has attracted significant attention. Finally, the spectrophotometric measurement technique has become common and is far superior to electrode based measurements. One result of this history is that reporting requirements for pH data were not previously standardized. When CARINA began, the

most accepted scale for oceanographic measurements was the seawater scale. During this project, however, agreement was finally reached that pH data should be reported on the total hydrogen ion scale at some specified temperature (generally 25 °C). By the time this decision was made, it was too late to change all of the CARINA data sets. Consequently, all CARINA pH values (both in the cruise files and in the data products) are reported on the seawater scale at 25 °C.

For GLODAP, Key et al. (2004) noted that the need for nutrient standards similar to the carbon CRMs. Progress has been made (Aoyama et al., 2008; Aminot and Kirkwood, 1995), but so far, the use of nutrient “CRMs” has not been generally adopted. Analysis of the CARINA data make it abundantly clear that this practice must stop. The community must adopt a set of CRMs and those “standards” should be used on every cruise. This change in methodology is absolutely critical if we are ever to understand subtle changes in nutrient distributions and stoichiometric ratios in a changing ocean environment.

The development of a dedicated web site for the CARINA work was extremely helpful. This site allowed team members to easily share data and ideas and provided a location to store all of the QC output and final adjustment tables. Now that the project is finished all of the CARINA website materials are being transferred to CDIAC for archive and public access.

#### 4.6. Conclusions

The CARINA data products represent the work of hundreds of scientists. The project has now extended for a decade with the final effort requiring half that time. The original goal, to assemble a collection of European data that would be useful to study the inorganic carbon system in the North Atlantic Ocean, was significantly expanded and, we believe, successfully completed. Not only were the data assembled, but the most critical parameters were subjected to very careful analysis to remove various data biases. An independent analysis of the CARINA data prod-

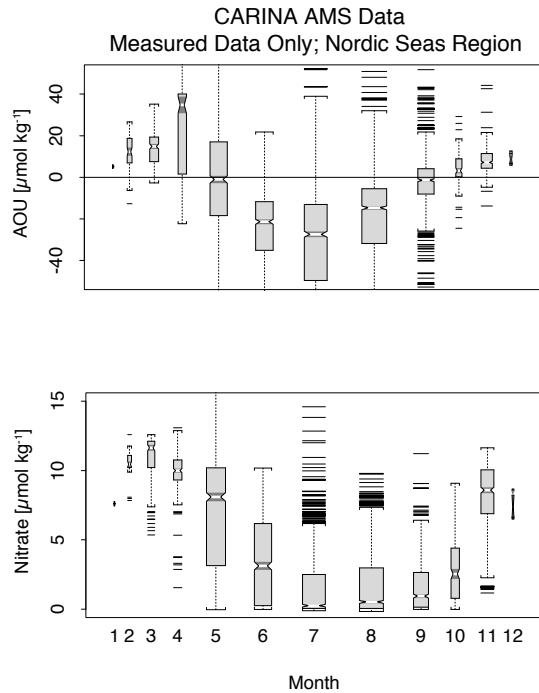


**Figure 4.4.** These two boxplots were generated using measured values from the AMS data product. The data selected are from the upper 25 m of the Nordic Seas region. The box widths are proportional to the number of data included. Even though a substantial fraction of the data were adjusted as part of the QC2 work, the seasonal cycle in these two parameters is retained. The near surface  $C_T$  data from this region have the same trend. Similar analyses with other parameters and other regions demonstrate that the QC2 procedure has not “erased” strong temporal signals. Investigation of more subtle signals such as the expected temporal increase in near surface  $C_T$  due to anthropogenic  $CO_2$  will require more careful analysis.

uct would undoubtedly show that overall the data quality of CARINA is not as high as GLODAP. This was expected. The CARINA cruises cover a longer time interval and more importantly the cruises were primarily carried out by individual scientists operating in small groups rather than being the result of a globally organized survey effort. Regardless, the secondary quality control activities have resulted in a data product that is sufficiently accurate for modern analyses including climate change issues. Equally important is the fact that CARINA both supplements and extends the global coverage provided by GLODAP. Chemical oceanographers now have a very nice

data set covering the northern North Atlantic and Nordic Seas, the beginning of coverage for the Arctic Ocean, and significantly more data for the Southern Ocean. Additionally, while the CARINA calibration techniques differed somewhat from those of GLODAP, the two data sets are thought to be compatible without alteration for large scale investigations.

The CARINA QC and adjustment procedures risk removing real signals from the original data. Without a much larger and higher initial quality data set such removal would be impossible to detect. As others use these data for independent research projects additional information will be gained. However, temporal signals still exist in the data products. As an example Fig. 4.4 shows boxplots of near-surface (0–25 dbar) nitrate and AOU (apparent oxygen utilization) data from the Nordic Seas region taken from the AMS data product. The data were taken after all adjustments had been applied. No interpolated values were included in this analysis. AOU was used rather than oxygen to remove the temperature dependence of oxygen solubility. It is abundantly clear that the seasonal cycle has not been removed from these data. A similar seasonal cycle exists for the near surface  $C_T$  data from this region, however, without removing the seasonal cycle, the expected anthropogenic increase is not readily apparent for these surface waters (it is visible in deep water). Detailed analyses are required to identify subtle signals. Such studies are planned, but not discussed here.

The seasonal signal demonstrated in Fig. 4.4 is so strong that it is not the most convincing demonstration that QC2 did not remove real signals from the data products. Fig. 4.5 illustrates a much sterner test. Here, deep water  $C_T$  data from the same region as Fig. 4.4 are summarized by measurement year. A significant fraction of the data variability for each year is due to spatial variability. Even though this test is crude, the increasing concentration trend

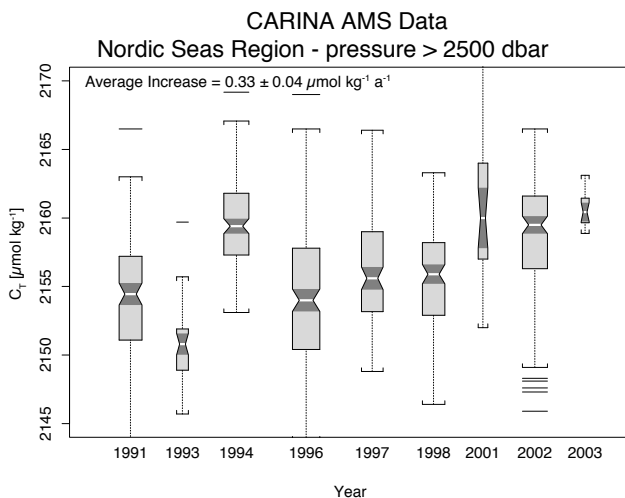


**Figure 4.5.** This boxplot shows deep water  $C_T$  measurements from the same region as Fig. 4.4. A significant fraction of the spread indicated by each box is due to spatial variability. In spite of the crude nature of this summary, the average concentration increase over time is statistically significant at a very high confidence level. The increase rate derived here is only about half that found for the Irminger Basin alone. For this discussion the important point is that the secondary QC adjustments have not erased subtle large scale temporal signals.

with time is clearly evident and statistically significant at a very high confidence level. The  $C_T$  increase rate derived from these combined data ( $0.33 \mu\text{mol kg}^{-1} \text{a}^{-1}$ ) is less than that derived from the near bottom data in the Irminger Sea time series ( $0.8 \mu\text{mol kg}^{-1} \text{a}^{-1}$ ; cruise #185). Again, detailed investigation will be required to determine if the difference in increase rate is real or due to the averaging incurred in the trend shown in Fig. 4.5.

The next planned step is to merge CARINA with GLODAP. Tests show the two data products to be consistently calibrated. The merge is, however, non-trivial because of differences in the parameters included and various detail differences such as sample indexing.





# Chapter 5

## Quality control procedures and methods of the CARINA database

Slightly adapted from the publication  
*Tanhua, T., S. van Heuven, R.M. Key, A. Velo, A. Olsen and  
C. Schirnick (2010). Quality control procedures and methods of  
the CARINA database. Earth System Science Data, 2, 35–49.*



## Abstract

Data on the carbon and carbon relevant hydrographic and hydrochemical parameters from previously not publicly available cruises in the Arctic, Atlantic and Southern Ocean have been retrieved and merged to a new data base: CARINA (CARbon IN the Atlantic). These data have gone through rigorous quality control (QC) procedures to assure the highest possible quality and consistency. All CARINA data were subject to primary QC; a process in which data are studied in order to identify outliers and obvious errors. Additionally, secondary QC was performed for several of the measured parameters in the CARINA data base. Secondary QC is a process in which the data are objectively studied in order to quantify systematic differences in the reported values. This process involved crossover analysis, and as a second step the offsets derived from the crossover analysis were used to calculate corrections of the parameters measured on individual cruises using least square models. Significant biases found in the data have been corrected in the data products, i.e. three merged data files containing measured, calculated and interpolated data for each of the three regions (i.e. Arctic Mediterranean Seas, Atlantic Ocean, and Southern Ocean). Here we report on the technical details of the quality control and on tools that have been developed and used during the project, including procedures for crossover analysis and least square models. Furthermore, an interactive website for uploading of results, plots, comments etc. was developed and was of critical importance for the success of the project, this is also described here.

### 5.1. Introduction

CARINA is a database of carbon and carbon-relevant data from hydrographic cruises in the Arctic Mediterranean Seas, Atlantic, and Southern Ocean. The project started as an essentially informal, unfunded project in Delmenhorst, Germany, in 1999 during the workshop on “CO<sub>2</sub> in the North Atlantic”, with the main goal to create a uniformly formatted database of carbon relevant variables in the ocean to be used for accurate assessments of oceanic carbon inventories and uptake rates. The collection of data and the quality control of the data have been a main focus of the CARINA project. Both primary and secondary QC of the data has been performed (“QC1” and “QC2”, respectively). Experience with the previous GLODAP synthesis project (Key et al., 2004) demonstrated that a consistent data product can be produced containing data from many different cruises by many different laboratories in different regions. But it is essential that the results obtained by the different methods of quality control are compared and systematically assessed. This assessment is required largely due to the fact that standards do not exist for many oceanographic measurements. Since CARINA included a large number of scientists from all over the world, communication of individual efforts and results were important. For this purpose, the individual data analysts and the working groups used an internet based platform for posting their results, including uploading/downloading and viewing of figures, data and comments. In this way, the data analysts were sharing experience and results in real time. In addition to the interaction over the web portal and email communication, 3 workshops were held where practical matters and the

adjustments of data were discussed, and finalized. This report provides an overview of the methods and techniques used for the quality control of the database.

## 5.2. Data provenance

The CARINA database includes data and metadata from 188 oceanographic cruises or projects, i.e. entries to the cruise summary table ([http://cdiac.esd.ornl.gov/oceans/CARINA/Carina\\_table.html](http://cdiac.esd.ornl.gov/oceans/CARINA/Carina_table.html)). A few of the cruises listed in the table are collections of several cruises or time series stations. In addition, 52 reference cruises are included in the secondary QC to ensure consistency with historical data (i.e., WOCE/GLODAP). These reference cruises are not included in the CARINA data base, but on several occasions are suggestions for adjustments made that are different from those applied to the GLODAP data base. Due to the volume of the data set, the CARINA data are divided in three regions: Arctic Mediterranean Seas (AMS); Atlantic Ocean (ATL), and Southern Ocean (SO), each of them with a working group that carried out the secondary QC. A few of the CARINA cruises are common to the ATL and SO groups, and a few cruises are common to the ATL and AMS groups. In these cases there has been agreement between the groups on all adjustments. This provides a consistency control in the secondary QC between the CARINA working groups.

The CARINA database consists of two parts: the first part is the individual cruise files where all the data reported by the measurement teams are stored. Quality flags are accompanying the data. In many cases the flags are those originally reported, in others cases the flags were assigned by R. Key. These files are in WHP (WOCE Hydrographic Program) exchange format (<http://whpo.ucsd.edu/format.html>). The first lines of each file are the condensed metadata. There are no calculated or interpolated values in the individual cruise files, except for pressure calculated from depth. No adjustments have been applied to any of these values with the exception that all pH measurements were converted to the seawater pH scale at 25 °C. Recently, the international ocean carbon measurement community decided that new pH measurements would be reported on the total hydrogen scale, but that decision occurred too late to be incorporated into this project.

The second part of CARINA consists of three merged data files; one each for the Atlantic Ocean, Arctic Mediterranean Seas and Southern Ocean regions. These files contain all the CARINA data judged to be “good”, and also include: (i) interpolated values for nutrients, oxygen and salinity if those data were missing and the interpolation could be made according to certain criteria, as described in Key et al. (2009; Chapter 4 of this thesis); and (ii) calculated carbon parameters; e.g. if  $C_T$  (total dissolved inorganic carbon, DIC, or  $TCO_2$ ) and  $A_T$  (total alkalinity, TA, ALK, TALK or alk) were measured, pH was calculated, (iii) instances where bottle salinity was missing or bad were replaced with CTD salinity, if possible. Values for any of these cases have been given the quality flag “0”. In many cases there are additional parameters in the individual cruise files which have not been included in the secondary QC, such as  $\Delta^{14}C$ ,  $\delta^{13}C$  and  $SF_6$ . Some of these are included in the merged data files as well.

A significant and time consuming part of the CARINA synthesis was the data collection, merging of subsets of data from individual cruises and conversion of units to a common format/standard, see Key et al. (2009; chapter 4 of this thesis). The next step in the synthesis was the quality control (QC). Our quality control procedures are comprised of two distinct

steps. First the reported measurements are studied in order to identify outliers and obvious errors, i.e. primary QC. Secondly, we quantify systematic differences in the reported values in a process called secondary QC. Essentially, primary QC is a check of precision and secondary QC is a check of accuracy. These QC processes were performed on the data sets reported by the measurements teams, and are distinct from the quality assurance (QA) procedures originally performed by each cruise measurement team in order to ensure sufficient quality, which is part of the data collection and analysis procedures. A flowchart of the procedures involved in the process of producing the CARINA data product is presented in Fig. 5.1.

### 5.3. Primary quality control (QC1)

Primary QC (or simply “QC1”) is a process in which data are studied in order to identify outliers and obvious errors. While the methods used to identify questionable or bad data are objective, the actual flag assignment is subjective and is also highly dependent on the overall measurement precision of each parameter for each cruise. These outliers are either flagged, or the data were revised via direct contact with the data generators, for instance calibration of  $A_T$  values with respect to CRM that had been analyzed but not certified for  $A_T$  by the time the cruise was carried out. During the WOCE program a system was developed to indicate the quality of each measured datum in a cruise data set. The system amounts to flagging each

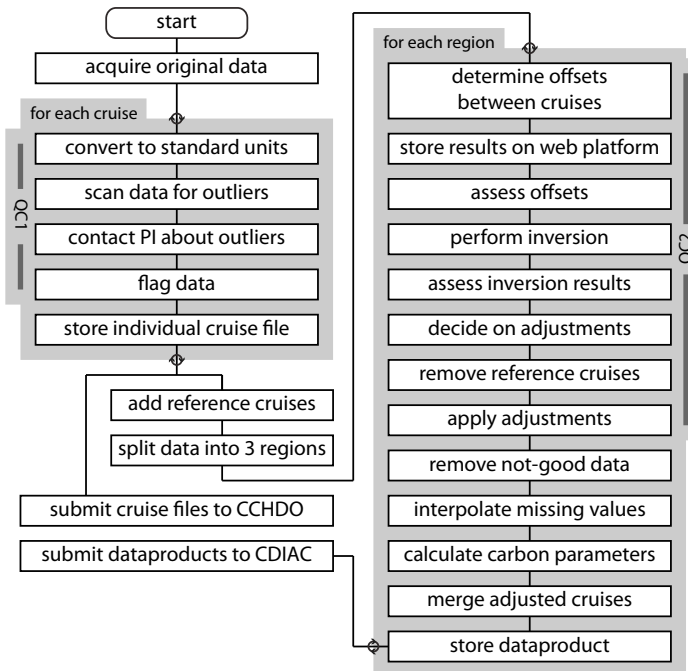


**Figure 5.1.** Flowchart describing the principal steps during the secondary quality control; see text for details.

datum with an integer. Nine different flag values were defined (0–9, see Table 5.1 for definitions). This system, which has been continued in subsequent major ocean sampling programs and was used for the GLODAP data synthesis, was adopted for CARINA. It is important to note that data flagging or QC1 deals only with data precision. The techniques used to assign these flags are usually insensitive to data bias particularly in cases where all of the measurements of any parameter for a cruise are biased relative to results from other cruises.

A large number of the CARINA cruises predate the custom of data flagging. Consequently, as the raw data files were accumulated, flags were initialized with flag value 2 (good) for each measured variable (except temperature) or 9 (not measured) when there was no measured value. Subsequently, the various measured parameters were analyzed with the same software and techniques used for modern cruises. Essentially, various property-property plots are examined for small groupings of stations looking for outliers. Notes were kept for each outlier in each plot. Measurements that were outliers, generally in more than one type plot, were flagged questionable (3) or bad (4) with the difference between these two flags being one of degree. Whenever possible, the data values flagged 3/4 were reported back to the person originally responsible for the measurements for confirmation. In cases of disagreement, the choice of the data generator was used. In general whenever a datum was borderline between good and questionable, the good flag was retained. Additionally, during the flagging significantly more variability was allowed for points that were in the upper thermocline or nearbottom. Near-surface values were virtually never flagged 3/4 with the only exception being totally unrealistic values and/or obvious clerical errors.

This method of data flagging is quite subjective regardless of who assigns the flags. With very few exceptions all of the CARINA cruises were flagged at Princeton (R. Key). This does not mean that the flags were assigned correctly, but does ensure that the assignment was done as consistently as possible and additionally that the flags were consistent with those assigned to the carbon parameters during preparation of GLODAP (Key et al., 2004). The only flags not assigned at Princeton were associated either with very recent cruises (generally WOCE or CLIVAR) or with data streams from labs which had participated in WOCE and assigned flags to their own data routinely (mostly CFC data from M. Rhein and/or R. Steinfeldt). Whenever data were submitted with flags, the flag values were simply checked for obvious/clerical errors. The CARINA data product incorporates one additional flag with value zero (0). This flag was also used in GLODAP. The zero flag indicates a datum that “could have been measured”, but was approximated in some manner. There are three different uses for the zero flag in the data products: 1) Instances where bottle salinity was missing or bad and consequently replaced with CTD salinity, 2) interpolated values for salinity, oxygen or nutrients, or 3) for calculated carbon parameters.

**Table 5.1.** Table listing the flags used for the CARINA data set. Only flags 0, 2 and 9 are used for the data product. Flag 0 (“approximated”) refers to interpolated values for nutrients, oxygen and salinity, and to calculated carbon parameters.

Flag value	Interpretation in CARINA
0	Approximated
1	Not used
2	Good
3	Questionable
4	Clearly bad result
5	Value not reported
6	Average of replicate
7	Not used
8	Not used
9	Not measured

The secondary quality control procedures used here (discussed below) critically examine the data using techniques quite different from the routine QC1 methods. In some cases additional data points are identified that are apparently spurious. In these cases the unusual data were reported back to Princeton to have the initial flag values reconsidered. Once all of the flag values are final, each cruise file was submitted to national data centers (CCHDO and CDIAC).

#### 5.4. Secondary quality control (QC2)

Secondary quality control (or simply “QC2”) is a process in which the data are objectively studied in order to quantify systematic biases in the reported values. The identified data biases are then subjectively compared to predetermined accuracy limits. Special consideration is given to the fact that some of the regions studied are known to have had real temporal change over the time period covered by the various cruises (1977–2007). Obviously, one does not want QC2 to “erase” real temporal change. The nature of the QC2 procedure is such that various data recording errors/outliers are also identified in the process, thus complementing the initial QC1. Data from cruises that show significant bias are given an adjustment (either multiplicative or additive), that is applied to the data product (i.e. the merged data files for the three regions), but not to the individual cruise files (those remain as reported with measured data). Data with lower than acceptable quality are also identified; questionable data are removed from the data product, but retained in the individual cruise files with appropriate flags. The parameters considered in QC2 are salinity (and in a few cases CTD salinity), oxygen, nitrate, phosphate, silicate, total alkalinity ( $A_T$ ), total dissolved inorganic carbon ( $C_T$ ), pH, CFC-11, CFC-12, CFC-113 and  $CCl_4$ .

The most important tool in the secondary quality control of the CARINA data was the crossover analysis. Other approaches that were used include multiple linear regression (MLR) analysis and relation between measured parameters, such as CFC-11 vs. CFC-12. This report focuses on the crossover analysis and the least square models (inversions) that followed to determine the corrections/correction factors needed to minimize the offsets between cruises.

##### 5.4.1. Crossover analysis

Crossover analysis is an objective comparison of deep water data from one cruise with data from other cruises in the same area. Crossover analysis has been performed earlier on, for instance, the WOCE and JGOFS data set (e.g. Sabine et al., 1999; Gouretski and Jancke, 2001; Johnson et al., 2001; Sabine et al., 2005), see also <http://cdiac.esd.ornl.gov/oceans/glodap/crossover.html>, where the concept was laid out. These results have increased the internal consistency of, for instance, the GLODAP data set. In CARINA we have used the basic concept of crossover analysis.

The result of a crossover analysis is an offset. Offsets are defined as the difference between two cruises, A and B, derived from a crossover analysis. If the offset for cruise A (relative to cruise B) is less than zero (or unity, for multiplicative parameters), then cruise A data would have to be increased in order to be consistent with cruise B (or vice versa). The offset were quantified as multiplicative factors for nutrients, oxygen and CFCs, and as additive constants for salinity,  $C_T$  and  $A_T$ . There are several reasons for this division between additive

and multiplicative offsets. Firstly, multiplicative offsets eliminate the problem of potentially negative values for any variable with measured concentration close to zero, i.e. in the surface water for nutrients, or oxygen concentrations in low oxygen areas. Also, for nutrients and oxygen analysis, problems in standardization are the most likely source of error, hence a multiplicative offset is deemed as appropriate. For  $C_T$ ,  $A_T$  and salinity an additive adjustment seemed most likely, due to, for instance, biases in the reference material used. Similarly, since pH is a logarithmic unit, only additive offsets can be considered. In the crossover analysis, clustering or cluster analyses was often performed. This refers to a subroutine in the crossover analysis for cruises that fall in more than one region, or for crossovers that cover such a large and diverse area that the crossover is divided into more “sub-crossovers”, i.e. clusters. When we discuss crossover analysis in the following, clustering is included, i.e. the crossover analysis between two cruises takes the geographic distribution of the cruises into consideration, either manually or automatically. The station distribution in CARINA was such that the definition of “same area” was variable and defined subjectively on a case by case basis, but the compared stations were normally within 2 degrees of latitude, i.e. ~222 km. Mostly, the two cruise tracks are crossing each other; hence the name “crossover analysis”, but it can also be repeat or parallel cruise tracks, which is often the case for the CARINA data. We identified and analyzed more than 2100 individual crossovers for the CARINA data set.

Since the upper water column is more sensitive to variability on various time-scales than the deep ocean, only the deep part of the water column was considered for the analysis. For the ATL and SO regions, this minimum depth (i.e. pressure) was 1500 dbar. However, due to the deep mixed layers sometimes found in the AMS region, the minimum depth was set to 1900 dbar for the Nordic Seas region as this is deeper than the ventilation depths observed over the time span covered by CARINA (Ronski and Budeus, 2005). The crossover analysis was performed on either pressure, density (i.e., sigma-4), or potential temperature surfaces. To account for vertical shifts of properties (i.e., internal waves etc.), the crossover analysis are normally done on density surfaces. However, in the Nordic Seas crossover analysis was made on depth surfaces due to the small density gradients there. Arguments for the use of theta over sigma include the superior measurement accuracy of temperature and its independence of other parameters (especially biases in salinity are impossible to clarify in sigma-space, since sigma itself is a function of salinity). One of the collections of software-routines that were developed for the CARINA effort determined offsets in each of the three spaces simultaneously, and its results allow for comparison. The quality of the determinations of offsets, as expressed by the standard deviation, was generally highest using density, followed closely by theta, and with comparisons in depth-space regularly yielding spurious results. In most cases however, there were only small differences in the offsets calculated in the three different ways, which gives us some confidence in the analysis, see below.

As a first step in the crossover analysis, the profiles of the parameter in question for all stations included in a crossover were interpolated with a Piecewise Cubic Hermite Interpolating scheme. An important feature of this algorithm is that interpolated values almost never exceed the range spanned by the data points. That is, the Hermitian function has low tendency to “ring”. Large vertical gaps in the data were not interpolated, the definition of “large” being depth-dependent; larger “gaps” were allowed in the deeper part of the profile. In the case of density, the profiles were interpolated in such a way that the interpolated val-



ues were roughly equally distributed in depth space. Practically this was done by letting a density profile that was typical for the area determine the interpolation distances in density space. This was done in order to have sufficient weight (or “interpolated data points”) in the deep water column where the properties of the water are supposed to change only slowly, and where the density gradients are often small.

Essentially, we distinguish between three routines for the crossover analyses carried out during the CARINA project: the manual crossover routine, and the two automatic routines; *running-cluster* and *cnaX-scripts*, see below. These codes and routines developed during the project, so that manual crossover results obtained in the early part of the project are not necessarily made with the same assumptions as those made in the later part of the project. This applies also for the automated routines, but in this case the full data set was analyzed again when new routines were developed. However, even if the codes are slightly different, the results were mostly very similar, as we will see below.

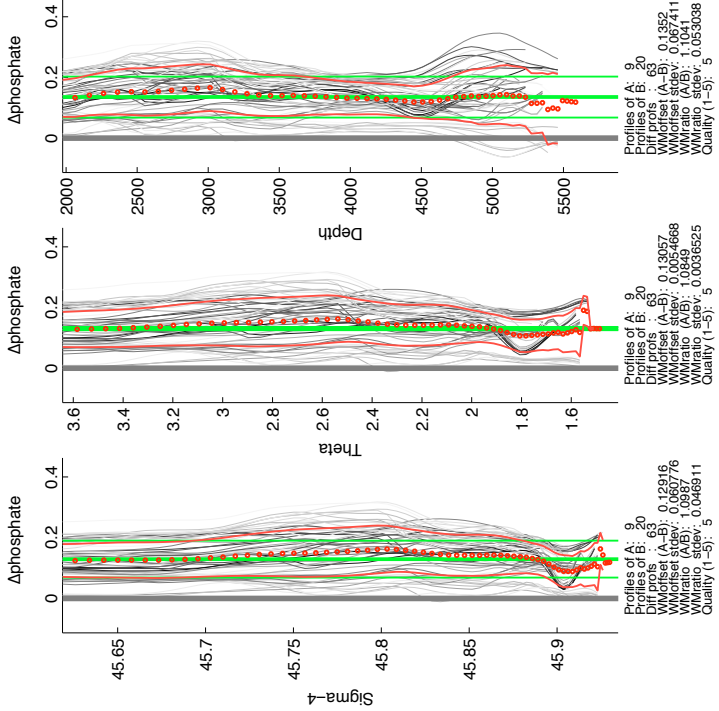
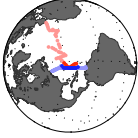
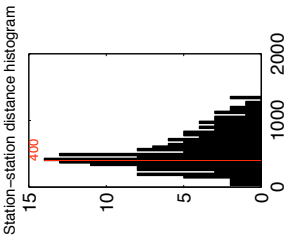
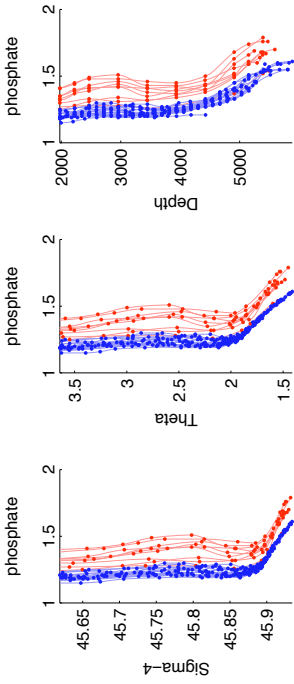
Due to the large number of crossovers in CARINA, the task of manually generating crossovers and entering the results in an online table soon become overwhelming in terms of workload. Even though the process of manually generating the crossovers lead to quality checked results, the process of manually entering the values in a table is prone to typos and errors that might bias the results of the inversions. Even though the automatically generated crossovers were, in general, used for the inversions, the manually generated crossovers were invaluable as reference points in the decision process for suggesting adjustments. The matlab routines used for QC2 of CARINA, as well as all figures generated during QC2 can be viewed and downloaded from [http://cdiac.ornl.gov/oceans/CARINA/Carina\\_inv.html](http://cdiac.ornl.gov/oceans/CARINA/Carina_inv.html).

#### 5.4.1.1. Manually generated crossovers

For the manually performed crossovers, an average profile (and its standard deviation) was calculated using all stations in each cruise that were closer to any station of the other cruise than the minimum horizontal distance. For this averaging process, the interpolated profiles were used. These two average profiles were then compared to each other in a second step, and the weighted offset and standard deviation of the crossover were calculated. The disadvantage of this method is that the crossover can cover large area with potentially very different hydrography, for instance for repeat cruise tracks, and the offset for the crossover might thus be biased. In this case, groups of stations for each cruise within a hydrographical regime were sought, and a crossover was divided into several sub-crossovers, “clusters”. The analyst then had the choice of using the average of all clusters to calculate the crossover offset, or to discard clusters in areas of known high variability, such as just south of the Greenland-Scotland Ridge. The analyst then entered the results from the crossover analysis to the CARINA website, and uploaded the figure for the crossover.

#### 5.4.1.2. The “running cluster”-crossover routine

The crossover version called “*running-cluster*” was mainly used for automatically generated crossovers. In this routine the interpolated profile from each station in cruise A was compared to each interpolated profile from all cruise B stations within the maximum distance for a valid crossover, and a difference profile was calculated for each such pair. This process was repeated



Cruise A (red). Date: Mar 2004. Cruise name: 103-06MT20040311  
 Cruise B (blue). Date: Nov 2003. Cruise name: 121-316N20031023

**Figure 5.2.** An example of a typical crossover made for phosphate in the western North Atlantic made by the running-cluster routine. The deep-ocean measurement data for phosphate of cruise A (red) can be seen to be about 8-10% higher than those of cruise B (blue).

for each station in cruise A which normally results in several, up to hundreds for a repeat section, difference profiles. The crossover offset and its standard deviation was calculated as the weighted mean and standard deviation of the difference profiles of each crossover pair, i.e. the part of the profile with low variability weigh higher in the calculation (often, but not always, the deeper part of the profile). This way of performing the crossover analysis has the advantage that only individual stations within the minimum horizontal distance are compared to each other. Hence, even for repeat cruises covering several different oceanographic regimes, the offset between these cruises can be calculated in a straight forward manner. An example of a crossover is shown in Fig. 5.2.

#### 5.4.1.3. cnaX crossover routine

This routine is essentially a fully automated implementation of the manual approach described above. Please note that, for the sake of readability, these paragraphs deal only with the determination of offsets in depth-space, but the software concurrently calculates offset profiles in density and thetaspace as well. The “cnaX” collection of matlab-routines was developed over several months during the CARINA project and incorporates many of the concepts mentioned above into a fully automatic analysis of the CARINA input dataset. The level of automation is variable and is set pre-run by the user. In its fastest form, user input is restricted to setting thresholds for criteria relating to cruise and sample inclusion and the automatic quality assessment of results. When set up, a full run from raw-data loading to output of a final set of recommendation for cruise parameter adjustments takes about 8 h on a regular computer for the complete CARINA data set. This includes the production of several tens of thousands figures and dozens of tables, useful for tracing the script’s steps to determine problem areas. At the highest level of user interaction, each of the steps concerning clustering and quality assessment require user input; a full run may take up to several days to complete this way. This method generally results in a somewhat reduced amount of uncertainty in the final output since badly determined offsets that may slip through the automatic quality check can be caught by the user manual interaction. A flowchart describing the various steps in the crossover routines is presented in Fig. 5.3 to help guide the reader.

In either form, the routine first loads all individual cruise data. During this step the user is allowed to specify subdivision of certain cruises if sufficient reason exists to assume changes in instrument calibration during, for instance, port calls or instrument changes. Maps showing cruise-track, station locations and bathymetry are created for each cruise for possible user inspection. After this a crude scan is made to check which cruises share a geographical area, and therefore may cross each other. During a subsequent refining step these potential matches are more closely analyzed. Stations are only considered for possible relevance for crossover analysis when certain criteria for parameter availability, minimum sample depth and number of samples are met. This approach saves considerable time over a full station-vs.-station proximity check.

Knowing which cruises can be compared with which other, i.e. cruise-pairs; a clustering method is employed to group stations from cruise A in close proximity to stations of cruise B into distinct geographical clusters. This clustering is either user-controlled, allowing the analyst to specify further clusters, reduced clustering or discard clusters, or fully automatic

mode in which stations are progressively further clustered until the spatial dimensions of each cluster meet pre-set criteria. Limits also apply to the minimum number of stations per cluster that should be retained. The results of the clustering operations are stored in tabular form as well as drawn on maps. After all cruise-pairs have had their “crossover stations” geographically clustered, offsets are determined for each parameter for each cluster. As a first step the profiles are interpolated to about 75 levels in the range between 2000 m to the deepest sample of either of the cruises. Offsets are determined and expressed both as additive offsets and multiplicative offsets taking considerations outlined above into account. These calculations closely follow the procedure outlined by Johnson et al. (2001).

After this “discrete clusters”-method of determining offsets, a “running cluster” approach is taken (as detailed above and comparable to the “running cluster”-routines) for another determination of offsets. For cruise-pairs in which both cruises have several dozens of stations in close proximity to stations of the other cruise (e.g. repeat lines) the running

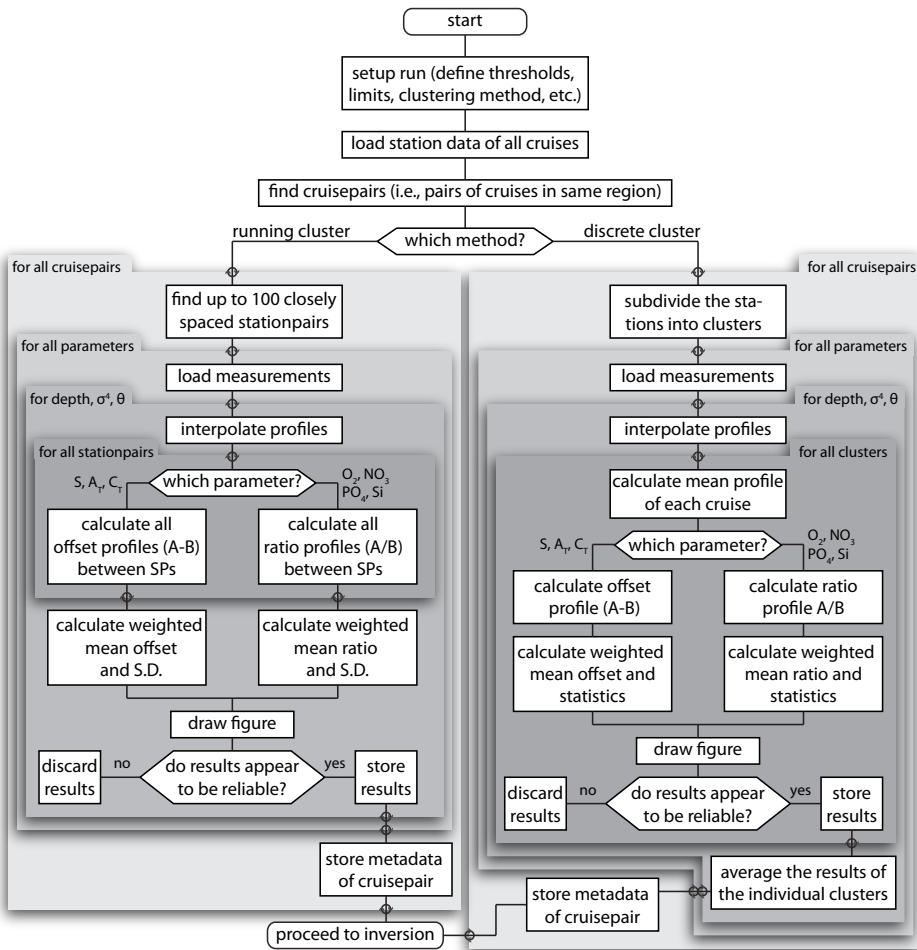


Figure 5.3. Flowchart describing the steps involved in the cnaX crossover routines.

cluster routine potentially results in several hundred station-pairs. Of these only the 100 most closely spaced station-pairs are further considered. The measurements at each of these stations are interpolated to  $\sim 75$  depth levels. For each station-pair the offset profile is determined by subtraction/division of B's interpolated profile from/by A's. The offset profiles are subsequently averaged to get the mean offset profile (MOP) and an associated offset standard deviation profile (OSDP) for this cruise-pair. The interpolated values in the MOP are averaged and weighted by the OSDP, resulting in a weighted mean offset (WMO) for this cruise-pair. The uncertainty of the value thus determined is expressed by the associated weighted mean offset standard deviation (WMOSD). It is these last two values that are used as input for the inversion. As mentioned above, the routine concurrently determines WMO and WMOSD in depth-, theta and sigma<sub>4</sub>-space. The determined WMO with the smallest associated WMOSD (generally the one in sigma<sub>4</sub>-space), is considered to be the best estimate of the cruise-pair's offset.

The overall quality of the offset determined this way is assessed through the use of several conditional statements considering number of stations, samples and difference profiles, and the OSDP. Alternatively, the user can manually rate the quality of the determined offset. This quality assessment and the WMOSD are later used in the inversion for weighing the offsets. The running-cluster-routine was determined to yield superior results to the discrete-cluster-routine as it offers more rapid processing and is more objective. The results of the cnaX routines were made available to the analysts on the website and used for determination of adjustments.

#### 5.4.2. Inversions

A second step in QC2 uses the offsets and standard deviations derived from the crossover analysis to calculate corrections of the parameters measured on individual cruises using least square models (Wunsch, 1996), i.e. inversions, following the methodology described in Johnson et al. (2001). The inversion produces a correction factor (for multiplicative corrections) or a correction (for additive corrections) for each of the cruises in the analysis. Indiscriminate application of these factors might produce the most uniform data set, but this would also remove real temporal trends, an undesirable side effect. Therefore the corrections and correction factors were manually evaluated; those that were actually applied to the data product are called adjustments, to avoid confusion with the corrections suggested by the inversion process.

Johnson et al. (2001) presented three models of different complexity to adjust five parameters for World Ocean Circulation Experiment (WOCE) cruises in the Pacific Ocean. The conclusion of Johnson et al. (2001) was that the intermediate complexity model Weighted Least Squares (WLSQ) performed most satisfactory for this analysis. In this model the standard deviation of each crossover is included in the calculation, but no a priori assumptions are made regarding the quality of the measurements. In the slightly more complex model, Weighted Damped Least Square (WDLSQ), a priori assumptions on the quality of the data are made; essentially the maximum allowed range of adjustments is set for each cruise, the model error. As Johnson et al. (2001) point out; this limitation tends to decrease the adjustments of individual cruises on cost of the overall performance of the model. Finally, the simplest of

the models, Simple Least Squares (SLSQ), do not take the uncertainty of the offset values into account, and is considered too simple.

For instance, both the work of Johnson et al. (2001) and Lamb et al. (2002) dealt with a set of cruises with presumable similar quality since they all aimed at meeting the WOCE Hydrographic Program (WHP) standards. The CARINA data base, in contrast, is a collection of cruises that covers more than 2 decades with different scope and standards of the measurements. The quality of the measurements is more heterogeneous for CARINA than for the WOCE data set. Therefore, the CARINA group performed both WLSQ and WDLSQ inversions of the crossover results, and the results from both were considered in determining the adjustment of a cruise. Since there is such a heterogeneity among the CARINA data, for the North Atlantic and Southern Ocean areas, a number of core cruises were identified, see above, where the quality of the data were, in general, assumed to follow WHP targets. The core cruises thus includes the reference cruises (i.e. WOCE/GLODAP cruises) for the SO area; for the NA area a number of non-reference cruises were additionally included as core-cruises (Tanhua et al., 2009). These core cruises were generally given low model error for the WDLSQ analysis whereas the non-core cruises were given high model errors, i.e. the corrections of the non-core cruises were allowed to be larger than those for the core cruises, Table 5.2. In this way, the model tended to adjust the CARINA dataset towards the values of the core-cruises. In most cases, however, there were only small differences between the WLSQ and WDLSQ inversions. As the CARINA project didn't blindly follow the inversion results we used both the WLSQ and WDLSQ models for the analysis; see Fig. 5.4 for an example of the result of an inversion for the multiplicative parameters for the CARINA-ATL data set.

There are some important additions/alterations to the inversion methods used in CARINA compared to Johnson et al. (2001). Firstly, since the time-span over which the hydrographic surveys took place is large (up to 3 decades) and trends in deep water properties can be expected on this time frame over large parts of the CARINA domain, a time factor,  $K_T$

**Table 5.2.** Table listing: (2<sup>nd</sup> column) the minimum adjustment applied to the data product; (3<sup>rd</sup> and 4<sup>th</sup> columns) the maximum model error in the Weighted Damped Least Square (WDLSQ) inversions for core cruises and non-core cruises; (5<sup>th</sup> column) the RMSE of the difference in offsets calculated by the running-cluster and the cnaX routines.

Parameter	Model error			
	Minimum adjustment	Core cruises	Non-core cruises	cnaX-RC
Salinity [ppm]	5	5	30	7.7
$C_T$ [ $\mu\text{mol kg}^{-1}$ ]	4	4	15	3.6
$A_T$ [ $\mu\text{mol kg}^{-1}$ ]	6	6	20	2.9
pH	0.005	0.005	0.01	NA
Nitrate [%]	2	2	20	2.9
Phosphate [%]	2	2	20	4.2
Silicate [%]	2	2	20	7
Oxygen [%]	1	1	10	1.1

, was weighted into the inversions. This factor was calculated as unity plus the time in years between the two cruises in a crossover times 0.1, i.e.,  $K_T = 1 + \Delta\text{year} \times 0.1$ , and multiplied to the standard deviation of a crossover. This reduces the impact of a crossover on the inversion if the time elapsed between the two cruises is large. One can argue that the time factor should be larger for more active parts of the ocean, for instance the Labrador Sea, than in “calmer” parts of the Ocean, such as the subtropical eastern Atlantic. However, since such classification tends to be rather arbitrary and difficult to implement, no such area dependent weighting was conducted for CARINA. This was rather done manually by the analyst in the final determination of the adjustment. That is, data from a “variable” area were generally allowed larger offsets (i.e. higher suggested corrections from the inversion) than data from a “quiet” area of the ocean before an adjustment was accepted.

### 5.4.3. Determination of adjustments

Many potential sources of uncertainty can complicate an otherwise straightforward assessment of cruise biases. Examples include: (1) temporal variability and long-time trends in parameter values on a particular location in the ocean, (2) drifting or variable measurement precision

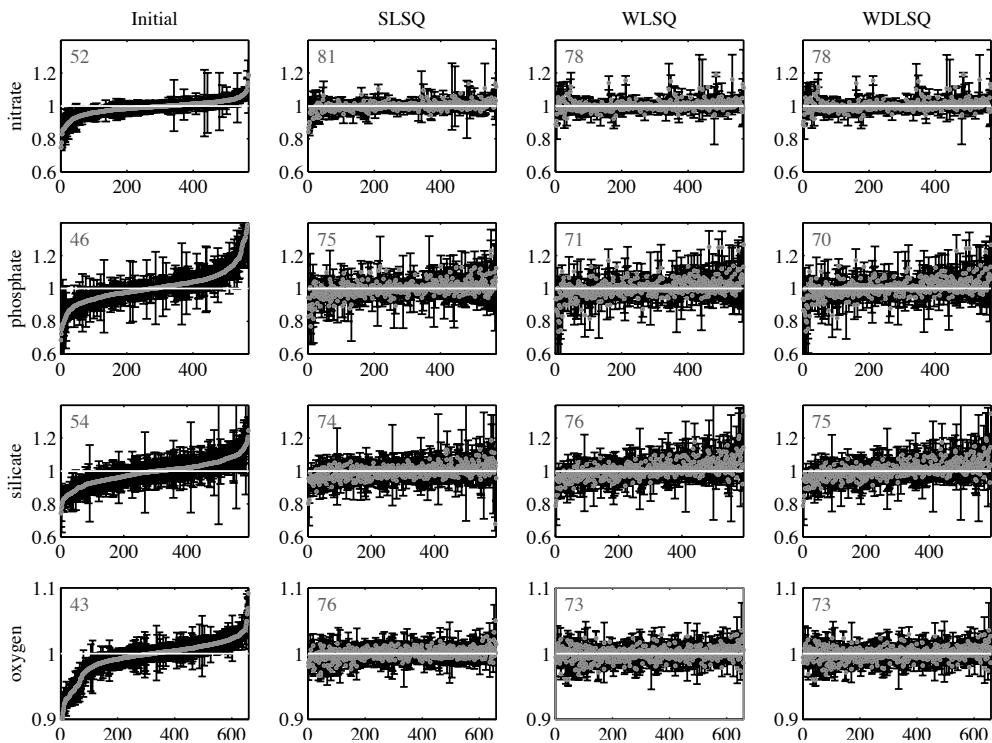


**Figure 5.4.** The results of an inversion of the North Atlantic nutrient and oxygen data: Left column (initial) shows the offsets of all the crossovers sorted by offset (red dots) and the weighted standard deviation of the crossover (black bars); the following columns shows the offsets after the corrections suggested by the SLSQ, WLSQ and WDLQS inversions has been applied to the data. The numbers in the panels indicate the percentage of crossovers that are indistinguishable from zero within their uncertainties.



and accuracy during a cruise, (3) profile interpolation errors, and (4) differences between routines used to determine offsets. Since biases cannot be determined with absolute accuracy, the CARINA working group agreed to correct only biases greater than a certain threshold value, Table 5.2. These thresholds reflect the expected minimum bias that should be possible to determine with reasonably certainty. For highly variable regions or for cruises with few deep data points, larger uncertainty was allowed in the manual evaluation of corrections.

Aided by the corrections suggested by the inversions and the offsets of all crossovers for a cruise/parameter combination, the potential bias for each cruise and parameter was scrutinized by the analyst. Particular emphasis was put on crossovers with core cruises and from crossovers with good statistics (i.e. larger number of stations/samples) in “quiet” parts of the ocean (i.e. with less variability). In many cases, additional evidence was considered by the analyst, such as the relation to another parameter (e.g. nitrate/phosphate or CFC-11/CFC-12 ratios) and whether or not certified reference material (CRM) was used. Finally, an adjustment was suggested by the analyst and entered into the online adjustment table. Only significant adjustments were applied, generally rounded to the nearest full percent,  $\mu\text{mol/kg}$  or ppm (for salinity). This somewhat subjective process makes the CARINA project different from most previously published consistency analyses of hydrographic data. The subjectivity possibly makes CARINA more prone to errors made by the analyst, but at the same time makes the CARINA adjusted data potentially more robust. In case of doubt, the CARINA team always tried to err of the side of not making an adjustment. The CARINA adjustment decision mechanism was similar to GLODAP, but the CARINA mechanics used to quantify the adjustment were much more sophisticated than those of GLODAP.

The lines of evidence for an adjustment (or the absence thereof) can be found at [http://cdiac.ornl.gov/oceans/CARINA/CARINA\\_QC.html](http://cdiac.ornl.gov/oceans/CARINA/CARINA_QC.html) in the form of comments and relevant figures, see Sect. 5.6. These adjustments were vetted during the final CARINA workshop in Paris in June 2008. Additionally, a second crossover analysis and inversion was made using the adjusted CARINA data. Any adjustments larger than the threshold were scrutinized again by the analysts. In a few cases, this step revealed cruises for which the adjustment needed revision. A few changes to the adjustment agreed on during the Paris meeting were made in consultation between the three group leaders.

### 5.5. Evaluation of the methods used

Since a few different routines and approaches were used for QC2 we have evaluated the consistency of the different methods and analyzed how these differences affect QC2.

#### 5.5.1. Manual vs. automatic crossovers

Both manually and automatically generated crossovers were used for the analysis. In order to evaluate any biases between the two methods we have plotted the difference between manually performed crossovers vs. crossovers generated automatically with the running-cluster routine for the Atlantic subset of CARINA in Fig. 5.5. The manual results are found in the crossover table on the CARINA website, see below. These crossovers were generated by a number of different analysts, potentially using different maximal horizontal length scales, clustering, minimum depth etc. Even though there are a number of data points that



are significantly different from zero, the mean difference is close to zero for all of parameters except phosphate. The few data points with large deviations from zero difference are due to miss-entered values in the crossover table and crossovers that were performed on few data points, i.e., that have low significance. It is clear that there are some differences in the results from the manually and automatically generated crossovers but that the overall difference is small, although it could potentially be important for some cruises.

### 5.5.2. Automatic crossover routines

The offsets determined by the two different automatic crossover routines discussed above (text sections 5.4.1.2 and 5.4.1.3) are compared to each other to evaluate any biases, Fig. 5.6.

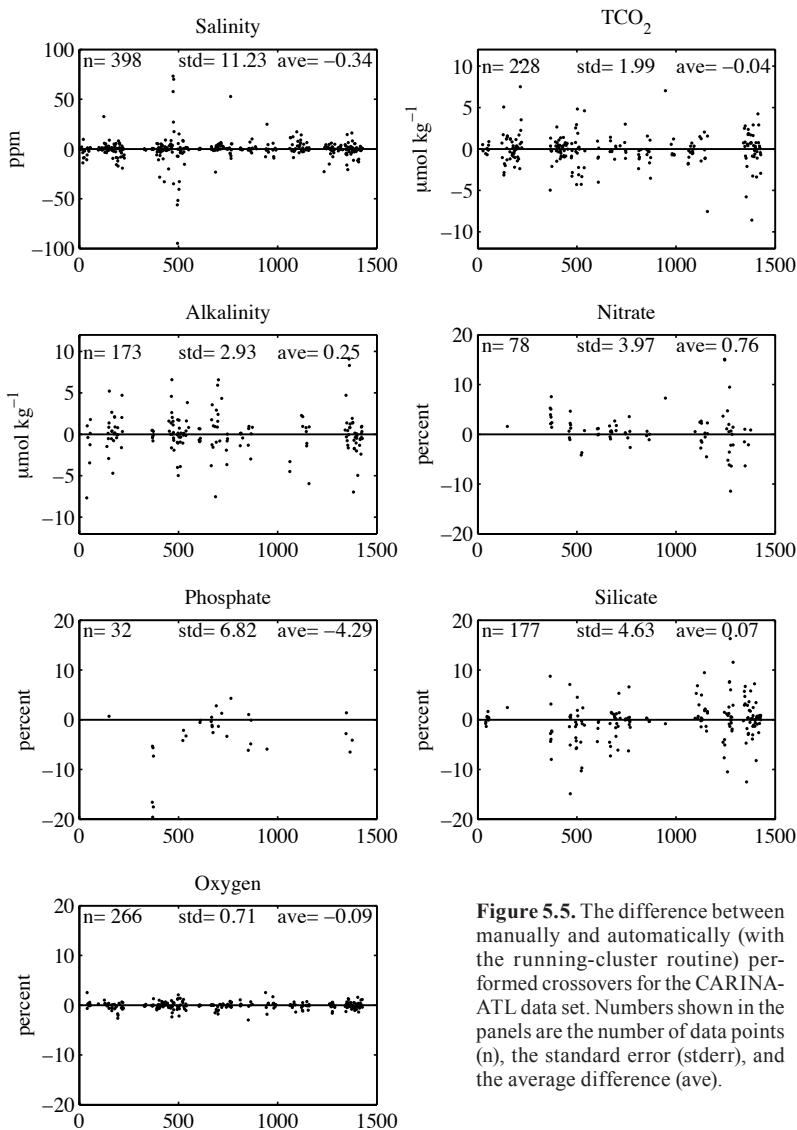


**Figure 5.5.** The difference between manually and automatically (with the running-cluster routine) performed crossovers for the CARINA-ATL data set. Numbers shown in the panels are the number of data points ( $n$ ), the standard error ( $stderr$ ), and the average difference ( $ave$ ).

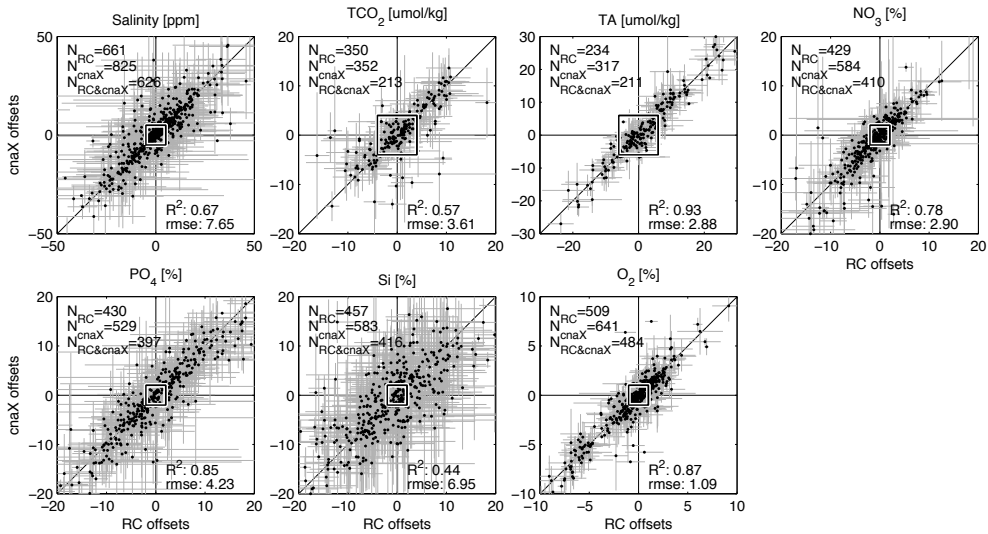


**Figure 5.6.** Figure comparing offsets determined by the cnaX method and the Running-Cluster (RC) method for the SO and ATL areas (black dots with gray error bars). The square in the middle of the figures indicate the minimum adjustment that were applied to the data. The numbers in the upper left corner states the number of crossover that the different methods found; the numbers in the lower right corner states the  $R^2$  value of the linear fit and the rmse of the difference between the methods. The methods are generally in good agreement, with the exception for silicate, where the standard deviation of differences between the two methods is around 7%. See text for discussion.

The first observation is that the cnaX routine generally found more crossovers than the RunningCluster (RC) routine. This is mostly due to the spatial distance within which to search for crossovers being larger for cnaX than for RC; cnaX will thus find more crossovers at an increased risk of introducing errors due to spatial variability. The second observation is that performance is different for different parameters. For instance, determinations of oxygen-offsets by the two routines are in agreement to approximately 1%, while silicate offsets are determined with a much lower agreement of about 7% (measured as the standard deviation of the difference from the two methods), Fig. 5.6. Given that each routine operates equally for all parameters, the cause for the difference must be the silicate data itself. Profile interpolation is assumed not to be cause of the problem since the vertical sample distribution is in most cases identical for nutrients and oxygen, both generally being sampled at full resolution. A possible cause of the difference is high station-to-station variability of silicate values either due to analytical difficulties or large natural variability of silicate values in the deep water. This would make the result of the offset determinations strongly dependent on the stations included in the crossover. The second alternative is certainly possible considering the large difference in silicate concentrations in the southern and northern end-members of the Atlantic deep waters. In this case the different “search radius” would be important for the result. On the other hand, offsets determined for alkalinity are in very good agreement between the two routines, suggesting that although large biases between cruises exist for this parameter, the alkalinity values within a cruise is measured with a constant bias.

Taking the RMSE of the difference between the offsets determined by the two routines as an upper limit of detection for biases, we conclude that the thresholds used by the

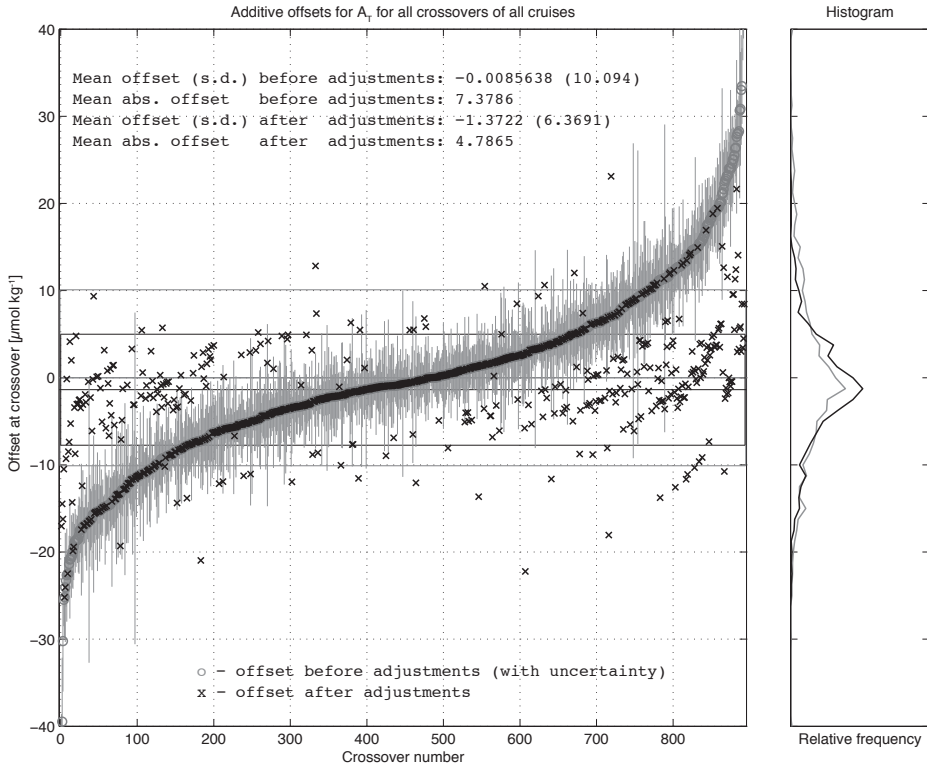


**Figure 5.7.** Figure showing the offsets for individual crossovers for alkalinity as determined by the `cnaX` routine. The gray circles are the offsets before adjustment, sorted from low to high; black crosses are the same offsets but after application of the adjustments suggested by the inversion (and that larger than the threshold value). The uncertainty of the crossovers is only shown for the uncorrected crossovers. The right panel shows the relative distribution of offsets (gray line before adjustment; black line after adjustment). This analysis includes also the GLODAP reference cruises.

CARINA team for applying adjustments (i.e., Table 5.2) are on the optimistic side for silicate and phosphate, about right for oxygen, nitrate, salinity and  $C_{Tr}$ , and too conservative for  $A_T$ .

### 5.5.3. Adjustments

As discussed above, the results of the inversions were only used as a guide by the analyst when determining the adjustments, and almost no adjustments below the threshold were applied to the data product. The inversions often suggest corrections that are smaller than these limits. In order to evaluate the effects of the threshold, we analyzed how the weighted mean offsets for all crossovers and parameters in the CARINA data set are affected by using two different sets of adjustments; in the first case all the corrections suggested by the inversion were blindly applied to all the data, in the second case we applied only adjustments larger than the threshold (see Table 5.2). The overall performance is somewhat better if all corrections are applied, Table 5.3, but the difference between the two cases is not particularly large. Thus, application of all corrections suggested by the inversion results in the most in-

ternally consistent dataset, but implicitly suggests a confidence in the adjustments that is not warranted for a relatively small gain in internal consistency. An example of the effect of the adjustments on the offsets for individual crossovers can be seen in Fig. 5.7 where the offsets of all crossovers for alkalinity are plotted; before any adjustments are applied as well as after adjustments larger than the threshold are applied. The mean absolute offset clearly decreases by application of the adjustments.

We have also directly compared the suggested corrections derived from the *cnaX* scripts with the adjustments that were actually applied to the CARINA data product, Fig. 5.8. The differences between the corrections and adjustments are a measure of the subjectivity of the CARINA QC2. There is generally a reasonable agreement between adjustments and corrections. However, this should not be considered to be an indication of the correctness of the adjustments since the two measures are not independent – the results from the inversions were generally followed with small modifications. Note several points with an adjustment value of zero but where a significant correction has been suggested by the inversion (x's in Fig. 5.8), particularly for cruises conducted in areas of known high temporal variability. The reverse is also true, although not as often, i.e. even if the inversion suggests a correction smaller than the threshold, an adjustment has been made. Further inversions could have been performed (with the adjusted system) to find new model solutions that iteratively maximizes the internal consistency of the system. A first step in this iterative process was taken, but as we found that the result did not significantly improve the result above the level of uncertainty, this was not further pursued.

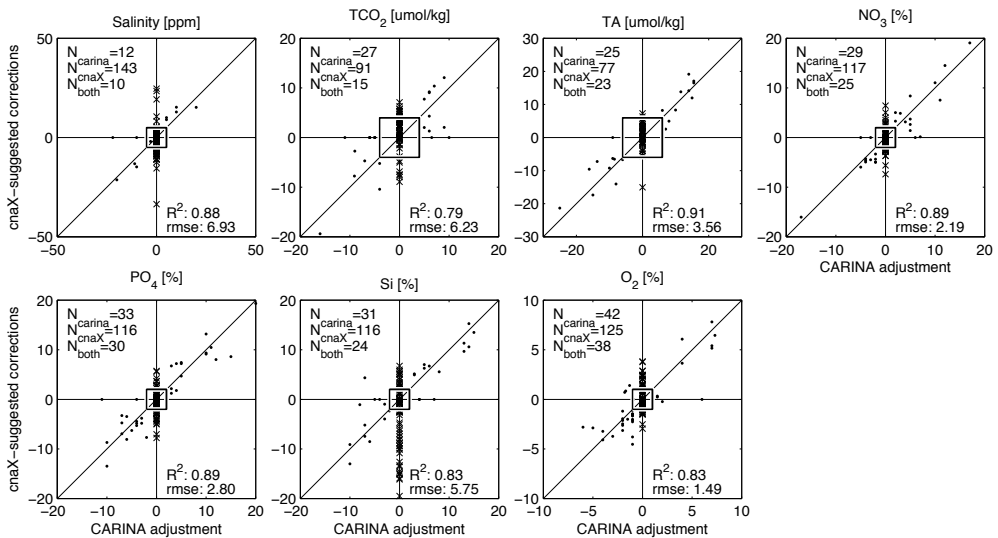


**Figure 5.8.** A comparison between the corrections suggested by the *cnaX* routine and the adjustments applied to the CARINA data product. Black dots denote that an adjustment was applied; black crosses that no adjustment was applied. The square in the middle of the figures indicate the minimum adjustment that were applied to the data. The numbers in the upper left corner states the number of cruises for which a correction was suggested by the *cnaX* method ( $N_{cnaX}$ ) and the number of adjustments applied to the CARINA data ( $N_{carina}$ ); the numbers in the lower right corner states the  $R^2$  value of the linear fit and the rmse of the difference between the methods for those cruises where an adjustment was applied.

**Table 5.3.** The internal consistency of the data set expressed as the weighted mean of the absolute offsets for all crossovers in CARINA. Various levels of consistency are acquired by applying varying corrections to the dataset: Uncorrected, before any adjustments are applied; Limited, no adjustments smaller than the cut-off limit (see Table 5.2) are applied; Unlimited, all corrections suggested by the inversion are applied. The statistics are determined by the *cnaX* routines using all crossovers from the complete CARINA data set.

Parameter	Uncorrected	Limited	Unlimited
Oxygen [%]	1.6	0.8	0.6
Nitrate [%]	3.5	1.7	1.4
Silicate [%]	6.2	2.8	2.6
Phosphate [%]	5.1	2.5	2.4
$C_T$ [ $\mu\text{mol kg}^{-1}$ ]	5	3.2	2.6
$A_T$ [ $\mu\text{mol kg}^{-1}$ ]	6.7	3.9	2.5
Salinity [ppm]	6.1	4	3.3

## 5.6. The web-based crossover workspace

The CARINA team included a large number of scientists from all over the world working simultaneously on the quality control and rapid communication of individual efforts and results were important for the success of the project. To facilitate this, an interactive internet based platform was developed. To the user, the website provides important functions and tables of which the crossover and adjustment tables are the most important. We will first briefly discuss some of the functionality of the website from a user's perspective, and will then describe its basic architecture. A non-user interactive version of the website, with all the information used by the CARINA team, is available at [http://cdiac.ornl.gov/oceans/CARINA/Carina\\_inv.html](http://cdiac.ornl.gov/oceans/CARINA/Carina_inv.html).

The crossover table provides the interface to enter offset values for crossovers for any of the 14 parameters considered for QC2. Also generic information to a crossover, such as position, number of stations etc. can be entered. Furthermore, files can be uploaded and comments can be posted. This allows several investigators to work on crossover analysis simultaneously without duplicating work and enables communication of information. The adjustment table is similar in its functionality. Adjustment values, files and comments can be entered or uploaded for any of the 14 parameters, or to the cruise as a whole. Furthermore, a quality flag (either "good" or "poor") is assigned for each cruise/parameter combination. The user can search the database for all figures relevant to a cruise/parameter combination, and create a link to the adjustment table. This allows the investigator to select important figures that motivate the choice of adjustment. There is also a link to the relevant readme (i.e. condensed cruise metadata) for each cruise entry in the adjustment table.

The cruise and ship tables provide easy access to basic information for each cruise or ship, if that information is not found in the readme files. More importantly, it provides means to keep track of the aliases for different cruises, i.e. old versions of the EXPCODE or project names associated to a cruise (this information is also displayed in the adjustment table). The information in the crossover and adjustment tables can be exported as csv-files that can be used by other applications. For instance, the adjustments are used for creation of the merged data product where the adjustments in the table are applied to the data in the individual cruise

files or the manually entered crossover values can be downloaded for the inversions. Another important aspect of the website is the possibility to post larger files and data volumes. This enable, for instance, rapid upload of inversion results that cannot be attributed to any specific cruise. Also draft versions of manuscripts etc. were posted on the website.

The CARINA website project started with the initial requirement of at least two tables; one where crossover results could be stored, and one for adjustment values of individual cruises. Supplemental information such as figures, comments and ReadMe files could be stored on the platform as well and be linked to submitted data. It soon became clear that this website would accumulate thousands of individual data points for crossovers and adjustments, and even more supplementary files and updates of these. All of this would then have to be available to all users during the data compilation and evaluation process. Manual creation or maintenance of contents and links would thus be impossible. Moreover, the need arose to batch submit a large number of automatically generated figures and data calculated by user scripts which should be automatically processed and reflected throughout the applications. The greatest demand (and challenge) was the linkage between an individual datum and multiple supplementary information with the ability to “share” these relations in other contexts. For example, a supplemental file uploaded to the crossover analysis of salinity (which involves two cruises) should be available in the context of the salinity adjustment value for each of the two cruises, and whenever the file is updated it would have to be reflected in every shared relation. To accommodate these demands, we decided in favor of open source software in order to be able to freely use and distribute the application, particularly after termination of this project and in case that offline usage is needed. We chose to use Ruby on Rails, which is based on the object-oriented programming language Ruby, as web application framework and PostgreSQL as relational database for storage of data and information snippets. Uploaded files are stored in the file-system, while their respective metadata are kept in the database.

According to the Ruby on Rails framework, the CARINA application is implemented using the model-view-controller architecture (MVC) which provides an out-of-the-box basic skeleton of all necessary methods to create, read, update or delete (CRUD) datasets of a particular model (i.e. a corresponding table) and to build HTML forms or pages to edit or display datasets in the end user’s browser. Due to the conventions of the Rails framework, all methods necessary for a quick and effortless implementation of links between a datum and its supplementing information are available as soon as the database models are setup such that they reflect the real world relations of the material in use. It is not mandatory, but the usage of AJAX (Asynchronous JavaScript and XML) in the CARINA web application greatly improved usability and performance.

All information of the CARINA web application is stored in a total of eleven database tables: ships, countries, cruises, crossovers, regions, adjustments, attachments, comments, postings, readmes and users. Datasets are then handled by Rails as objects with automatically created methods. This provides access to both a dataset’s parameters (i.e. columns) and to other related datasets; these are also treated as objects. This allows syntactically simple access to the parameters/attributes (i.e. columns) of datasets and their supplements as well as to the relations between different models. It also avoids formulation of any SQL-based queries or handling of interactions with the back-end database. We have used polymorphic relations for comments, readmes, postings and attachments. This allows a single model (e.g.

attachment representing an uploaded file) to be used for datasets of different models to which files can be uploaded (i.e. attached). In the CARINA site, most models can thus have multiple files uploaded to a single dataset. We even extended this feature by an additional attribute for attachment and comment records holding the parameter to which an uploaded file or a comment is attached. Thus, a file uploaded to a crossover can be specifically “attached” to any parameter, for instance salinity.

In numerous cases crossovers are assigned to more than one working group (see section 5.2 on data provenance). It was required that each working group could store values for their regional crossover separately. This is accomplished by insertion of two additional crossovers as subsets with a simple parent-child relation to the parental crossover (parent id as foreign key) representing the two data provenances. Members of either working group can click a dynamically inserted link in the list view whenever subsets are present and both subsets are then retrieved from the server and displayed in the context without reloading the entire page. One of the subsets is always assigned as primary subset yielding a priority for automatic display of values; as long as a parameter value is not finalized and entered in the primary (i.e. parent) dataset, the web application displays the value of the parameter from the primary subset or, if no value has been entered, from the secondary subset. A trailing “c” as subscript to the value indicates such a copy. Another parent-child relation is used for the adjustments table when a cruise or campaign may have to be split in sections due to temporal variations in the proper adjustment value (e.g. mid-cruise change of standards or different instrument performance after a port call). In this case multiple copies of the dataset are inserted, but as there is no unique solution to this case, multiple datasets are either exported or displayed and sorted according to the sets of stations which apply.

All authenticated users can upload files individually via the web-interface and some authorized users can upload directly into a separate folder accessible via WebDAV. This allows uploads of large file batches created by script routines which, when compliant with naming and file/folder hierarchy conventions, can be ingested upon request of the uploading user, and will “attach” each discovered plot file to the appropriate crossover (or adjustment). Uploaded figures are commonly provided in PostScript format, unsuitable for display in web browsers. These files are automatically converted to PNG formatted files using the ImageMagick utilities and available for quick views of the figure via an autogenerated weblink while the original PostScript file is only sent to the user when a download is explicitly requested. Special forms allow users to make a selection of crossovers or adjustments which they wish to export and download. An entry which is not a number may be exported as a string (e.g. NaN) or as a special number (e.g. -999) based on individual user settings. Similarly, overview lists of all comments posted to each adjustment can be generated and saved to disk.

Overall statistics reflect busy usage of the CARINA working platform: 2102 crossovers (with additional 556 subsets to 278 crossovers), 238 cruises and respective adjustment datasets, 35063 attached plot files, 1919 comments, 173 readmes and 107 postings, all together consuming about 10 Gigabytes of disk space.





# Chapter 6

## **Direct observation of increasing CO<sub>2</sub> in the Weddell Gyre along the Prime Meridian during 1973-2008**

Published as:

*van Heuven, S., M. Hoppema, O. Huhn, H.A. Slagter, and  
H.J.W. de Baar (2011). Direct observation of increasing CO<sub>2</sub> in  
the Weddell Gyre along the Prime Meridian during 1973–2008.  
Deep-Sea Research II, 58, 2613–2635.*



## Abstract

The World Ocean takes up a large portion of the anthropogenic  $\text{CO}_2$  ( $C_{\text{ant}}$ ) emitted into the atmosphere. Determining the resulting increase in dissolved inorganic carbon ( $C_T$ , expressed in  $\mu\text{mol kg}^{-1}$ ) is challenging, particularly in the subsurface and deep Southern Ocean where the time rate of change of  $C_T$  (in  $\mu\text{mol kg}^{-1} \text{decade}^{-1}$ ) is often expected to be low. We present a determination of this time trend of  $C_T$  in a dataset of measurements that spans 35 years, comprising 10 cruises in the 1973–2008 period along the  $0^\circ$ -meridian in the Weddell Gyre. The inclusion of many cruises aims to generate results that are more robust than may be obtained by taking the difference between only one pair of cruises, each of which may suffer from errors in accuracy. To further improve consistency between cruises, data were adjusted in order to obtain time-invariant values of  $C_T$  (and other relevant parameters) over the 35 years in the least ventilated local water body, this comprising the deeper Warm Deep Water (WDW) and upper Weddell Sea Deep Water (WSDW). It is assumed that this normalization procedure will allow trends in  $C_T$  in the more intensely ventilated water masses to be more clearly observed.

Time trends were determined directly in measurements of  $C_T$ , and alternatively in back-calculated values of preformed  $C_T$  ( $C_T^0$ ; i.e., the  $C_T$  of the water at the time that it lost contact with the atmosphere). The determined time trends may be attributed to a combination of natural variability (in hydrography or biogeochemistry) and increased uptake of anthropogenic  $\text{CO}_2$  from the atmosphere. In order to separate these natural and anthropogenic components, an analysis of the residuals of a multivariate linear regression (MLR), involving the complete time series of all 10 cruises, was additionally performed. This approach is referred to as the Time Series Residuals (TSR) approach.

Using the direct method, the time trends of  $C_T$  in the WSDW are quite small and non-significant at  $+0.176 \pm 0.321 \mu\text{mol kg}^{-1} \text{decade}^{-1}$ . On the other hand, the measured concentration of  $C_T$  in the Weddell Sea Bottom Water (WSBW) is shown to rise slowly but significantly over the period from 1973 to 2008 at a rate of  $+1.151 \pm 0.563 \mu\text{mol kg}^{-1} \text{decade}^{-1}$ . The spatial distribution of these determined increases of  $C_T$  in the deep Weddell Gyre closely resembles that of the increase of the anthropogenic tracer CFC-12, this strong similarity supporting a mostly anthropogenic cause for the increasing trend of  $C_T$ . Time trends in back-calculated values of  $C_T^0$  appear to be obscured due to uncertainties in the measurements of  $\text{O}_2$ . Finally, the shallow waters (<200 m depth) do not allow for interpretation since these are strongly affected by seasonality.

Due to the small time trend signal in the WSBW, the TSR approach does not allow for unambiguous attribution of the observed trend in  $C_T$  in the WSBW. The residuals of the TSR method do exhibit a time trend (considered representative of the time trend of  $C_{\text{ant}}$ ) of  $+0.445 \pm 0.405 \mu\text{mol kg}^{-1} \text{decade}^{-1}$  (i.e., only 38% of the direct observed time trend in  $C_T$ ) thus only partly supporting the attribution of the measured time trend of  $C_T$  to uptake of anthropogenic  $\text{CO}_2$ . Another TSR-derived result suggests that there is no significant time trend of biogeochemical changes. A time trend in hydrography of mixing between two deep water masses does exist, as evidenced by a slight positive time trend in the temperature of the WSBW, but is inadequate to explain the time trend of  $C_T$ .

After all, the time trend in measured  $C_T$  is most straightforwardly ascribed entirely to uptake of  $C_{ant}$ , and assuming an exponentially growing history of storage, the observed increase of  $C_T$  in the WSBW suggests that a total amount of  $C_{ant}$  of  $6 \pm 3 \mu\text{mol kg}^{-1}$  has accumulated in this water mass between the onset of the industrial revolution and 1995. Extrapolating this result, the rate of storage of  $C_{ant}$  in the deep Weddell Gyre (>3000 m, west of 20 °E) is calculated to be about  $12 \pm 6 \text{ TgC a}^{-1}$  over the 1973-2008 period. This rate of storage is likely somewhat lower than the rate of export of  $C_{ant}$  from the surface water into the deep Weddell Gyre, this due to continuous loss of  $C_{ant}$  with WSDW flowing out of the Weddell Gyre into the deep basins of the other oceans as AABW.

## 6.1. Introduction and outline

### 6.1.1 Introduction

Since the onset of the Industrial Revolution around 1780, the combustion of fossil fuels has led to increasing concentrations of  $\text{CO}_2$  in the atmosphere. In 1957 the now world famous time series of atmospheric  $\text{CO}_2$  measurements at Mauna Loa, Hawaii was started (Keeling, 1960). After a few years, a rise in  $\text{CO}_2$  was apparent, and already in the early 1960s it was recognized that the steady increase was attributable to the burning of fossil fuels. Moreover, it was realized that a portion of the fossil fuel  $\text{CO}_2$  would enter into the ocean. Postma (1964) suggested that this invasion of anthropogenic  $\text{CO}_2$  into the oceans can in principle be quantified. However, at the time, the analytical precision was inadequate to distinguish within the measured dissolved inorganic carbon (DIC, hereafter  $C_T$ ; in  $\mu\text{mol kg}^{-1}$ ), the small anthropogenic (or 'excess') component ( $C_{ant}$ ; in  $\mu\text{mol kg}^{-1}$ ) from the large and variable natural background.

The extensive and at the time state-of-the-art dataset for  $C_T$  and alkalinity collected during the GEOSECS expeditions in the 1970s (Bainbridge, 1981) led to renewed efforts to quantify  $C_{ant}$  in the oceans (Brewer, 1978; Chen and Millero, 1979). Although their approach worked quite well for certain water masses, it was deemed unsuitable for worldwide application. Additionally, at the time the quality of the data was still only modest. Nevertheless, Chen (1993) did produce an estimate of the global ocean inventory (in PgC, equal to  $10^{15}$  grams of C) of anthropogenic  $\text{CO}_2$  in the year 1980.

The next major improvement was the  $\Delta C^*$  approach (Gruber et al., 1996) that in combination with the higher accuracy TTO dataset (Transient Tracers in the Ocean, 1981), led to improved estimate of  $C_{ant}$  and its corresponding inventory in the North Atlantic Ocean. In the early 1990s, the introduction of certified reference material for  $C_T$  (CRM; Dickson, 2001) as well as detailed measurement protocols (Dickson, 1993, updated in 2007), were other major steps forward in accuracy. New high quality datasets of the world oceans, obtained by the WOCE/JGOFS programs, in combination with the  $\Delta C^*$  approach, led to the first high accuracy estimate of the inventory of  $C_{ant}$  of the world oceans (Sabine et al., 2004).

Consensus now exists concerning the inventory of  $C_{ant}$  for most of the world ocean. However, the determination of the inventory of  $C_{ant}$  in the Southern Ocean remains a challenge, largely because the validity for the application in the Southern Ocean of the various approaches to derive  $C_{ant}$  is debatable. Vázquez-Rodríguez et al. (2009) clearly demonstrate the large range in estimates of  $C_{ant}$  in the South Atlantic Ocean that are produced by the various approaches. For

the deep and bottom water masses, Vázquez-Rodríguez et al. (2009), show these estimates of  $C_{\text{ant}}$  to range from negligible to values as high as one-third of the concentrations in the surface water.

This study aims to determine the rate of increase of actually measured  $C_T$  over 35 years (1973-2008) in the Weddell Gyre using ocean interior data from 10 successive cruises. In the little-ventilated (or 'old') lower Warm Deep Water (WDW) and upper WSDW, no time trend of  $C_T$  is expected or observed, therefore all cruise datasets are normalized to a common level in this water body. Next, the normalized  $C_T$  is gridded. From these grids, the spatial distribution along the section (55°S-70°S) of the generally increasing time trend of  $C_T$  is obtained, with striking resemblance to the similar distribution of time trends in the independent anthropogenic transient tracer chlorofluorocarbon-12 (CFC-12). Moreover, for two individual key water masses (the Weddell Sea Deep Water (WSDW) and Weddell Sea Bottom Water (WSBW)) the time trend of  $C_T$  (in  $\mu\text{mol kg}^{-1} \text{decade}^{-1}$ ) is calculated, from which a new improved estimate of the  $C_{\text{ant}}$  and its inventory in Weddell Gyre is reported. Obviously, the time trend of  $C_T$  may partly be due to natural variability of water mass mixing and biogeochemistry. Any effect of water mass mixing is assessed in a simple mixing model, relying on observed temperature trends. Moreover, the novel Time Series Residuals (TSR) method is designed to extract the sought after increase of anthropogenic  $C_{\text{ant}}$  and distinguish this from the natural variability. The novel TSR method relies on the measured  $C_T$  and a suite of independent ancillary measured variables of all 10 cruises.

Several stations of the 1973 GEOSECS expedition comprised the first suitable observations along the Prime Meridian in the Weddell Gyre. Since then, this hydrographic section along the 0°-meridian has been (more or less extensively) occupied by at least another 9 expeditions that performed high-quality measurements of  $C_T$  and additional relevant oceanic properties, (Tables 6.2 and 6.3). To the best of our knowledge this is the longest existing ocean section time series of  $C_T$  data. Therefore this is a uniquely promising section for assessing the rate of increase of  $C_T$ . Moreover it serves as a field test of the novel TSR approach for extracting the increasing  $C_{\text{ant}}$  signal from noise due to natural variability. On the other hand the Southern Ocean south of 50°S is often considered to feature only low concentrations of anthropogenic carbon (e.g., Sabine et al., 1999; Hoppema et al., 2001; but see Lo Monaco et al., 2005a,b). This conceivably constitutes a challenge for the demonstration of the direct  $C_T$  time trend and the TSR approach for discerning  $C_{\text{ant}}$ . However in the coming decades, and already in regions with a higher rate of increase (notably the North Atlantic Ocean; Perez et al., 2008 and 2010, Olafsson et al., 2009, Peng and Wanninkhof, 2010), both the direct  $C_T$  time trend approach and the Time Series Residuals method are expected to deliver a strong signal of increasing  $C_T$  and increasing  $C_{\text{ant}}$ , respectively.

### 6.1.2. Outline

After a brief introduction of the unique hydrography of the Weddell Gyre (text section 6.2), we will discuss in more detail the preceding concepts and approaches for quantifying the invasion of anthropogenic  $\text{CO}_2$  into the oceans (section 6.3). Firstly, five different published original approaches for determining the **total inventory** of  $C_{\text{ant}}$  in the ocean interior are recognized, and discussed with regards to assumptions and uncertainties, notably for the Southern Ocean (sec-

tion 6.3.1). Secondly, we mention three approaches for quantifying the **change** of such  $C_{ant}$  (i.e.,  $\Delta C_{ant}$ ) between two successive cruises along one and the same transect (section 6.3.2). Thirdly we introduce the novel Time Series Residuals (TSR) approach for extracting from a suite of several cruises along one transect the **rate of increase** of  $C_{ant}$  (section 6.3.3). Next, in text sections 6.4 through 6.7, both the direct  $C_T$  time trend method and the TSR-approach are applied to the suite of 10 cruises over 35 years along the Prime Meridian transect in the Weddell Gyre, aiming to establish the rate of increase of  $C_T$  and  $C_{ant}$ , respectively.

## 6.2. Hydrography

The Southern Ocean comprises all waters south of the Subtropical Front situated at about 40°S, while the Antarctic Ocean proper comprises all waters south of the Polar Front situated at about 50°S (Deacon, 1984). The hydrography of the Antarctic Ocean is dominated by the wind-driven Antarctic Circumpolar Current (ACC), which flows relatively unhindered around Antarctica at all depths (Figure 6.1). The eastward flows of wind and ocean currents also drive the Weddell Gyre, which rotates cyclonically (i.e., clockwise) between the Antarctic continent to the south, the Antarctic Peninsula to the west and the ACC to the north and east. The easternmost extension of the Weddell Gyre is located at 25-30 °E. Several water masses flow into and out of the ACC and the Weddell Gyre (Figure 6.2). From the north, at depths below about 1500 meters, North Atlantic Deep Water (NADW) mixes into the ACC. However, before reaching the ACC, as well as within it, the NADW is deflected upward by the denser Antarctic Bottom Water (AABW) from the south, which wedges itself underneath the NADW. In the ACC there

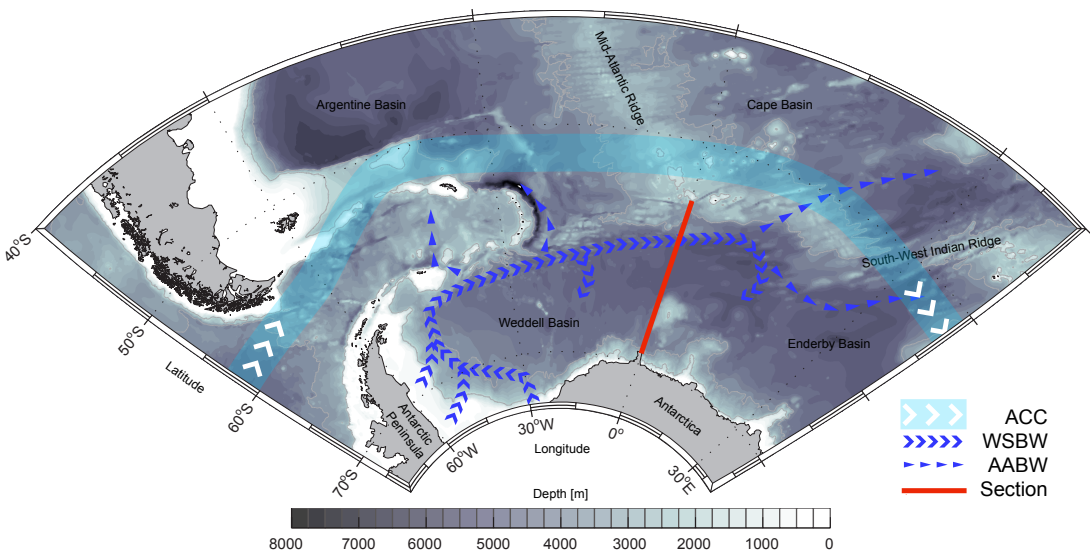


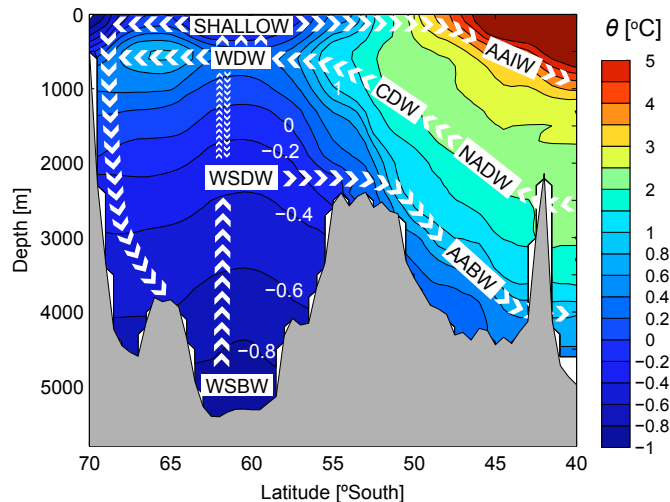
**Figure 6.1.** Map of the Weddell Basin and its surroundings, indicating the extent of the Weddell Gyre to about 30°E, the generalized course of the Antarctic Circumpolar Current (ACC; blue shaded with white chevrons) and the pathways of the WSBW (blue chevrons) and AABW (blue triangles). The formation areas of WSBW are situated at the southwestern perimeter of the Weddell Basin. Also shown is the general location of the oceanographic research section along the 0°-meridian.

**Table 6.1:** Definition of water mass cores as used throughout this paper. ‘Shallow’ is obviously not a formal water mass but this layer is defined because it potentially shows most clearly the time trends in properties related to the uptake of anthropogenic  $CO_2$  from the atmosphere. Note that the WSDW does not have a formal core since it is part of the gradient between WDW and WSBW. Of the three deeper water masses the limits of salinity and  $\theta$  follow the definition by Carmack and Foster (1975), although the temperature range for WSDW has been slightly constricted in order to retain just the samples from the core (or rather ‘middle layer’) of the water mass. The latitudinal constraint of 58 °S to 63 °S was added to prevent inclusion of samples (or grid points) close to the continental slope of Antarctica and to restrict the sampling to the meridional range that included data from the most cruises. Actual water masses may have a wider extent than those defined here. Note that the ‘1WDW/uWSDW-normalization’ performed in this study uses data of ( $\theta$ : -0.4 to 0.2 °C and latitude: 57 °S to 66 °S), i.e., from the deeper extent of the WDW and the upper extent of the WSDW, and from a slightly wider latitudinal range than the water masses defined in this table.

Water mass / layer	abbreviation	Latitude [°S]	Depth [m]	Salinity	$\theta$ [°C]
(upper 200 metres)	SHLLW	58 - 63	<200	-	-
Warm Deep Water	WDW	58 - 63	-	>34.6	>0
Weddell Sea Deep Water	WSDW	58 - 63	-	>34.64	-0.5 to -0.2
Weddell Sea Bottom Water	WSBW	58 - 63	-	>34.6	<-0.7

is large-scale mixing of several water masses including the NADW, resulting in a relatively homogeneous water mass called Circumpolar Deep Water (CDW). South of the ACC, the shallowing CDW penetrates southward toward the Antarctic continent at a depth of about 250 to 750 meters. Being distinctly warmer (potential temperature ( $\theta$ )>0 °C, see Table 6.1 for definitions) and saltier than the overlying, frigid and fresh polar water masses, it is locally referred to as Warm Deep Water (WDW). Strong and continuous circumpolar westerly winds cause upwelling of the WDW at latitudes between 60 °S and 65 °S in the Weddell Gyre. The upwelled waters are subsequently redistributed. A small fraction flows southward, replenishing the downwelling waters near the continent. A larger fraction flows northward where, between 50 °S and 45 °S, it subducts to depths of about 1000 m, and subsequently flows toward the equator as Antarctic Intermediate Water (AAIW).

**Figure 6.2.** Section along the 0°-meridian in the Southern Ocean showing potential temperature ( $\theta$ ) [°C] and the generalized locations and movements of various water masses. The ~45°S to ~55°S region represents the Antarctic Circumpolar Current. The 55°S to 70 °S region represents the actual Weddell Gyre, subject of this study. AAIW = Antarctic Intermediate Water; NADW = North Atlantic Deep Water; CDW = Circumpolar Deep Water; AABW = Antarctic Bottom Water; SHALLOW = the shallowest 200 meters of the water column; WDW = Warm Deep Water; WSDW = Weddell Sea Deep Water; WSBW = Weddell Sea Bottom Water.





The AABW, spilling from the intermediate and deep depths of the Weddell Basin over and through the Mid Atlantic Ridge (MAR) and the South-West Indian Ridge (SWIR), flows northward into the South Atlantic and South Indian basins (Figure 6.1). In the Weddell Basin, the pool of AABW (locally referred to as Weddell Sea Deep Water, WSDW) is replenished from below, by formation of dense water at sites along the edge of the Antarctic continent and the ice shelves of the Weddell Sea. The dense water flows downslope, entraining significant amounts of WDW, and accumulates near the bottom or at depths according to the density it achieves. This continuous supply of cold ( $\theta < -0.7$  °C) water - referred to as Weddell Sea Bottom Water (WSBW) - forces the near-bottom pool to extend upward where it is mixed into the overlying water (Foster and Carmack, 1976; Klatt et al., 2005). Typical features of the surface water at the margin of the Weddell Sea (i.e., relatively low temperature, salinity, nutrients and  $C_T$ ; high oxygen and CFCs) are retained during its transfer to depth. The characteristics of the WDW, the water mass that influences the intermediate depth Weddell Gyre from above, are diametrically opposed to this, and the resulting mixing gradients are clearly distinguishable for these properties. The intermediate state between WDW and WSBW, generally between 2000 and 4000 meters depth, constitutes the WSDW, and is the main source of AABW. This study is restricted to the sub-surface water masses within the Weddell Sea: WDW, WSDW and WSBW.

Much of the uncertainty about the inventory of  $C_{ant}$  of the Antarctic Ocean stems from this unique local hydrography. In the North Atlantic and Arctic oceans, deep water formation is generally thought to result from deep convection of cool, dense surface waters in wintertime. These waters have been cooled during extensive contact with the overlying atmosphere, meanwhile also exchanging gases such as CFCs,  $O_2$  and  $CO_2$ . Deep water formation in the Weddell Sea on the other hand, largely takes place along the Antarctic continent, under strong influence of the ice shelves (i.e., often preventing direct air/sea gas exchange). The waters contributing to the nascent deep water generally have only recently upwelled. The unknown and likely variable degree to which they equilibrate with the atmosphere before reaching the shelf zones, makes their ability to sequester anthropogenic  $CO_2$  difficult to predict or quantify.

### 6.3. Concepts and approaches to derive $C_{ant}$ and its change in the ocean interior

Firstly, five different published original approaches for determining the **total inventory** of  $C_{ant}$  in the ocean interior (section 6.3.1) are recognized, and discussed with regards to assumptions and uncertainties, notably for the Southern Ocean. Secondly, we mention three approaches for quantifying merely the **change** of such  $C_{ant}$  (i.e.,  $\Delta C_{ant}$ ) between two successive cruises along one and the same transect (section 6.3.2). Thirdly we introduce our novel approach for extracting from a suite of several cruises along one transect the **rate of increase** of  $C_{ant}$  (section 6.3.3): the Time Series Residuals (TSR) approach. Finally, all three groups of approaches are summarized in Table 6.2.

#### 6.3.1. Determination of the concentration of $C_{ant}$ in the ocean interior

##### 6.3.1.1. $C_{ant}$ : the $C_T^0$ approach

The gradual uptake by the ocean of anthropogenic  $CO_2$  from the atmosphere is detectable, in principle, as the ensuing gradual rise of  $C_T$  at the surface and eventually within the ocean in-



**Table 6.2:** A selection of techniques available for the calculation of the concentration of anthropogenic  $CO_2$  ( $C_{ant}$ ), or the increase therein ( $\Delta C_{ant}$ ), in the ocean. Some of the major perceived strengths and drawbacks of each are given in the table. See further text section 6.3.

Technique	Reference	Comment	Required measurements	Strengths	Assumptions made	Drawbacks / sensitivities
<i>Determining <math>C_{ant}</math></i>						
$C_T^0$	Brewer, 1978; Chen and Millero, 1979	Shiller, 1981	$O_2, C_T, A_T$	Conceptually simple	Surfaces histories of $C_{ant}, O_2$ and $A_T$ . No diapycnal mixing.	Requires pre-industrial reference watermass; hence difficult for world-wide application
$\Delta C^*$	Gruber et al., 1996	Matsumoto and Gruber, 2005	$O_2, C_T, A_T$ , transient tracer	Reduced sensitivity to some assumptions. No requirement of reference watermass	Surfaces histories of $C_{ant}, O_2$ and $A_T$ . No diapycnal mixing.	Must obtain ventilation age estimate of sample
TTD	Hall et al., 2002	---	transient tracer	Independent of biogeochemical data. Inherently allows for mixing	General shape of TTD. Surface histories of CFC and $C_{ant}$ .	TTD difficult to infer for certain regions.
TrOCA	Touratier et al. 2004a,b	Yool et al., 2010	$O_2, C_T, A_T$	Easily implemented	TrOCA <sup>0</sup> -parameterization may be extrapolated to higher temperatures	TrOCA <sup>0</sup> -parameterization likely not widely valid
TSS	Tanhua et al., 2007	---	$\Delta C_{ant}$ (see below)	Conceptually straightforward	TSS has been reached. Surface history of $C_{ant}$ .	Requires $\Delta C_{ant}$ of samples.
<i>Determining <math>\Delta C_{ant}</math></i>						
change in $C_T$	this study (trend)	---	$C_T$	Uses only high accuracy data ( $\pm 0.1\%$ )	Biogeochemical noise smaller than $\Delta C_{ant}$	Aliases in hydrographically and biogeochemically dynamic regions
change in $C_T^0$	Peng et al., 1998	---	$O_2, C_T, A_T$	Insensitive to variable biogeochemistry	Uncertainty of biogeochemical corrections applied are smaller than $\Delta C_{ant}$	Requires use of lower accuracy ancillary data ( $\pm 2\%$ ). Aliases in hydrographically dynamic regions
MLR	Wallace, 1995	Levine et al., 2008	$O_2, C_T, A_T$ , nutrients	Insensitive to variable hydrography and biogeochemistry	Ancillary data are independent. $\Delta C_{ant}$ is linearly representable by ancillary data. No "secular" trends.	Requires use of lower accuracy ancillary data ( $\pm 2\%$ ). Interpretation of results is ambiguous.
eMLR	Friis et al., 2005	Levine et al., 2008	$O_2, C_T, A_T$ , nutrients	Insensitive to variable hydrography and biogeochemistry	$\Delta C_{ant}$ is linearly representable by ancillary data. No "secular" trends.	Requires use of lower accuracy ancillary data ( $\pm 2\%$ ). Interpretation of results is ambiguous.
TSR	This study	---	$O_2, C_T, A_T$ , nutrients	Insensitive to variable hydrography and biogeochemistry. Use of many cruises reduces sensitivity to biases	Ancillary data are independent. $\Delta C_{ant}$ is linearly representable by ancillary data. No "secular" trends.	Requires use of lower accuracy ancillary data ( $\pm 2\%$ ).

terior. However, the presence and variability of biogeochemical processes in the ocean interior obscure these trends, and may need to be compensated for in order to be able to observe the increasing  $C_T$ . Remineralization of organic matter and the dissolution of calcium carbonate ( $\text{CaCO}_3$ ) do not only influence  $C_T$  but also the concentrations of dissolved oxygen ( $\text{O}_2$ ) and total alkalinity ( $A_T$ ), respectively. The stoichiometric ratios of these biogeochemical reactions have been shown to be fairly uniform in the oceans (Redfield et al., 1963; Anderson and Sarmiento, 1994). Therefore, by conversely using the changes in  $\text{O}_2$  and  $A_T$  from their preformed (i.e., at the time a water mass by its subduction loses contact with the atmosphere) values in the original surface water, these biogeochemical effects on  $C_T$  can be quantified and subtracted from the measured  $C_T$  in the ocean interior. This yields the reconstructed (or 'back-calculated')  $C_T$  that a water parcel had at the time of formation at the surface (preformed  $C_T$ :  $C_T^0$ ):

$$C_T^0 = C_T - \psi_{\text{O:C}}(\text{AOU}) - 0.5(A_T - A_T^0 + \psi_{\text{O:N}}(\text{AOU})) \quad (6-1)$$

Here, AOU (apparent oxygen utilization) represents the amount of oxygen consumed by remineralization of organic matter. The AOU is defined as the difference between the measured  $\text{O}_2$  of an ocean interior water sample and the preformed concentration,  $\text{O}_2^0$ , which is calculated (following Weiss, 1970) as the dissolved  $\text{O}_2$  presumably in equilibrium with atmospheric  $p\text{O}_2$ , using the measured values of salinity and temperature of the sample. The term  $\psi_{\text{O:C}}(\text{AOU})$  yields the amount of carbon released (as  $\text{CO}_2$ ) during biological respiration, calculated from the stoichiometry of consumption of  $\text{O}_2$  and production of  $\text{CO}_2$  ( $\psi_{\text{O:C}}$ ), and AOU. The value of preformed  $A_T$  ( $A_T^0$ ) is estimated from conservative properties of a water mass (any one or a combination of  $\theta$ , S, PO or NO; Broecker, 1974), using relationships determined between the measured  $A_T$  and these properties in the formation region of the subducted water mass. The factor of 0.5 here reflects the fact that the dissolution of  $\text{CaCO}_3$  increases  $C_T$  at half the rate at which it increases  $A_T$ . The extra term  $\psi_{\text{O:N}}(\text{AOU})$  corrects the estimate of dissolution of  $\text{CaCO}_3$  (derived from the change of  $A_T$ ) for the slight effect on alkalinity of the release of nitrate ion during remineralization of organic matter (Brewer and Goldman, 1976).

In a case study of the AAIW, flowing from its formation region at the Antarctic Polar Front to the low latitude South Atlantic, Brewer (1978) was able to calculate  $C_T^0$  over the 45 °S to 4 °S range, and from this derived the corresponding atmospheric  $p\text{CO}_2$  value to decrease from ~300  $\mu\text{atm}$  at 45 °S to ~250  $\mu\text{atm}$  between 20 °S and the Equator. Taking into account the  $-30 \pm 10 \mu\text{atm}$  range of the  $p\text{CO}_2$  disequilibrium with the atmosphere at the formation region at 50 °S, a preindustrial atmospheric  $p\text{CO}_2$  of ~280  $\mu\text{atm}$  was obtained. Similarly, Chen and Millero (1979) reported the gradual increase of oceanic  $\text{CO}_2$  for the intermediate depth salinity minimum and the deep temperature minimum along a complete Atlantic section (50 °S-50 °N).

The  $C_{\text{ant}}$  of a water sample can be calculated by subtracting from  $C_T^0$  the *pre-industrial* value of  $C_T^0$  ( $C_{T \text{ preind}}^0$ ; Poisson and Chen, 1987; Körtzinger et al., 1998):

$$C_{\text{ant}} = C_T^0 - C_{T \text{ preind}}^0 \quad (6-2)$$

The  $C_{T \text{ preind}}^0$  is assumed to be equal (and constant through time) for all samples within a water mass, and is generally obtained from the interior of the water mass under consideration, if that can be determined (from absence of anthropogenic tracers such as tritium or CFCs) to be still uncontaminated with  $C_{\text{ant}}$  (i.e.,  $C_{T \text{ preind}}^0 = C_{T \text{ interior}}^0$ ). For more shallow water masses, however,

even the inner part may have already become contaminated with  $C_{ant}$ . For such cases, one needs to resort to calculating  $C_{T\ preind}^0$  using Eq. (6-3):

$$C_{T\ preind}^0 = f(S, T, A_T^0, pCO_{2,preind}) \quad (6-3)$$

where  $pCO_{2,preind}$  is the assumed  $pCO_2$  of the surface water in preindustrial times. However, because subducting waters are generally not in equilibrium with the overlying atmosphere (Gruber et al., 1996; Takahashi et al., 2009), any assumed value of  $pCO_{2,preind}$  is debatable, which jeopardizes the application of the  $C_T^0$  approach in shallower, more recently ventilated waters masses. Several additional problems of the  $C_T^0$  approach should be mentioned. The inherent assumption of  $pO_2$  equilibrium (for calculation of AOU) with the atmosphere may be invalid, and is of strong influence on the calculated  $C_{ant}$ . For example, in the Southern Ocean the air-sea gas exchange is hampered by ice cover and Lo Monaco et al. (2005a,b) assume a mean undersaturation of 12%, yielding an about  $7 \mu\text{mol kg}^{-1}$  higher  $C_{ant}$  in the WSBW than in the case of  $O_2$  equilibrium with the atmosphere. Moreover, the stoichiometric ratio between the consumption of oxygen and production of  $CO_2$  ( $\psi_{O,C}$ ) is not uniform but varies between oceans and depth intervals, significantly affecting the  $C_{ant}$  (Wanninkhof et al., 1999). Furthermore, over the years, progressively less of the old waters will remain suitable to serve as pre-industrial reference. Moreover, although the detection of more recently emitted transient tracers (notably CFCs,  $^3H$ , ~1950-1960 era) shows a water sample is not pristine anymore, the absence of such tracers does not necessarily imply the absence of  $C_{ant}$ , for which emission commenced already at ~1780. Finally, a constant disequilibrium value of  $pCO_2$  between air and sea is assumed, yet in reality this value likely varies over the years (Metzl, 2009).

### 6.3.1.2. $C_{ant}$ : the $\Delta C^*$ approach

The  $\Delta C^*$  technique (Gruber et al., 1996) overcomes an important shortcoming of the  $C_T^0$  method in that it allows the  $pCO_2$  disequilibrium in the formation region to be quantified from measurements even for water masses that are contaminated with  $C_{ant}$ , provided that the age of the water sample is known. The  $\Delta C^*$  technique defines  $C_{ant}$  as follows:

$$C_{ant} = C_T^0 - C_{eq280} - C_{diseq} \quad (6-4)$$

The first two terms on the right hand side of (4) comprise “ $\Delta C^*$ ” such that:

$$C_{ant} = \Delta C^* - C_{diseq} \quad (6-5)$$

Here,  $C_T^0$  of the water sample is calculated according to Eq. (6-1),  $C_{eq280}$  is the hypothetical  $C_T^0$  of the water if it were in  $pCO_2$ -equilibrium with the preindustrial atmosphere of  $280 \mu\text{atm}$  (at the  $S$ ,  $T$  and  $A_T^0$  of the sample), and  $C_{diseq}$  represents the small difference versus  $C_{eq280}$  due to air-sea  $pCO_2$  disequilibrium in the formation area. Because  $C_{diseq}$  is not expected to be the same for all water masses, it is generally determined for each of a number of isopycnal intervals (layers of water between distinct lines of equal density).

For the deepest isopycnal intervals,  $C_{diseq}$  is obtained by observing  $\Delta C^*$  versus (generally) latitude. Such a plot shows  $\Delta C^*$  decreasing from the higher latitude formation regions toward the equator (reflecting the higher  $C_T$  in recently ventilated waters) where at some lati-

tude it reaches a baseline level (extending toward the equator) comprising all samples that have a pre-industrial ventilation history. The mean of these pre-industrial samples is taken to represent the mean  $C_{\text{diseq}}$  of the isopycnal interval. For example, Gruber et al., (1996) show that the deep (>2000 m) water masses in the North Atlantic south of Iceland have a  $C_{\text{diseq}}$  of about  $-16 \mu\text{mol kg}^{-1}$ , corresponding to a  $\Delta p\text{CO}_2$  of about  $-32 \mu\text{atm}$ . This suggests that these waters generally have not completed the process of taking up  $\text{CO}_2$  from the atmosphere before they were subducted.

For shallower isopycnal intervals, no such baseline of  $\Delta C^*$  may be observed, due to the fact that the whole interval is already contaminated with  $C_{\text{ant}}$ , such that  $C_T$  and thereby  $\Delta C^*$  are elevated above preindustrial levels. However, with knowledge of the ventilation age of the samples (obtained independently from CFCs,  $^3\text{H}$ - $^3\text{He}$  or other transient tracers), an alternative may be calculated for  $C_{\text{eq}280t}$  that is, a  $C_{\text{eq}t}$  referenced to the known atmospheric  $p\text{CO}_2$  of the year  $t$  of formation. For instance, for a sample with ventilation age dating from the year 1990, one would calculate  $C_{\text{eq}353}$ . Subsequent assessment, over a range of latitudes (or ages), of  $\Delta C^*$  (now called  $\Delta C^*$ ) once again yields a baseline that may be taken to represent  $C_{\text{diseq}}$ . Gruber et al., (1996) in this manner show that relatively shallow water masses (those originally formed in the seas north of Iceland) exhibit a  $\Delta p\text{CO}_2$  of about  $-85 \mu\text{atm}$ . Once  $C_{\text{diseq}}$  is determined for each isopycnal interval, the value of  $C_{\text{ant}}$  is easily calculated using Eq. (6-5).

Because  $C_{\text{diseq}}$  is inferred as the mean difference between  $C_T^0$  and  $C_{\text{eq}280}$  (or  $C_{\text{eq}t}$ ), its value not only represents the effects of the air-sea disequilibrium of  $p\text{CO}_2$  at the time of subduction, but also the effects of a conceivable  $p\text{O}_2$  disequilibrium (which affects  $C_T^0$ ). Because  $C_{\text{diseq}}$  is subtracted from  $\Delta C^*$  to obtain  $C_{\text{ant}}$ , any effect on  $C_{\text{ant}}$  is cancelled out. In the same way,  $C_{\text{diseq}}$  includes the effects of any inaccuracy of the remineralization ratio values  $\psi_{\text{O,C}}$  and  $\psi_{\text{O,N}}$  of Eq. (6-1), which are also cancelled out (again through  $C_T^0$ ), thereby removing another source of uncertainty that is present in the  $C_T^0$  method.

Using the  $\Delta C^*$  method, Sabine et al. (2004) used ocean interior measurements obtained during WOCE and JGOFS studies of the 1990s to constrain the inventory of  $C_{\text{ant}}$  of the world ocean to  $118 \pm 19 \text{ PgC}$  in 1994.

Matsumoto and Gruber (2005) assessed the  $\Delta C^*$  method and realized that biases in its results are introduced by the assumption of constant (over time)  $C_{\text{diseq}}$  and the simplified derivation of ventilation age from transient tracers (see also Hall et al., 2004). Matsumoto and Gruber (2005) suggest that these two biases can be minimized by (i) varying  $C_{\text{diseq}}$  as a function of the uptake of  $C_{\text{ant}}$  itself, and by (ii) taking into account the age spectrum of water when determining ventilation ages, respectively. However, for the Southern Ocean the second suggestion (ii) is notably difficult, because the age spectrum of the locally formed water masses is strongly bimodal (Khatiwala 2002; Hall, 2002; Peacock and Maltrud, 2005), and therefore difficult to establish using tracer measurements. Therefore, application to the Southern Ocean of the  $\Delta C^*$  approach remains challenging.

### 6.3.1.3. $C_{\text{ant}}$ : the TrOCA approach

Application of the TrOCA approach (Tracer combining Oxygen, Carbon and Alkalinity; Touratier and Goyet, 2004a,b) is more straightforward. The approach requires less variables to be measured (only  $\text{O}_2$ ,  $C_T$ ,  $A_T$  and  $\theta$ ), and avoids the rather complex estimation of air-sea disequi-

libria for  $pCO_2$ . In the TrOCA method, first the effects of remineralization of organic matter and dissolution of calcium carbonate are compensated:

$$\text{TrOCA} = O_2 + 1.2 \cdot C_T - 0.6 \cdot A_T \quad (6-6)$$

The resulting value of TrOCA includes the  $C_{\text{ant}}$  component. Next, if the preindustrial TrOCA ( $\text{TrOCA}^0$ ) value of the water sample can be obtained, this  $C_{\text{ant}}$  component can be calculated:

$$C_{\text{ant}} = (\text{TrOCA} - \text{TrOCA}^0) / 1.2 \quad (6-7)$$

For old, deep water masses that have not been in contact with the modern atmosphere, the value of  $\text{TrOCA}^0$  is assumed to be equal to TrOCA. In order to obtain values of  $\text{TrOCA}^0$  in shallower water masses (ventilated after 1780), the observed relationship in the deep waters of TrOCA and potential temperature (and in subsequent work also  $A_T$ ; Touratier et al., 2007) is extrapolated to the higher  $\theta$  of the shallower, warmer, water masses. However, Yool et al., (2010) argue that the extrapolation of a single  $\text{TrOCA}^0$ -versus- $\theta$  relationship toward shallower, warmer waters cannot represent the full range of  $pO_2$ - and  $pCO_2$ -disequilibria encountered in the different involved formation regions and processes. Therefore, the TrOCA approach necessarily can likely only be applied on a sub-basin scale. In the deep Southern Ocean, no required pristine water mass exists anymore, as suggested by the fact that anthropogenic CFCs are found at all depths (Klatt et al., 2002), which complicates the derivation of a locally predictive relationship for  $\text{TrOCA}^0$ .

#### 6.3.1.4. $C_{\text{ant}}$ : the Transit Time Distribution (TTD) approach

The Transit Time Distribution approach (TTD; Hall et al., 2002; McNeil et al., 2003; Waugh et al. 2006) relies on a combination of measurements of one or more oceanic anthropogenic transient tracers (e.g., CFCs,  $SF_6$ ), their atmospheric time histories, and hydrographic data to estimate the most likely ventilation age distribution (i.e. the TTD) of water parcels in the ocean interior. The inferred TTDs are then combined with the assumed surface water time history of  $C_{\text{ant}}$  to calculate the ocean interior concentrations of  $C_{\text{ant}}$ . Waugh et al. (2006) have used the TTD method to estimate a total inventory of  $C_{\text{ant}}$  for the global ocean of 94-121 PgC for 1994.

The complete independence of the TTD method from measurements of oceanic  $C_T$  makes it a valuable complement to  $C_T$ -based approaches. However, like some of the previous approaches, the TTD approach requires assumptions of the time histories of  $C_{\text{ant}}$  and CFC in the surface ocean, which are strongly dependent on the unknown (and likely variable) time histories of equilibration with the atmosphere. Additionally, as already mentioned in text section 6.3.1.2, the shape of the TTD may be difficult to quantify specifically in the Weddell Gyre, where upwelling, subduction and entrainment occur on small temporal and spatial scales. The concurrent measurements of transient tracers with strongly differing atmospheric time histories (e.g., CFC-12 and  $SF_6$ ; Walker et al., 2000; Tanhua et al., 2008; Fine, 2011) in principle allows for some of the uncertainty of the shape of the TTDs to be resolved. However, no datasets of  $SF_6$  in the Weddell Gyre have been described in the literature yet.

### 6.3.1.5. $C_{\text{ant}}$ : the Transient Steady State (TSS) approach

Given a sufficiently long time, an exponentially increasing concentration of  $C_{\text{ant}}$  at the surface of the ocean will result in a similar exponential increase of  $C_{\text{ant}}$  at depth, the so called Transient Steady State (TSS; Tanhua et al., 2007). Therefore the *rate of increase* of  $C_{\text{ant}}$  at any location in the ocean interior is proportional to the *concentration* of  $C_{\text{ant}}$  (Gammon et al., 1982; Tanhua et al., 2007). This method thus allows the derivation of a value of  $C_{\text{ant}}$  given only the rate of change of  $C_{\text{ant}}$ . However, just as for most of the above methods, the finally derived  $C_{\text{ant}}$  concentration depends strongly on the assumed time history of surface water  $p\text{CO}_2$ . Nevertheless, this technique will be used in below section 6.7.5 to convert the determined rate of increase of  $C_{\text{ant}}$  in the deep Weddell Sea into an estimate of the total concentration of  $C_{\text{ant}}$ .

### 6.3.2. Determination of the increase $\Delta C_{\text{ant}}$ between two consecutive cruises

The expected increase of  $C_T$  at the ocean surface due to the accumulation of  $C_{\text{ant}}$  is about  $1 \mu\text{mol kg}^{-1} \text{a}^{-1}$ , against a background concentration in the order of  $2000 \mu\text{mol kg}^{-1}$ . In deeper waters, this increase will be smaller and therefore more difficult to discern against the large background value. Moreover, the signal may be obscured by variability of formation and mixing of deep water masses (Fahrbach et al., 2004) and variability of biological processes (Sabine et al., 2008). We discuss three published approaches for quantifying the increase in  $C_{\text{ant}}$  ( $\Delta C_{\text{ant}}$ ) between two successive cruises along one and the same transect.

#### 6.3.2.1. $\Delta C_{\text{ant}}$ : determination of the change in $C_T$ or $C_T^0$

Early determinations of the increase of  $C_{\text{ant}}$  between (once-)repeated ocean sections were reported by Hoppema et al. (1998) and Peng et al. (1998). The former study in the western Weddell Sea explicitly considered variable formation properties of water masses. The latter study accounted for the confounding effects of variability in such natural processes as water mass mixing and biology, evaluating the increases of  $C_T^0$  along isopycnal surfaces.

#### 6.3.2.2. $\Delta C_{\text{ant}}$ : the Multivariate Linear Regression (MLR) approach

Wallace (1995) proposed the use of a Multivariate Linear Regression (MLR) technique to assess the changes in  $C_{\text{ant}}$  between two subsequent occupations of the same ocean station or section. The technique correlates measured values of  $C_T$  with a suite of ancillary tracers in order to determine these changes, while accounting for some of the variability in hydrographic conditions and biological activity.

Firstly, for one single cruise, a mathematical relationship is derived between the measured  $C_T$  and the values of ancillary physical and biogeochemical properties that are known to be related to the natural subsurface variability of  $C_T$ . These properties (generally  $\theta$ ,  $S$ , one or more nutrients,  $\text{O}_2$  or AOU and  $A_T$ ) are independent of increasing  $C_{\text{ant}}$ , but represent the natural processes affecting  $C_T$ : the mixing of water masses, remineralization of organic matter and dissolution of  $\text{CaCO}_3$ . The approach does not require knowledge about remineralization ratios or mixing processes. The derived MLR is used to predict the values  $C_T^{\text{MLR}}_1$ , and by comparison with the actually measured  $C_T$  values, the residuals ( $C^{\text{MLR}}_{\text{residual},1}$ ) are obtained. In



practice, these residuals are normally distributed around zero, with a typical standard deviation in the order of  $4 \mu\text{mol kg}^{-1}$ . Subsequently, for a second cruise some years later, the MLR relationship of the first cruise is combined with the ancillary values of the second cruise, to derive  $C_{\text{residual},2}^{\text{MLR}}$ . Finally, by comparison of the depth profiles of  $C_{\text{residual},1}^{\text{MLR}}$  and  $C_{\text{residual},2}^{\text{MLR}}$  the apparent increase  $\Delta C_{\text{ant}}$  is derived.

Application in the Indian Ocean by Sabine et al. (1999) resulted in an estimate of the increase of  $C_{\text{ant}}$  in the Indian Ocean north of  $35^\circ\text{S}$ . McNeil and coworkers used this technique to demonstrate the invasion of both  $C_{\text{ant}}$  and the  $\delta^{13}\text{C}_T$ -signal into the Southern Ocean south of Australia (McNeil et al., 2001a,b). Peng et al. (2003) reported an increase of anthropogenic  $\text{CO}_2$  in the Pacific Ocean over two decades. Matear and McNeil (2003) found reasonable agreement between the MLR-method and the TTD technique (section 6.3.1.4) in the Southern Ocean.

### 6.3.2.3. $\Delta C_{\text{ant}}$ : the Extended Multivariate Linear Regression (eMLR) approach

In the original MLR approach (section 6.3.2.2), the derived  $\Delta C_{\text{ant}}$  is affected by errors of both the suite of ancillary measurements and the measured  $C_T$  values. The extended MLR (eMLR; Friis et al., 2005) aims to minimize the effect of the errors of the ancillary measurements. Here one derives, again using MLR, a unique relationship for each of two cruises and uses the difference between the coefficients of the two relationships as a predictor of  $\Delta C_{\text{ant}}$  between the cruises. The eMLR approach has been applied by several investigators (e.g., Olsen et al., 2006; Tanhua et al., 2007; Sabine et al., 2008; Hauck et al., 2010). The approach is deemed less sensitive than the original MLR-method to systematic errors (biases) in the ancillary data of each cruise. Nevertheless, the sensitivity of the results to biases in the measurements of  $C_T$  of either involved cruise remains. This jeopardizes the application of this method, notably in the Weddell Gyre where time trends in  $C_{\text{ant}}$  are deemed to be small.

Every technique used to determine anthropogenic changes in  $C_T$  between two cruises is sensitive to biases in the data of either cruise. Such biases are not uncommon: before the introduction of certified reference material (CRM: Dickson, 2001), analytical biases in  $C_T$  and  $A_T$  could be more than  $10 \mu\text{mol kg}^{-1}$  (Stoll et al., 1993). Even today, now that values of  $C_T$  and  $A_T$  are more accurate, the measurements of dissolved nutrients and oxygen occasionally remain inaccurate by several percent. Dataset synthesis efforts like GLODAP (Key et al. 2004) and CARINA (Key et al. 2010) aim to identify and remove these biases (Tanhua et al., 2010), but the resulting datasets are obviously not as good as what could analytically have been achieved at the time, or can be achieved nowadays. Until primary measurements of required ancillary parameters reach a level of accuracy comparable to that attained in the measurements of  $C_T$  and  $A_T$  themselves, the interpretation of results of the back-calculations and MLR-type methodology will be ambiguous to some extent. Moreover, Levine et al. (2008) argue and illustrate that the (e)MLR approaches do not necessarily yield accurate results in the presence of trends in the ancillary data that persist over the period of interest (so-called *secular trends*). The warming of shallow water masses due to global warming is a case in point.

### 6.3.3. The Time Series Residuals (TSR) approach for multiple repeat cruises along one transect

Here we introduce an approach for extracting from a suite of multiple cruises along one transect the rate of increase of  $C_{\text{ant}}$  during the time interval spanning these cruises. This TSR-approach is applied to a suite of 10 cruises along the Prime Meridian transect in the Southern Ocean during the 1973-2008 time interval. The inclusion of 10 cruises aims to minimize the effects of systematic errors in both the suite of ancillary measurements and in the measured  $C_T$  values. For 10 cruises, one overall MLR relationship is determined. Next, this overall relationship is used to calculate  $C_T^{\text{TSR}}$ , and by comparison with actually measured  $C_T$ , the  $C_{\text{residual}}^{\text{TSR}}$  is derived. Finally  $C_{\text{residual}}^{\text{TSR}}$  is regressed against sampling date (1973-2008). Following the same premises as the MLR and eMLR approaches, it is expected that increasing (over time) values of  $C_{\text{residual}}^{\text{TSR}}$  reflect the increase in the concentration of  $C_{\text{ant}}$  in a water mass. As with the MLR method, the application of the TSR approach does not require knowledge of the surface water gas disequilibrium or remineralization ratios.

Seasonal variability in  $C_T$  in shallow waters is to a large extent represented by the MLR (Friis et al., 2005). Therefore, the TSR method allows the determination of time trends in  $C_{\text{ant}}$  (i.e.,  $C_{\text{residual}}^{\text{TSR}}$ ) in shallow waters. This in contrast with  $C_T^0$  and  $C_T$ , which both are expected to show strong variations in shallow waters between the different seasons in which the data were collected.

## 6.4. Data collection.

The shipboard methods of the most recent cruise are described (section 6.4.1), followed by the chosen database of the preceding nine cruises (section 6.4.2). Of all ten cruises, stations south of  $\sim 55^\circ\text{S}$  and (generally) within  $5^\circ$  of longitude from the Prime Meridian were selected, representative for the Weddell Gyre. The locations of all stations are shown in Figure 6.3. The cruises span the period from 1973 to 2008.

### 6.4.1. Shipboard analyses

The most recent data used in this paper, from *PFS Polarstern* cruise ANT-XXIV/3 (Cape Town – Punta Arenas, 10 February – 16 April 2008; Fahrbach and De Baar, 2010) have not been published before. During this cruise, about 2800 samples were analyzed on two identical instruments (VINDTA 3C, MARIANDA, Kiel, Germany), with each instrument measuring both  $C_T$  and  $A_T$ . Collection and analysis was in accordance with the standard operating procedures outlined by Dickson et al. (2007). Samples were analyzed immediately after sampling, hence were not poisoned. Occasionally, samples were analyzed on both instruments concurrently, thereby allowing for instrument-to-instrument comparison.

Measurements of  $C_T$  were performed using the coulometric method (Johnson et al., 1993). Determinations of  $A_T$  were performed by an acid titration following the standard settings of the VINDTA (Mintrop et al., 2000). In order to set the measurement accuracy, certified reference material (CRM, Dickson 2001) was analyzed at least three times per day. On both instruments, measurements of CRM deviated from the certified values less than 0.5% for both  $C_T$  and  $A_T$  (i.e., less than circa  $12 \mu\text{mol kg}^{-1}$ ). Post-cruise processing and correction of the data



resulted in a dataset that is deemed to be of excellent quality for  $C_T$ , with typical short-term reproducibility of around  $1.4 \mu\text{mol kg}^{-1}$  for both instruments. Intercomparability of the instruments is considered to be excellent, with the difference in final  $C_T$  values between them (as inferred from about 400 samples that were run on both instruments) being  $0.1 \pm 1.9 \mu\text{mol kg}^{-1}$ . Results of  $C_T$  of the two instruments were merged into one dataset, of which the overall accuracy is estimated to be better than  $\pm 2 \mu\text{mol kg}^{-1}$ . Results for  $A_T$  of one of the two instruments were discarded due to excessive drift. The estimated accuracy of the retained  $A_T$  dataset of the other instrument is  $\pm 4 \mu\text{mol kg}^{-1}$ .

Data for dissolved oxygen was obtained from *in situ* sensors that were regularly calibrated against Winkler titrations, with a reported final accuracy of  $\pm 4.5 \mu\text{mol kg}^{-1}$ . Measurements of dissolved nutrients (silicate, phosphate and nitrate) were performed colorimetrically and on board with an auto-analyzer. The combined accuracy and precision of these three measurements is considered to be better than  $\pm 0.5\%$ ,  $\pm 0.5\%$  and  $\pm 1.0\%$ , respectively. Measurements that were concurrently made on a preliminary batch of the novel reference material for nutrients in seawater (RMNS, distributed by KANSO co. [www.kanso.co.jp](http://www.kanso.co.jp); Aoyama et al., 2008) confirm this accuracy.

#### 6.4.2. Additional data

From the GLODAP 1.1 database (Key et al., 2004) and the CARINA database (Key et al., 2010) the data of six cruises in the vicinity of the  $0^\circ$ -meridian were extracted (Table 6.3). For each cruise, we used the data that had received primary quality control (outliers removed, conversion to common units), but were not yet adjusted for internal consistency, because for our application the desired internal consistency will be tailored to the local region. (Please notice that the final product of GLODAP and CARINA has been adjusted for global internal consistency). Data of  $C_T$  of cruises ANT-XV/4, ANT-XXII/3 and ANT-XXIV/2, which are not available in GLODAP or CARINA, have been described before and were obtained from the respective investigators (see references in Table 6.3).

#### 6.5. Data processing

This study aims to quantify the rates of storage of  $C_{\text{ant}}$  in the Weddell Gyre, using data from 10 cruises conducted between 1973 and 2008. The use of multiple cruises is expected to reduce the susceptibility of the results to biases in individual cruises. Firstly, we will determine time trends directly in the actual measured data of  $C_T$  that have been collected during multiple cruises along the same ocean section. Secondly, we perform a similar time trend assessment but now using calculated  $C_T^0$  (section 6.3.1.1), relying on additional measured variables ( $\theta$ ,  $S$ ,  $O_2$  and  $A_T$ ). Lastly, the determined time trends of  $C_T$  will be separated into their natural components and anthropogenic (i.e.  $C_{\text{ant}}$ ) components using the TSR method outlined in section 6.3.3. Moreover, for the sake of comparison with previous studies in the region, the concentration of  $C_{\text{ant}}$  will be determined with another approach, the TrOCA method.

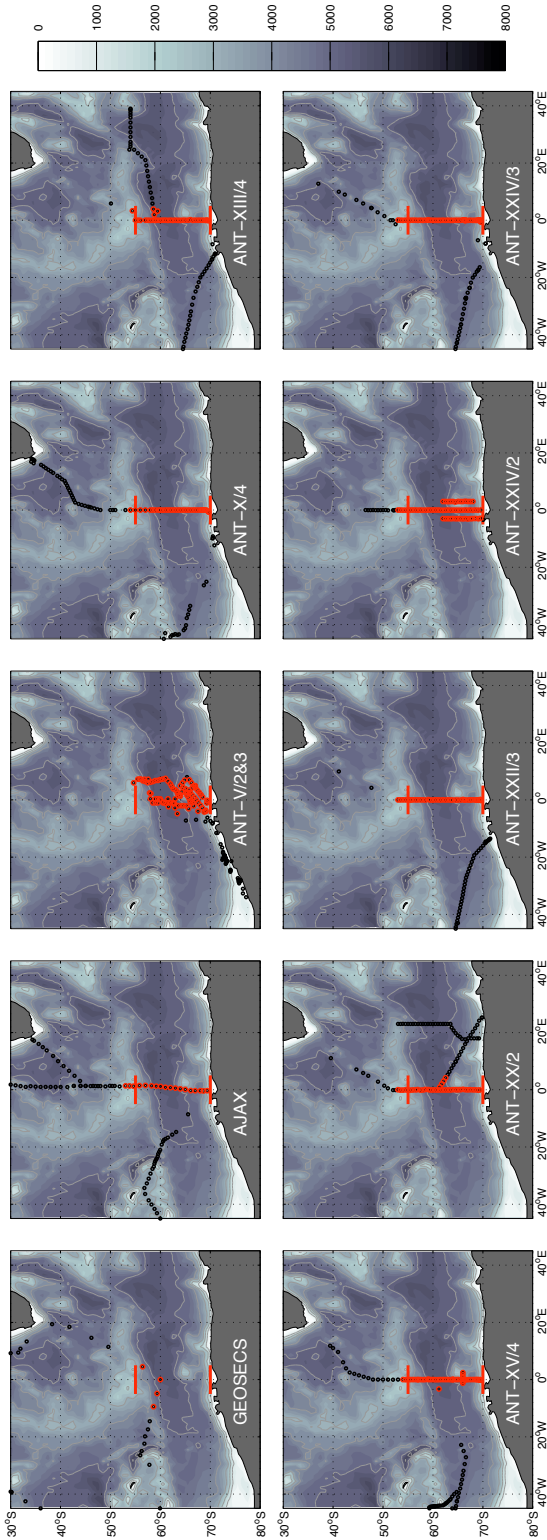


**Figure 6.3.** Locations of the oceanographic sampling stations (red dots) of the 10 cruises used in this study. Black dots indicate locations of stations that were not used. The color scale represents the bottom topography, in 1000 m intervals. The two horizontal red lines (at 55°S and 70°S) in each panel respectively indicate the northern and southern extent of the part of the section that is investigated in this study. For several cruises, data from a few stations north of 55°S are used in the data gridding procedure.

### 6.5.1. Normalization in lower Warm Deep Water (WDW) and upper Weddell Sea Deep Water (WSDW).

In the Weddell Gyre, the southernmost part of the  $0^\circ$ -meridian section, the lower extent of the WDW together with the upper part of the WSDW, is considered the least ventilated water body (Fahrbach et al., 2011, this issue; to be concise, this combined water body will in the context of the normalization procedure be referred to as IWDW/uWSDW). Indeed, over the 1973-2008 period of observations, the  $C_T$  in this water body is in steady state (Figure 6.4), except for the strongly outlying data of AJAX (1984) and ANT-V/2&3 (1986). Moreover, the observed values of major nutrients (silicate, nitrate and phosphate) and dissolved oxygen in the IWDW/uWSDW also are in steady state, i.e., there are no systematic changes discernable in biogeochemical processes (data not shown). Nevertheless, for each cruise there may exist a systematic offset due to calibration uncertainties. In order to remove these offsets (that in turn might give rise to erratic time trends), a normalization is applied to bring the values in the WDW of each cruise to the mean of all 10 cruises. Following Hoppema et al. (2001), for each cruise a subset of the data (latitude:  $57^\circ\text{S}$  to  $66^\circ\text{S}$ , potential temperature ( $\theta$ ):  $-0.4^\circ\text{C}$  to  $0.2^\circ\text{C}$ ) of the parameter to be adjusted is linearly regressed against  $\theta$  and the intercept at  $\theta=0^\circ\text{C}$  is determined. For each cruise, the difference between this intercept and the mean intercept at  $0^\circ\text{C}$  of the entire dataset (in the case of  $C_T$ :  $2262.7 \mu\text{mol kg}^{-1}$ , see Figure 6.4) is taken as the required adjustment. Adjustments determined in this manner for all relevant parameters of all cruises are listed in Table 6.3 (i.e.,  $C_T$ ,  $A_T$ ,  $O_2$ ,  $\text{NO}_3$ ,  $\text{PO}_4$ , Si. Data of CFCs were not adjusted). At the latitudinal range considered, the used temperature range coincides with a depth range of about 800 m to 2200 m, i.e., the IWDW/uWSDW. The NADW in the South Atlantic Ocean is

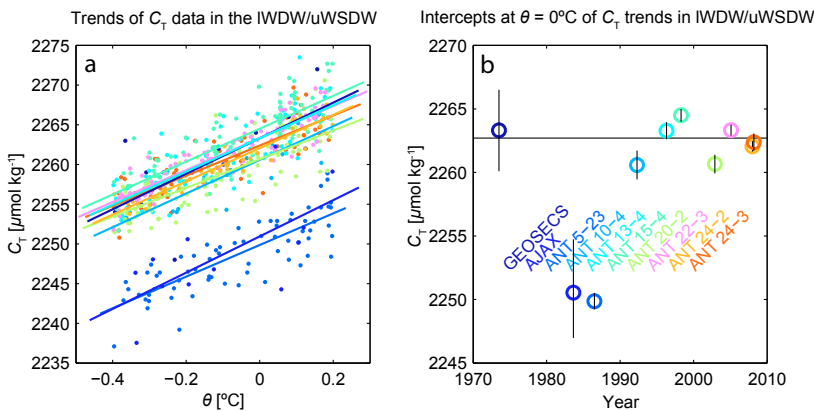


**Figure 6.4.** Example for  $C_T$  of the procedure followed to normalize cruise data in the lower WDW and upper WSDW (IWDW/uWSDW). See section 6.5.1 for details. **(a)** Regressions of measured  $C_T$  [ $\mu\text{mol kg}^{-1}$ ] versus potential temperature ( $\theta$ ) [ $^\circ\text{C}$ ] of all 10 cruises. The strongly outlying regression lines represent the data of cruises AJAX (1984) and ANT-V/2&3 (1987). **(b)** The determined intercepts at  $\theta=0^\circ\text{C}$  of the regressions in panel a). The black horizontal line indicates the mean intercept ( $2262.7 \mu\text{mol kg}^{-1}$ ) of all cruise data (ANT-V/2&3 excepted). The black vertical lines represent the 95% confidence interval of each intercept. Data of each cruise were adjusted to make the cruise-specific intercept coincide with the mean intercept of all (non-outlying) cruises.

**Table 6.3.** Relevant details of the cruises of which data are used in this study. Date refers to the months of relevant sampling at the Prime Meridian. Adjustments applied to the data are additive in  $\mu\text{mol kg}^{-1}$  for  $C_T$  and  $A_T$ , and multiplicative for the other parameters (rounded to the nearest 0.5%). Adjustments without brackets are those applied in the current study, required to obtain consistency in the IWDW/uWSDW (text section 6.5.1). Adjustments between brackets are those suggested in the CARINA and GLODAP dataset compilation efforts, for comparison. The column ‘CRM’ states the use of Certified Reference Material (CRM; Dickson, 2001) during the analyses of  $C_T$  and  $A_T$ . In the most recent cruise ANTE-XXIV/3 (2008) reference material (Aoyama et al., 2008) was additionally used in nutrient analyses. For background information regarding these cruises please refer to the listed references or the CARINA (<http://cdiac.ornl.gov/oceans/CARINA/>) or GLODAP (<http://cdiac.ornl.gov/oceans/GLODAP/>) literature.

Cruise	Date	Ship	Adjustments performed to the data										CRM	$C_T$ -relevant reference
			$C_T$	$A_T$	$O_2$	$NO_3$	$PO_4$	Si						
GEOSECS	Jan 1973	Knorr	-0.6 (a) (0)	-5 (-10)	0% (-1%)	+1% (0%)	+1% (+2%)	-2% (0%)	no	Bainbridge, 1981				
AJAX	Jan-Feb 1984	Knorr	+10.9 (+8)	+8 (0)	-2% (-1%)	-1% (0%)	+2% (0%)	-1% (-2%)	no	Chipman, 1986				
ANT-V/2-3	Jul-Dec 1986	Polarstern	+12.8 (+12)	+7 (b) (0)	0% (0%)	+3% (+3%)	+0.5% (0%)	-0.5% (0%)	no	Schmack-Schiel, 1987				
ANT-X/4	Jun-Jul 1992	Polarstern	+2.1 (0)	no data	-1% (0%)	-0.5% (-2%)	-0.5% (-2%)	0% (-2%)	no	Hoppema et al., 1995				
ANT-XXIII/4	April 1996	Polarstern	-0.6 (-4)	no data	-0.5% (+1%)	+3.5% (+2%)	+2.0% (1%)	+2.0% (+5%)	yes	Hoppema, 1998				
ANT-XV/4	May 1998	Polarstern	-1.8 (NA)	no data	-0.5 (NA)	-1.0% (0%)	-2.0% (0%)	-0.5% (NA)	yes	Hoppema, 2004				
ANT-XX/2	Dec 2002	Polarstern	+2.0 (NA)	no data	+0.5% (NA)	-2.0% (NA)	no data	-2.0% (NA)	yes	Bakker et al., 2008, Geibert et al., 2010				
ANT-XXII/3	Feb 2005	Polarstern	-0.6 (NA)	no data	+2.5% (NA)	-1.5% (NA)	0% (NA)	0% (NA)	yes	Hoppema, 2007				
ANT-XXIV/2	Jan 2008	Polarstern	+0.6 (NA)	0 (NA)	0% (NA)	0 (NA)	no data	no data	yes	Hauck et al., 2010				
ANT-XXIV/3	Feb 2008	Polarstern	+0.3 (NA)	-1 (NA)	+1.5% (NA)	0% (NA)	0% (NA)	0% (NA)	yes	this work				

(a)  $C_T$  of GEOSECS was measured potentiometrically, for all other cruises  $C_T$  was measured coulometrically.  
 (b)  $A_T$  of ANTE-V/2&3 was calculated by GLODAP from  $C_T$  and  $pCO_2$ .

much larger and even less ventilated than the IWDW/uWSDW and is deemed an even more suitable reference water mass, but cannot serve that purpose because five of the ten cruises in this study did not sample the NADW.

The spread of measurements around the regression line (Table 6.4, column 'rmse') is illustrative of the precision of the data of each cruise. Clearly, the precision of the analysis of  $C_T$  has generally improved over time, from  $4.0 \mu\text{mol kg}^{-1}$  during GEOSECS in 1973 to  $1.3 \mu\text{mol kg}^{-1}$  or  $2.2 \mu\text{mol kg}^{-1}$  for ANT-XXIV/2 and ANT-XXIV/3, respectively. The thus adjusted datasets for  $C_T$  and other parameters are highly internally consistent within the IWDW/uWSDW. However, the  $C_T$  data of AJAX (1984) are deemed to be of insufficient quality for this study due to low spatial sampling resolution and significant station-to-station biases that cannot be objectively resolved. Therefore, the  $C_T$  data of AJAX are excluded from further analysis (the remaining data of CFCs and  $A_T$  of AJAX will be used). Similarly, the southerly deep data (south of  $63^\circ\text{S}$  and deeper than 1500 m) of cruise ANT-X/4 are considered erroneously high by up to  $7 \mu\text{mol kg}^{-1}$  and are also excluded from analysis. Figure 6.5 shows sections of the IWDW/uWSDW-normalized  $C_T$  data. Although they are not (all) used in further analyses, the data of AJAX and ANT-X/4 are shown in Figure 6.5 for completeness. The performed adjustments are of similar magnitude as those applied in CARINA and GLODAP (Table 6.3).

### 6.5.2. Data gridding

Toward discerning a time trend over 35 years, all cruises are assigned equal weight. If this is not done, then a straightforward regression would cause overrepresentation of those cruises that have most measurements. Equal weighting of the data of each cruise is accomplished by resampling all data of interest ( $S$ ,  $\theta$ , CFC-12,  $C_T$ ,  $A_T$ ,  $O_2$ , nutrients) onto a common grid (spacing: 100 m depth and  $0.5^\circ$  latitude). The longitude of all data is set to  $0^\circ\text{E}$ . Bottom topography is assumed to be the same for all cruises, as extracted from a bathymetric dataset of the mean

**Table 6.4.** Details of the regression of  $C_T$  versus potential temperature of cruise data from the deeper part of the WDW and the upper part of the WSDW (IWDW/uWSDW). rmse: root mean square error (i.e., measure of spread of data around the regression line). Data were adjusted to yield an intercept of  $2262.7 \mu\text{mol kg}^{-1}$ . Although not obvious from these results, the data of  $C_T$  of AJAX (1984) were deemed to be of insufficient quality for inclusion in this study. Southerly, deep data of ANT-X/4 are deemed to be erroneously high, and are also not further used in this study either (see also Figure 6.5). See text section 6.5.1 for details.

Cruise	Intercept	Slope $^\circ\text{C}^{-1}$	rmse $\mu\text{mol kg}^{-1}$	$n$	adjustment $\mu\text{mol kg}^{-1}$	discarded data
GEOSECS	2263.3 $\pm$ 3.2	22.4 $\pm$ 13.5	4.0	15	-0.6	none
AJAX	2250.8 $\pm$ 2.1	21.2 $\pm$ 9.9	3.9	23	+10.9	all data
ANT-V/2&3	2249.2 $\pm$ 0.9	18.7 $\pm$ 4.4	2.7	48	+12.8	none
ANT-X/4	2260.5 $\pm$ 1.0	21.0 $\pm$ 5.1	2.1	22	+2.1	<63 $^\circ\text{S}$ & <1500 m
ANT-XIII/4	2263.3 $\pm$ 0.6	20.9 $\pm$ 2.9	2.4	91	-0.6	none
ANT-XV/4	2264.5 $\pm$ 0.5	20.7 $\pm$ 2.6	2.4	105	-1.8	none
ANT-XX/2	2260.8 $\pm$ 0.7	18.7 $\pm$ 3.3	3.3	116	+2.0	none
ANT-XXII/3	2264.3 $\pm$ 0.4	20.2 $\pm$ 2.1	1.7	79	-0.6	none
ANT-XXIV/2	2262.0 $\pm$ 0.4	20.9 $\pm$ 2.0	1.3	54	+0.6	none
ANT-XXIV/3	2262.4 $\pm$ 0.7	18.9 $\pm$ 3.1	2.2	64	+0.3	none

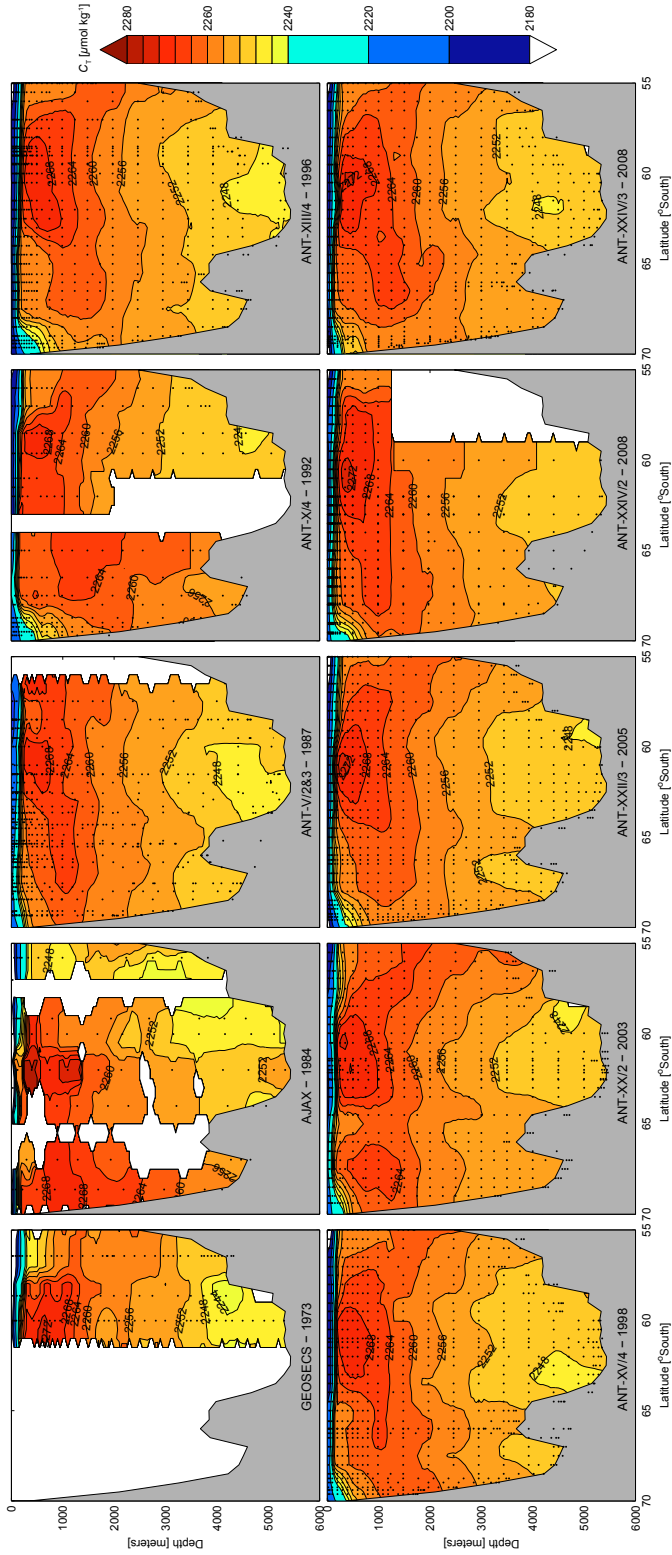


**Figure 6.5.** Section plots for the 10 cruises used in this study of  $C_T$  (after normalization in the IWDW/uWSDW; see text section 6.5.1 for details). Note that southerly, deep data ( $>63^\circ\text{S}$ ,  $>1500\text{ m}$ ) for ANT-X/4 and all data of AJAX are shown in this figure, although these data are not further considered in this study.



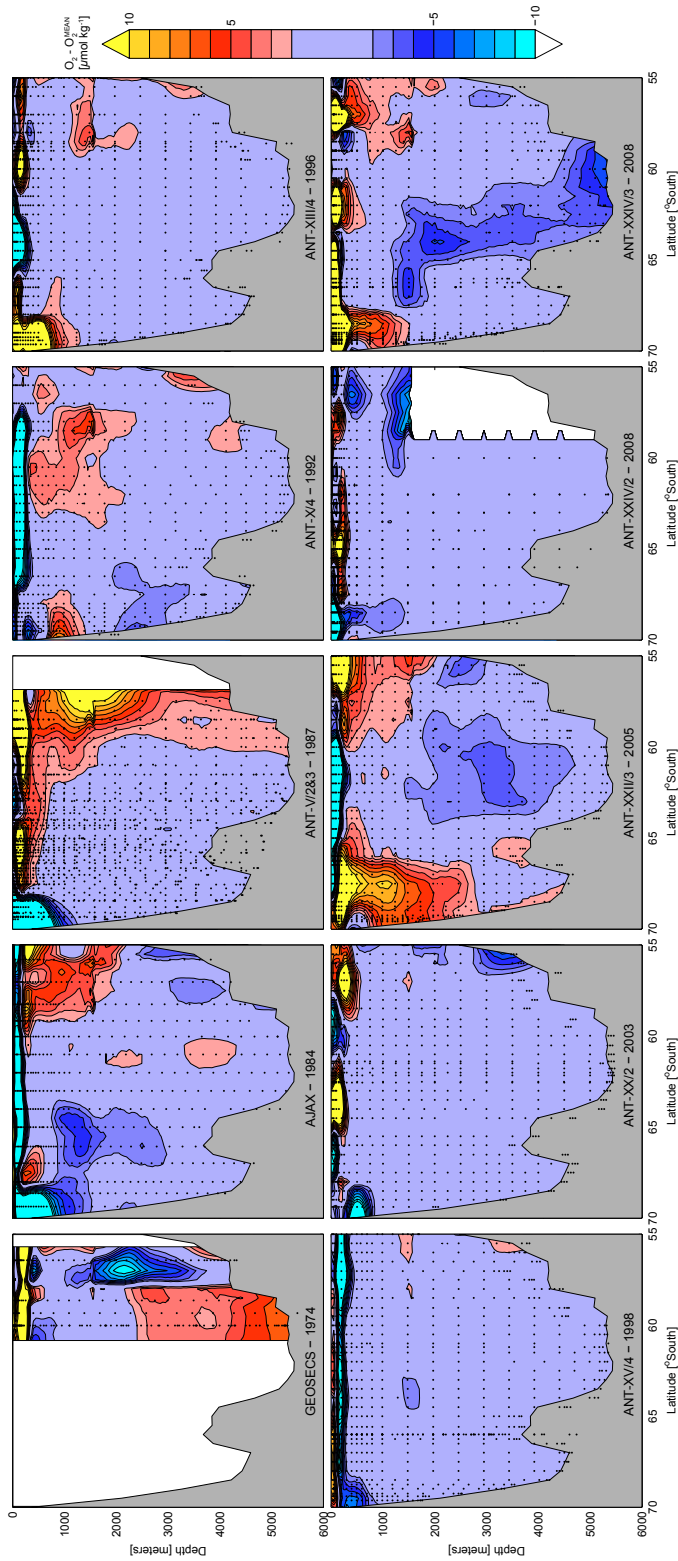


**Figure 6.6.** Section plots for the 10 cruises used in this study of the difference between (IWDW/uWSDW-normalized)  $O_2$  and  $O_2^{mean}$ . The latter is defined as the mean IWDW/uWSDW-normalized  $O_2$  of four selected, mutually consistent cruises: ANT-XIII/4, ANT-XV/4, ANT-XX/2 and ANT-XXIV/2. These section plots are deemed to be indicative of station-to-station bias in the reported data of  $O_2$ . These biases are not accounted for by the single normalization performed in this study. Because the data of  $O_2$  of ANT-XXIV/3, ANT-XXII/3 and of selected stations of ANT-V/2&3 (north of 63°S) and GEOSECS (north of 57°S) exhibit such bias they are excluded from this study, but are retained in this figure.

topography between 2 °W and 2 °E. Care was taken not to allow the gridding routine to extrapolate data too far into depths or latitudes where in fact no samples were collected.

### 6.5.3. Consideration of oxygen

Some cruises retain significant localized bias for  $O_2$ , even after the IWDW / uWSDW-normalization procedure outlined above. In order to illustrate this, we obtain a ‘best’ or ‘mean’ section of  $O_2$  by averaging the very consistent  $O_2$  sections of recent cruises ANT-XIII/4, ANT-XV/4, ANT-XX/2 and ANT-XXIV/2, and make section plots of the difference of this  $O_2^{\text{mean}}$  and each of the  $O_2$  datasets of all ten cruises used in this study (Figure 6.6). It may be observed that the applied single-adjustment approach is not sufficient for eliminating all biases in the  $O_2$  datasets of all cruises. For example, an offset may be seen for ANT-XXIV/3 in the deep water between 60 °S and 65 °S. This anomaly is not observed for ANT-XXIV/2 only 2 months earlier. Similarly, cruises GEOSECS, ANT-V/2&3 and ANT-XXII/3 also appear to have calibration problems, although for GEOSECS, which is far in the past from the subsequent cruises, deviations in the deep water arguably might be reflective of genuine changes in the deep Weddell Sea.

Based on these observations, this study ignored the  $O_2$  data of ANT-XXII/3 and ANT-XIV/3, and of selected stations of ANT-V/2&3 (north of 63 °S) and GEOSECS (north of 57 °S). The magnitude of these (local) offsets (about 2-5  $\mu\text{mol kg}^{-1}$ ) is about as large as the stated overall accuracy of  $O_2$  of cruise ANT-XXIV/3 ( $\pm 4.5 \mu\text{mol kg}^{-1}$ , see supplementary material), and much larger than the  $\pm 1\%$  (locally about  $\pm 2\text{-}3 \mu\text{mol kg}^{-1}$ ) that is often stated for the accuracy of oxygen measurements in general. The uncertainty about the accuracy of  $O_2$  measurements (in this study and in general) may jeopardize the application and interpretation of the back-calculation techniques that require  $O_2$  ( $C_T^0$ , TrOCA). In the back-calculation concept, an erroneously low  $O_2$  yields a  $C_T^0$  that is also too low, because a too large fraction of the measured  $C_T$  is considered to result from remineralization of organic matter (see Eq. 6-1).

### 6.5.4. Derivation of necessary variables

The following variables were derived from the gridded original data.

$C_T^0$ . Values of preformed  $C_T$  (i.e.,  $C_T^0$ ) were calculated for each grid point of each cruise using equation (6-1) (section 6.3.1.1). The required values of  $A_T^0$  and  $O_2^{\text{sat}}$  were obtained using the parameterizations of Sabine et al. (1999) and of Weiss (1970), respectively. Because the present study concerns the increase in  $C_T^0$  over a certain period rather than its exact value, the determination of the  $pO_2$  disequilibrium is not required, and we assume  $\Delta pO_2 = 0\%$ . The values of the ratios  $\psi_{O,C}$  and  $\psi_{O,N}$  are taken from Anderson and Sarmiento (1994) as 117/170 and 16/170 respectively.

$A_T^{\text{MLR}}$ . Measurements of  $A_T$  are available from 4 of the 10 cruises. To improve the availability of  $A_T$  (a requirement for the application of the  $C_T^0$  and TrOCA methods), an MLR was performed of the available (WDW-adjusted) data of  $A_T$  versus [salinity,  $\theta$ , silicate, depth, latitude]. With the derived coefficients, an artificial variable  $A_T^{\text{MLR}}$  was generated. In order to optimally represent the measured values of  $A_T$  over the entire section, separate MLRs were performed for each of four intervals of potential density. The procedure was performed both for non-gridded and gridded data, in order to verify the robustness of the gridding routine.



The resulting residuals of the regressions are presented in Figure 6.7 (panels a, c). It can be observed that the residuals are small and neutrally distributed around zero ( $0.1 \pm 2.3$  and  $0.0 \pm 1.5 \mu\text{mol kg}^{-1}$  for non-gridded and gridded data respectively). The shapes of the profiles are highly comparable, confirming the suitability of the employed gridding method. Since the predictive parameters were measured more often than  $A_T$  itself, values of  $A_T^{\text{MLR}}$  could be obtained for 9 of the 10 cruises (no silicate data of cruise ANT-XXIV/2 are available). At any location, the values of derived variable  $A_T^{\text{MLR}}$  are much more homogenous between the cruises than the original  $A_T$  values, which are not further used in this study. It must be noted that this application of an MLR removes any conceivable time trend from the  $A_T$  data if this trend is not reflected in any of the constituent parameters of  $A_T^{\text{MLR}}$ . This is in accordance with the common assumption that, as yet, there has been no anthropogenic influence on  $A_T$  distributions since the onset of the industrial revolution.

$C_T^{\text{TSR}}$  and  $C_{\text{residual}}^{\text{TSR}}$ . As part of the TSR approach (section 6.3.3), we performed an MLR between the measurements of  $C_T$  and ancillary variables [salinity,  $\theta$ , depth,  $A_T^{\text{MLR}}$ , phosphate, silicate], both for the gridded dataset and for the non-gridded dataset. All relevant data from all cruises in this study (i.e., the full 1973-2008 era) were used in a single MLR. As outlined in section 6.4.4, we suspect the presence of significant inaccuracies in some of the measurements of  $O_2$ . To avoid complicating the attribution of resulting time trends in  $C_{\text{residual}}^{\text{TSR}}$ , the MLR did not use  $O_2$  as an estimate of remineralization but relied solely on phosphate and silicate for this purpose. This is akin to the approach of Friis et al. (2005), who opted for the use of a nutrient (phosphate) instead of  $O_2$ -based AOU, because use of the latter resulted in a non-normal and depth-varying distribution of residuals. The residuals of the regression (Figure 6.7, panels b, d) are reasonably small ( $-0.1 \pm 2.9$  and  $-0.1 \pm 1.9 \mu\text{mol kg}^{-1}$  for non-gridded and gridded data respectively) and provide confidence that a suitable selection of independent parameters was chosen. The slanted shape of the residuals profile does not jeopardize our application, since we are solely interested in the *time trends* of the residuals, rather than their actual values.

### 6.5.5. Determination of time trends along the section

For each of the measurements (and derived variables) of interest, time trends were determined at each of the grid points as follows: of each of the cruises, the value of the grid point of interest and those of the grid points immediately surrounding it, were extracted. These values (up to 90 for each grid point: there are up to 10 cruises present at each grid point, and each grid point is surrounded by up to 8 other grid points) were regressed against their time of sampling, using an ordinary least squares linear fitting routine. All grid points weighted equally in the regression. This procedure makes the results slightly less sensitive to an occasional outlying value in the grids. Since no resolvable gradients are expected on the short spatial scale from one grid point to another, this step does not sacrifice spatial resolution. The results of the regression at each grid point allow for the derivation of parameter values for those years where data is not available. In general, trends derived in this way in the upper ~400 meters of the Weddell Gyre should not be taken to be representative of the underlying data, due to seasonality in the upper shallow waters and the limited resolution of used grid relative to the vertical variability of the water column at these depths. However, trends in  $C_{\text{residual}}^{\text{TSR}}$  do allow for interpretation in the shallow water column (section 6.3.3).

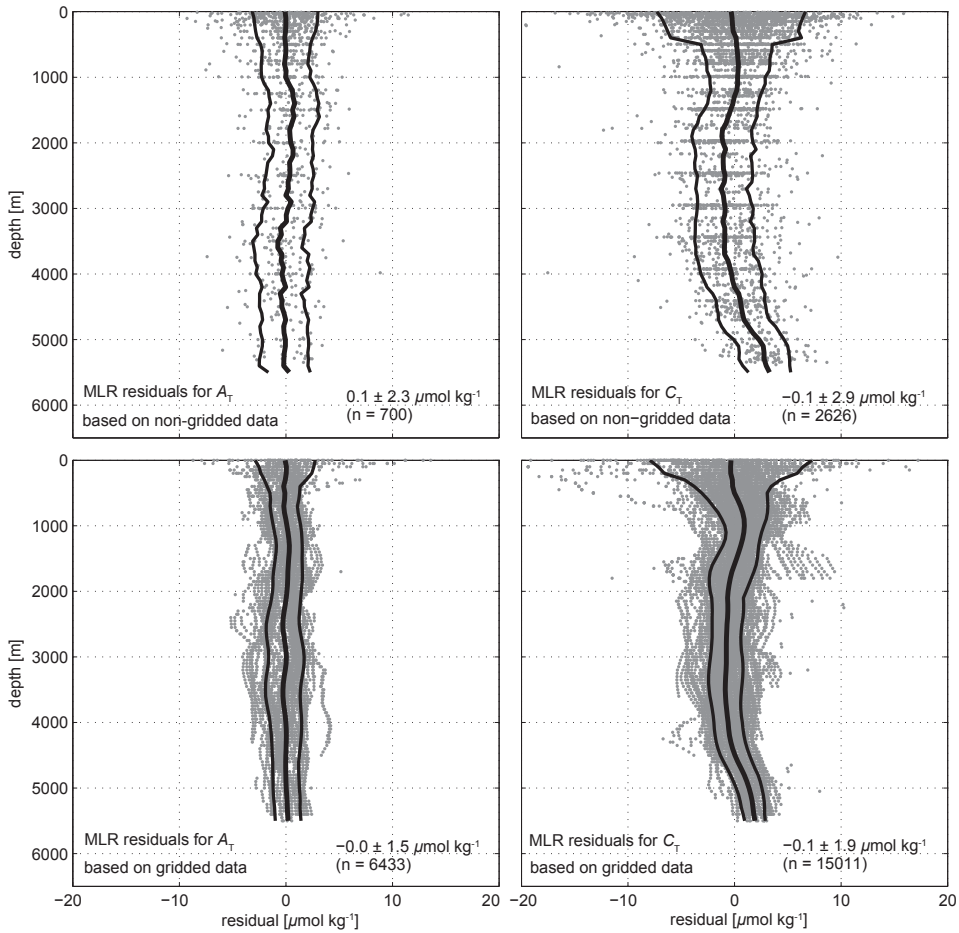


**Figure 6.7.** Depth profiles of the residuals of multivariate linear regressions (see section 6.5.4) of data of (left column)  $A_T$  versus [salinity,  $\theta$ , silicate, depth, latitude] and (right column)  $C_T$  versus [salinity,  $\theta$ , silicate, phosphate, depth]. The top row comprises non-gridded data, bottom row comprises gridded data. Thick lines indicate the mean and standard deviation of the residuals over a moving 500 m interval. The overall standard deviation of each profile is provided as text in each panel.

To illustrate this approach of linear fitting through gridded data, we process data of CFC-12. Figure 6.8 shows the concentrations of CFC-12 in 1992 as inferred from the time trends through the measurements obtained on the 7 coverings of the section (AJAX, 1984 to ANT-XXII/3, 2005). Also shown are actual measurements in 1992 (ANT-X/4), as well as the inferred time trends and the uncertainty associated with these time trends. The inferred concentrations in 1992 compare very well with the gridded data of ANT-X/4 (slope of regression of data below 1000 meters depth:  $0.98 \pm 0.02$ ,  $r^2 = 0.87$ ,  $p < 0.001$ ).

Even though the results obtained from CFC-12 serve an illustrative purpose only, we note that the use of linear regressions for CFC-12 does not do justice to the well known, distinctly nonlinear concentration history of this compound in the atmosphere and the surface

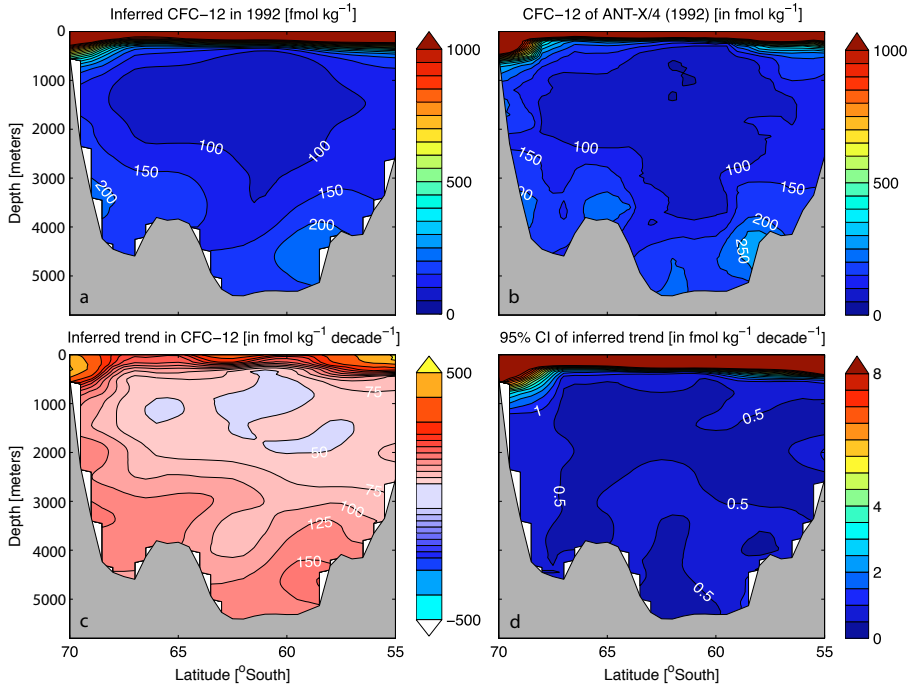


**Figure 6.8.** Example of results of the determination of linear trends in CFC-12, using all available data (i.e., from 1984 to 2005). **a)** inferred CFC-12 section in 1992; **b)** actual section from 1992, measured during cruise ANT-X/4; **c)** determined linear time trends of CFC-12 over the 35 year period; **d)** standard error of the time trend estimates of panel 8c. Trends with high relative standard errors are generally located in shallow waters. This is where the diminishing atmospheric increase is most closely tracked and, additionally, where temperature-driven seasonal oscillation of the concentrations of CFC-12 may further invalidate the assumption of linearity of time trends.

ocean. However, the stabilization and decrease of the atmospheric concentration of CFC-12 since approximately 2003 has not likely penetrated into the deep Weddell Sea yet (Klatt et al., 2002; Huhn et al., 2008). Therefore, an approximately linear rise in ocean interior concentrations may still be expected, and is indeed observed (Figure 6.9, see text section 6.5.6 for details).

### 6.5.6. Determination of time trends in water mass cores

The determination of time trends at fixed locations (latitude, depth) as outlined in section 6.4.7, yields results that may be plotted to reveal the spatial pattern of such trends (for example, Figure 6.8c). However, the results of that procedure may occasionally be ambiguous not only because of the sometimes small amount of samples represented by each grid point, but also because of hydrographical variability at each grid point. For example, the location of a particular water mass may vary somewhat through time and is thus not always present at the same location on the grid. Detection and quantification of time trends at such a location may therefore be jeopardized. To ensure that time trends within the proper cores of water masses are nonetheless optimally quantified, an additional analysis of the data was performed in which all grid points

that belonged to the core of a particular water mass (as determined by their  $S$  and  $\theta$  properties, see Table 6.1) were pooled, and time trends were determined for the data in each of these data pools. This procedure was performed for both the gridded and the non-gridded data, again in order to be able to verify that no inaccuracies result from the gridding routine. The time trends were determined by calculating for each cruise the mean values of the data in the water mass cores. Subsequently, an ordinary least squares linear fit against time was determined through these averages.

A sensitivity analysis was performed using a simple statistical model. We assume that the remaining inaccuracy (after the IWDW/uWSDW-adjustment) of the measurements of  $C_T$  performed before the introduction of CRM (i.e., the cruises in the period 1973-1992) is smaller than  $4 \mu\text{mol kg}^{-1}$ . The subsequent 6 cruises did use CRM and are assumed to be accurate to within  $2 \mu\text{mol kg}^{-1}$ . Under those assumptions, and taking into account the analytical noise in the measured  $C_T$  data (section 6.5.1), trends smaller than circa  $1 \mu\text{mol kg}^{-1} \text{decade}^{-1}$  fall within the statistical uncertainty of the method (at the  $p < 0.05$  level).

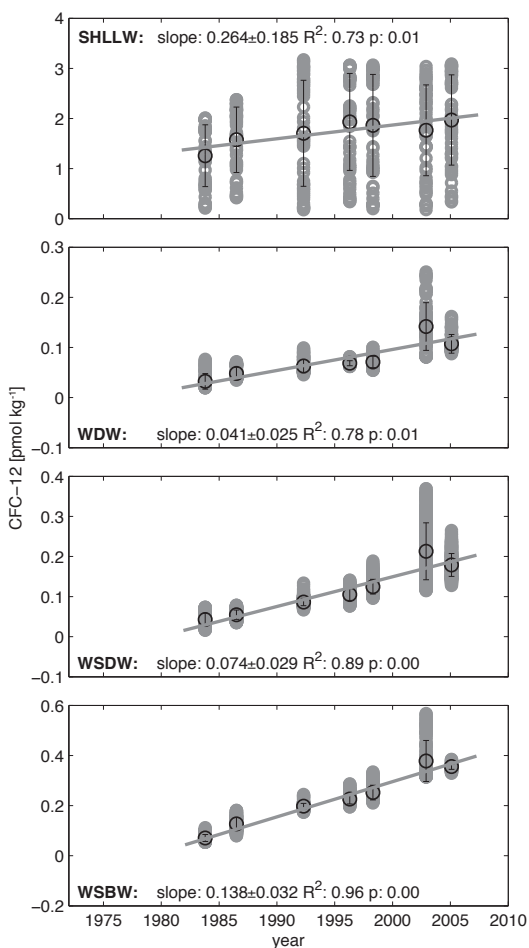


**Figure 6.9.** Time trends in the gridded data of CFC-12 [ $\text{pmol kg}^{-1} \text{decade}^{-1}$ ] in the cores of four watermasses (SHALLOW, WDW, WSDW, WSBW; see Table 6.1), determined using ordinary least squares regression. See text section 6.5.6 for details.

### 6.5.7. Determination of $C_{\text{ant}}^{\text{TrOCA}}$ for 2005

For the sake of comparison with the findings of previous studies, the concentration of  $C_{\text{ant}}$  along the section is determined for the nominal year 2005 using the TrOCA method (section 6.3.1.3). The required values of  $O_2$ ,  $C_T$  and  $A_T$  (or rather  $A_T^{\text{MLR}}$ ; section 6.5.4) are obtained by taking the mean values of all cruises in the time interval from 2002 to 2008. We use the same  $\theta$ -based  $\text{TrOCA}^0$ -parameterization as used by Lo Monaco et al. (2005b), which is only a slight adaptation of the parameterization originally provided by Touratier and Goyet (2004b).

### 6.5.8. The carbonate system of the Weddell Gyre in a high- $CO_2$ world

The continued uptake by the oceans of anthropogenic  $CO_2$  from the atmosphere will cause shifts in the oceanic carbonate system. Most notably, a strong reduction is predicted of the concentrations of carbonate ion  $[CO_3^{2-}]$  and hydroxide ion  $[OH^-]$ . These changes are of major importance for the solubility of (biogenic)  $CaCO_3$  (Feely et al., 2004; Orr et al., 2005) and for the speciation of trace metals (Millero et al., 2009). In order to briefly investigate the presence of these effects in the Weddell Gyre, values were calculated of  $[CO_3^{2-}]$ , pH (representing the decreasing  $[OH^-]$ ), and of the saturation states of the  $CaCO_3$ -structures aragonite and calcite ( $\Omega_{AR}$  and  $\Omega_{CA}$ ) from the gridded data of  $[S, T, C_T, A_T^{MLR}, \text{phosphate and silicate}]$  using CO2SYS for MATLAB (van Heuven et al., 2009). Trends were determined in these data as in text section 6.5.6.

## 6.6. Results

### 6.6.1. Spatial distribution of time trends along the section

#### CFC-12

The pattern of trends found in CFC-12 (Figure 6.8c) in the deep waters reflects current knowledge about the ventilation processes of the Southern Ocean (*e.g.*, Klatt et al., 2005). The strongest sub-surface increases are visible in the WSBW, flowing eastward along the southern side of the Mid-Atlantic Ridge (MAR), and along the Antarctic continental slope in the westward flowing water that makes up the southern limb of the Weddell Gyre. The core of the WDW (at 500-1500 m, 57-63 °S) shows a very low rate of increase in CFC-12. Because the CFC-12 concentrations at the surface of the water column tightly track the (distinctly non-linear) atmospheric CFC-12 concentration history, the method of linear fitting is not applicable at these shallower depths, as is also evidenced by the high uncertainties associated with the trends (Figure 6.8d). Therefore, results obtained in the upper 400 m will not be discussed and should not be taken to accurately reflect the rates of accumulation of CFC-12. In deeper waters, this problem is likely not yet as prominent (see section 6.5.1). A detailed look at the trends in the cores of the water masses (Figure 6.9, Table 6.5) shows the CFC-12 to still increase approximately linearly.

#### $C_T$

The spatial distribution of determined time trends in  $C_T$  (Figure 6.10a) qualitatively resembles that of CFC-12 in the deep region of the Weddell Gyre (Figure 6.8c). Notably in the WSBW and the deeper ranges of the WSDW, rates of increase of  $C_T$  are between 0.5 and 1.75  $\mu\text{mol kg}^{-1} \text{decade}^{-1}$ . A spatial distinction is observed between the cores of the increases in the southern and northern limb of the Weddell Gyre, in agreement with the pattern of trends in CFC-12. Again, we consider trends in  $C_T$  that were determined in the upper 400 meters of the water column not to accurately reflect real trends. It is interesting to note, though, that a near-zero (or even negative) rate of increase, associated with the upwelling region south of ~60 °S, prominently appears, as does an area of strong uptake (rates over 5  $\mu\text{mol kg}^{-1} \text{decade}^{-1}$ ) to the north of this divergence zone.

The near-zero rate of increase of  $C_T$  within the WDW has been dictated by the method. The inherent assumption of a constant  $C_T$  in the WDW is largely corroborated by the time trends

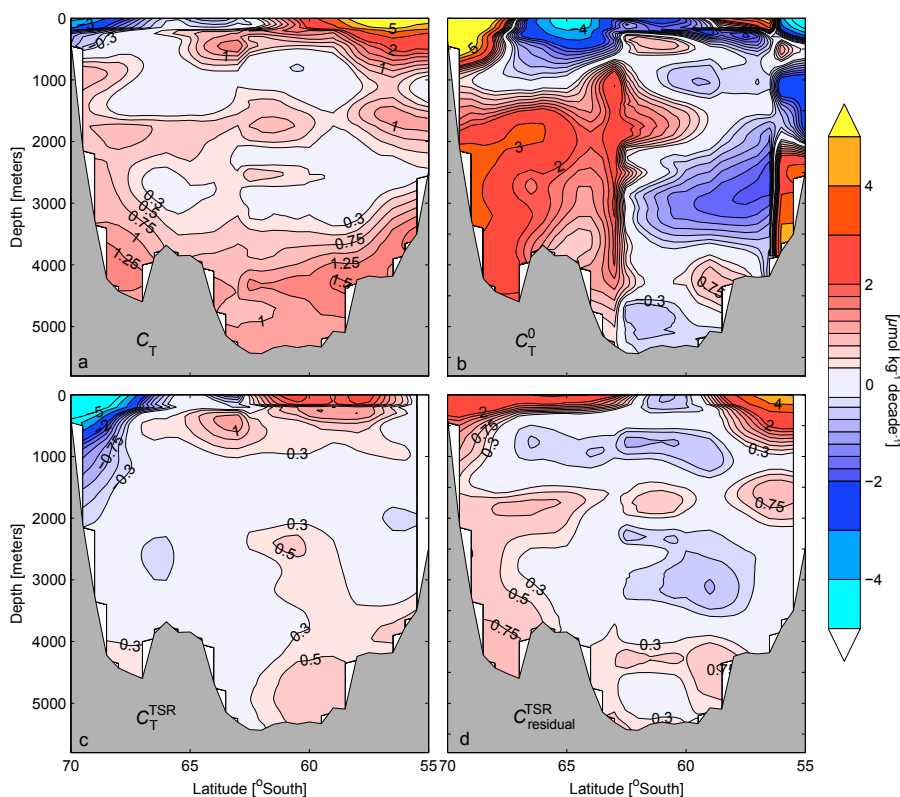


**Figure 6.10.** Section plots of the linear time trends [ $\mu\text{mol kg}^{-1} \text{decade}^{-1}$ ] determined through the gridded data of **a)** measured  $C_T$ ; **b)**  $C_T^0$ , the values of back-calculated performed  $C_T$ , which are assumed to reflect a time trend in  $C_{\text{ant}}$ , due to compensation for variable biogeochemical modification of  $C_T$ ; **c)**  $C_T^{\text{TSR}}$ , the values of  $C_T$  predicted using a multivariate linear regression of  $C_T$  versus a suite of independent parameters, deemed to represent the component of the trends in  $C_T$  that are attributable to natural variability; **d)**  $C_{\text{residual}}^{\text{TSR}}$ , the residuals of the TSR method, the trends in which are expected to reflect the component of the variability of  $C_T$  that is due to uptake of  $C_{\text{ant}}$  at the ocean surface. All results are based on data that were adjusted for consistency in IWDW/uWSDW. See text sections 6.5.5 and 6.6.1 for details.

**Table 6.5.** The time trends in  $C_T$  (derived in both the non-gridded and the gridded data) and in  $C_T^{\text{TSR}}$ ,  $C_{\text{residual}}^{\text{TSR}}$ , and CFC-12 as determined within the cores of each of the four water masses SHALLOW, WDW, WSDW and WSBW. Definitions of the water mass cores are given in Table 6.1. Significant time trends are in bold print. Time trends in the shallow waters that are expected to be susceptible to the influence of seasonality at the surface are shown in brackets. As opposed to the underlying data of the other results in this table, the CFC data were not normalized in the IWDW/uWSDW and indicate that the core of the WDW is not entirely unventilated. Rather, it shows a rate of increase of about 30% of that of the WSBW. Although this suggests that an upward correction may conceivably have to be applied to the  $C_T$ -based results, we opt not to perform this adjustment. See text section 6.7.2.

Water mass	$C_T$	$C_T$	$C_T^{\text{TSR}}$	$C_{\text{residual}}^{\text{TSR}}$	CFC-12
	$\mu\text{mol kg}^{-1} \text{decade}^{-1}$ non-gridded data	$\mu\text{mol kg}^{-1} \text{decade}^{-1}$ gridded data	$\mu\text{mol kg}^{-1} \text{decade}^{-1}$ gridded data	$\mu\text{mol kg}^{-1} \text{decade}^{-1}$ gridded data	$\text{pmol kg}^{-1} \text{decade}^{-1}$ gridded data
SHALLOW	(+1.846 ± 3.693)	(+2.979 ± 3.181)	<b>(+3.878 ± 3.656)</b>	+0.332 ± 1.797	<b>(0.264 ± 0.185)</b>
WDW	+0.086 ± 0.298	-0.213 ± 0.720	+0.340 ± 0.362	-0.436 ± 0.520	<b>0.041 ± 0.025</b>
WSDW	+0.241 ± 0.318	+0.176 ± 0.321	+0.268 ± 0.613	-0.363 ± 0.636	<b>0.074 ± 0.029</b>
WSBW	<b>+1.250 ± 0.563</b>	<b>+1.151 ± 0.563</b>	+0.512 ± 0.832	+0.445 ± 0.405	0.138 ± 0.032

in CFC-12, which are very small there (only about 30% of the bottom water trends). Additionally, we note again that pre-correction values of  $C_T$  in the WDW did not exhibit a trend, and that the applied corrections are small. The positive trend in  $C_T$  is also visible along the Antarctic continental slope from circa 1000 m downward, and tentatively also around 57 °S, as a protrusion from the surface downward to circa 2000 m depth. These columnar features at the southern and northern limits of the Weddell Gyre resemble the observed spatial distribution of CFC-12 and the trends therein (Figure 6.8a, b and c). Discussing data of CFC-11, the northern structure is interpreted by Klatt et al. (2002) as resulting from vertical mixing at the interface between the ACC and the Weddell Gyre, while the southern feature reflects the inflow from east of the Weddell Gyre of recently ventilated water.

By simple linear regression of the time trends in  $C_T$  versus those in CFC-12 for all grid points below 750 m and between 57 °S and 68 °S we find a significant correlation (Figure 6.11):

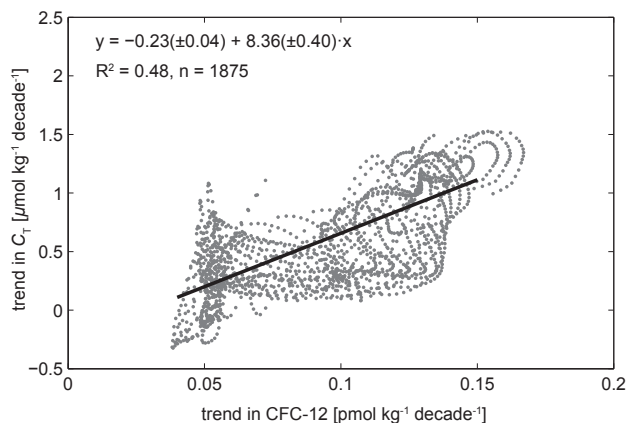
$$dC_T/dt = 8.4 \pm 0.4 \cdot dCFC12/dt - 0.23 \pm 0.04 \quad (n=1875, R^2=0.48, p<0.001) \quad (6-8)$$

The above relationship between the increases of CFC-12 and  $C_T$  is not highly significant. A better correlation than this is not likely to be expected, in part due to different equilibration times of the gases in the region of water mass formation, measurement inaccuracies and the distinctly different atmospheric histories of these gases (for a detailed treatment of the latter factor, see Tanhua et al., 2006). However, the relationship provides evidence that the observed distribution of time trends in  $C_T$  is consistent with the much more clearly resolved accumulation of CFC-12 in the deep Weddell Sea.

$C_T^0$ .

The spatial distribution of time trends in the derived concentrations of  $C_T^0$  along our section (see Figure 6.10b) is not at all in agreement with the time trends found directly in the originally measured  $C_T$  (Figure 6.10a). Strongly positive trends in  $C_T^0$  can be seen from the Antarctic continental slope northward to 62 °S, whereas the WSWB shows near-zero or negative trends. The observed pattern of time trends in  $C_T^0$  does not conform to known hydrographic pathways as exemplified by CFC-12 (Figure 6.8c), suggesting that the observed time trends in  $C_T^0$  are likely spurious. The erratic pattern of trends in  $C_T^0$  is found to be mainly attributable to localized

**Figure 6.11.** Regression between the time trends determined in  $C_T$  [ $\mu\text{mol kg}^{-1} \text{decade}^{-1}$ ] and in CFC-12 [ $\text{pmol kg}^{-1} \text{decade}^{-1}$ ] at the 1875 gridpoints deeper than 750 m and between 68 °S and 57 °S. Although the non-identical atmospheric concentration histories of  $C_{\text{ant}}$  and CFC-12 formally would invalidate the use of a linear regression as performed here, the agreement is quite apparent ( $R^2 = 0.48$ ) and provides confidence that the spatial distribution of the rates of increase of  $C_T$  is indeed related to spatial distribution of the accumulation of CFCs in the deep Weddell Gyre.





biases in data of  $O_2$  (see section 6.4.4), which results in a reduced ability to determine time trends through use of this parameter. This sensitivity of the  $C_T^0$  approach (and likely other approaches that use  $O_2$ ) to biases of measurements of  $O_2$  illustrates the need for future more accurate determinations of the dissolved  $O_2$ .

*TSR.*

The spatial distribution of time trends of  $C_T^{TSR}$  (Figure 6.10c; representing natural variability) are close to zero everywhere in the deep Weddell Sea except for in the WSBW, where a moderate increase is observed. The latter would suggest that part of the time trend in measured  $C_T$  (Figure 6.10a) in the WSBW may be attributed to variability in hydrographical or biogeochemical processes in the ocean interior. Indeed, the time trend in  $C_{residual}^{TSR}$  (Figure 6.10d; representing the anthropogenic influence) in the WSBW is clearly smaller than the time trend in measured  $C_T$  (Figure 6.10a). This is further quantified in below section 6.6.2. However, away from the core of the WSBW, several features of the distribution of the time trends in measured  $C_T$  are reflected in the distribution of time trends in  $C_{residual}^{TSR}$ . Most notably, the columnar feature adjacent to the Antarctic continental slope (see also section 6.6.1) and the southernmost deepest core (66 °S to 69 °S, >3500 m) are observed (although their magnitude is slightly smaller than the time trends observed directly in measured  $C_T$ , Figure 6.10a). Additionally, in both  $C_T$  and  $C_{residual}^{TSR}$ , a strong time trend is seen in the upper waters (<500 m) north of the diversion zone at 60 °S. These results indicate that at these locations, a significant fraction of the time trends observed in measured  $C_T$  may be attributed to uptake of  $C_{ant}$  at the surface of the Weddell Sea.

Lastly, a striking difference between time trends in  $C_T$  and  $C_{residual}^{TSR}$  is noted that, as we will argue, may be explained by the fact that values of (and time trends determined in)  $C_{residual}^{TSR}$  are insensitive to seasonality. Namely, in the upper waters near the Antarctic continent (south of 66 °S and shallower than 500 m), the  $C_{residual}^{TSR}$  shows a marked increase with time (about 2 to 3  $\mu\text{mol kg}^{-1}$  decade<sup>-1</sup>; Figure 6.10d) indicating that the anthropogenic component of  $C_T$  is increasing there. This increase is not evident from in  $C_T$  or  $C_T^{TSR}$ , which both show a negative time trend (Figure 6.10a,c). Both these latter two inferred decreases are conceivably strongly influenced by the combination of strong seasonal variability in these upper waters and the unbalanced seasonal distribution of the cruises, and are indeed statistically not significant (data not shown). Because the natural seasonal variability in  $C_T$  over the 1973-2008 era is by the TSR method related to independent parameters (mainly temperature), this variability is nicely replicated in the values of  $C_T^{TSR}$ . However, the gradually increasing  $C_{ant}$  in these waters is not expressible in terms of an independent variable, and is therefore visible as a time trend in  $C_{residual}^{TSR}$ .

## 6.6.2. Time trends determined in water mass cores.

Figure 6.12 and Table 6.5 present the determined time trends in the four water masses defined in Table 6.1 (SHALLOW, WDW, WSDW, WSBW). On the one hand the time trends of  $C_T$  in the WSDW are quite small and non-significant at  $+0.241 \pm 0.318$  and  $+0.176 \pm 0.321$   $\mu\text{mol kg}^{-1}$  decade<sup>-1</sup> for the gridded and non-gridded data, respectively. On the other hand, the time trends of  $C_T$  in the WSBW are sizable and significant at  $+1.151 \pm 0.563$  and  $+1.250 \pm 0.563$   $\mu\text{mol kg}^{-1}$  decade<sup>-1</sup> for the gridded and non-gridded data, respectively. These values resemble the results shown



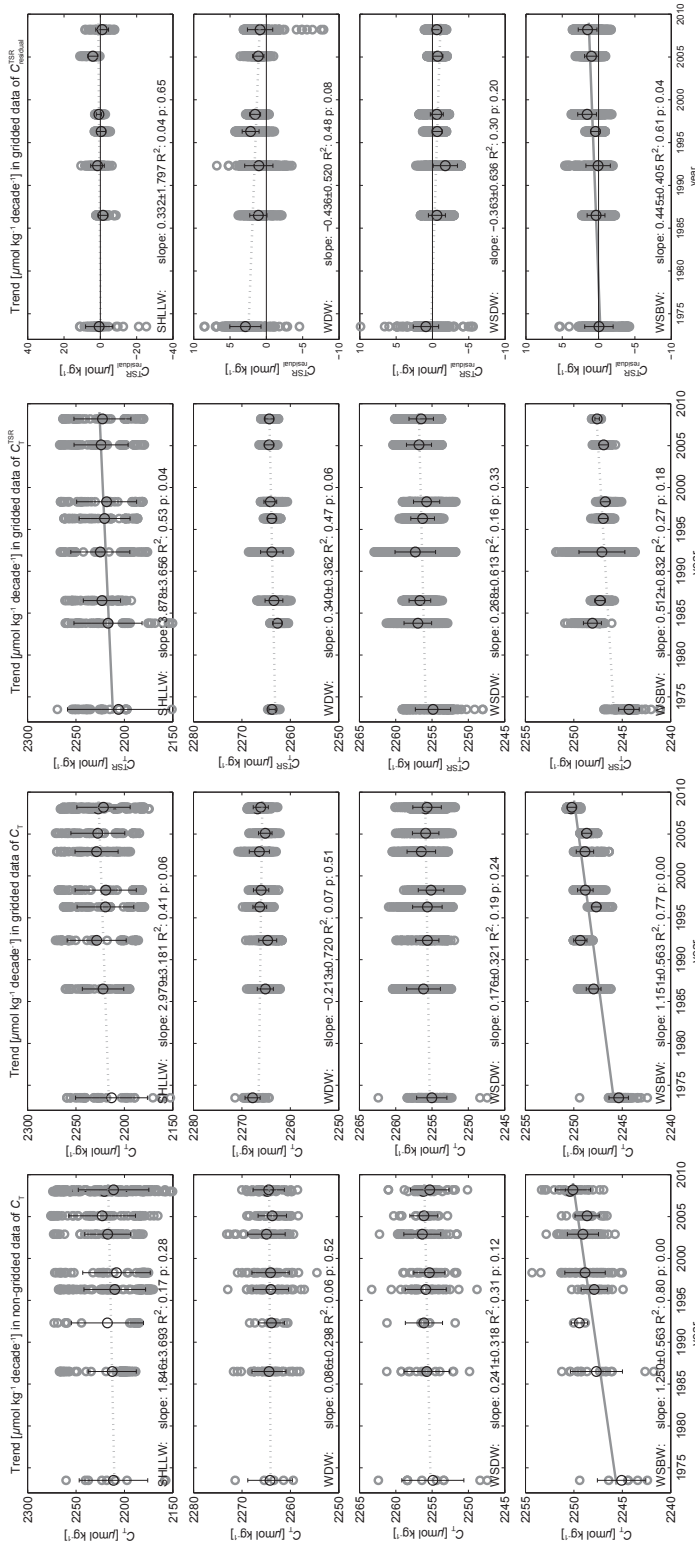


**Figure 6.12.** Time trends [ $\mu\text{mol kg}^{-1} \text{ decade}^{-1}$ ] in the cores of four water masses (SHALLOW, WDW, WSDW, WSBW; see Table 6.1) computed using ordinary least squares regression. All results are based on data that were adjusted for consistency in IWDW/uWSDW. See text sections 6.5.6 and 6.6.2 for details. **a)** non-gridded data of  $C_T$ ; **b)** gridded data of  $C_T$ ; **c)**  $C_T^{residual}$ , the values of  $C_T$  predicted using a multivariate linear regression of the gridded  $C_T$  versus a suite of gridded independent parameters. These trends are deemed to represent the component of the variability in  $C_T$  that is attributable to natural variability; **d)**  $C_T^{residual}$ , the residuals of the Time Series Residuals method, the trends through which are expected to reflect the component of the variability of gridded  $C_T$  that is due to uptake of  $C_{int}$  at the ocean surface.

for the WSBW in the section plot of the time trends in  $C_T$  (Figure 6.10a), providing confidence that the results are robust. No significant trends in (gridded or non-gridded)  $C_T$  are found in the three overlying water masses, although there is a hint at increase in the shallow waters (<200 m), notwithstanding seasonality and the upwelling character of the SHALLOW water mass at the defined 58 °S-63 °S latitude (Table 6.1).

The time trends in  $C_T^{\text{TSR}}$  (deemed to represent influences on  $C_T$  of natural variability) are not significantly different from zero in the three deeper water masses. This is deemed to confirm that there are no systematic time trends of hydrographic or biogeochemical origin over the 35 years. The variability in  $C_T$  in the upper waters (Figure 6.12; top panels of leftmost two columns), that likely is a result of uneven distribution of sampling in various seasons, is partly reproduced by  $C_T^{\text{TSR}}$ , suggesting that seasonality indeed obscures conceivable trends in  $C_T$  there.

The time trend of  $C_{\text{residual}}^{\text{TSR}}$  (deemed to represent the time trend of  $C_{\text{ant}}$ ) in the WSBW equals about one third of that observed in measured  $C_T$ :  $0.445 \pm 0.405 \mu\text{mol kg}^{-1} \text{decade}^{-1}$ . This difference was also observed in the section plots of trends (Figure 6.10a,d; text section 6.6.1), and will be further discussed in text section 6.7.3. The time trends in the other three water masses are not significantly different from 0. Finally, no increase in  $C_{\text{residual}}^{\text{TSR}}$  is observed in the upper waters, suggesting very little penetration of  $C_{\text{ant}}$  into the upwelling waters.

### 6.6.3. Determined $C_{\text{ant}}^{\text{TrOCA}}$

The section of  $C_{\text{ant}}$  derived using the TrOCA method (Figure 6.13) resembles the distribution of the concentration of (and trends in) CFC-12 (Figure 6.8). Specifically, the low values in the WDW (circa  $10 \mu\text{mol kg}^{-1}$ ) and higher concentrations in two distinct bottom water cores (circa  $16 \mu\text{mol kg}^{-1}$ ) are clearly discernable in both properties. These values are in general accordance with earlier published data (Lo Monaco et al., 2005b; Vázquez Rodríguez, 2009).

### 6.6.4. The carbonate system of the Weddell Gyre in a high- $\text{CO}_2$ world.

Significant decreasing time trends are observed for all calculated parameters of the carbonate system ( $[\text{CO}_3^{2-}]$ , pH,  $\Omega_{\text{AR}}$  and  $\Omega_{\text{CA}}$ ) in the shallow waters (<200 m; Table 6.1) and the WSBW (Figure 6.14). For the shallow waters these trends exceed beyond the expected strong influence of seasonality there. In the WSBW, the time trend in the concentration of carbonate ion is  $-0.7 \pm 0.3 \mu\text{mol kg}^{-1} \text{decade}^{-1}$ , which equates to almost -1% per decade. Orr et al. (2005) used a set of ocean carbon cycle models to predict the global evolution of  $[\text{CO}_3^{2-}]$  for the 2000-2100 era under a 'business-as-usual' scenario for anthropogenic emissions of  $\text{CO}_2$ . For the surface waters of the Southern Ocean, they computed an approximately linear trend of about  $-5 \mu\text{mol kg}^{-1} \text{decade}^{-1}$  (their Figure 6.5), resulting in aragonite undersaturation around the year 2065. That estimate is considerably more pronounced than the  $-1.6 \pm 1.5 \mu\text{mol kg}^{-1} \text{decade}^{-1}$  that we derive from measurements over the period 1973-2008, which would not result in undersaturation within the current century. Hauck et al. (2010), also note the projection of Orr et al. (2005) to be markedly higher than their own data-based estimates. However, we note here that 'shallow water' in the present study is defined to be located in, or close to, the upwelling region (cf. Table 6.1), and will therefore likely exhibit more modest rates of accumulation of  $C_{\text{ant}}$  compared to the

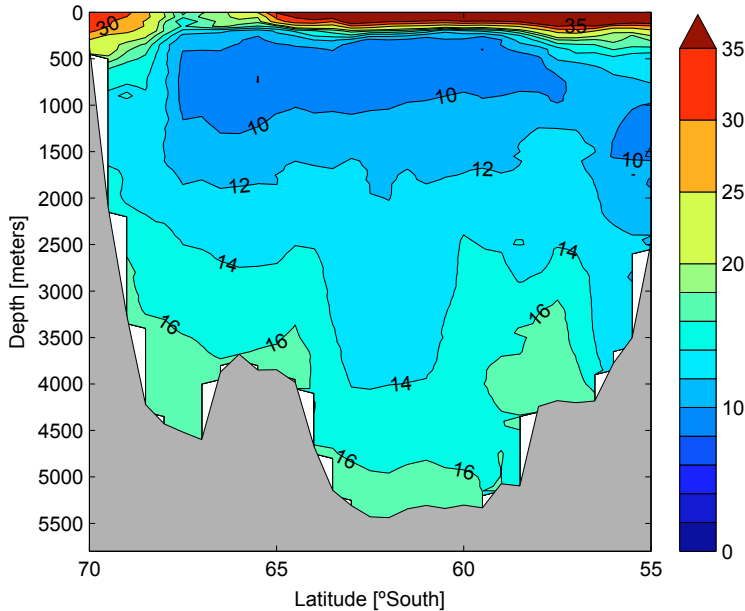


**Figure 6.13.** Section plot of  $C_{\text{anti}}$  [ $\mu\text{mol kg}^{-1}$ ] as determined with the TrOCA approach, valid for the year 2005. For the required input values of  $C_T$ ,  $A_T^{\text{MLR}}$ ,  $O_2$ ,  $S$ ,  $\theta$ , phosphate and silicate we used the means of the cruises between 2002 and 2008 (see text sections 6.5.7, 6.6.3). All results are based on data that were adjusted for consistency in IWDW/uWSDW.

rates in waters to the north and south of this region (text section 6.2), which the estimate of Orr et al. did include.

## 6.7. Discussion

This discussion contains a treatment of some of the uncertainties associated with the followed methodology, a comparison of our finding with earlier work, and an extrapolation of the results obtained at the Prime Meridian to the larger Weddell Gyre.

### 6.7.1. GEOSECS bias

The GEOSECS (1973) data are so far in the past compared to the 1984-2008 era of the other cruises that a conceivably remaining bias in the GEOSECS data will have excessive leverage in the linear regression. For example, if these data would, after the WDW normalization, still be  $2 \mu\text{mol kg}^{-1}$  too low, time trends in  $C_T$  would be overestimated by about 25% (i.e.,  $+1.5$  instead of  $+1.2 \mu\text{mol kg}^{-1} \text{ decade}^{-1}$ ). We are confident, however, that any remaining bias in the GEOSECS is of limited influence on our results. Some justification for the used correction of  $-0.6 \mu\text{mol kg}^{-1}$  is found in the literature. Peng and Wanninkhof (2010) determined corrections for  $C_T$  for individual GEOSECS stations in the Atlantic Ocean. Their results indicate that  $C_T$  at the stations that are used in this study should be corrected by between  $0 \pm 4 \mu\text{mol kg}^{-1}$  (their Figure 6.5) and  $-2 \pm 4 \mu\text{mol kg}^{-1}$  (their Figure 6.7). The fact that we observe a time trend in  $C_T$  also in

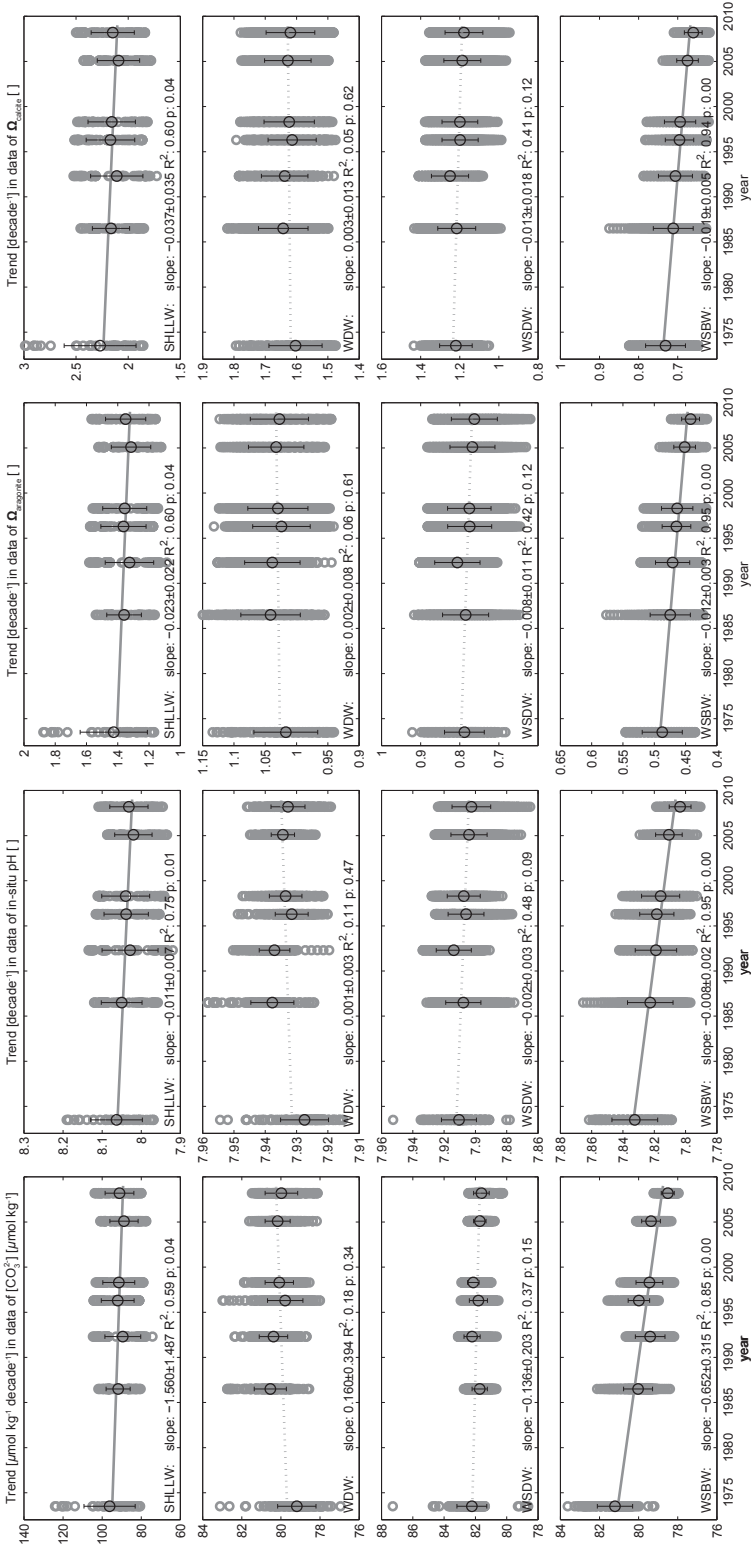


**Figure 6.14.** Time trends in the cores of four water masses (SHALLOW, WDW, WSDW, WSBW; see Table 6.1), determined using ordinary least squares regression, of the calculated values of **a)** the carbonate ion concentration [CO<sub>3</sub><sup>2-</sup>]; **b)** the concentration of hydroxide ion ([OH<sup>-</sup>]), expressed as in-situ pH (see text section 6.6.4); **c)** the saturation state Ω of aragonite; **d)** the saturation state Ω of calcite. Trends in **a)** in μmol kg<sup>-1</sup> decade<sup>-1</sup>, trends in **b), c)** and **d)** in units of decade<sup>-1</sup>. For the last two panels **c)** and **d)**, values of Ω below 1 indicate that the seawater is undersaturated with respect to the aragonite or calcite crystal/lime state of CaCO<sub>3</sub>, respectively. See text sections 6.5.8 and 6.6.4 for details. All results are based on data that were adjusted for consistency in IWDW/uWSDW.

the waters that were not sampled by GEOSECS (Figures 6.5, 6.10a) is an additional indication that the derived results are robust and not an artifact of GEOSECS bias.

### 6.7.2. Effects of WDW normalization

The absence of the trends in  $C_T$  in the WDW (Figure 6.12, second row, first two columns) indicates that the normalization of values in the WDW was valid and effective. However, the spread that was observed in the WDW before normalization may have contained an obscured real-world trend. The detection of trends of CFC-12 hints at the slow but definite ventilation of this water mass. The trend in CFC-12 in the WDW is  $0.041 \pm 0.025 \text{ pmol kg}^{-1} \text{ decade}^{-1}$ , versus  $0.138 \pm 0.032 \text{ pmol kg}^{-1} \text{ decade}^{-1}$  in the WSBW (see Table 6.5, Figure 6.9). Translated to the results for  $C_{\text{ant}}$  this suggests that the real world trends in WSBW and WDW conceivably may be as large as  $+1.65$  and  $+0.49 \text{ } \mu\text{mol kg}^{-1} \text{ decade}^{-1}$ , respectively. However, the trend in non-adjusted data of  $C_T$  in the WSBW (excluding the strongly outlying data of ANT-V/2&3 and AJAX) is  $1.1 \pm 1.0 \text{ } \mu\text{mol kg}^{-1} \text{ decade}^{-1}$ , (i.e., less clearly resolved, but of similar slope as the adjusted data). Therefore, although we acknowledge the possibility that real-world trends in the WSBW might be up to 30% higher than the  $+1.2 \pm 0.6 \text{ } \mu\text{mol kg}^{-1} \text{ decade}^{-1}$ , we opt not to perform such an upward correction of our results.

### 6.7.3. Attribution of trends

We show a distinct and unambiguous increase in  $C_T$  in the WSBW of about  $1.2 \pm 0.6 \text{ } \mu\text{mol kg}^{-1} \text{ decade}^{-1}$ . This trend is only partly consistent with the significant time trend in  $C_{\text{residual}}^{\text{TSR}}$  (about  $0.4 \pm 0.4 \text{ } \mu\text{mol kg}^{-1} \text{ decade}^{-1}$ ), deemed representative of an increase of  $C_{\text{ant}}$  over time. However, there is no significant time trend in the WSBW of  $C_T^{\text{TSR}}$  ( $0.512 \pm 0.832 \text{ } \mu\text{mol kg}^{-1} \text{ decade}^{-1}$ ), implying that there are no clear systematic time trends of biogeochemical and/or hydrographic origin over the 35 years that would explain the remainder of the observed time trend in  $C_T$ . In order to more satisfyingly attribute the observed time trend in  $C_T$  to either natural variability or accumulation of anthropogenic  $\text{CO}_2$ , we below consider alternative lines of evidence, and eventually opt to ascribe the entire increase of  $C_T$  (i.e., about  $1.2 \pm 0.6 \text{ } \mu\text{mol kg}^{-1} \text{ decade}^{-1}$ ) to accumulation of anthropogenic  $\text{CO}_2$  in the WSBW.

From an absence of trends in (IWDW/uWSDW-normalized)  $\text{NO}_3$ ,  $\text{PO}_4$  and  $\text{O}_2$ , we rule out enhanced remineralization as cause of the observed trend in  $C_T$ . Due to the limited accuracy of the  $A_T$  data and the lack of time trends in  $A_T^{\text{MLR}}$  (section 6.4.6) no such statement can be made for the influence of  $\text{CaCO}_3$  dissolution, but the rate of that process and the variability therein may be considered to be too small to suffice as an explanation (Sabine et al., 2002). Alternatively, part of the time trend in  $C_T$  in the WSBW might be the result of a changing formation process of the water mass. In order to explain the observed increasing temperature of the WSBW, Fahrbach et al. (2004) suggest that increases in the penetration of CDW into the Weddell Sea and in the amount of entrainment of (CDW-derived) WDW during the convective formation of WSBW from Ice Shelf Water (ISW) would increase the temperature of the WSBW. Lenton et al. (2009) provide a tentative mechanism for this increased penetration of CDW involving anthropogenically driven changes in atmospheric circulation. Such increased entrainment of WDW would inevitably also increase the  $C_T$  of the WSBW and can be quantified

as follows. The WSBW is considered to be a mixture of Ice Shelf Water and near-continental slope WDW (ISW:  $\theta = -1.85$  °C, salinity-normalized  $C_T = 2250$   $\mu\text{mol kg}^{-1}$ ; WDW:  $\theta = 0.25$  °C, salinity-normalized  $C_T = 2285$   $\mu\text{mol kg}^{-1}$ ), with a gradient of the mixing line of  $16.7$   $\mu\text{mol kg}^{-1} \text{ } ^\circ\text{C}^{-1}$  (Hoppema et al., 1998). This gradient multiplied with the observed time trend of  $\theta$  in the WSBW of  $+0.015 \pm 0.006$   $^\circ\text{C decade}^{-1}$  (comparable to the trend observed by Fahrbach et al., 2004) yields a time trend of  $C_T$  of  $0.25 \pm 0.10$   $\mu\text{mol kg}^{-1} \text{ decade}^{-1}$ . In other words, an increase in the amount of WDW entrained by ISW during the formation of WSBW may at most explain  $\sim 20\%$  of the observed trend in  $C_T$ .

Overall, we reckon that the observed increase of  $C_T$  in the WSBW at a rate of about  $1.2 \pm 0.6$   $\mu\text{mol kg}^{-1} \text{ decade}^{-1}$  may best be completely ascribed to a true invasion of anthropogenic  $\text{CO}_2$  into the deep Weddell Gyre. This attribution is at least partly supported by the significant time trend in  $C_{\text{residual}}^{\text{TSR}}$  ( $0.4 \pm 0.4$   $\mu\text{mol kg}^{-1} \text{ decade}^{-1}$ ). More importantly, the strong spatial correlation of the increase of  $C_T$  and the increase of CFC-12 (Figure 6.11), is most convincing. However, the given rate of  $1.151 \pm 0.56$   $\mu\text{mol kg}^{-1} \text{ decade}^{-1}$  is deemed to be an upper limit, because natural variability of hydrography may account for a part of the trend ( $0.25 \pm 0.10$  to  $0.5 \pm 0.8$   $\mu\text{mol kg}^{-1} \text{ decade}^{-1}$ , as suggested above by the mixing consideration and the TSR approach, respectively).

#### 6.7.4. Comparing the time trend of $C_{\text{ant}}$ with other estimates

Hoppema et al. (2001), following the method of Poisson and Chen (1987), report a ‘negligible’ increase in  $C_{\text{ant}}$  between 1973 and 1998 from a comparison of cruise data from the mid 1990’s with data of GEOSECS and AJAX. Although no significant change was determined, the authors concluded from statistical considerations that the increase of  $C_{\text{ant}}$  in the WSBW is almost certainly smaller than  $2$   $\mu\text{mol kg}^{-1} \text{ decade}^{-1}$ . That upper limit estimate is in agreement with the  $1.2 \pm 0.6$   $\mu\text{mol kg}^{-1} \text{ decade}^{-1}$  found in the present study.

Another recent determination of  $\Delta C_{\text{ant}}$  in the Weddell Sea, also along the  $0^\circ$ -meridian, relies on the eMLR method (Friis et al., 2005; see text section 6.3.2.3) to derive an increase of  $C_{\text{ant}}$  between the two cruises ANT-X/4 (1992) and ANT-XXIV/2 (2008) (Hauck et al., 2010). The magnitude of the reported increases over 16 years is similar to our findings. However, for individual water masses significant discrepancies exist with our results. Firstly, in the WSDW, the reported pronounced increase ( $\sim 1.5$ - $2.0$   $\mu\text{mol kg}^{-1}$  over 16 years), is incompatible with the about fivefold smaller and non-significant time trend in  $C_T$  found in our study ( $0.2 \pm 0.3$   $\mu\text{mol kg}^{-1} \text{ decade}^{-1}$ ; Figure 6.12, Table 6.5). Moreover, we do not find a significant time trend of  $C_{\text{residual}}^{\text{TSR}}$  ( $-0.4 \pm 0.6$   $\mu\text{mol kg}^{-1} \text{ decade}^{-1}$ ; Figure 6.12, Table 6.5) either, representative of  $C_{\text{ant}}$ . In favor of the findings of Hauck et al., one might argue that the procedure of WDW-normalization performed in the present study has inadvertently also removed the trend in the WSDW. However, that argument is mutually exclusive with our concurrent finding of a significant positive trend in  $C_T$  in the WSBW (about  $+1.2 \pm 0.6$   $\mu\text{mol kg}^{-1} \text{ decade}^{-1}$ ), where Hauck et al. report an increase that is significantly smaller than  $1$   $\mu\text{mol kg}^{-1}$  over 16 years. On the other hand, the reported low increase in the WSBW *does* coincide with our TSR-based results for  $C_{\text{residual}}^{\text{TSR}}$  (WSBW  $+0.4 \pm 0.4$   $\mu\text{mol kg}^{-1} \text{ decade}^{-1}$ ). However, we do not hold this resemblance to demonstrate the veracity of the results of either study, mainly in light of the fact that the two studies indicate different water masses to dominate the storage of  $C_{\text{ant}}$  (namely, WSDW in the study of Hauck et al., and



WSBW in the present study). Instead, the discrepancies between the two studies may be due to the fact that the used datasets are not the same. Specifically, although Hauck et al. (2010) showed the overall quality of the used data to be satisfactory, we have chosen to exclude the southerly deep  $C_T$  measurements (south of 63 °S and deeper than 1500 m) of the ANT-X/4 (1992) cruise, which we consider to be erroneously high by up to 7  $\mu\text{mol kg}^{-1}$  on the basis of a regression versus  $\theta$  (see above section 6.5.1). The exclusion we performed (and the additional exclusion of  $C_T$  measurements of AJAX, 1983) is corroborated by the distribution of time trends in our remaining data base of actually measured  $C_T$  (Figure 6.10a), which closely resembles the distribution of time trends of CFC-12 in the deep region of the Weddell Gyre (section 6.6.1; Figure 6.8c), comprising the WSDW and WSBW. In the study of Hauck et al., the presence of a bias in part of the data may have led to increased uncertainty (but not necessarily inaccuracy) in the applied MLR and the results derived from it. Additionally, the low number of samples qualifying as WSBW in the study of Hauck et al. (Figure 6.5) may have affected their results obtained for this water mass.

### 6.7.5. The concentration of $C_{\text{ant}}$ derived from the observed decadal time trend

The Transient Steady State approach (Tanhua 2007; section 6.3.1.5) implies that the per-decade increase in  $C_{\text{ant}}$  represents a fraction of about  $0.2 \pm 0.03$  of the total concentration of  $C_{\text{ant}}$  (i.e.,  $C_{\text{ant}} [\mu\text{mol kg}^{-1}] \approx 5 \cdot \Delta C_{\text{ant}} [\mu\text{mol kg}^{-1} \text{decade}^{-1}]$ ; notice the informal use of units in this expression). Assuming that the time trend of  $C_{\text{ant}}$  in the WSBW equals that of  $C_T$  (i.e., about  $1.2 \pm 0.6 \mu\text{mol kg}^{-1} \text{decade}^{-1}$ ), we infer a  $C_{\text{ant}}$  of  $6 \pm 3 \mu\text{mol kg}^{-1}$ . We will take 1995 as the year for which this estimate is valid, that is, slightly more recent than the midpoint of the 1973–2008 period. The error bound of this estimate is not formally determined, due to several assumptions inherent to the taken approach. Nonetheless, the estimate may serve as a rough guide to assess the validity of our study versus various other estimates of  $C_{\text{ant}}$  previously reported by other investigators.

Table 6.6 lists the  $C_{\text{ant}}$  estimates derived in this study, as well as various estimates of the concentration of  $C_{\text{ant}}$  in the Weddell Gyre that were obtained by other investigators (Poisson and Chen, 1987; Lo Monaco et al., 2005b; Waugh et al., 2006; Vázquez-Rodríguez et al., 2009). Poisson and Chen (1987), using a back-calculation approach (section 6.3.1.1), reported a concentration of  $C_{\text{ant}}$  in the deep Weddell Sea (for 1984) of circa  $6 \pm 5 \mu\text{mol kg}^{-1}$ , which is in agreement with the results of this study. However, several estimates of  $C_{\text{ant}}$  in the WSBW that have been derived using the  $\Delta C^*$  method are close to zero (Sabine et al., 2004; Waugh et al., 2006; Vázquez-Rodríguez et al., 2009). On the other hand, results from application of the TTD approach (e.g., Waugh et al., 2006; Vázquez-Rodríguez et al., 2009) are generally somewhat higher than our results. Both authors report estimates of  $C_{\text{ant}}$  in the WDW and the (largely WSDW-derived) AABW at 30 °E of about 9  $\mu\text{mol kg}^{-1}$ . These estimates are significantly higher (WDW) or slightly higher (AABW) than the results obtained in the present study (0 and  $6 \pm 3 \mu\text{mol kg}^{-1}$ , respectively). On the other hand, by assuming an undersaturation of dissolved oxygen of 12%, Lo Monaco et al. (2005a,b) used the  $C_T^0$  method to determine a  $C_{\text{ant}}$  concentration in 1996 of circa 22  $\mu\text{mol kg}^{-1}$  in the core of the AABW at 30 °E. This estimate is very significantly higher than what is obtained in this study using the Transient Steady State method.

Results of the applications of the TrOCA method agree fairly well between the different studies, which is not surprising given the strict definition and application of the method.

**Table 6.6.** Comparison of several estimates of  $C_{\text{ant}}$  from previously published literature. Reproduced values necessarily are simplified from originally reported depth profiles and section plots. Many of these estimates are from data obtained along the section at 30 °E (WOCE section I06), which is located at the easternmost extent of the Weddell Gyre (as indicated in the column ‘section longitude’), and thus does not cover the exact same water masses as the present study. Most notably, the composition of the bottom water at 30 °E (Antarctic Bottom Water, AABW) is alike (and largely derived from) the WSDW, rather than WSBW. Although the AABW at 30 °E to some extent is formed in areas to the East of the Weddell Sea, the involved formation processes are likely comparable, and since significant mixing and horizontal homogenization takes place in the Southern Ocean, and CFC-12 concentrations are comparable (data not shown), we consider the comparison between results from these two sections not perfect but informative.

Source	$C_{\text{ant}}$ estimate ( $\mu\text{mol kg}^{-1}$ )	Nominal year	Section longitude	Method	Remarks
<b>Warm Deep Water</b>					
Lo Monaco et al., 2005a	~ 6	1996	30 °E	$C_T^0$ (assuming $O_2$ saturation)	from their figure 5a
Lo Monaco et al., 2005a	~ 9	1996	30 °E	$C_T^0$ (assuming 12% $O_2$ undersaturation)	from their figure 5b
Sabine et al., 2004	~ 0	1996	30 °E	$\Delta C^*$	from GLODAP data product
Lo Monaco et al., 2005b	~ 6	1996	30 °E	$\Delta C^*$ (assuming 12% $O_2$ undersaturation)	from their figure 4c
Waugh et al., 2006	~ 0	1996	30 °E	$\Delta C^*$	from their figure 6b
Vázquez-Rodríguez et al., 2009	~ 1	1996	30 °E	$\Delta C^*$	from their figure 4
Waugh et al., 2006	~ 8	1996	30 °E	TTD	from their figure 6b
Vázquez-Rodríguez et al., 2009	~ 10	1996	30 °E	TTD	from their figure 4
Lo Monaco et al., 2005b	~ 10	1996	30 °E	TrOCA	from their figure 4a
Vázquez-Rodríguez et al., 2009	~ 7	1996	30 °E	TrOCA	from their figure 4
This study	~ 9	2005	0 °E	TrOCA	text sections 6.5.7, 6.6.3
This study	0	1995	0 °E	a priori assumption	text section 6.5.1
<b>WSBW / AABW</b>					
Poisson & Chen, 1987	6±5	1984	0 °E	diff. of $C_T^0$ between WDW and WSBW	
Lo Monaco et al., 2005a	~ 8	1996	30 °E	$C_T^0$ (assuming $O_2$ saturation)	from their figure 5a
Lo Monaco et al., 2005a	~ 22	1996	30 °E	$C_T^0$ (assuming 12% $O_2$ undersaturation)	from their figure 5b
Sabine et al., 2004	~ 0	1996	30 °E	$\Delta C^*$	from GLODAP data product
Lo Monaco et al., 2005b	~ 18	1996	30 °E	$\Delta C^*$ (assuming 12% $O_2$ undersaturation)	from their figure 4c
Waugh et al., 2006	~ 0	1996	30 °E	$\Delta C^*$	from their figure 6b
Vázquez-Rodríguez et al., 2009	~ 1	1996	30 °E	$\Delta C^*$	from their figure 4
Waugh et al., 2006	~ 9	1996	30 °E	TTD	from their figure 6b
Vázquez-Rodríguez et al., 2009	~ 8	1996	30 °E	TTD	from their figure 4
Lo Monaco et al., 2005b	~ 15	1996	30 °E	TrOCA	from their figure 4a
Vázquez-Rodríguez et al., 2009	~ 13	1996	30 °E	TrOCA	from their figure 4
This study	~ 16	2005	0 °E	TrOCA	text sections 6.5.7, 6.6.3
This study	6±3	1995	0 °E	from time trend in $C_T$ (using TSS)	text section 6.7.5



However, all TrOCA-based estimates for the WSBW (or AABW) (all around  $15 \mu\text{mol kg}^{-1}$ ) are higher than results obtained by this study or by studies employing the TTD or  $\Delta C^*$  methods.

Obviously, the highest of the above discussed, previously published estimates of  $C_{\text{ant}}$  for the WSBW/AABW presented in Table 6.6, are incompatible with the results of this study. We here assume the central argument of the Transient Steady State method to be valid. That is, the exponential accumulation of  $C_{\text{ant}}$  in the atmosphere and the ocean surface will lead to exponentially increasing concentrations in the ocean interior (Tanhua et al., 2007). The time trends in  $C_{\text{ant}}$  that would therefore necessarily be associated with high concentrations of  $C_{\text{ant}}$  (for example, a  $C_{\text{ant}}$  of  $\sim 20 \mu\text{mol kg}^{-1}$  requires a trend in  $C_{\text{ant}}$  of  $\sim 4 \mu\text{mol kg}^{-1} \text{decade}^{-1}$ ) are irreconcilable with the observed time trends in measured  $C_T$  (about  $+1.2 \pm 0.6 \mu\text{mol kg}^{-1} \text{decade}^{-1}$ ). Moreover, the trends in  $C_T$  observed in this study are deemed to represent an upper limit of the trend in  $C_{\text{ant}}$  (see text section 6.7.3), which further reduces the likelihood that the highest previously published estimates of  $C_{\text{ant}}$  in Table 6.6 are accurate.

### 6.7.6. The rate of increase of the inventory of $C_{\text{ant}}$ of the deep Weddell Gyre.

The determined time trend in the concentration of  $C_{\text{ant}}$  along the section may be spatially extrapolated and integrated to obtain a first estimate of the time trend of the inventory of  $C_{\text{ant}}$  in the Weddell Gyre over the period of this study (i.e., 1973-2008), as follows. The mean rate of increase in  $C_T$  (taken to represent an upper bound to rate of increase of  $C_{\text{ant}}$ , see section 6.7.3) of all grid points along the section between  $70^\circ\text{S}$  and  $55^\circ\text{S}$  and below 3000 meters depth is  $0.9 \pm 0.4 \mu\text{mol kg}^{-1} \text{decade}^{-1}$ . Assuming this rate of increase of the concentration to be representative of the deep Weddell Gyre as a whole (here taken as west of  $20^\circ\text{E}$  and deeper than 3000 m, and thus having a volume of approximately  $11 \cdot 10^6 \text{ km}^3$ ), the rate of increase of the inventory of  $C_{\text{ant}}$  in the Weddell Gyre is calculated to be about  $12 \pm 6 \cdot 10^{12} \text{ gC a}^{-1}$  ( $\text{TgC a}^{-1}$ ), which is about  $0.15 \pm 0.07\%$  of the current rate of anthropogenic emissions. Please note that this rate of local storage of  $C_{\text{ant}}$  does not include the additional  $C_{\text{ant}}$  transferred into other oceans with the northeastward spreading AABW. Moreover, the storage of  $C_{\text{ant}}$  in the shallower layers (typically  $< 200 \text{ m}$ ), that actually have the highest  $C_{\text{ant}}$  component, could not be included in this approximation due to seasonal variability.

The calculated rate of storage of  $C_{\text{ant}}$  in the deep Weddell Gyre appears to be compatible with the results of Anderson et al. (1991), who estimated an export of  $C_{\text{ant}}$  from the continental shelf into the deep Weddell Gyre of  $8\text{-}16 \text{ TgC a}^{-1}$  from observations in the Filchner Depression in the southern Weddell Sea in 1988-1989. The latter rate of export would on the one hand include the transfer with AABW into other oceans, yet on the other hand, just as in our study exclude the shallower layers.

## 6.8. Conclusions

Time trends in the concentration of  $C_T$  were determined directly from measured values along the  $0^\circ$ -meridian in the Weddell Gyre in the Southern Ocean. A significant positive trend in  $C_T$  of  $+1.2 \pm 0.6 \mu\text{mol kg}^{-1} \text{decade}^{-1}$  is determined in the WSBW. The determined time trends in back-calculated preformed  $C_T$  ( $C_T^0$ ) appear affected by inaccuracies of the oxygen data. Within the observed trend in  $C_T$ , we attempted to separate the contributions of natural variability and the

uptake of anthropogenic CO<sub>2</sub> from the atmosphere, by use of a novel MLR-based technique: Time Series Residuals (TSR). In the taken approach, trends in the residuals ( $C_{\text{residual}}^{\text{TSR}}$ ) of an MLR encompassing all data of 10 cruises are assumed to represent the anthropogenic component of the observed trends in  $C_T$ , whereas trends in the MLR-predicted  $C_T$  values ( $C_T^{\text{TSR}}$ ) are assumed to reflect natural variability in  $C_T$ . Use of this approach regrettably did not allow for a convincing attribution of the observed time trend in measured data of  $C_T$  to either natural variability or uptake of anthropogenic CO<sub>2</sub> from the atmosphere.

However, the significant resemblance between the spatial distributions of time trends determined in  $C_T$  and CFC-12 provides compelling evidence that the results reflect genuine changes in  $C_T$  of the deep Weddell Gyre that are propagated from the surface into the interior. From a consideration of the formation process of the WSBW and observed temperature changes of that water mass, we rule out a strong influence on the observed time trend in  $C_T$  of variable entrainment of WDW into the forming WSBW, thereby strengthening the case for an anthropogenic (rather than a hydrographic) origin of the observed increases in  $C_T$  in the deep Weddell Gyre. If indeed assuming the trend in  $C_{\text{ant}}$  to equal the trend in  $C_T$  (i.e., the trend in  $C_{\text{ant}}$  equals about  $+1.2 \pm 0.6 \mu\text{mol kg}^{-1} \text{decade}^{-1}$ ), and further assuming an exponential buildup of  $C_{\text{ant}}$  in the deep ocean (as in the atmosphere and surface ocean), we calculate a total concentration of  $C_{\text{ant}}$  in the WSBW of  $6 \pm 3 \mu\text{mol kg}^{-1}$  for the year 1995. This estimate is significantly lower than estimates obtained with the TrOCA method, but higher than what is generally obtained using the  $\Delta C^*$  method. Results from investigators using the TTD method compare more favorably with our estimate. Extrapolating the determined rate of increase of the concentration of  $C_{\text{ant}}$  to the deep Weddell Gyre as a whole (>3000 m, west of 10 °E), we obtain a rate of increase of the inventory of  $C_{\text{ant}}$  of about  $12 \pm 6 \text{TgC a}^{-1}$  for 1995, or about 0.15% of current anthropogenic emissions to the atmosphere. This case study of the Weddell Gyre demonstrates the value of the direct determination of time-trends of  $C_T$  in the deep ocean.

## 6.9. Recommendations for future research

While we arguably have been successful in using historical data of  $C_T$  to determine time trends in the deep Weddell Sea, we experienced difficulties in separating the natural and anthropogenic components of the observed changes, whether with the proposed TSR method or the classical  $C_T^0$  approach. In part, this was due to uncertainties about the accuracy of the ancillary parameters required for such an exercise. Dataset compilation efforts like GLODAP and CARINA may to some extent eliminate systematic cruise biases of these properties. Nevertheless it has become obvious that further improvement of the original measurements is needed in future cruises. Variable biases of up to 3% are quite common in the used datasets of nutrients and dissolved O<sub>2</sub>, while in fact the state-of-the-art does permit an order of magnitude lower uncertainty (i.e., circa 0.2%), approaching what is common nowadays for  $C_T$  and A<sub>T</sub>. Reference standards for measurements of the major nutrients are being developed and made available to the international community under the flag of the Meteorological Research Institute, Tsukuba, Japan (Aoyama et al., 2008). The determination of the increase of inventories of  $C_T$  and the separation of the natural and anthropogenic components of this increase will likely benefit greatly from the widespread adoption of these reference materials. The development of reference material (or another method of standardization) for dissolved oxygen would similarly be

of great benefit. A simple standardization method for oxygen exists, namely, the measurement of seawater saturated with oxygen at stable temperature and air pressure conditions, where the oxygen concentration is known from the theoretical solubility (Reinthal et al., 2006). Analysts are encouraged to use this method until reference material becomes available.

The further long term pursuance of repeated ocean interior measurements of  $CO_2$ , ideally accompanied by continued measurements of CFCs and the broad adoption of  $SF_6$  as an additional anthropogenic tracer, will be crucial for further constraining the oceanic uptake and storage of anthropogenic  $CO_2$  from the atmosphere on decadal time scales, both locally in the Weddell Gyre and in the ocean at large.

## 6.10. Acknowledgements

The diligent work performed by the officers, crew and scientists that participated in the many expeditions of which results are used in this study is immensely appreciated. Without this measurement effort, sustained over more than three decades already, this work would not have been possible. The excellent cooperation with the officers, crew and scientific party during *PFS Polarstern* expedition ANT-XXIV/3 is specifically acknowledged. Valuable suggestions by two anonymous reviewers have helped to substantially improve this manuscript.



# Chapter 7

## **Determination of the rate of storage of anthropogenic CO<sub>2</sub> in the South Atlantic Ocean from 35 years of ocean interior observations**

*This manuscript will be adapted for submission a scientific journal.*



## Abstract

Uptake and storage of atmospheric anthropogenic  $\text{CO}_2$  by the oceans are part of a major perturbation of the global carbon cycle. This study attempts to determine the rate of storage of anthropogenic  $\text{CO}_2$  ( $C_{\text{ant}}$ , part of the total amount of dissolved inorganic carbon  $C_{\text{T}}$ ) in the South Atlantic Ocean. We use measured data of the oceanic  $\text{CO}_2$ -system and ancillary variables, obtained from the CARINA and GLODAP data products as well as from original contributions by the authors and others. The time rate of change of  $C_{\text{ant}}$  ( $dC_{\text{ant}}/dt$ ) is assessed using an adaptation of the Time Series Residuals method (TSR; van Heuven et al., 2011), which is based on multivariate linear regression (MLR) techniques. The results are scaled up to the entire basin using climatological information.

An optimum multiparameter (OMP) analysis is used to separate the contributions of 7 distinct water masses to the measured samples of 53 cruises. Subsequently, in the core of each of the water masses, a characteristic multivariate linear relationship between measured  $C_{\text{T}}$  ( $C_{\text{T}}^{\text{meas}}$ ) and ancillary parameters is determined, using all locally available cruise data, irrespective of sampling date. Using these relationships, a synthetic value for  $C_{\text{T}}$ ,  $C_{\text{T}}^{\text{TSR}}$ , is generated for each sample in the database. As is commonly done, we assume that changes over time in the difference between  $C_{\text{T}}^{\text{meas}}$  and  $C_{\text{T}}^{\text{TSR}}$  (i.e., the *residuals* of the relationship,  $C_{\text{res}}^{\text{TSR}}$ ) are representative of changes over time in the  $C_{\text{ant}}$  component of  $C_{\text{T}}$ . We therefore assume the time rate of change of  $C_{\text{ant}}$  to be commensurate with the time rate of change of  $C_{\text{res}}^{\text{TSR}}$ . We assume all such time trends to be linear in first approximation. For three of the 7 water masses discerned in this study,  $dC_{\text{ant}}/dt$  is further expressed as a linear function of apparent oxygen utilization (AOU). Accounting for this dependence of  $dC_{\text{ant}}/dt$  on AOU is necessary because within a water mass,  $dC_{\text{ant}}/dt$  is expected to be high in the most recently ventilated part of the water mass and low in the ‘older’ part of the water mass, since the latter was ventilated in times where the atmospheric concentrations of anthropogenic  $\text{CO}_2$  were lower. The analysis reveals values of  $dC_{\text{ant}}/dt$  as high as  $1 \mu\text{mol kg}^{-1} \text{a}^{-1}$  for the most recently ventilated parts of surface water masses and as zero for the North Atlantic Deep Water, observations which are consistent with expectations. We note that values of  $dC_{\text{ant}}/dt$  for the deep water masses of southern origin (Antarctic Bottom Water, Weddell Sea Bottom Water) are slightly above zero – indicating the accumulation of significant amounts of  $C_{\text{ant}}$  in these voluminous water masses. The storage rates in the different water mass cores, as thus obtained from measured data, are extrapolated to the World Ocean Atlas 2005 climatology. We calculate the overall rate of storage of  $C_{\text{ant}}$  in the South Atlantic Ocean (poleward of the equator and extending to the Antarctic continent) to be  $0.39 \pm 0.08 \text{ PgC a}^{-1}$ .

Assessing trends in  $C_{\text{T}}^{\text{meas}}$  itself (rather than using  $dC_{\text{ant}}^{\text{TSR}}/dt$ ) yields markedly similar results, although the error estimates on the TSR-based estimated are smaller, especially for the warmer waters. This comparison corroborates the robustness of the methodology. Adopting the concept suggested by Rios et al. (2012), we additionally express the rate of change of  $C_{\text{ant}}$  as a function of the concentration of atmospheric anthropogenic  $\text{CO}_2$  (in  $\mu\text{atm}$ ). The resulting metric (in units of  $\mu\text{mol kg}^{-1} \mu\text{atm}^{-1}$  rather than  $\mu\text{mol kg}^{-1} \text{a}^{-1}$ ) allows for scaling of the inferred oceanic



accumulation of  $C_{\text{ant}}$  to past and (not-too-far) future concentrations of atmospheric anthropogenic  $\text{CO}_2$ , provided that the atmospheric increase continues approximately exponentially.

Our results compare favorably with those obtained by other investigators, further strengthening and constraining the significant storage of  $C_{\text{ant}}$  in the South Atlantic Ocean.

## 7.1. Introduction

Only about 45% of the  $\text{CO}_2$  that is emitted by human activities (anthropogenic  $\text{CO}_2$  or  $\text{CO}_{2\text{ant}}$ ) is retained in the atmosphere (Solomon et al., 2007; Le Quéré et al., 2009). The remainder is accounted for by net uptake by the terrestrial biosphere and the surface ocean. In the latter, it contributes to the pool of dissolved inorganic carbon (DIC, hereafter  $C_T$ , in units of  $\mu\text{mol kg}^{-1}$ ). The anthropogenic fraction of  $C_T$  is commonly referred to as  $C_{\text{ant}}$ . A quantitative understanding of this uptake of anthropogenic  $\text{CO}_2$  and its subsequent transport as  $C_{\text{ant}}$  into the ocean interior is a prerequisite for robust projections of the future behavior of Earth's perturbed carbon cycle.

The South Atlantic Ocean, here including the Atlantic sector of the Southern Ocean, is of particular importance to the process of uptake and storage of anthropogenic  $\text{CO}_2$ . The formation regions of mode- and intermediate waters and, to a lesser extent, of deep waters (the Subantarctic Convergence Zone (SCZ) and the vicinity of major ice sheets surrounding the Antarctic continent, respectively) are considered to be responsible for up to 40% of the global oceanic uptake of anthropogenic  $\text{CO}_2$  (Takahashi et al., 2009; Gruber et al., 2009; Khatiwala et al., 2009). However, specifically in the Southern Ocean, estimates of the inventory of  $C_{\text{ant}}$  and of the flux of  $\text{CO}_{2\text{ant}}$  across the sea surface vary substantially between authors and methodologies, both in total amount and in the vertical and horizontal distribution.

Sabine et al. (2004) use ocean interior carbon measurements to estimate a total global inventory of  $C_{\text{ant}}$  ( $^{\text{INV}}C_{\text{ant}}$ ) of  $118 \pm 19 \text{ PgC}$  ( $1 \text{ PgC} = 1 \cdot 10^{15}$  grams of carbon) in 1995. The South Atlantic Ocean (defined here as all waters south of the Equator, between  $30^\circ\text{E}$  and Drake Passage) contributes circa  $17.3 \text{ PgC}$  (~15%) to this global total. According to Sabine et al. (2004), deep waters (>1500 m), and waters south of the Polar Front are typically devoid of anthropogenic carbon. Conversely, by using a different ocean interior carbon-based method, Lo Monaco et al. (2005a; 2005b) report very significant concentrations of  $C_{\text{ant}}$  in the deep and bottom waters of the Eastern South Atlantic Ocean at  $30^\circ\text{W}$ . Khatiwala et al. (2009) present a reconstruction of the history of concentrations of  $C_{\text{ant}}$  in the ocean that is constrained by observations of chlorofluorocarbon (CFCs),  $\Delta^{14}\text{C}$  and additional tracers of gas exchange and ocean circulation. The global inventory and rate of uptake for the year 2008 are by Khatiwala et al. (2009) inferred to be  $140 \pm 25 \text{ PgC}$  and  $2.3 \pm 0.6 \text{ PgC a}^{-1}$ , respectively. For the South Atlantic Ocean as defined in the current study, these values are  $23 \pm 5 \text{ PgC}$  and  $0.39 \pm 0.10 \text{ PgC a}^{-1}$ , respectively (Khatiwala, personal communication; uncertainties scaled, but are likely somewhat larger). From a local study, Van Heuven et al. (2011) report a modest rate of increase in  $C_{\text{ant}}$  in the deep Weddell Gyre (intermediate to the results of Sabine et al. (2004) and Lo Monaco et al. (2005a; 2005b), and more in line with the results of Khatiwala et al. (2009)), thereby strengthening the case for at least a moderate rate of storage of  $C_{\text{ant}}$  in the deep South Atlantic Ocean. In a study confined to the western South Atlantic Ocean between  $10^\circ\text{N}$  and  $55^\circ\text{S}$ , Rios et al. (2012) use measurements of  $C_T$ , total alkalinity ( $A_T$ ) and dissolved oxygen ( $\text{O}_2$ ), taken over 30 years, to infer an inventory and rate of storage of  $C_{\text{ant}}$  that are significantly higher than suggested by many other studies,

and attribute the difference in large part to (not earlier reported) non-negligible amounts of  $C_{\text{ant}}$  in the very large volumes of Antarctic Bottom Water (AABW) and North Atlantic Deep Water (NADW).

Carbon cycle models currently offer little help in constraining (the rate of storage of)  $C_{\text{ant}}$  because they have difficulty to determine the net flux across the ocean surface in the important formation regions south of 45 °S due to their present inability to sufficiently resolve the intrinsically small-scale processes of water mass formation in this area (Gruber et al., 2009). From the above, it becomes clear that for the South Atlantic Ocean, consensus exists neither on the inventory of  $C_{\text{ant}}$  nor on the uptake of  $\text{CO}_{2,\text{ant}}$ . However, a well constrained understanding of the rates of uptake and storage of  $C_{\text{ant}}$  in the South Atlantic Ocean is much needed for the validation and further improvement of global carbon cycle models, which will be indispensable for projections of the impact of human activity on the Earth's biosphere.

The present study aims to provide an estimate of the rate of storage of  $C_{\text{ant}}$ , based on measurements of ocean interior  $C_T$  and ancillary data collected in the South Atlantic Ocean over the period of 1973 to 2008. We employ an adaptation of the Time Series Residuals technique (Van Heuven et al., 2011) that allows the assessment of trends in  $C_{\text{ant}}$  in the cores of the dominant locally present water masses. The method aims to avoid some of the uncertainties that have plagued the studies mentioned above. It aims to minimize the confounding influence of natural variability in hydrography and biogeochemistry by the use of a technique based on multivariate linear regression. Additionally, the sensitivity of the result to unknown biases in the individual cruise datasets is reduced by including data from 53 cruises, mostly obtained from databases that have been processed for optimal internal consistency. The rates of increase of  $C_{\text{ant}}$  determined for individual water masses, are extrapolated to a high resolution climatology and compared to the results from other investigators.

## 7.2. Outline of study

This section summarizes the methods used in this study to estimate the rate of storage of anthropogenic carbon in the South Atlantic Ocean. After an introduction of the hydrography of the South Atlantic Ocean, more detailed descriptions of these methods and their application will follow in subsequent sections, together with results. A discussion of the results is found at the end of this paper (section 7.9).

Briefly, the employed methodology assumes that the rate at which anthropogenic carbon accumulates in the ocean ( $dC_{\text{ant}}/dt$ ) may be quantified by tracing over time the portion of the variability of  $C_T$  that is not explained by variability in hydrography and biogeochemistry. We employ the Time Series Residuals method (TSR; Van Heuven et al., 2011) that is a variant of the MLR technique (Wallace 1995; Friis et al., 2005).

The products of the GLODAP and CARINA data synthesis projects (Key et al., 2004, 2010) have been merged with several datasets that are not available in these products (section 7.4). The resulting global dataset contains data from about 250 cruises, 53 of which are used in the present analysis of the South Atlantic Ocean. After thus preparing the data, the contributions of seven water masses to the samples in the dataset are quantified by use of an optimum multiparameter analysis (OMP, Tomczak, 1981; Mackas et al., 1987; section 7.5). Next, in section 7.6, for each sample in the dataset, a 'synthetic' value for  $C_T$  ( $C_T^{\text{TSR}}$ ) is generated using a predic-

tive relationship obtained using multivariate linear regression (MLR) between the measured concentration of dissolved inorganic carbon (DIC, hereafter  $C_T^{\text{meas}}$ ) and predictive hydrographic and chemical parameters, using all available data (i.e., not only the newer cruises). The difference between the  $C_T^{\text{TSR}}$  and  $C_T^{\text{meas}}$  is referred to as the *residual*:  $C_{\text{res}}^{\text{TSR}}$ . Its change over time is assumed to represent the change over time of the anthropogenic component  $C_{\text{ant}}$  of  $C_T^{\text{meas}}$ . In section 7.7, for each water mass core a multi-linear relationship is derived between  $C_{\text{res}}^{\text{TSR}}$ , AOU and time. This relationship is assumed to describe for a water mass how the concentration of  $C_{\text{ant}}$  increases over time at different apparent 'distances' from the ventilation region (where 'distance' is represented by the apparent oxygen utilization, AOU). For example, at high AOU (i.e., far removed from the formation region) the relationship between  $C_{\text{res}}^{\text{TSR}}$  and time may be found to be neutral (i.e., no change in  $C_{\text{ant}}$  over the time span of observations), while at low AOU (i.e., at or near the formation region)  $C_{\text{res}}^{\text{TSR}}$  (i.e.,  $C_{\text{ant}}$ ) may be determined to be increasing sharply with time. After having obtained such typical relations for the individual water masses in the South Atlantic Ocean, these rates are projected onto the World Ocean Atlas 2005 climatology (section 7.8). The resulting rates of increase of  $C_{\text{ant}}$  may be integrated to obtain the total rate of storage of  $C_{\text{ant}}$  in the South Atlantic Ocean. Finally, section 7.9 evaluates the obtained results in light of earlier estimates.

### 7.3. Hydrography of the South Atlantic Ocean

The South Atlantic Ocean in this study encompasses all waters between the Equator and the Antarctic continent, west of 30 °E and east of Drake Passage at 65 °W (Figure 7.1). This section details the general hydrological features of the South Atlantic Ocean, as well as several details that are of specific interest to this study. Throughout this treatment of the hydrography of the South Atlantic Ocean, refer to Figures 7.1 and 7.2.

#### 7.3.1. Bottom topography

The Atlantic Ocean is divided meridionally by the Mid-Atlantic Ridge, which at places rises to depths as shallow as 700 m. In the South Atlantic Ocean it prohibits all abyssal flow between the eastern and western basins at levels below 3300 m, the southernmost connection being formed by the Romanche Fracture Zone just north of the Equator, which connects the east and west basins to a depth of 4500 m. Further impediments to abyssal flow are Walvis Ridge and Rio Grande Rise, located around 30 °S in the eastern and western basins, respectively. Walvis Ridge inhibits abyssal flow below 4000 m, while the Rio Grande Rise gives way to the Rio Grande Gap to its west, allowing bottom currents passage down to 4700 m depth. These and other subsea ridges divide the South Atlantic Ocean into (clockwise from the north east) the Guinea Abyssal Plain, Angola Basin, Cape Basin, Weddell-Enderby Abyssal Plain, Argentine Basin and the Brazil Basin (Tomczak and Godfrey, 2003).

### 7.3.2. Deep Currents and water masses

#### *North Atlantic Deep Water (NADW)*

The NADW is a relatively warm, saline water mass of arctic and sub-arctic origin. From high northern latitudes, it moves southward as a deep western boundary current and enters the South Atlantic Ocean from the northwest. Entrainment of lenses of Eurafrian Mediterranean Water (EMW) increases potential temperature ( $\theta$ ) and salinity ( $S$ ) of the NADW as it travels southward, reaching values of  $\theta=4.4^{\circ}\text{C}$  and  $S=35.0$ . Through entrainment and mixing, the NADW defines the makeup of large parts of the deep South Atlantic Ocean. During its movement southward, its upper and lower layers gradually mix with the overlying Antarctic Intermediate Water (AAIW, see below) and underlying Antarctic Bottom Water (AABW, see below), respectively. However, the core of the NADW between 3500 and 2000 m depths can be clearly identified across the width of the South Atlantic Ocean as far south as  $50^{\circ}\text{S}$ . At these latitudes, NADW is entrained into the Antarctic Circumpolar Current, and referred to as Circumpolar Deep Water (CDW; see below). Concentrations of dissolved oxygen and nutrients are fairly uniform over the latitudinal range, due to a moderate influx of organic material from overlying water combined with a high overall flow toward the south.

Although the recently ventilated, northern extent of the NADW is generally considered to constitute the main conduit of anthropogenic  $\text{CO}_2$  into the deep ocean (Sabine et al., 2004), the southern extent of the NADW is generally considered to still be free of  $C_{\text{ant}}$ .

#### *Circumpolar Deep Water (CDW)*

The NADW, which can be recognized as far south as circa  $50^{\circ}\text{S}$ , gets deflected upwards by the AABW, which wedges itself underneath the NADW from the south. Reaching shallower layers, the NADW becomes part of the CDW, one of the main water masses transported in eastward direction by the Antarctic Circumpolar Current (ACC). The ACC flows rapidly around Antarctica in the zonal band between  $45^{\circ}\text{S}$  and  $65^{\circ}\text{S}$ , its eastward movement extending along the full depth of the water column. The characteristics of this rapidly moving volume of water do only change slightly throughout the three great oceans. The NADW may be considered to be the main constituent of CDW although the CDW is also fed from below by the AABW and from above by the AAIW. The continuous supply of NADW from the north and wind-driven surface divergence to the south force the upper layers of the CDW gradually further southward and upward, i.e., over the AABW. Upon reaching the depths of the wind-mixed layer – in the Atlantic around  $65^{\circ}\text{S}$  – the thus upwelled CDW is split into north- and south-bound surface flows in a process referred to as the Antarctic Divergence. Part of the northbound fraction may subduct to become AAIW, while a further part may reach the sub-tropical convergence zone and may contribute to the South Atlantic Central Water (SACW; see below). The south-bound waters will reach close to the continent, and may contribute to the formation of AABW.

Vertical mixing occurs at the interfaces of CDW with AABW and AAIW. This changes the properties of the CDW. Mixing of the CDW with the overlying AAIW creates the approximately equally warm but less saline mixture referred to as Upper Circumpolar Deep Water (UCDW). Mixing of the CDW with the underlying AABW freshens and cools the CDW, resulting in a water type is referred to as Lower Circumpolar Deep Water (LCDW). In between the two

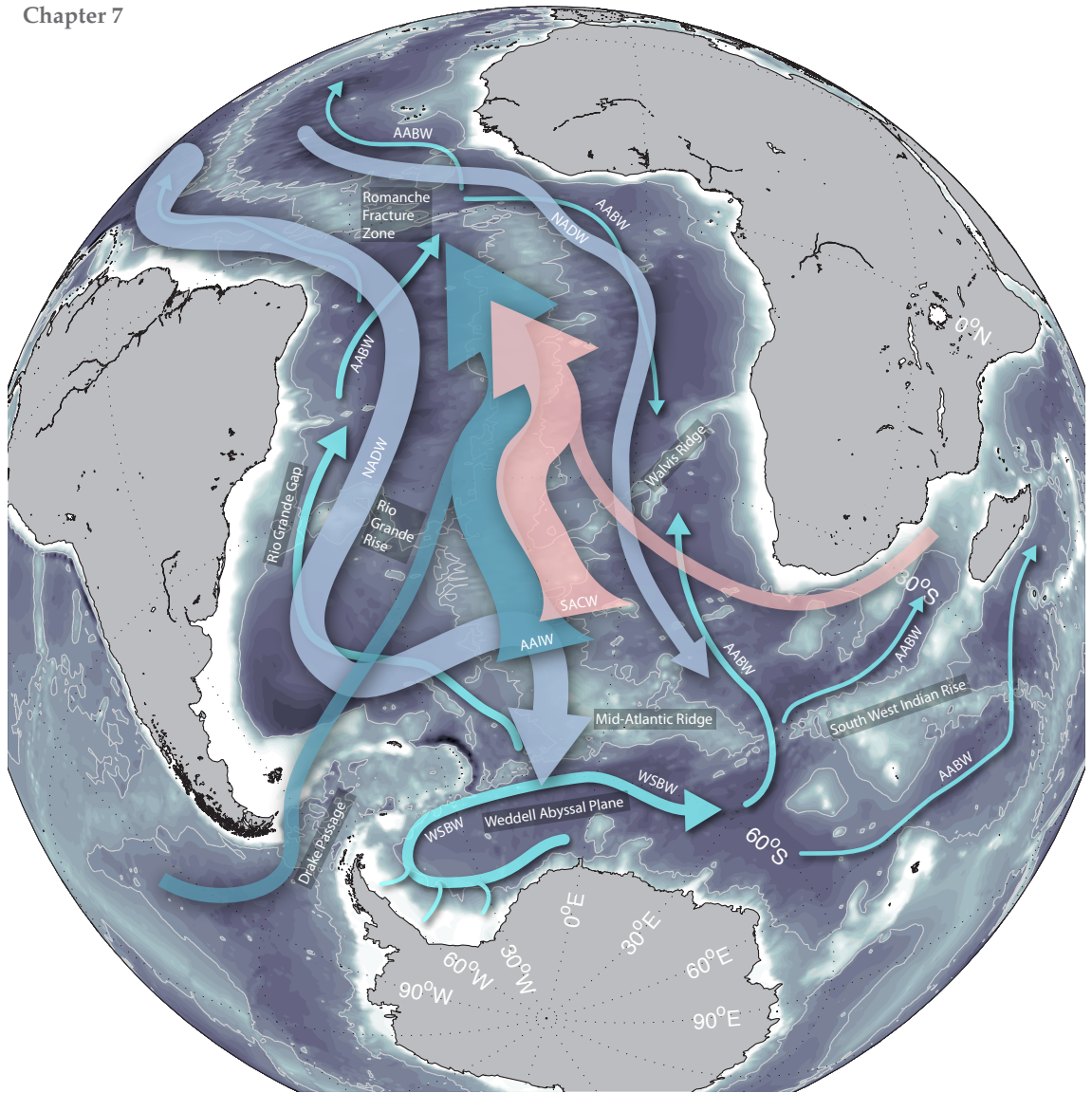


**Figure 7.1.** Map of the South Atlantic Ocean, schematically showing some of the major local bathymetric and hydrographic features of the ocean interior. SACW: South Atlantic Central Water; AAIW: Antarctic Intermediate Water; NADW: North Atlantic Deep Water; AABW: Antarctic Bottom Water; WSBW: Weddell Sea Bottom Water. Not shown are the strong, westward flowing Antarctic Circumpolar Deepwater and the equatorial surface water masses. Arrow width is not indicative of watermass volume or formation rate. Refer to text section 7.3 for details.

mixing layers, the dominant characteristic is that of NADW, although that gets progressively further eroded as the CDW moves south.

Because of its origin in the 'old' NADW with only very limited contributions from AABW (which is not considered well ventilated with respect to  $\text{CO}_2$ ), the  $C_T$  of LCDW may be considered to be relatively insensitive to rises in atmospheric  $\text{CO}_2$ .



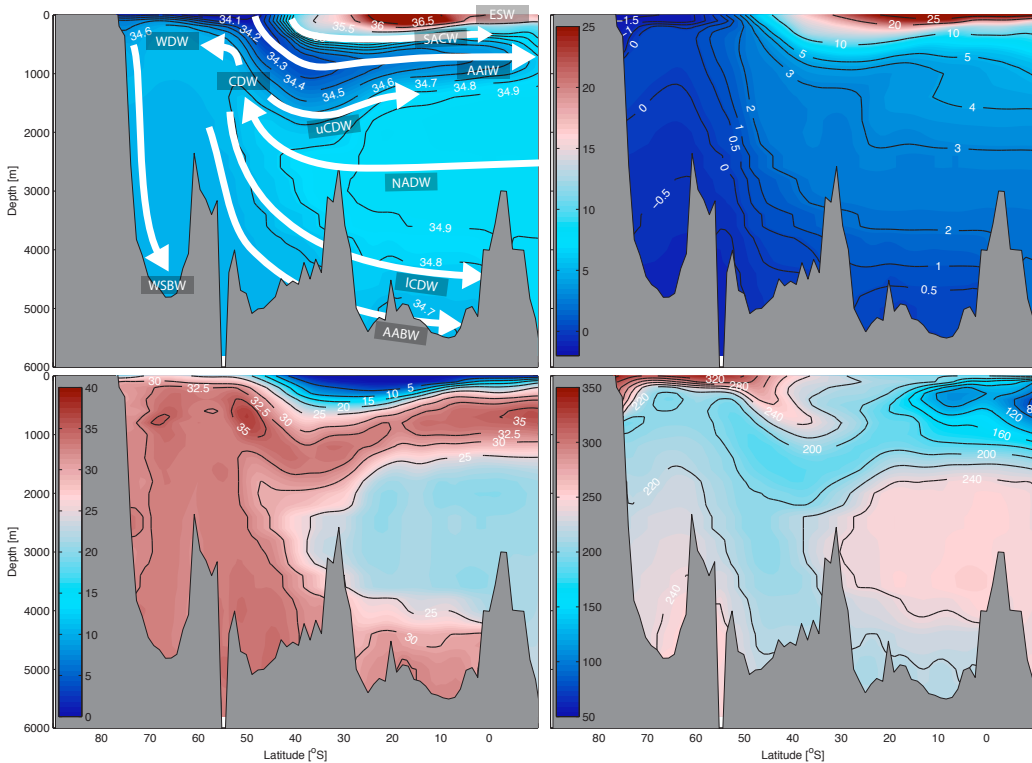


**Figure 7.2.** Meridional section along  $30^{\circ}\text{W}$ , showing major bathymetric and hydrographic features, as well as the generalized locations and movements of various water masses in the South Atlantic Ocean. Please refer to text section 7.3 for details. Panel a: salinity (in psu); Panel b: potential temperature ( $\theta$ ) [ $^{\circ}\text{C}$ ]; panel c: nitrate [ $\mu\text{mol kg}^{-1}$ ]; panel d: oxygen [ $\mu\text{mol kg}^{-1}$ ]. Water mass abbreviation is in Figure 7.1, with the addition of CDW: Circumpolar Deep Water; WDW: Warm Deep Water; WSDW: Weddell Sea Deep Water; ESW: Equatorial Surface Water.

### *Antarctic Surface Water (AASW) and Winter Water (WW)*

All surface layer waters south of the Polar Front are referred to as Antarctic Surface Water (AASW). Violent storms during the austral autumn and winter stir the water column to significant depth, generating a rather homogenous layer of cold, fresh ( $\theta > -1.8^{\circ}\text{C}$ ,  $S=34$ ) water. In summer, temporarily, a shallow, warm and stratified surface layer may form. The cold, fresh water mass that persists underneath the AASW is known as Winter Water (WW). Due to brine rejection during the formation of pack ice, WW may become more saline, and under the right conditions (generally under the influence of ice shelves and polynyas) may contribute to the formation of Weddell Sea Deep Water and Weddell Sea Bottom Water (WSDW and WSBW, respectively; see below).

The WW and AASW are expected to exhibit an only moderately rising concentration of  $C_{\text{ant}}$  because of being constantly replenished from below with  $C_{\text{ant}}$ -poor CDW. Also due to seasonal ice cover, the AASW and WW may not be ventilated well enough to fully track the rising atmospheric concentrations of  $\text{CO}_2$  (Ito et al., 2004).

### *Weddell Sea Bottom Water (WSBW) and Weddell Sea Deep Water (WSDW)*

Along the Antarctic continent, surface water loses heat to the atmosphere and becomes more saline during the formation of pack ice. Subsequent cooling, often at a depth of several hundreds of meters, along the side and bottom of (floating) ice sheets increases the density of these waters to the point that convective sinking to great depths may take place. The most important areas in the (circumpolar) Southern Ocean for such convective formation of bottom waters are the southern and western boundaries of the Weddell Sea, where the Weddell Sea Bottom Water is formed (Huhn et al., 2008). During its descent and flow towards the bottom of the Weddell Abyssal Plain, the characteristically low temperature ( $\theta \approx -1.8^\circ\text{C}$ ) of the freshly forming WSBW is eroded away by entrainment of encountered water masses, which are derived from warmer, slightly more saline CDW. The rotation of the Weddell Gyre and the continuous replenishment of the deepest WSBW with fresh input from the ice-shelves forces the bottom water mass at the interior abyssal plain slowly upwards. The ascending water mass is generally referred to as the Weddell Sea Deep Water (WSDW). The WSDW is not a water mass with a distinct core, because it constitutes the gradient between WSBW (below) and the CDW above, although we note that several authors point to direct contributions to WSDW of the descending ice shelf water (e.g., Weppernig et al., 1996). The WSDW spills out of the Weddell-Enderby Basin over and through the Mid-Atlantic Ridge and the West-Indian Ridge into the surrounding basins, from where it proceeds northward as part of the Antarctic Bottom Water.

The formation process of WSBW takes place under the influence of ice shelves (i.e., not necessarily in contact with the atmosphere). It therefore does not necessarily exhibit strong uptake of anthropogenic  $\text{CO}_2$  from the atmosphere. However, tentative gradual increases in  $C_{\text{ant}}$  in the WSWB have been inferred (Hoppema et al., 1998, Van Heuven et al., 2011).

### *Antarctic Bottom Water (AABW)*

The global ocean's densest common water mass, the AABW, is formed by convective processes at several locations around the Antarctic continent. Significant source areas are the ice shelves surrounding the Weddell Sea (see WSBW, above), the Ross Sea and the Adelie Coast. This water mass flows northward into all three oceans, underlying all other water masses. In the eastern basin of the South Atlantic Ocean, continuous northward flow of the AABW is restricted by the presence of Walvis Ridge. In the western basin the flow of AABW is unhampered and traces of AABW are found as far north as  $50^\circ\text{N}$ . During its journey from the Southern Ocean, the characteristics of AABW (cold, fresh) are slowly modified by the overlying warm, saline NADW. The eastern basin of the Atlantic Ocean (north of Walvis Ridge) is filled with AABW through the equatorial Romanche Fracture zone. Thus, Walvis Ridge is bordered by AABW on both sides, with the variety to the north being about  $1^\circ\text{C}$  warmer and more saline.

The capacity of AABW to take up anthropogenic  $\text{CO}_2$  from the atmosphere is considered to be limited (Poisson and Chen, 1987; Klatt et al., 2002). The formation of the water mass does not necessarily take place in contact with the atmosphere, and significant entrainment of sub-surface water masses by the convective downwelling streams will dilute (on a concentration basis) the modest uptake that does take place at the surface.

*Antarctic Intermediate Water (AAIW) and Subantarctic Upper Water (SAUW)*

The high salinity ( $S=34.7$ ) of the upwelled CDW is at the surface rapidly decreased (to  $S=33-34$ ) by the melting of ice and snow-on-ice (from the south) and by strong precipitation. The north-bound part of the upwelled water warms to 4-10 °C at lower latitudes, and becomes Subantarctic Upper Water (SAUW). In winter, at latitudes of 35-45 °S, SAUW becomes homogenized by strong wintertime mixing, and is referred to as Subantarctic Mode Water (SAMW). Around 50 °S, i.e., north of the Polar Front, convective subduction forms the Antarctic Intermediate Water (AAIW). This water mass initially sinks to a depth of circa 1000 m, while being deflected northward by the underlying CDW), exchanging characteristics with it. As indicated above, the resulting 'AAIW-tainted' CDW is referred to as 'Upper' CDW, or UCDW. The AAIW gradually rises to about 800 m while continuing its northward journey as a distinct layer of low-salinity water. This layer is slowly eroded away by the more saline over- and underlying water masses (SACW and UCDW/NADW, respectively), and the AAIW can no longer be clearly discerned north of ~20 °N.

A significant fraction of the AAIW found in the South Atlantic Ocean is believed to be transported through Drake Passage after having been formed from Subantarctic Mode Water (SAMW) in the southeast Pacific Ocean (Talley, 1996). Intense and extended contact of this water mass with the atmosphere during formation is expected to result in strong uptake of  $\text{CO}_{2,\text{ant}}$ .

*South Atlantic Central Water (SACW)*

As stated above, intense wintertime mixing in the subantarctic frontal zone results in the rather homogenous Subantarctic Mode Water (SAMW), which contributes both to the AAIW and the South Atlantic Central Water.

The main component of the South Atlantic thermocline distinguished in this study is South Atlantic Central Water (SACW). This water mass forms in a subductive process (i.e., being pushed down by convergence of surface water masses), as opposed to AAIW, which may be understood to be formed in a more convective (i.e., density-driven) manner. Formation of SACW takes place in the subtropical frontal zone (STF) around 45 °S. The cold and fresh ( $\theta > 8^\circ\text{C}$ ,  $S \approx 34.6$ ) southern component of this convergence is a warm variety of SAMW (the southern extent of the SAMW is the source of AAIW). The northern component of the SACW on the other hand is warmer and more saline to ( $\theta \approx 17^\circ\text{C}$ ,  $S \approx 35.75$ ). All intermediate varieties of SACW have properties on the mixing line between these two extremes. The SACW extends northwards from the STF (around 45 °S) to about 15 °N, where the North Atlantic Central Water becomes the dominant water mass in the thermocline with its own, distinct characteristics.

Part of the SACW does not actually form in the Atlantic Ocean, but rather was formed in the Indian Ocean, and is transported around South Africa by the Agulhas Current (Tomczak, 2003; Provost et al., 1999) as part of the upper limb of the meridional overturning circulation. In the literature the distinction between these two varieties of SAMW is often made (referred to as East- and West-SAMW). However, for reason of simplicity that will become evident in section 7.5, in this study we limit ourselves to using just one definition.

Due to their prolonged exposure to the atmosphere, both the southern and northern source waters that contribute to the SAMW are expected to be able to fully track the increasing atmospheric levels of  $\text{CO}_2$ .



### Equatorial Surface Water (ESW)

Temperatures of the tropical surface waters encountered north of circa 30 °S exceed 25 °C. Salinity of this very warm surface water varies greatly due to excess precipitation at the equator, and excess evaporation around between 15° and 30° on either side of the equator. These waters will contribute to the Central Waters of both the North and South Atlantic Oceans after reaching the subtropical subduction zones as part of the surface circulation. There, they will have lost much of their heat. These water masses may thus be understood to constitute the surface return flow of the SACW. However, due to the evaporation/precipitation-driven transformation upon upwelling near the equator these hot surface waters are classified as a distinct water type: Equatorial Surface Water (ESW).

The high CO<sub>2</sub> content of ESW (largely due to deep remineralization of organic matter) causes these upwelled waters to be a source of CO<sub>2</sub> to the atmosphere. The CO<sub>2</sub> efflux must have become smaller as the *p*CO<sub>2</sub> of the atmosphere increased due to anthropogenic emissions. The resultant increase over time of C<sub>T</sub> of these water masses is expected to follow the increasing atmospheric concentration only qualitatively, because the continuous upwelling of C<sub>ant</sub>-poor waters from below will keep concentrations below equilibrium with the atmosphere.

## 7.4. Data provenance

### 7.4.1. Cruise datasets

The present study uses data from 53 cruises (Table 7.1). These data are obtained from the GLODAP and CARINA data synthesis projects (Key et al., 2004 and 2010, respectively; both available at <http://cdiac.ornl.gov>), as well as several cruises that are not part of either data product: three cruises on board *PFS Polarstern* in 2002, 2005 and 2008 in which the authors took part, as well as two cruises (on *RV Ron Brown* in 2005 and on *RV Revelle* in 2008), downloaded from the CLIVAR & Carbon Hydrographic Data Office (CCHDO, <http://cchdo.ucsd.edu>). For analytical details of these cruises, see the references in Table 7.1. The spatial and temporal coverage of the dataset is presented in Figures 7.3 and 7.4.

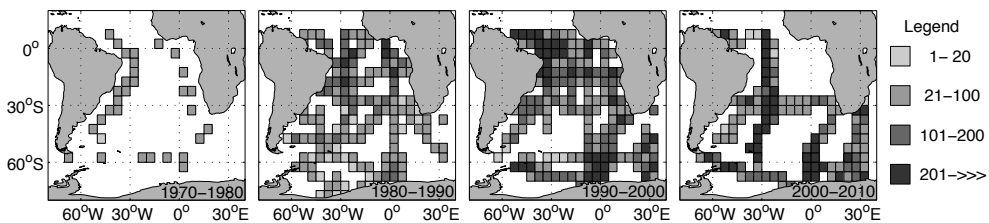


**Figure 7.3.** The spatial distribution of samples of C<sub>T</sub> in the dataset, divided into four one-decade periods. The samples in the leftmost panel are exclusively from the GEOSECS expeditions. The 1980-2000 period can be seen to be highly representative of the basin as a whole. In the vast majority of cases, samples can be assumed to cover the entire water column. The southern Weddell Sea is not well represented in any period.

## GLODAP

During the World Ocean Circulation Experiment (WOCE; Wunsch, 1996) enough  $\text{CO}_2$ -system related data were collected to derive the global distribution of anthropogenic carbon in the oceans. Such studies (e.g., Sabine et al., 2004) rely heavily on accurate measurements of Dissolved Inorganic Carbon ( $\text{DIC}$ , hereafter  $C_{\text{T}}^{\text{meas}}$ ), total alkalinity ( $A_{\text{T}}^{\text{meas}}$ ), the dissolved major nutrients nitrate ( $\text{NO}_3$ ), phosphate ( $\text{PO}_4$ ), silicate ( $\text{Si}$ ), and dissolved oxygen ( $\text{O}_2$ ). Although these variables are generally analyzed with very high precision, the accuracy of the analyses has occasionally been questioned, mainly due to problems with calibration standards, although for  $C_{\text{T}}$  and  $A_{\text{T}}$  this problem has been alleviated to a large extent by the use of certified reference material since the early 1990s (Dickson, 2001).

In order to optimize the internal consistency of the WOCE dataset, the GLODAP project was conceived (Key et al., 2004). This project aimed to assemble all  $\text{CO}_2$ -related data from WOCE and earlier cruises and to adjust the measurements of the individual cruises in such a way as to minimize the deep-water offsets between cruises at crossover locations. Assuming that biases were the result of a single, constant calibration error (i.e., drift of the calibration over time was not considered), at most one adjustment per variable per cruise (or per cruise leg) was performed. The result of this effort was a trio of data products (for the Atlantic, Indian and Pacific oceans), containing all WOCE and historic cruise data (Key et al., 2004). The WOCE-era cruises were adjusted for optimal internal consistency, but data of historic cruises was not altered beyond the removal of obvious outlying data.

During the CARINA effort (see next section; Key et al., 2010; also Chapter 4 of this thesis), in which another 188 cruises were adjusted for internal consistency, the GLODAP data were re-analyzed and this time, adjustments were also suggested for the historical data. These suggestions may be found on the CARINA website (above). Although adjustments were suggested, the CARINA consortium did not apply these adjustments to the historical GLODAP

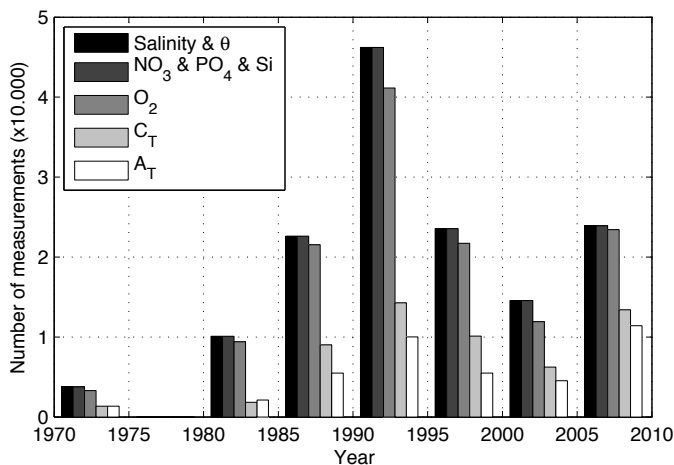


**Figure 7.4.** Distribution of relevant carbon-related measurements over time, binned into periods of five years. The strong measurement effort in the 1990's during the World Ocean Circulation Experiment (WOCE) is prominent.

**Table 7.1.** Cruises of which data were used in this study. The ‘adjustment’ columns list adjustments (in  $\mu\text{mol kg}^{-1}$ ) made in this study to the CARINA cruises. For several cruises, although samples of  $C_T$  are available, the lack of nutrient data precludes the derivation of values for  $C_T^{\text{TSR}}$  (section 7.6). Please refer to text section 7.4.1 for details.

Data origin <sup>4</sup>	Cruisename	Ship	Start date	End date	adjustments		number of samples <sup>6</sup>			
					$C_T$	$A_T$	$C_T$	$A_T$	$C_T^{\text{TSR}}$	
1	GLODAP	GEOSECS-2	Knorr	1972-Oct-17	1972-Oct-29			259	259	455
2	GLODAP	GEOSECS-3	Knorr	1972-Nov-07	1972-Nov-24			369	369	738
3	GLODAP	GEOSECS-4	Knorr	1972-Dec-05	1972-Dec-13			116	117	579
4	GLODAP	GEOSECS-5	Knorr	1972-Dec-31	1973-Feb-02			393	392	809
5	GLODAP	GEOSECS-6	Knorr	1973-Feb-12	1973-Mar-01			206	206	577
6	GLODAP	WEPOLX	Somov	1981-Oct-22	1981-Nov-13			0	304	0
7	GLODAP	TTOTAS_1-3	Knorr	1982-Dec-15	1983-Feb-18			916	917	1404
8	GLODAP	316N83_a,c	Knorr	1983-Oct-07	1984-Feb-15			914	896	4845
9	GLODAP	06AQANTV-2,3	Polarstern	1986-Jul-17	1986-Sep-08			819	790	620
10	GLODAP	INDIGO-3	Dufresne	1987-Jan-28	1987-Feb-07			321	308	259
11	GLODAP	SAVE-HYDROS-1	Knorr	1987-Nov-24	1987-Dec-11			673	548	1330
12	GLODAP	SAVE-HYDROS-2	Knorr	1987-Dec-20	1988-Jan-21			1443	424	2511
13	GLODAP	SAVE-HYDROS-3	Knorr	1988-Jan-29	1988-Mar-06			1733	736	3095
14	GLODAP	SAVE-HYDROS-4	Melville	1988-Dec-09	1989-Jan-13			1088	1062	2747
15	GLODAP	SAVE-HYDROS-5	Melville	1989-Jan-27	1989-Mar-06			908	634	2892
16	CARINA	58A119890214	Stena Arctica	1989-Feb-15	1989-Mar-15	8 <sup>h</sup>	6 <sup>i</sup>	530	223	253
17	GLODAP	SAVE-HYDROS-6	Melville	1989-Mar-14	1989-Apr-12			1513	774	2700
18	GLODAP	06MT11_5	Meteor	1990-Feb-03	1990-Mar-06			994	994	1647
19	GLODAP	06MT15_3	Meteor	1991-Feb-13	1991-Mar-18			751	141	923
20	GLODAP	OACES91_1-2	Baldrige	1991-Jul-12	1991-Aug-04			726	570	0
21	GLODAP	06AQANTX_4	Polarstern	1992-May-28	1992-Jul-28			959	0	1818
22	CARINA	06AQ19920929	Polarstern	1992-Oct-05	1992-Nov-23	5 <sup>j</sup>		509	592	2531
23	GLODAP	06AQANTX_7	Polarstern	1992-Dec-17	1993-Jan-18			1255	0	1636
24	GLODAP	06MT22_5	Meteor	1992-Dec-30	1993-Jan-28			1349	602	1482
25	GLODAP	35MFCIVA_1	Dufresne	1993-Feb-05	1993-Mar-10			1455	1431	1469
26	GLODAP	OACES93	Baldrige	1993-Jul-06	1993-Jul-14			561	507	641
27	GLODAP	3230CITHER_1-2	Ewing	1994-Jan-10	1994-Mar-20			2724	2339	6314
28	GLODAP	06MT28_1	Meteor	1994-Apr-01	1994-May-07			1530	1401	0

29	GLODAP	316N142_3	Knorr	1994-Apr-04	1994-May-19	1462	1432	4900
30	GLODAP	35A3CITHER3_1	L'Atalante	1995-Jan-17	1995-Feb-11	834	939	2278
31	GLODAP	35A3CITHER3_2	L'Atalante	1995-Feb-22	1995-Mar-28	1233	416	3156
32	GLODAP	316N145_9	Knorr	1995-Jun-22	1995-Jun-24	184	157	285
33	CARINA	35LU19950909	LeNoroit	1995-Sep-09	1995-Oct-07	493	486	1731
34	GLODAP	06AQANTXIII_4	Polarstern	1996-Mar-25	1996-May-09	1920	0	2464
35	CARINA	33LK19960415	Edwin.Link	1996-Apr-16	1996-May-16	718	706	308
36	GLODAP	320696_3	Palmer	1996-May-16	1996-May-20	245	149	482
37	CARINA	91AA19971204	Agulhas	1997-Dec-31	1998-Feb-02	483	472	0
38	CARINA	06AQ19980328	Polarstern	1998-Apr-01	1998-May-19	2116	0	2513
39	CARINA	35TH19990712	Thalassa	1999-Jul-16	1999-Aug-20	1639	1634	0
40	CARINA	29HE20010305	Hesperides	2001-Mar-08	2001-Mar-31	386	386	382
41	CARINA	74AB20020301	C. Darwin	2002-Mar-04	2002-Mar-07	167	182	354
42	CARINA	29HE20020304	Hesperides	2002-Mar-06	2002-Mar-28	354	357	263
43	CARINA	06MT20021013	Meteor	2002-Oct-18	2002-Oct-29	48	48	1173
44	Authors <sup>c</sup>	ANT-XX/2	Polarstern	2002-Nov-24	2003-Jan-23	1703	0	0
45	CARINA	33RO20030604	R.H. Brown	2003-Jul-29	2003-Aug-09	672	634	1281
46	CARINA	49NZ20031106	Mirai	2003-Nov-07	2003-Dec-02	1459	1458	3661
47	CARINA	74DI20041103	Discovery	2004-Nov-05	2004-Nov-05	8	9	21
48	CARINA	90AV20041104	A.S. Vavilov	2004-Nov-08	2004-Nov-25	902	906	1707
49	CARINA	33RO20050111	R.H. Brown	2005-Jan-17	2005-Feb-21	5086	5016	8048
50	CCHDO <sup>p</sup>	33RO200501	R.H. Brown	2005-Jan-17	2005-Feb-21	2244	2192	3148
51	Authors <sup>f</sup>	ANT-XXII/3	Polarstern	2005-Jan-02	2005-Apr-6	2228	0	2849
52	CCHDO <sup>f</sup>	33RR20080204	Revelle	2008-Feb-05	2008-Mar-08	1495	2563	2916
53	Authors <sup>g</sup>	ANT-XXIV/3	Polarstern	2008-Feb-13	2008-Apr-13	2093	1348	2636

<sup>A</sup> "GLODAP" here refers to the author's unpublished re-analysis of GLODAP, see text section 7.4.

<sup>B</sup> In the Atlantic Ocean, south of 10°N

<sup>C</sup> Bakker et al., 2008.

<sup>D</sup> Wanninkhof et al., 2010

<sup>E</sup> Hoppema et al., 2007.

<sup>F</sup> No scientific reference available at time of writing

<sup>G</sup> Van Heuven et al., 2011.

<sup>H</sup> MLR and cnaX suggest +14. CARINA already adjusted by +6

<sup>I</sup> MLR and cnaX suggest - 9. CARINA already adjusted -15

<sup>J</sup> No correction performed in CARINA. MLR and cnaX suggest +5 necessary

data. In the present study, the adjustments determined by software written by the author of this study (detailed in Tanhua et al., 2010; also Chapter 5 of this thesis) and used during the CARINA effort, will be applied to all GLODAP cruises (i.e., historical and WOCE-era). These adjustments may occasionally differ slightly from the official suggestions of CARINA or GLODAP.

### CARINA

The CARINA effort (Key et al., 2010) had goals similar to GLODAP. Data from 188 cruises, spanning 1980 to 2005, were collected and the internal consistency of the dataset was optimized. In contrast to GLODAP, the CARINA effort made use of automated, objective software routines for the determination of the offsets between deep-water measurements of cruises at crossover locations, and for the determination of adjustments that would minimize these offsets (Tanhua et al., 2010). Suggested adjustments were critically evaluated by working groups of experts before a decision was made to apply them.

This study uses the CARINA data that are publicly available, with very minor alterations (listed in Table 7.1). These additional adjustments were suggested by analysis of the data using multivariate linear regression (detailed in section 7.6), and were in all cases corroborated by (partly unpublished) crossover results from the CARINA effort, which did at the time not appear robust enough to warrant an adjustment.

One cruise in the CARINA dataset that did fall into the region of interest (i.e., the South Atlantic Ocean) was removed: “33SW20010102” (MANTRA/PIRANA 1, 2001; Cooley and Yager, 2006), which was performed close to Brazil in the outflow of the Amazon river. This data contained mostly river-plume samples, which are ill-suited to the MLR and OMP approaches followed in this study.

Whereas CARINA applied adjustments to  $C_T$  and  $A_T$  of cruise “58A119890214” (SWEDARP 1989, Anderson et al., 1991) of +6 and -15  $\mu\text{mol kg}^{-1}$ , respectively, my estimates of the crossover offsets for this cruise were +14 and -9  $\mu\text{mol kg}^{-1}$ , respectively. Before performing additional adjustments, MLR analysis performed during the present study (section 7.6) yielded residual offsets for this cruise of +8 and +6  $\mu\text{mol kg}^{-1}$  for  $C_T$  and  $A_T$ . These consistent results suggest that the adjustments performed during CARINA were too weak and too strong, respectively. After applying the additional adjustments, results of SWEDARP 1989 for the deep waters of the South Atlantic Ocean are in line with results from other cruises.

Values of  $C_T$  of cruise “06AQ19920929” (PFS *Polarstern* cruise ANT-X/6) are adjusted +5  $\mu\text{mol kg}^{-1}$ , again based on the observation of a severe offset during the application of an MLR (section 7.6). The CARINA group had made no adjustment due to lack of local crossovers.

### 7.4.2. World Ocean Atlas 2005

The World Ocean Atlas 2005 (Antonov et al., 2005; Garcia, 2005a,b; Locarnini et al., 2005) is used in this study to extrapolate results to basin scale. As opposed to the dataset assembled in this study, the World Ocean Atlas is a climatology – that is, its contents are not specific to a particular year, but rather are the ‘mean’ state of the ocean, as inferred from a long period of measurements. Within the World Ocean Atlas, different climatologies are available for the different months and seasons, as well as one of the yearly mean. The climatology has a zonal

and meridional resolution of 1 degree, and discerns 33 depth levels with an increasingly high vertical resolution towards the surface. From the larger World Ocean Atlas, we used the objectively mapped (i.e., gridded) values of temperature (Locarnini et al., 2005), salinity (Antonov et al., 2006), dissolved nutrients  $\text{PO}_4$ ,  $\text{NO}_3$  and silicate (Garcia et al., 2006a) and dissolved oxygen (Garcia et al., 2006b). These are the same parameters (after deriving  $\theta$  from temperature) as are used to separate the water mass fractions of the samples in the dataset assembled in this study, and both datasets (i.e., ours and the World Ocean Atlas) may thus be processed using near-identical methodology, as far as applicable.

### 7.4.3. Derived data

For both the our dataset and the World Ocean Atlas climatology, several additional parameters were derived (as far as not already present): potential temperature ( $\theta$ ), potential density, oxygen saturation ( $\text{O}_2^{\text{sat}} = f(T,S)$  following Weiss, 1970) and Apparent Oxygen Utilization ( $\text{AOU} = \text{O}_2^{\text{sat}} - \text{O}_2^{\text{meas}}$ ).

## 7.5. Separating water masses with Optimum Multiparameter (OMP) analysis

### 7.5.1. Introduction

This section will lay out the concept of Optimum Multiparameter (OMP) analysis, as well as detail its implementation in the present study. Before proceeding to the next section, the results of the OMP analysis will be presented.

#### *Water types and water masses*

A water sample from the interior of the ocean can be considered to consist of a mixture of contributions from several water masses. A water mass is in this context defined as a body of water derived from a unique source area, and having a unique formation process (Tomczak, 1999). Different such formation processes may be distinguished; strong wintertime cooling, often combined with salinization (through brine rejection by forming pack ice), may result in a surface water mass that is so dense that *convective overturning* takes place: dense parcels of surface water sink away from the surface, while underlying parcels of water rise to replace them. Due to the ensuing turbulent mixing, a water mass of vertically and horizontally homogenous physico-chemical properties is formed. Examples of such convectively formed water masses are the AAIW and the WSBW. Both water masses have very tightly constrained physico-chemical properties in their formation regions. They can be said to each occupy a *point* in T-S-space (or any other relevant property-property space).

A second process of water mass formation is *subduction*. This formation process is associated with convergence of mostly wind-driven surface waters. The resulting dome of water is gravitationally forced to depth. The characteristics of the formed water mass may vary horizontally (generally meridionally), since the different surface components may well have different characteristics and do not fully mix before or during subduction. An example of a subduction water mass is the SACW, which is formed in the Subtropical Frontal Zone, from the merging of the Subantarctic Mode Water (SAMW) from the south and warmer surface wa-

ters from the north. The resulting water mass is colder and fresher on the southern (at depth: lower) side, and warmer and saltier on the northern (at depth: upper) side, with a gradient between two extremes occupying the intermediate layers. As opposed to a convectively formed water mass, subductively formed water masses thus occupy a *line* in property-property space. For instance, all waters in the South Atlantic Ocean on the mixing line in T-S-space between [ $S=34.60$ ;  $\theta=8$  °C] and [ $S=35.75$ ;  $\theta=17$  °C] are considered to be part of the water mass SACW. The endpoints of this mixing line that describes the water mass are referred to as water *types*. Every water mass may thus be defined by one or more water types. For sake of simplicity, this study is restricted to water masses defined by at most two water types.

#### *Separating water types in a mixture*

The values of  $S$  and  $\theta$  of any mixture of two water types will be located on the (nearly) straight line (in  $\theta$ - $S$  space) between the two defining water types (the 'mixing line'). This fact has been exploited in classical oceanography to infer the spreading and mixing of the waters of the deep ocean (Wüst, 1931). This approach allows for the separation of three water types, if their respective characteristics of  $S$  and  $\theta$  are distinct enough: any sample composed of any combination of three water types will be located in the 'mixing-triangle' defined by the three water types. The relative contributions of the water types to the mixture can be inferred from the distance of the sample to each of the three corners of the triangle. If one desires to distinguish contributions of more than 3 water types to a mixture, additional variables (for which the water types of interest have distinct properties) need to be measured. Generally, the number of water types that may be discerned is defined by the number of measured variables ( $n$ ) as  $n+1$ , provided that all variables yield additional information. Optimum Multiparameter analysis (OMP), developed by Tomczak (1981) and Mackas et al (1987), offers a mathematical framework that allows such multi-component multiparameter mixtures to be separated in a well-defined manner.

#### *Non-conservative variables*

Measurements of 6 common variables are available in many oceanographic datasets: salinity, temperature, dissolved oxygen, and the major nutrients phosphate, nitrate, and silicate ( $S$ ,  $T$ ,  $O_2$ ,  $PO_4$ ,  $NO_3$ ,  $Si$ , respectively). In principle, this would allow for distinguishing 7 water types. However, the use of the  $O_2$ ,  $NO_3$ ,  $PO_4$  and  $Si$  is complicated by the fact that these properties take part in biogeochemical cycles and are thus affected by more processes than just water type mixing (i.e., they are *non-conservative* properties). The main process affecting these variables in the sub-surface ocean is remineralization of organic matter. This process gradually increases the concentration of the dissolved nutrients in the water mass, while at the same time decreasing the concentration of dissolved oxygen. Due to the low rate of this process, values of nutrients and  $O_2$  can safely be considered constant when analyzing water masses on sub-basin scale because over small spatial distances, water masses do not 'age' much. However, over large distances (and thus longer timescales), the water type definitions of oxygen and nutrients lose their representiveness of samples. Conveniently however, because remineralization affects these variables according to fairly well-constrained ratios (Redfield et al., 1963), the effect of remineralization can to a large extent be compensated for by inferring the amount of remineralization that most likely has taken place (see next sections). Karstensen and Tomczak (1998) presented a mathematical approach, the extended OMP or eOMP, to infer the most likely



amount of remineralization that has taken place in each sample, allowing the eOMP approach to be applied over very large spatial scales.

*Details vs. scale*

Generally, in doing OMP analysis, a trade-off has to be made between the desired amount of hydrographical detail and the size of the region under consideration. On small spatial scales, where mixing is the dominant driver of water sample characteristics, detailed studies may be made of the interaction between water types with highly alike properties (e.g., Poole and Tomczak, 1999). However, on larger spatial scales (and, inherently, longer times since ventilation) remineralization becomes an additional dominating influence on the characteristics of water samples. Since the influence of this process cannot be perfectly compensated for, the finer details of the water mass structure may not be resolvable. For basin-scale application of OMP analysis, simplification of the hydrological details of the area under consideration is inevitable.

*Variable information content of variables: weighting required*

The value of a measured variable for discerning water types depends on the relative accuracy with which the variable was measured, and on the distinctiveness of the water type definitions for this variable. These considerations make  $S$  and  $\theta$  the most valuable variables for OMP: both are measured with extremely high accuracy, both are fully conserved and the properties of  $S$  and  $\theta$  differ significantly between the various water types. These variables therefore get a high weight in the OMP.

Dissolved nutrients, as an opposed example, are of much less value for discerning water types. This is because the inaccuracies of (i) the primary measurements and of (ii) the employed remineralization ratios are in many cases larger than the differences in the definitions of the various water masses. Additionally, due to the very high co-variation between  $NO_3$  and  $PO_4$ , the information content of the two is not as high as for the couple  $S$  and  $\theta$ . Thus, nutrients generally get a reduced weight compared to  $S$  or  $\theta$ . Although a formal criterion may be considered for the assignment of weights to variables, weights are generally (as in this study) applied more arbitrarily:  $S$  and  $\theta$  get intermediate weight, nutrients and oxygen get low weight, and a very high weight is assigned to *mass conservation*. That is, the requirement that the various water type fractions must add up to a total of 100%.

$$\begin{matrix}
 \begin{bmatrix}
 \theta_1 & \theta_2 & \dots & \theta_j & 0 \\
 S_1 & S_2 & \dots & S_j & 0 \\
 O_{2,1} & O_{2,2} & \dots & O_{2,j} & -170 \\
 PO_{4,1} & PO_{4,2} & \dots & PO_{4,j} & 1 \\
 NO_{3,1} & NO_{3,2} & \dots & NO_{3,j} & 17 \\
 Si_1 & Si_2 & \dots & Si_j & 25 \\
 1 & 1 & \dots & 1 & 0
 \end{bmatrix} &
 \begin{bmatrix}
 x_1 \\
 x_2 \\
 \dots \\
 x_j \\
 \alpha
 \end{bmatrix} &
 = &
 \begin{bmatrix}
 \theta_{obs} \\
 S_{obs} \\
 O_{2,obs} \\
 PO_{4,obs} \\
 NO_{3,obs} \\
 Si_{obs} \\
 1
 \end{bmatrix} &
 + &
 \begin{bmatrix}
 \theta_{res} \\
 S_{res} \\
 O_{2,res} \\
 PO_{4,res} \\
 NO_{3,res} \\
 Si_{res} \\
 Mass_{res}
 \end{bmatrix} &
 (7-1)
 \end{matrix}$$

$$\begin{matrix}
 (G) & & (X) & = & (O) & + & (R)
 \end{matrix}$$

In Equation 7-1 (adapted from Budillon et al., 2003), the matrix  $G$  contains the source water type definitions for  $\theta_j$ ,  $S_j$ ,  $NO_{3,j}$ ,  $PO_{4,j}$ ,  $Si_i$  and  $O_{2,j}$  of water types 1 through  $j$  as well as, in the last column, the remineralization ratios that connect the concentrations of nutrients and oxygen. The vector  $X$  holds the (unknown) contributions of source water types 1 through  $j$ , and

remineralization amount  $\alpha$  to a measured sample. The values of the observed properties are in vector  $O$ . The last row of  $G$ , and the last element of  $O$ , together form the mass conservation constraint, i.e., the contributing fractions must add up to one. The process of remineralization obviously does not add to the total mass. Both the observed values ( $O$ ) and the source water type definitions ( $G$ ) are normalized to the mean and standard deviation of the water type definitions and subsequently weighted before solving. A non-negative solver function attempts to find the vector  $X$  that minimizes, in a least square sense, the vector of residuals  $R$ . This procedure can be understood as mathematically answering the question «which combination of water type contributions, together with which amount of remineralization of organic matter, is most likely to have produced the measured water sample?

The non-negativity constraint prohibits negative water type fractions and biological production (i.e., the negative of remineralization) to be considered for the solution.

Using uncertainties defined for the water type definitions, one may opt to perform a ‘stability analysis’ of the solution of the OMP by slightly varying the water type definitions within these uncertainties. Such an additional analysis is beyond the scope of this study.

## 7.5.2. Application of OMP in this study

### *Defining water types and water masses*

Section 7.3 presented a descriptive treatment of the water masses distinguished in this study. The current section will formalize those descriptions. Due to the restrictions inherent to the application of an OMP analysis, the amount of hydrographic detail that can be represented in any study is limited. This restriction has led to the source water type definitions listed in Table 7.2. Also, see Figure 7.5 for a graphical representation of these properties. Several details mentioned in the previous sections on the hydrography of the South Atlantic Ocean, although conceptually important, are not further taken into account in our analysis. Most notable in this regards is the absence of the Circumpolar Deep Water. We believe this exclusion is justified because this water mass is strictly a mixture of other water masses, without featuring its own surface exposure. Inclusion of this water type would moreover destabilize the solution of the OMP. Additionally, we note that the water mass that is called ‘AASW’ in the remainder of this study, by the definition in Table 7.2 comprises both the AASW proper and the Winter Water (section 7.3).

### *Spatial restrictions to presence of water types*

This study distinguishes, for the whole South Atlantic Ocean, 11 water types (Table 7.2). Clearly then, the 6 measured variables are not nearly enough to give reliable results if all water types are considered potential contributors to every sample. Conveniently, certain water types can safely be excluded in certain analyses. For example, AABW is unlikely to contribute to a sample collected in the equatorial surface waters, and it therefore will not need to be considered there. Restrictions to the assumed spatial extent of water types contributions are imposed using latitude, longitude, depth and temperature (Table 7.3). These restrictions limit the number of water types to be considered to a maximum for all samples, with most samples having only 3 or 4 potential contributing source water types (Figure 7.6). For example, the algorithm would

**Table 7.2.** The definition of water types. The uncertainties in the definitions define the amount of perturbation allowed during perturbation runs (not performed in this study), and should be indicative of the variability of the watertype in the ocean (e.g., Weddell Sea Bottom Water is of very constant composition, whereas both endmembers of the Equatorial Surface Water have a highly variable temperature). AABW: Antarctic Bottom Water; WSBW: Weddell Sea Bottom Water; NADW: North Atlantic Deep Water; AAIW: Antarctic Intermediate Water; SACW: South Atlantic Central Water; AASW: Antarctic Surface Water; ESW: Equatorial Surface Water. MC: mass conservation constraint.

Watermass	Watertype	$\theta$ °C	Salinity	$\text{NO}_3$ $\mu\text{mol kg}^{-1}$	$\text{PO}_4$ $\mu\text{mol kg}^{-1}$	Si $\mu\text{mol kg}^{-1}$	$\text{O}_2$ $\mu\text{mol kg}^{-1}$	MC
AABW	AABW-1	0.30±0.02	34.66±0.01	33.0±0.8	2.30±0.05	120.0±4.0	210±4	1
WSBW	WSBW-1	-0.70±0.02	34.650±0.002	32.5±0.8	2.30±0.05	120.0±8.0	256±3	1
NADW	NADW-1	2.40±0.05	34.90±0.01	22.0±1.0	1.40±0.07	40.0±3.0	255±15	1
	NADW-2	3.80±0.07	34.95±0.01	22.0±0.5	1.50±0.05	22.5±1.0	240±5	1
AAIW	AAIW-1	5.00±0.10	34.20±0.03	26.0±1.0	1.90±0.05	15.0±2.0	270±7	1
SACW	SACW-1	8.15±0.20	34.61±0.05	16.0±2.0	1.56±0.10	8.0±3.0	295±10	1
	SACW-2	17.00±0.20	35.74±0.05	1.0±0.2	0.30±0.10	2.3±0.5	250±10	1
AASW	AASW-1	-1.78±0.05	33.27±0.04	25.8±2.0	1.75±0.10	64.0±3.0	347±5	1
	AASW-2	-1.90±0.05	34.63±0.02	30.8±2.0	2.19±0.10	85.0±3.0	332±5	1
ESW	ESW-1	29.00±3.00	33.30±0.30	0.3±0.1	0.03±0.01	4.8±1.0	202±5	1
	ESW-2	27.10±3.00	37.40±0.30	0.2±0.1	0.10±0.01	2.6±1.0	202±5	1
Weight		10	10	3	3	2	4	40

**Table 7.3.** The allowed extent of water types, as determined by location, and potential temperature. These definitions restrict the number of watermasses that the OMP analysis may consider to contribute to a certain sample. See text section 7.5.2.

Watertype	Latitude °N	Longitude °E	Depth m	$\theta$ °C
AABW-1	-90 -44	-70 to 30	0 to 9999	-3.0 to 4.0
	-45 to 20	-70 to 30	700 to 9999	-3.0 to 4.0
WSBW-1	-90 to -40	-70 to 30	0 to 9999	-3.0 to 1.0
NADW-1	-60 to 20	-70 to 30	700 to 9999	-3.0 to 8.0
	-90 to -60	-70 to 30	0 to 9999	-3.0 to 8.0
NADW-2	-60 to 20	-70 to 30	700 to 9999	-3.0 to 8.0
	-90 to -60	-70 to 30	0 to 9999	-3.0 to 8.0
AAIW-1	-60 to 20	-70 to 30	0 to 2500	1.0 to 10.0
SACW-1	-60 to 20	-70 to 30	0 to 1200	4.0 to 50.0
SACW-2	-60 to 20	-70 to 30	0 to 1200	6.0 to 50.0
AASW-1	-90 to -45	-70 to 30	0 to 1000	-3.0 to 4.0
AASW-2	-90 to -45	-70 to 30	0 to 1000	-3.0 to 4.0
ESW-1	-45 to 20	-70 to 30	0 to 500	10.0 to 50.0
ESW-2	-45 to 20	-70 to 30	0 to 500	10.0 to 50.0

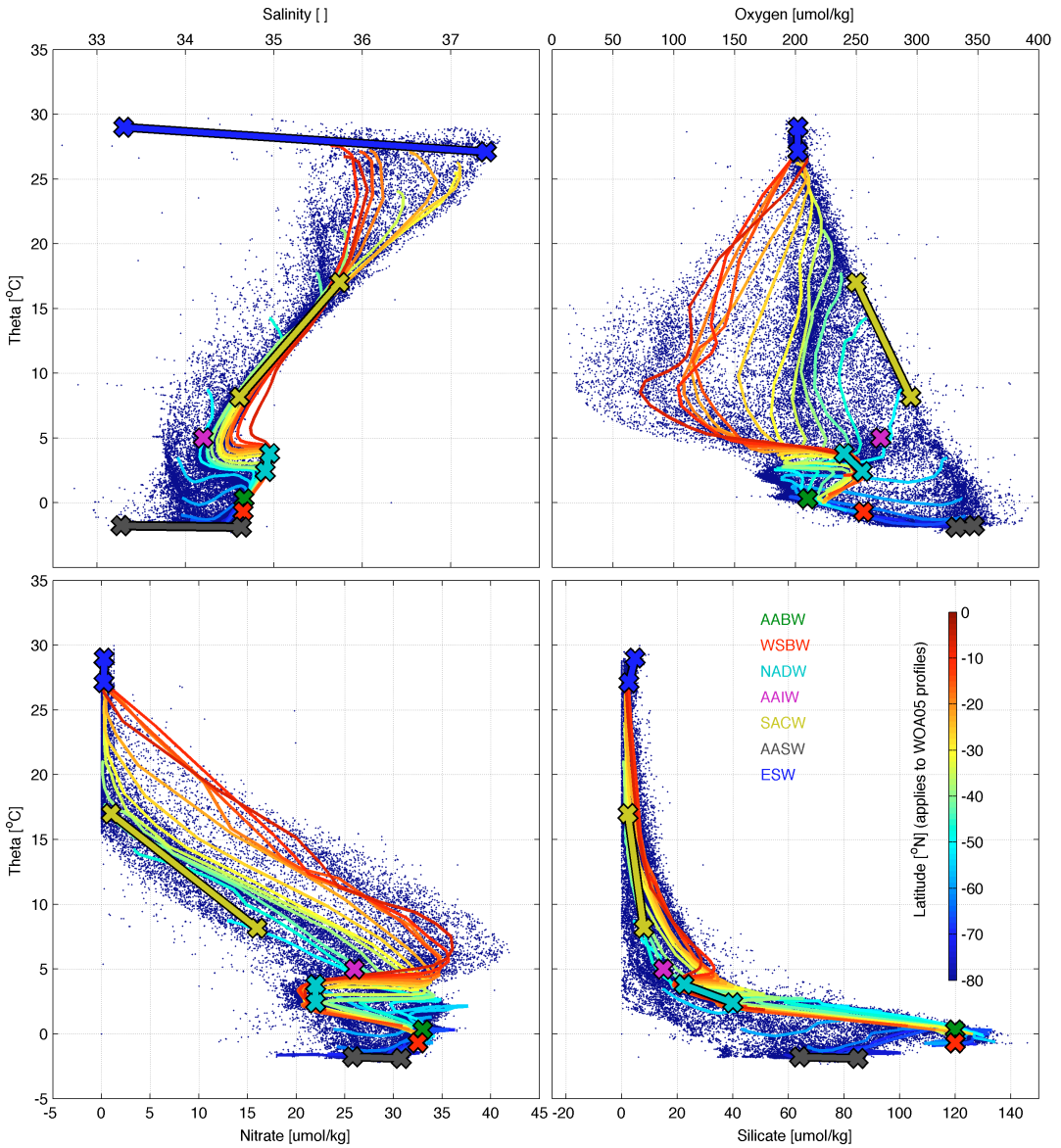


**Figure 7.5.** Property-property plots illustrating the definitions of the watermasses for the optimum multiparameter (OMP) analysis. Panel **a**) salinity versus potential temperature ( $\theta$ ) ; **b**) dissolved oxygen ( $O_2$ ) versus  $\theta$ ; **c**) nitrate ( $NO_3$ ) versus  $\theta$ ; **d**) silicate (Si) versus  $\theta$ . Thick crosses define the definitions of the watertype(s) that constitute(s) a watermass. If multiple watertypes constitute a watermass, thick crosses are connected by a thick line. Colors of the crosses and lines correspond to a particular watermass (names listed in panel **d**). Small blue dots: the measurements in the GCC dataset. Thin colored lines: profiles along  $30^\circ W$  (every  $5^\circ$  of latitude between  $10^\circ N$  and Antarctica) from the World Ocean Atlas climatology (color indicates the latitude of the profile).

Frequency distribution of number of water types allowed for consideration in OMP analysis

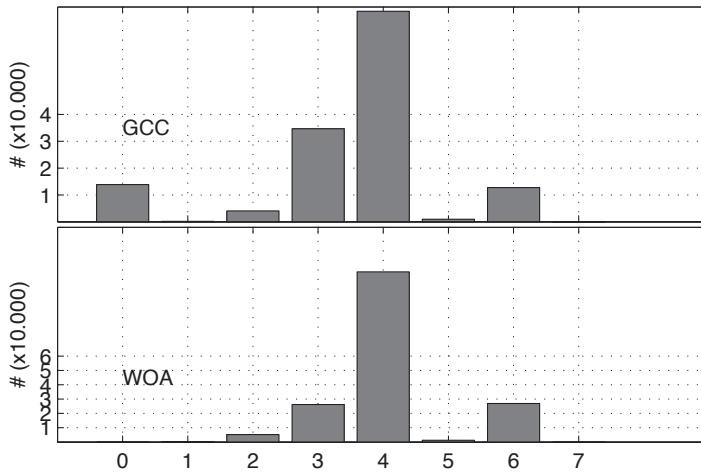


**Figure 7.6.** Frequency distribution of the number of watertypes allowed in the OMP analysis of samples in the two datasets that are subjected to this procedure: GCC (top) and WOA (bottom). Since only six variables are available ( $S$ ,  $q$ ,  $O_2$ ,  $NO_3$ ,  $PO_4$  and  $Si$ ), and we allow for remineralization in the calculations, the system is underdetermined if more than 6 watertypes are allowed for each particular sample. This can be seen to be the case for about 11000 samples (~5%) in the GCC dataset, and for some 22000 samples in the WOA data. The circa 13000 samples in the GCC dataset that are not considered for any watermass, are samples that do not have a value for salinity and/or  $q$ . Most of these are from the GLODAP dataset, which contains circa 26000 samples without salinity data.

consider as water types potentially contributing to a sample at [30 °S, 0 °E, 75 m] only the five water types AAIW, SACW-1, SACW-2, ESW-1 and ESW-2.

### *Weighting*

The variables were assigned individual weights before solving Equation 7-1 (see Table 7.2, last row). Mass conservation was assigned the highest relative weight (40) in order to assure that, irrespective of the accuracy of the solution for each sample, the sum of the fractions will be very close to 1. In other words, almost all imperfection of the solution would be contained in the residuals of the measured variables, and not in the mass conservation residual. Salinity and  $\theta$  were assigned high weights (10, reflecting their very high value for the separation of water types, which follows from the high accuracy with which they are measured and their highly conservative nature. For the variables  $O_2$ ,  $NO_3$  and  $PO_4$ , uncertainties about the exact definition of the Redfield ratios, relatively low accuracy of measurement (circa  $\pm 1\%$ ) and the limited value of these variables in the separation of (nutrient-depleted) surface water masses lead to relatively low weights (2, 2 and 5, respectively). Although silicate is a highly informative variable for discerning between water types of northern and southern origins, it is assigned the lowest weight (1), since its remineralization does not follow constant ratios but is strongly depth-dependent (Hupe and Karstensen, 2000), and a higher weight would therefore be detrimental to the results in the high-remineralization regions towards the equator.

### 7.5.3. Results

Figures 7.7a-c show the mean solution of the OMP for the meridional sections along 30 °W, 0 °E and 30 °E (the various water masses have been grouped into different subfigures for clarity). The following brief description of results pertains to the section along the Prime Meridian at 0° East).

The resultant distribution of water masses generally conform to the hydrography outlined in section 7.3. The core of the WSBW can be seen to occupy the bottom of the Weddell-Enderby Basin. Overlying it is the AABW, which at this longitude is seen to ‘spill over’ the rim of the Mid-Atlantic Ridge (or Southwest-Indian Ridge). The clear northward advance of AABW is halted by Walvis Ridge at 30 °S. To the north of that ridge, the water has a strong characteristic of NADW. The upward deflection and admixture of the NADW into the CDW is seen between 40 °S and 55 °S, where the mixture contains AAIW, NADW and AABW. Higher in the water column, the low-salinity AAIW separates the WW and the SACW (to the south and north, respectively). The core of the SACW is confined to the latitudinal band between 40 °S and 20 °S. At tropical latitudes, the SACW is overlain by the warm and shallow Equatorial Surface Water (ESW).

Results from the World Ocean Atlas climatology (right hand column of Figures 7.7a-c) are in excellent agreement with those obtained from the dataset assembled in this study.

## 7.6. Determining $C_T^{\text{TSR}}$

### 7.6.1. Rationale

The  $C_T$  of the surface ocean varies with the solubility of  $\text{CO}_2$  (which is dependent on temperature and salinity) and with the biological production and remineralization of organic matter, and the formation and dissolution  $\text{CaCO}_3$ . In the deep ocean, remineralization is the dominant process that, over time, increases  $C_T$ . Mixing between water masses is an additional cause of temporal variability in  $C_T$  at any particular location. These processes affect not only  $C_T$  but also the concentrations of nutrients, dissolved oxygen and total alkalinity according to fairly well-established ratios (Redfield et al., 1963; Anderson and Sarmiento, 1994;). Since these conditions and processes affect  $C_T$  and associated variables in approximately linear fashion, it follows that  $C_T$  must to a large extent be predictable from these associated variables, provided that the numerical dependencies are quantified. Multivariate linear regression (MLR) has been shown to be well able to capture the relationships between  $C_T$  and the independent parameters  $S_T$ , AOU and one or more nutrients (e.g., Wallace 1995, Friis et al., 2005, Van Heuven et al., 2011).

The residuals of such an MLR (referred to as  $C_{\text{res}}^{\text{TSR}}$ , i.e., difference  $C_T^{\text{meas}} - C_T^{\text{TSR}}$ ) are inherently distributed around zero. The deviations from zero are of interest here, and are the result of a combination of (a) non-applicability of a (multi-) linear model to represent the

---

**Figure 7.7.** Meridional sections along (from top to bottom, 6 panels each): (a) 30 °W (b) 0 °E and (c) 30 °E, showing the presence of water masses as inferred by the OMP analyses of the GCC and WOA datasets (left and right column of each subfigure, respectively). The sections of GCC data contain all samples from within a 4°-wide longitudinal band. Non-overlapping water masses have been grouped into different panels for clarity. Black dots indicate the locations of samples (GCC) or gridpoints (WOA).







relationships between  $C_T^{\text{meas}}$  and the independent variables, **(b)** the presence of bias or **(c)** noise in the measurements of either  $C_T^{\text{meas}}$  or of any of the independent variables, **(d)** real changes in one or more of the independent variables that are not associated with changes in one or more of the other independents and **(e)** real changes in the values in  $C_T^{\text{meas}}$  that are not accounted for by concurrent changes in the independent variables (or vice versa).

Of the above five sources of spread in residuals, (a)-(c) are considered to be of only limited importance, while (d) is necessarily assumed to be negligible, following the concept of a steady state ocean. The source of 'error' (e) is of interest to the MLR-based methods for the detection of  $C_{\text{ant}}$  in the ocean. The effect of (a) is generally (though often implicitly) considered to be small. Support for this assumption may be found in the relatively small residuals of the deep water samples of about  $5 \mu\text{mol kg}^{-1}$ , which is only about twice as much as the measurement inaccuracy of  $C_T^{\text{meas}}$  itself, on samples spanning a range of about  $100 \mu\text{mol kg}^{-1}$ . The effect of error source (b) may be minimized by ensuring that the employed dataset is internally consistent (i.e., biases between cruises are minimized). The used CARINA and GLODAP datasets have been processed for optimized internal consistency (Key et al., 2004, 2010). Measurement noise (c) is likely a prime contributor to the spread observed in the profiles of  $C_{\text{res}}^{\text{TSR}}$ . Error source (d) is more problematic. The time rate of increase in  $C_{\text{ant}}$  may be underestimated if concurrent (but unassociated) secular trends are present in any of the predictive variables (Levine et al., 2008). In the presence of such secular trends, a conceivable time trend of  $C_T$ , in reality due to uptake to  $C_{\text{ant}}$ , would by the MLR be numerically related with the secular trend in the predictive variable, and would therefore not be detectible as a time trend of the residuals. Although localized secular changes to ocean physics and biogeochemistry have been documented (Solomon et al., 2007), we necessarily assume these to be of minor influence. This assumption is regarded as valid over the large spatial scale of this analysis. An exception to this is the gradual rise of sea surface temperatures, which is observed globally (Levitus et al., 2005). However, the small magnitude of this process ( $<0.1 \text{ }^\circ\text{C decade}^{-1}$  for the sea surface of the South Atlantic Ocean) with respect to the temperature range of the sea surface in the present study is expected to minimize the influence of this secular change on the obtained results.

Exclusion of the influence of the above four sources of error allows us to attribute all the residual to the fifth source of spread in  $C_{\text{res}}^{\text{TSR}}$ . The enhanced uptake of  $\text{CO}_2$  from the atmosphere does not affect any of the independent parameters, and such samples will be calculated to have a positive  $C_{\text{res}}^{\text{TSR}}$ . Although the mean of all values of  $C_{\text{res}}^{\text{TSR}}$  of the dataset on which the MLR is performed is inherently zero, the older cruises may be expected to have, on average, more negative residuals than the more recent cruises. The increase in the value of the residuals over time is thus assumed to reflect the enhanced  $\text{CO}_2$  uptake from the atmosphere.

### 7.6.2. Method

For every sample, a synthetic value of  $C_T$  (i.e.,  $C_T^{\text{TSR}}$ ) is calculated on the basis of independent parameters, and additionally using results of the OMP analysis. First, for each water type  $i$ , all samples are selected that contain at least 25% of that water type  $i$  and were collected from deeper than 100 m and after 1985. This should give a selection of samples that have been measured by fairly modern techniques and are not too much influenced by transitory biological or air-sea gas exchange processes. Using these selected samples, an MLR is performed between

$C_T^{\text{meas}}$  and a selection of ancillary data. The coefficients yielded by the MLR (one set per water mass) are used to generate the synthetic variable  $C_T^{\text{TSR}}$  for all samples in the dataset, according to Equation 7-2.

$$C_T^{\text{TSR}} = \sum_{i=1}^j x_i \cdot (C_i + a_i \cdot S + b_i \cdot \theta + c_i \cdot \text{NO}_3 + d_i \cdot \text{PO}_4 + e_i \cdot \text{Si} + f_i \cdot \text{AOU} + g_i \cdot \text{depth}) / \sum_{i=1}^j x_i \quad (7-2)$$

The last term in Eq. 7-2 is to compensate for the effect on  $C_T^{\text{TSR}}$  of conceivable mass conservation residuals. Because the sum of the first term of Eq. 7-2,  $x_i$ , may not exactly equal unity (i.e., the OMP solution of a certain sample has a mass conservation residual),  $C_T^{\text{TSR}}$  for that sample would be erroneous by the same amount in absence of this correction.

### 7.6.3. Results

The resulting values of  $C_T^{\text{TSR}}$  are in very good agreement with measured  $C_T$  (Figure 7.8, Tables 7.4 and 7.5). The standard deviation of the residuals is  $4.7 \mu\text{mol kg}^{-1}$  throughout the basin below 500 meters depth. For the more shallow samples the residuals are slightly more dispersed, with the largest residuals found in the upper part of the water column, occasionally being as

**Table 7.4.** Coefficients determined for MLR for  $C_T$  (i.e., the terms C and a through g of Eq. 7-2).

Watermass	Constant	Salinity	$\theta$	Si	NO <sub>3</sub>	PO <sub>4</sub>	O <sub>2</sub>	Depth
			°C	$\mu\text{mol kg}^{-1}$	$\mu\text{mol kg}^{-1}$	$\mu\text{mol kg}^{-1}$	$\mu\text{mol kg}^{-1}$	km
AABW	1158.0±83.3	27.7±2.3	-7.1±0.3	0.1±0.0	1.0±0.1	11.9±1.7	0.5±0.0	0.1±0.1
WSBW	832.9±663.9	39.0±19.2	10.2±1.0	-0.0±0.0	1.3±0.2	11.4±2.7	0.1±0.0	0.2±0.1
NADW	2329.3±97.5	-6.3±2.8	1.0±0.5	0.6±0.0	0.3±0.2	-12.0±2.2	0.6±0.0	2.7±0.2
AAIW	1566.6±65.9	16.0±1.9	-4.1±0.3	0.6±0.0	1.9±0.1	-12.5±2.0	0.5±0.0	-8.9±0.7
SACW	486.8±41.2	47.3±1.2	-6.4±0.2	-1.0±0.2	2.8±0.3	-2.5±4.3	0.4±0.0	-9.2±2.5
AASW	241.5±46.7	53.6±1.4	-1.2±0.2	0.3±0.0	2.1±0.2	21.8±2.6	0.1±0.0	-6.2±2.3
ESW	483.6±40.5	46.8±1.2	-5.5±0.3	-2.2±0.5	0.6±0.8	40.6±9.3	0.5±0.1	-10.8±16.6

**Table 7.5.** Means and standard deviations of the residuals  $C_{\text{res}}^{\text{TSR}}$  (in  $\mu\text{mol kg}^{-1}$ ), presented for all samples in a given depth range, and separately for each of the cores (75% purity) of the seven water masses used in this study.

Watermass	depth range			
	0 m-100 m	100 m-500 m	500 m-bottom	full water column
AABW	not enough data	$0.8 \pm 3.4$ (n=1990)	$0.5 \pm 3.9$ (n=4711)	$0.6 \pm 3.8$ (n=6708)
WSBW	not enough data	not enough data	$0.0 \pm 3.3$ (n=2358)	$0.0 \pm 3.3$ (n=2358)
NADW	not enough data	not enough data	$-0.2 \pm 4.9$ (n=4911)	$-0.2 \pm 4.9$ (n=4911)
AAIW	$0.4 \pm 8.2$ (n=242)	$-0.6 \pm 6.2$ (n=955)	$-0.9 \pm 5.7$ (n=2113)	$-0.8 \pm 6.1$ (n=3310)
SACW	$0.8 \pm 11.2$ (n=891)	$-0.6 \pm 8.6$ (n=2903)	$3.0 \pm 8.5$ (n=91)	$-0.2 \pm 9.3$ (n=3885)
AASW	$1.5 \pm 7.6$ (n=2181)	$1.1 \pm 7.0$ (n=662)	$5.9 \pm 6.2$ (n=24)	$1.4 \pm 7.5$ (n=2867)
ESW	$0.8 \pm 13.3$ (n=1075)	$-6.7 \pm 10.7$ (n=46)	not enough data	$0.5 \pm 13.3$ (n=1121)
All samples	$0.9 \pm 10.5$ (n=6465)	$0.1 \pm 7.2$ (n=9628)	$-0.3 \pm 4.7$ (n=24040)	$-0.0 \pm 6.6$ (n=40133)

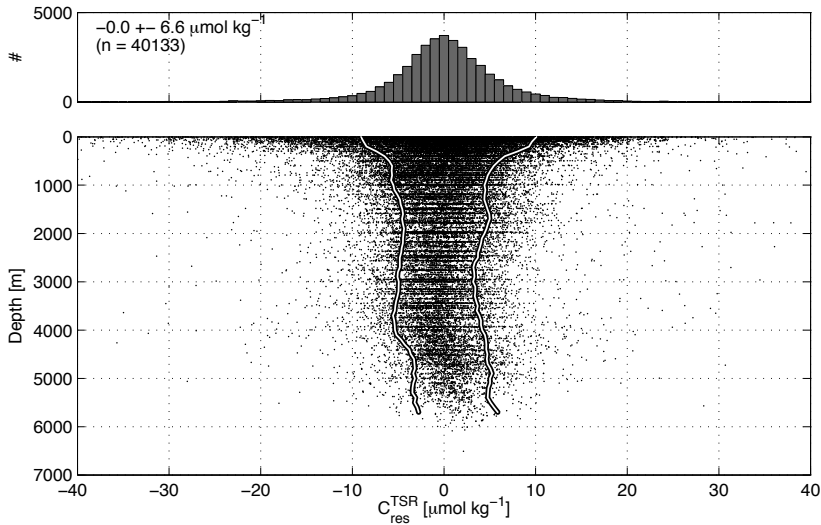


**Figure 7.8.** Frequency distributions (top) and depth profiles (bottom) of  $C_{res}^{TSR}$ . Please refer to text section 7.6 for details on how this variable is derived. Clearly,  $C_{res}^{TSR}$  is more variable in shallow waters than in the deep ocean. Part of the variability in  $C_{res}^{TSR}$  appears not to be random, but rather stems from unresolved measurement bias in the individual cruises (see figure 7.9).

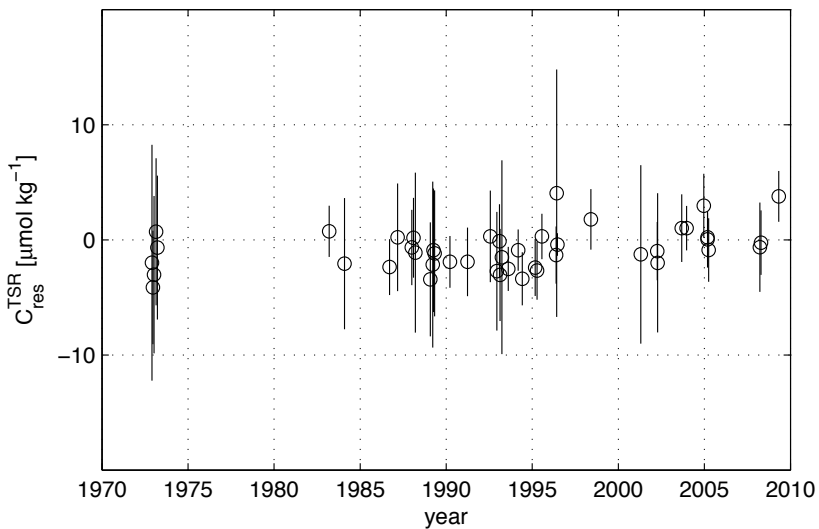


**Figure 7.9.** Time series of the means and standard deviations of all  $C_{res}^{TSR}$  values between 2000-3500 m depth of the individual cruises. Deviations from zero are indicative of minor biases in the measurements of the predicted parameters ( $C_T^{meas}$ ,  $A_T^{meas}$ ) and/or of the independent parameters ( $S$ ,  $\theta$ ,  $Si$ ,  $NO_3$ ,  $PO_4$  and  $O_2$ ) of an individual cruise. At these depths, no time trend is clearly discernable in  $C_{res}^{TSR}$ , which is in line with expectations.

large as  $30 \mu\text{mol kg}^{-1}$  (either positive or negative). However, this spread is expected, because the uptake of  $C_{\text{ant}}$  at the ocean surface will be contained in these residuals. We expect that the spread reflects not only 'noise' but also the gradual shift over time from negative to positive residuals. Figure 7.9 shows a time series of the per-cruise mean and standard deviation of  $C_{\text{res}}^{\text{TSR}}$  for all samples between 2000 and 3500 meters depth. No significant increase in  $C_{\text{ant}}$  is expected here, and therefore these means should fall on a horizontal line at  $C_{\text{res}}^{\text{TSR}}=0$ . The slight spread around this line is likely indicative of minor measurement biases that remain in spite of the adjustments performed in GLODAP and CARINA.

## 7.7. Determining time trends of $C_{\text{res}}^{\text{TSR}}$ in each water mass

### 7.7.1. Rationale

*Trends in  $C_{\text{res}}^{\text{TSR}}$  equal trends in  $C_{\text{ant}}$*

Trends in  $C_{\text{res}}^{\text{TSR}}$  may be considered commensurate with trends in  $C_{\text{ant}}$ . For surface water samples,  $C_{\text{T}}^{\text{meas}}$  will increase over time, due to accumulation of anthropogenic  $\text{CO}_2$ , taken up from the atmosphere. The difference between the two,  $C_{\text{res}}^{\text{TSR}}$  (defined as  $C_{\text{res}}^{\text{TSR}}=C_{\text{T}}^{\text{meas}}-C_{\text{T}}^{\text{TSR}}$ ), will thus increase over time. A quantification of the rate of increase of  $C_{\text{res}}^{\text{TSR}}$  will thus be commensurate with quantification of the rate of increase of  $C_{\text{ant}}$ .

*Expected dependence of trends on AOU*

Time trends in  $C_{\text{res}}^{\text{TSR}}$  are expected to be strongest in well-ventilated surface waters. Over the 35 years spanned by the measurements,  $C_{\text{ant}}$  of these samples may have increased by as much as  $30 \mu\text{mol kg}^{-1}$  (in the case of  $p\text{CO}_2$ -equilibrium with the atmosphere). At any particular location further into the interior of the ocean (i.e., away from the ventilation areas), the time rate of increase is expected to become progressively smaller, towards complete absence in the old deep waters, which were ventilated before significant amounts of anthropogenic  $\text{CO}_2$  had accumulated in the atmosphere.

*Removing sampling bias*

The amount of samples collected each year has increased substantially since the 1970s. The WOCE campaign of the mid-1990s yielded a larger amount of  $C_{\text{T}}$  and ancillary data than any period before or since (>50% of the total; Figure 4). If these differences in sampling density are not properly accounted for, valuable information may be lost. For instance, the data obtained during the GEOSECS campaign in the 1970s will not likely exert much influence on the resulting trends, even though the few data that we have from that era are of good quality. In order to address this problem, the data for  $C_{\text{res}}^{\text{TSR}}$  were binned over time and over AOU. This approach condensed the (for some water masses) more than 10000 data points for  $C_{\text{res}}^{\text{TSR}}$  into just a few dozen means.

*Surface fitting.*

It thus seems appropriate to fit a surface through the data of TIME, AOU and  $C_{\text{res}}^{\text{TSR}}$ . Two methods have been considered here. One is to fit a time trend through the data in each AOU bin (for example, through all binned  $C_{\text{res}}^{\text{TSR}}$  values in the AOU range 90-100, and another fit in

the AOU range 100-110, etc.). This would yield distinct  $dC_{\text{res}}^{\text{TSR}}/dt$  (i.e.,  $dC_{\text{ant}}/dt$ ) results in each of these classes, but many classes would turn out to be undersampled. The second approach, which is the one that we followed, fits a surface through all data points at once, allowing the surface to curve as a function of AOU, i.e., the surface is allowed to rise steeper (over time) at low values of AOU while becoming progressively ‘flatter’ at increasing AOU.

*The time-derivative of the fitted surface*

What is of interest for the remainder of this study is the dependence of the time rate of change at a particular location in a water mass on the AOU (as a proxy of ventilation age) at that location. The time derivative is obtained through differentiation to TIME of the mathematical formula that specifies the shape of the fitted surface.

*Linearity*

We argue that both the time trend of  $C_{\text{res}}^{\text{TSR}}$  and the dependence of this time trend on AOU may be assumed to be linear. Between 1973 and 2008 the atmospheric concentration of  $\text{CO}_2$  increased from about 330 to 385  $\mu\text{atm}$ . In surface water of [ $\theta=10\text{ }^\circ\text{C}$ ;  $S=34.5$ ;  $A_T=2350\text{ }\mu\text{mol kg}^{-1}$ ] that is in  $p\text{CO}_2$  equilibrium with the atmosphere, the commensurate change in the  $C_T$  is from 2130 to 2157  $\mu\text{mol kg}^{-1}$ , i.e., an increase of 0.8  $\mu\text{mol kg}^{-1}\text{ }\mu\text{atm}^{-1}$ . The time history of atmospheric  $\text{CO}_2$  is not exactly linear: as a result in the early 1970s the value  $dC_T/dt$  of such seawater was 0.6  $\mu\text{mol kg}^{-1}\text{ a}^{-1}$ . In 2008, this had increased to circa 1.0  $\mu\text{mol kg}^{-1}\text{ a}^{-1}$ . However, for the purpose of this study, we opted for use of linear trends, both for the rise of  $C_{\text{res}}^{\text{TSR}}$  over time, and for the dependence on AOU. Not enough data is available to warrant the fitting of more complex, and potentially more realistic, surfaces.

**7.7.2. Method**

For each water mass, using the results of the OMP analysis, those samples are selected that contain more than 70% of it. Every water mass is represented by at least 250 samples of such high purity. A good selection criterion for removing occasional spurious samples and thus to improve the representativeness of the selection of the core of the water mass of interest is to narrow the selection to just those samples that fall in the median 90% of the range of AOU spanned by the original selection. The remaining samples are binned in two dimensions: TIME (year the sample was collected) and AOU; bin width is 5 years and 5  $\mu\text{mol kg}^{-1}$ , respectively. Thus, a selection of samples from between 1982 and 2008, spanning a range of AOU from 64 to 113 will be binned into 66 bins (6 bins span 1980-2010, 11 bins span 60-115). If at least 4 values of  $C_{\text{res}}^{\text{TSR}}$  are present in a bin, the average of these values is stored, and later on used for determination of time trends. If less than 4 values are present, the bin is considered to be underrepresented by the data and will not be used in subsequent analyses. Initially, the routine tries to fit a curved surface through the binned values of  $C_{\text{res}}^{\text{TSR}}$  by minimizing (in a least squares sense) the residuals  $R$  of Eq. 7-3.

$$C_i + a_i \cdot \Delta\text{AOU} + b_i \cdot \text{TIME} + c_i \cdot \text{TIME} \cdot \Delta\text{AOU} = C_{\text{res}}^{\text{TSR}} + R \tag{7-3}$$

Here,  $\Delta\text{AOU}$  denotes the difference between the mean AOU of a bin and the mean AOU of all samples considered to belong to the core of a water mass  $i$ . If  $c_i$  (the coefficient that specifies

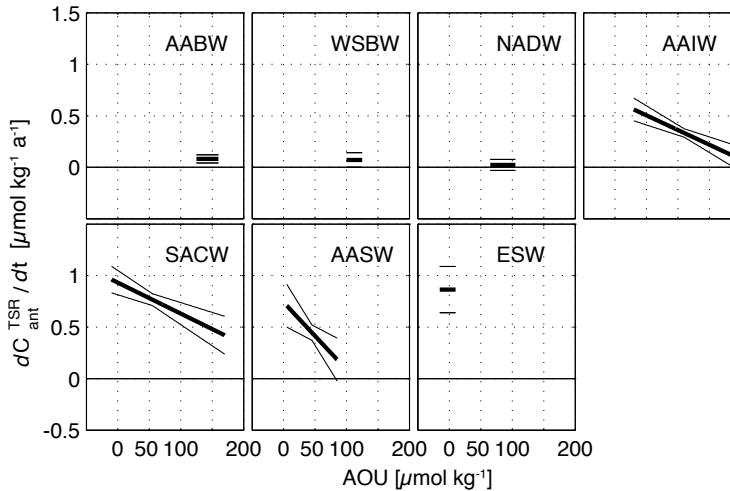
how the steepness of the surface depends on AOU) is not significantly different from 0 (at the 95% level), a plane (i.e., a non-curved surface) is fit through the binned values of  $C_{\text{res}}^{\text{TSR}}$ , as in Eq. 7-4. This is equivalent to performing a regular linear regression between TIME and  $C_{\text{res}}^{\text{TSR}}$ .

$$C_i + a_i \Delta \text{AOU} + b_i \text{TIME} = C_{\text{res}}^{\text{TSR}} + R \quad (7-4)$$

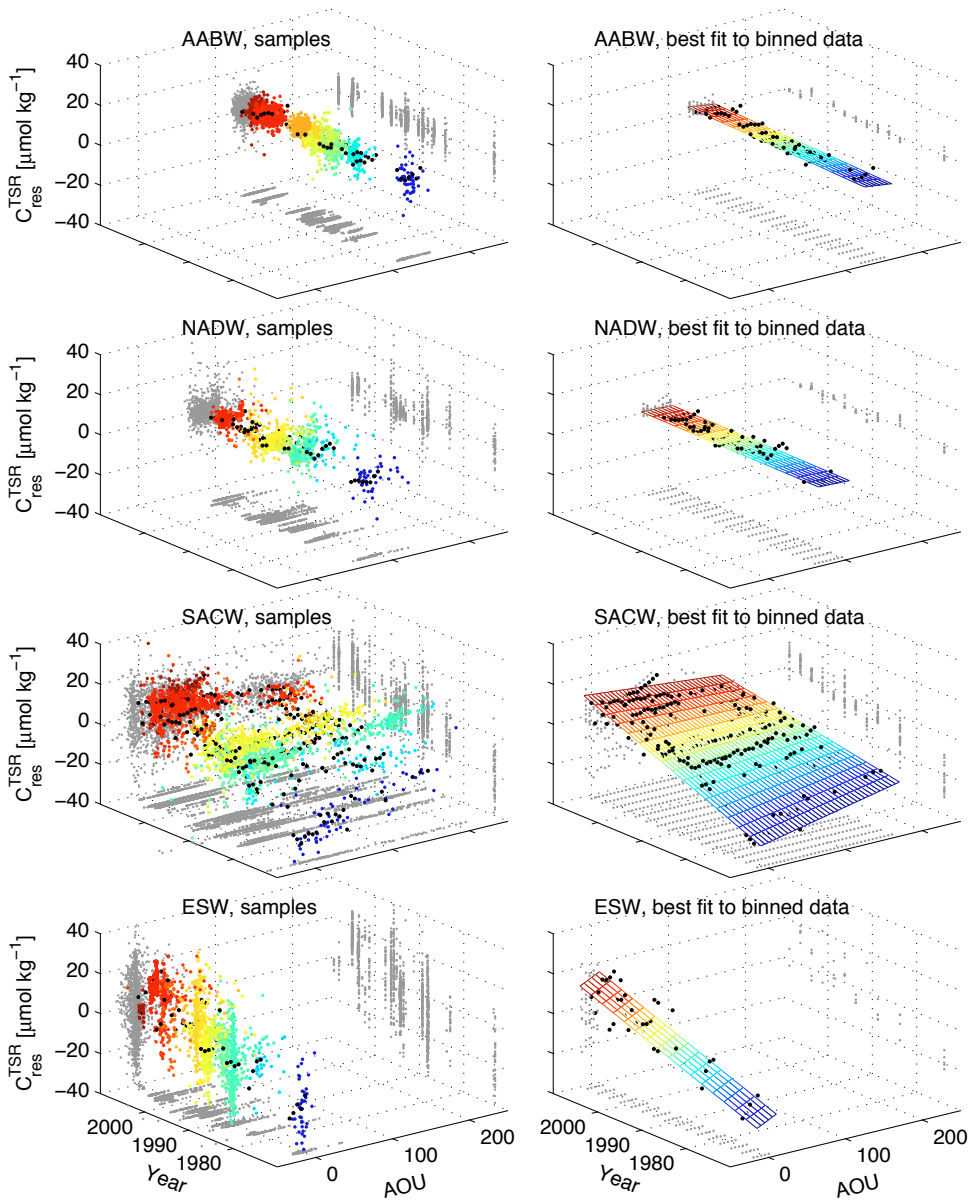
The coefficients  $b_i$  and (if determined)  $c_i$  are the two that are of interest to the remainder of this study, because they describe the time rate of change of  $C_{\text{res}}^{\text{TSR}}$  (i.e., the rate of storage of  $C_{\text{ant}}$ ) over the range of AOU that cover the core of the water mass.

### 7.7.3. Results

Figure 7.10 shows the sample data and the regressions between  $C_{\text{res}}^{\text{TSR}}$ , AOU and TIME for the cores of the seven distinguished water masses. Figure 7.11 shows the determined relationship of  $dC_{\text{res}}^{\text{TSR}}/dt$  (i.e.,  $dC_{\text{ant}}/dt$ ) on AOU. In only 3 of the considered water masses a significant relationship with AOU is determined (i.e., in the AAIW, SACW and AASW). The other four water masses (AABW, WSBW, NADW and ESW) all have ranges of AOU that are too limited to infer a slope of regression surface in AOU. The deep water masses WSBW and AABW have time trends of  $C_{\text{ant}}$  that are significantly above zero, albeit only barely for the WSBW. The time trend in NADW is indistinguishable from zero.



**Figure 7.11.** The relationship between AOU and  $dC_{\text{ant}}^{\text{TSR}}/dt$  (commensurate with  $dC_{\text{res}}^{\text{TSR}}/dt$ ), as determined in the cores of the 7 watermasses of interest (see figure 10, text section 7.7). In each panel, the thick line represents the time-derivative (i.e., the slope in the time-direction) of the surface fitted through the binned data of TIME, AOU and  $C_{\text{res}}^{\text{TSR}}$  from the core of a particular watermass (all of which are shown in figure 10). The horizontal extent of the black lines is indicative of the range of AOU spanned by the cores of the watermasses. The thin lines represent the 95% confidence interval of the fit. The overall uncertainty may be higher than this due to unresolved measurement biases and methodological errors. These relationships are used to project values of  $dC_{\text{ant}}^{\text{TSR}}/dt$  onto the WOA05 climatology (see Section 7.8).





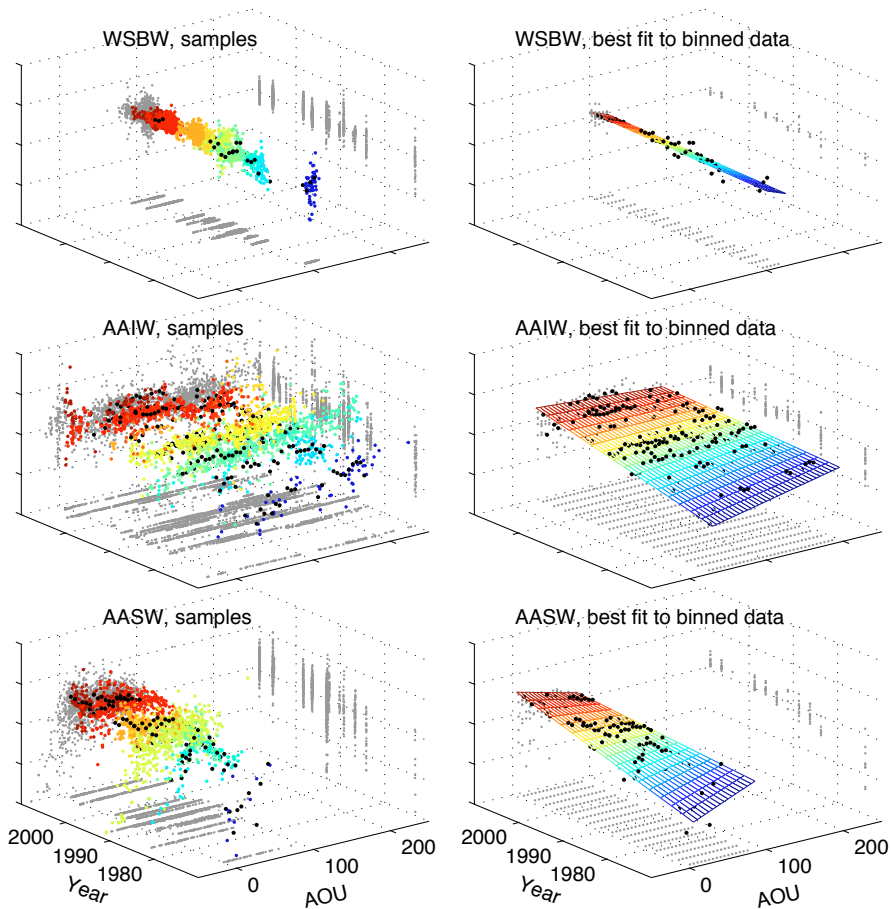


**Figure 7.10.** The relationship between time, AOU and  $C_{\text{res}}^{\text{TSR}}$ , in the cores of water masses. Individual samples and surface fits are shown side-by-side for each water mass (4 water masses in left 2 columns, 3 water masses in right two columns). To aid understanding, two examples of interpretation follow:

In the core of the NADW (left two columns, second row; water mass purity from OMP: >70%), no obvious trend is visible over the whole range of AOU, suggesting that ventilation of this part of the NADW predates the rise in atmospheric anthropogenic  $\text{CO}_2$ .

Conversely, in the South Atlantic Central Water (left two columns, third row; water mass purity: >70%),  $C_{\text{res}}^{\text{TSR}}$  is seen to rise gradually over the years. This increase is stronger at low AOU than at high AOU, reflecting the fact that the low-AOU samples were ventilated in more recent times, i.e., at a time where the anthropogenic  $\text{CO}_2$  concentrations were rising more sharply than at the time that the high-AOU samples were ventilated. See text section 7.7 for more details

## 7.8. Projecting $dC_{\text{ant}}^{\text{TSR}}/dt$ onto the World Ocean Atlas 2005

### 7.8.1. Rationale

In the previous paragraphs, the an adaptation of the TSR technique has been outlined with which is obtained, for each water mass, an estimate of the (inverse) relationship between AOU (which is indicative of ventilation age) and the time trend of the concentration of anthropogenic carbon,  $dC_{\text{ant}}^{\text{TSR}}/dt$ . In order to obtain basin-scale totals of the rate of change of the oceanic inventory of  $C_{\text{ant}}$ , we project these water mass-specific results onto the World Ocean Atlas, a large-scale, high-resolution climatology (see section 7.4) for which water mass distributions have been inferred using OMP (section 7.5).

### 7.8.2. Methods

In the remainder of this manuscript, the following abbreviations are used:

$C_{\text{ant}}^{\text{TSR}}$	Concentration of anthropogenic carbon ( $\mu\text{mol kg}^{-1}$ ) calculated using TSR
$dC_{\text{ant}}^{\text{TSR}}/dt$	Time trend of the above concentration (in $\mu\text{mol kg}^{-1} \text{a}^{-1}$ )
$\text{INV}C_{\text{ant}}^{\text{TSR}}$	Inventory of anthropogenic carbon in a volume (e.g., gridbox, basin) (in TgC)
$d^{\text{INV}}C_{\text{ant}}^{\text{TSR}}/dt$	Time trend of that inventory (in TgC $\text{a}^{-1}$ )
$^{\text{Cl}}C_{\text{ant}}^{\text{TSR}}$	Column (or ‘specific’) inventory of anthropogenic carbon (in $\text{mol m}^{-2}$ )
$d^{\text{Cl}}C_{\text{ant}}^{\text{TSR}}/dt$	Time trend of the column inventory (in $\text{mol m}^{-2} \text{a}^{-1}$ )

#### *Gridpoints to gridboxes*

The calculation of inventories of  $C_{\text{ant}}$  necessitates knowledge of the volume (or rather, the mass) of water represented by each gridpoint of the World Ocean Atlas. Each gridpoint in the World Ocean Atlas is considered to be representative of the water in a gridbox at the center of which it is located. Each gridbox is assumed to extend from halfway the next shallower gridpoint (or the surface) to halfway the next deeper gridpoint (or 5750 meters). The top gridpoint (at 0 m) thus represents the gridbox extending from 0 m to 5 m, the next one down (at 10 m) represents the gridbox [5-15 m], etc. The deepest gridpoint (at 5500 m) represents the gridbox between 5250-5750 m. No deeper waters are assumed to exist in the South Atlantic Ocean.

The volume of each gridbox depends on its latitude and vertical position in the water column: boxes towards the poles have a smaller horizontal area than those at the Equator, and boxes near the surface are vertically ‘thinner’ than those deeper down. The largest volumes of gridboxes (about 75,000  $\text{km}^3$ ) are thus encountered in deep waters at the equator, while the smallest volumes (about 40  $\text{km}^3$ ) are found in the far-southern surface waters.

The volumes of all gridboxes of the World Ocean Atlas are calculated under the assumption that the lower extent of the deepest gridbox at each horizontal gridpoint represents the ocean floor. Since the vertical extent of gridboxes below 2000 m is 500 m, this assumption potentially leads to significant errors (at 5000 m depth, a likely error of 250 m error is 5% of the local volume of the water column). This source of error is troublesome for an accurate determination of the rate of increase of the storage of  $C_{\text{ant}}$  in the WSBW, which occupies a relatively narrow layer above the bottom (Fahrbach et al., 2001), and exhibits an only small trend. Under

the untested assumption that positive and negative excursions of this error compensate each other, no further action is taken to mitigate the influence of this less-than-perfect near-bottom resolution.

Finally, because the rate of storage of  $C_{\text{ant}}$  is expressed in gravimetric units (i.e., per kg rather than per liter), gridbox *volume* is converted to gridbox *mass* (GBM) by multiplication by the in-situ density of the gridbox.

#### *Calculating rates of increase at each gridpoint*

Several water masses may contribute to the water at each gridpoint. For each contributing water mass  $i$ , a value  $dC_{\text{ant}}^{\text{TSR}}/dt$  (in units of  $\mu\text{mol kg}^{-1} \text{a}^{-1}$ ) is calculated at each gridpoint, that expresses the time trend (or rate of storage) of  $C_{\text{ant}}$  contributed by that water mass  $i$ :

$$\frac{dC_{\text{ant } i}^{\text{TSR}}}{dt} = x_i \cdot (a_i + \Delta\text{AOU} \cdot b_i) \quad (7-5)$$

Here,  $x_i$  signifies the fraction of water mass  $i$  that is present at the gridpoint (as determined by the OMP analysis of the World Ocean Atlas dataset). The constant  $a_i$  represents for each water mass  $i$  the time trend of  $C_{\text{ant}}$  at the mean AOU of the core of the water mass. The coefficient  $b_i$  represents the dependence of that trend on the AOU of the sample ( $\Delta\text{AOU}$  is the difference between the AOU of a sample and the mean AOU in the core of the water mass).

Summing the contributions of the  $j$  different water masses at each gridpoint results in the total rate of storage of  $C_{\text{ant}}$  ( $dC_{\text{ant}}^{\text{TSR}}/dt$ , also in units of  $\mu\text{mol kg}^{-1} \text{a}^{-1}$ ) at that gridpoint:

$$\frac{dC_{\text{ant}}^{\text{TSR}}}{dt} = \sum_{i=1}^j x_i \cdot (a_i + \Delta\text{AOU} \cdot b_i) \quad (7-6)$$

Multiplication of the results of Eq. 7-6 (i.e.,  $dC_{\text{ant}}^{\text{TSR}}/dt$ , in units of  $\mu\text{mol kg}^{-1} \text{a}^{-1}$ ) with the mass of the water contained by each gridbox (in units of kg) yields the rate of change of the inventory of  $C_{\text{ant}}$  ( $d^{\text{INV}}C_{\text{ant}}^{\text{TSR}}/dt$ , in units of  $\mu\text{mol a}^{-1}$ ) at that gridpoint.

$$\frac{d^{\text{INV}}C_{\text{ant}}^{\text{TSR}}}{dt} = \sum_{i=1}^j x_i \cdot (a_i + \Delta\text{AOU} \cdot b_i) \cdot \text{GBM} \quad (7-7)$$

Comparably, multiplication of the water mass-specific results of Eq. 7-5 with the gridbox mass yields the rate of storage of  $C_{\text{ant}}$  in each water mass  $i$  present at a gridpoint:

$$\frac{d^{\text{INV}}C_{\text{ant } i}^{\text{TSR}}}{dt} = x_i \cdot (a_i + \Delta\text{AOU} \cdot b_i) \cdot \text{GBM} \quad (7-8)$$

The terminology outlined above allows to obtain various metrics of interest, such as:

- the rate of increase of the inventory of  $C_{\text{ant}}$  in the AAIW (in  $\text{TgC a}^{-1}$ )
- the rate of increase of the inventory of  $C_{\text{ant}}$  in the whole South Atlantic Ocean (in  $\text{TgC a}^{-1}$ ).
- the mean rate of increase of  $C_{\text{ant}}$ , south of 30 °S, shallower than 1000 m (in  $\mu\text{mol kg}^{-1} \text{a}^{-1}$ )
- the mean rate of increase of  $C_{\text{ant}}$  in the NADW (in  $\mu\text{mol kg}^{-1} \text{a}^{-1}$ )

## Chapter 7

### Integrations of total accumulation

Two integrations are performed in order to permit a comparison between the results of this study and those of others:

- vertical integration yields the column inventory of the rate of increase of  $C_{\text{ant}}$  ( $\text{mol m}^{-2} \text{a}^{-1}$ ). This result can be compared, for instance, to the map produced by Sabine et al. (2004).
- a three-dimensional integration yields the rate of storage of  $C_{\text{ant}}$  ( $\text{TgC a}^{-1}$ ) in the South Atlantic Ocean as a whole. This estimate may, for instance, be compared with ocean general circulation models or large-scale atmospheric inversions.

### 7.8.3. Results

#### Rates of increase at gridpoints

Resulting values of  $dC_{\text{ant}}/dt$  are generally between 0 and  $1 \mu\text{mol kg}^{-1} \text{a}^{-1}$ . The near-zero values are mostly located in the deep and bottom waters, whereas the higher rates of increase  $C_{\text{ant}}$  are

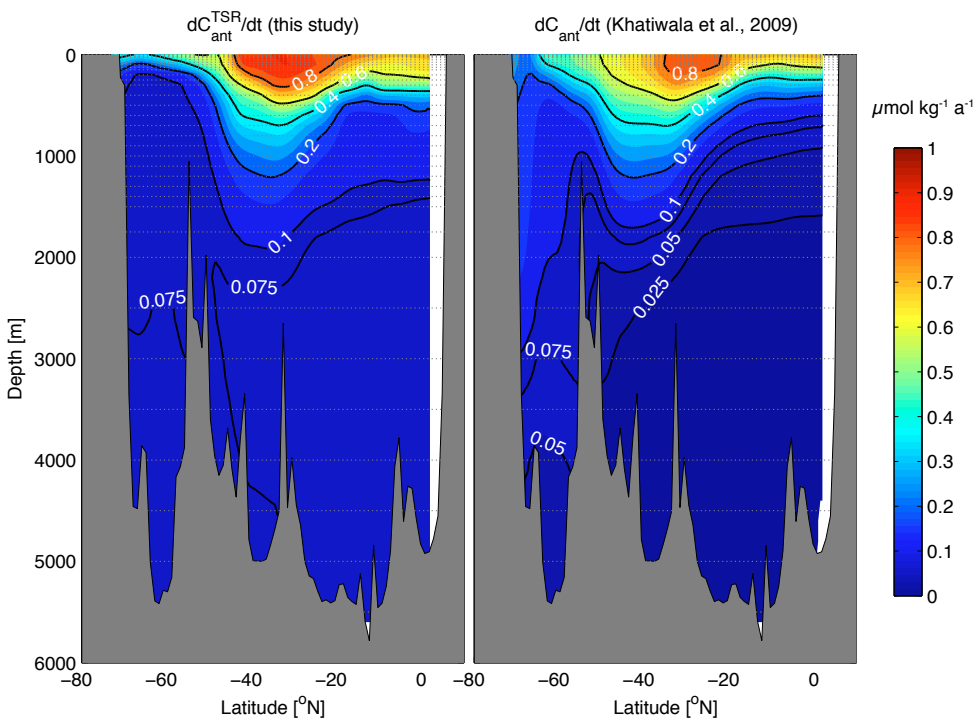


**Figure 7.12.** Panel **a**) A section along 0°E in the South Atlantic Ocean showing the rate of increase of  $C_{\text{ant}}$  ( $dC_{\text{ant}}^{\text{TSR}}/dt$ ) inferred from data spanning the period 1973–2008. High values of  $dC_{\text{ant}}/dt$  are observed for the surface waters north of 50°S, and in the descending AAIW. Further along the path of AAIW the rate of increase is lower, likely due to the lower levels of atmospheric  $C_{\text{ant}}$  around the time that these waters were ventilated. The surface waters south of 50°S show little accumulation of  $C_{\text{ant}}$ , likely due to continuous upwelling and subsequent divergence of old,  $C_{\text{ant}}$ -poor NADW at these latitudes. Panel **b**) Same, but showing the result of the study of Khatiwala et al., 2009. Please refer to text section 7.9 for a discussion of the differences between these studies.

located in the most shallow, well-ventilated (low-AOU) waters. Figure 7.12 shows a section of  $dC_{\text{ant}}/dt$  through the World Ocean Atlas dataset along  $0^\circ\text{E}$ , which clearly illustrates this pattern.

#### Rates of increase in individual water masses

The calculated rates of increase of the inventory of  $C_{\text{ant}}$  of the different water masses distinguished in this study are listed in Table 7.6. The biggest contributors to the accumulation of  $C_{\text{ant}}$  are the AAIW and SACW ( $108\pm 20$  and  $107\pm 12 \text{ TgC a}^{-1}$ , respectively). This is to be expected, since both are relatively large bodies of water and both are well ventilated. Due to its even larger volume, the AABW is another large contributor ( $81\pm 40 \text{ TgC a}^{-1}$ ), in spite of its relatively low  $dC_{\text{ant}}/dt$ , which moreover has a rather high uncertainty ( $0.08\pm 0.04 \mu\text{mol kg}^{-1} \text{ a}^{-1}$ ). Accumulation in the NADW is not significantly different from zero ( $26\pm 62 \text{ TgC a}^{-1}$ ). Although the  $dC_{\text{ant}}/dt$  in the ESW is as high as  $0.85\pm 0.21 \mu\text{mol kg}^{-1} \text{ a}^{-1}$ , the associated accumulation of  $d^{\text{INV}}C_{\text{ant}}/dt$  is limited due to the small volume of the ESW.

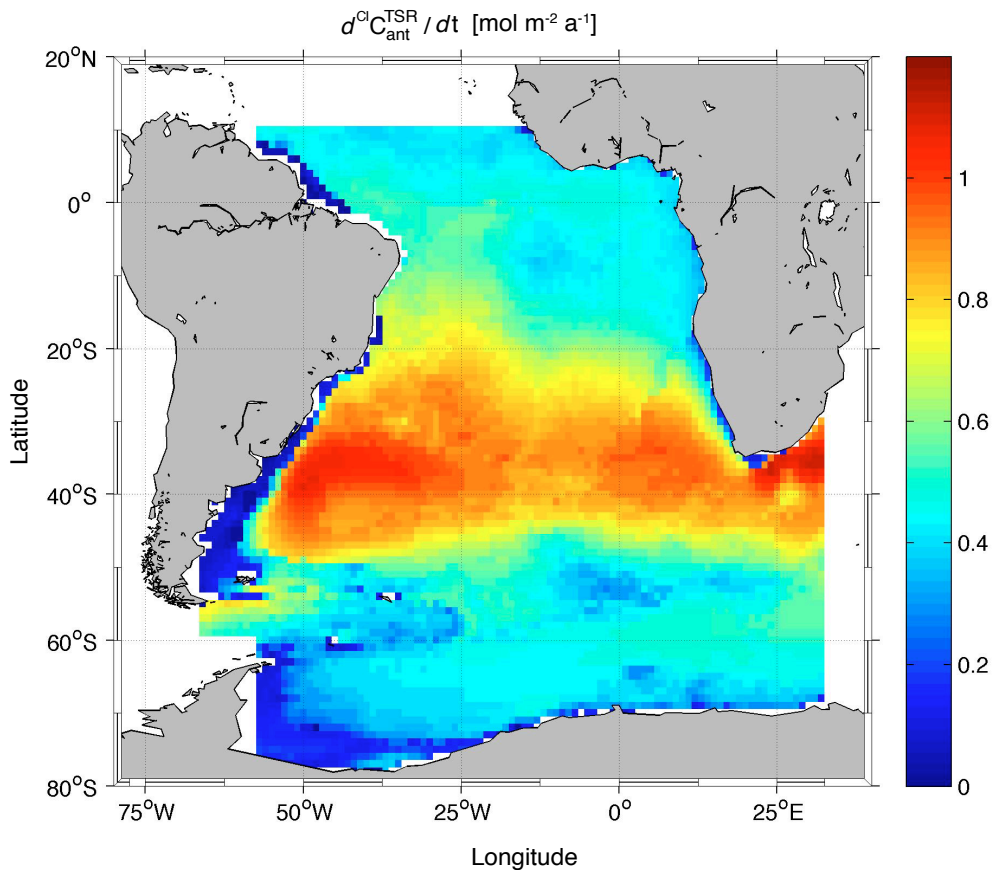


**Figure 7.13** Map of the Southern Ocean showing the column inventories of  $dC_{\text{ant}}/dt$  (in  $\text{mol m}^{-2} \text{ a}^{-1}$ ). Significant accumulation of  $C_{\text{ant}}$  (as high as  $1.2 \text{ molC m}^{-2} \text{ a}^{-1}$ ) takes place to the north of the region of subduction of intermediate and mode waters around  $50^\circ\text{S}$ . Intermediate rates of storage are observed in the Weddell Gyre and in the Gulf of Guinea.

**Table 7.6.** The rate of storage of  $C_{\text{ant}}$ , determined in each of the seven water masses discerned in this study (text section 7.8). Columns 3 and 4 pertain to the discussion of results from slightly modified versions of the TSR methodology (text section 7.9). For reference, the last column of the table lists the volumes of the watermasses (the sum of the products of gridbox volumes and watermass fractions; from OMP, section 7.5).

Watermass	$dC_{\text{ant}}^{\text{TSR}}/dt$ TgC a <sup>-1</sup>	$dC_{\gamma}/dt$ TgC a <sup>-1</sup>	$dC_{\text{ant}}^{\text{TSR}}/dAP$ TgC $\mu\text{atm}^{-1}$	Volume 10 <sup>6</sup> km <sup>3</sup>
AABW	81 ± 40	49 ± 63	38 ± 23	80.04
WSBW	19 ± 18	28 ± 20	12 ± 10	21.04
NADW	26 ± 62	36 ± 98	15 ± 46	92.83
AAIW	108 ± 20	114 ± 33	65 ± 14	29.9
SACW	107 ± 12	102 ± 15	61 ± 8	12.19
AASW	12 ± 3	9 ± 9	7 ± 2	2.53
ESW	36 ± 9	63 ± 37	22 ± 6	3.4
TOTAL	389 ± 80	401 ± 130	218 ± 55	241.94

#### Column inventories and total accumulation

Figure 7.13 shows a map of the rate of increase of the column inventory of  $C_{\text{ant}}$  ( $d^{\text{Cl}}C_{\text{ant}}^{\text{TSR}}/dt$ ) in the South Atlantic Ocean. The highest rates of storage (circa 1 mol m<sup>-2</sup> a<sup>-1</sup>) are seen between 30 and 45 °S on the westernmost side of the basin, representing the  $C_{\text{ant}}$  contained in the AAIW and SACW, being transported northward at intermediate depth by the large scale basin circulation. The overall rate of accumulation of  $C_{\text{ant}}$  in the South Atlantic Ocean as a whole is calculated to be 389±80 TgC a<sup>-1</sup>. The accumulation below 3000 m depth comprises about 15% of the total (i.e., ~60±50 TgC a<sup>-1</sup>), restricted to the AABW and the WSBW. Above 1500 m depth, SAMW and AAIW are the major contributors.

The error estimates of the accumulation in the individual water masses reflects both the uncertainty in the distribution of the water mass (as yielded by the stability analysis of the OMP) and the uncertainty of the determination of the trends. The error of the total accumulation is calculated as the square root of the sum of the squared individual errors. This implicitly assumes the errors are random and independent, which is, however, formally not the case.

#### 7.8.4. Discussion

##### Improvements of $C_{\text{res}}^{\text{TSR}}$

The methodology that was followed may be understood to be an attempt to explain part of the spread in  $C_{\text{res}}^{\text{TSR}}$  in terms of uptake of anthropogenic CO<sub>2</sub> from the atmosphere (or reduced outgassing of natural CO<sub>2</sub>, which amounts to the same). Obviously, not all spread in  $C_{\text{res}}^{\text{TSR}}$  will be explainable, since a large part of the spread results from measurement noise and inaccuracies. However, if one subtracts from  $C_{\text{res}}^{\text{TSR}}$  the inferred  $dC_{\text{ant}}/dt$  (times the time difference with the year 1997 - the nominal year of the dataset), the spread in  $C_{\text{res}}^{\text{TSR}}$  is reduced significantly (Figure 7.14). This suggests that a time-and-AOU-dependent parameterization of  $dC_{\text{ant}}^{\text{TSR}}/dt$  is valid.

If one takes the spread in  $C_{\text{res}}^{\text{TSR}}$  that is due to analytical inaccuracies to amount to 4  $\mu\text{mol}\cdot\text{kg}^{-1}$  (i.e., the value observed in the deep, stable water masses), the improvement due

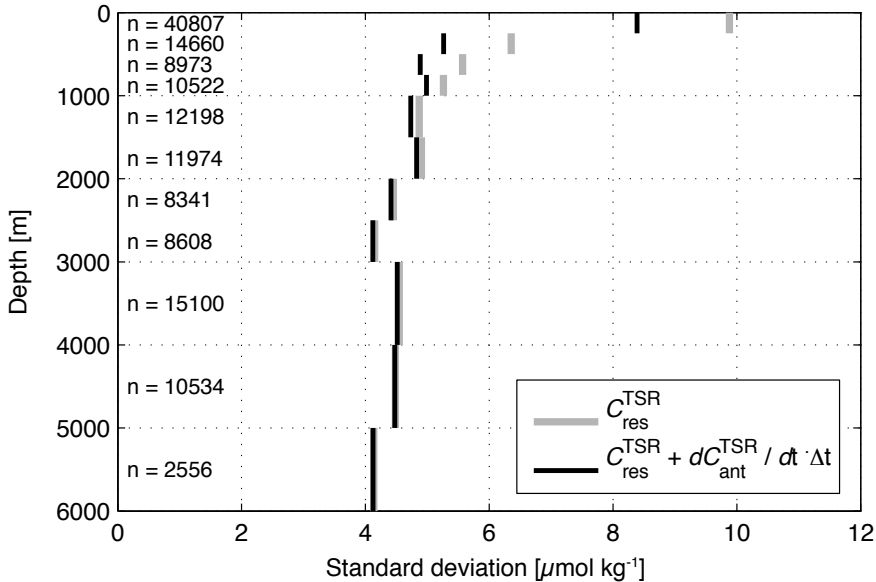


**Figure 7.14.** Illustration of the reduction of the spread in  $C_{\text{res}}^{\text{TSR}}$  by correction for the accumulation of  $C_{\text{ant}}$  over time. See text section 7.8.4 for more details.

to consideration of  $dC_{\text{ant}}/dt$  is about 30% for the surface 250 meters (i.e., from 5.3 (9.3 above the baseline noise of 4) to 3.8). For the three following depth bins, i.e., down to 1000 m, 57%, 52% and 37% of the spread is removed. The remaining spread necessarily stems from errors in various assumptions of linearity, from non-steady state of the ocean, etc. Consideration of the accumulation of  $C_{\text{ant}}$  does not seem to reduce the spread of  $C_{\text{res}}^{\text{TSR}}$  in the waters below 2000 m depth.

The exact amount that the individual water masses contribute to the total accumulation is sensitive to the definition of the source water types in the OMP analysis. However, the *total* amount is considered to be fairly insensitive to such variations in the source water type definitions.

An additional point of critique may be that the underlying GLODAP and CARINA datasets have themselves been adjusted such as to be internally consistent in the deep waters. The weighting scheme employed in these studies (Tanhua et al. 2010) should preclude the removal of time trends, but no formal evidence for the success of this approach is given. To get an idea of the sensitivity of the results of this study to the partly arbitrary corrections applied to the original data by the CARINA and GLODAP data synthesis efforts, an analysis of the uncorrected CARINA/GLODAP data is warranted. We expect the results of such an analysis not to differ significantly in the surface layers. Results for the deep water masses may be more susceptible to the relatively large biases of the pre-1990s cruises.



## 7.9. Discussion

The approach that was detailed in the previous sections relies on a suite of assumptions and somewhat arbitrary choices. For example, we opted to not include the Circumpolar Deep Water in the optimum multiparameter analysis. Also, we assumed that our scheme for determining  $C_T^{\text{TSR}}$  does not lead to appreciable biases.

Each section elaborates qualitatively on these assumptions. In the current section we present some compelling quantitative evidence of the robustness of the obtained results. Firstly, we present an additional analysis, performed with a slight modification and simplification of the outlined approach, with resulting trends that are near-identical to the original ones, albeit with larger error estimates.

Secondly, in order to maximize the applicability of the current approach, we adopt the methodology outlined by Rios et al. (2012) that allows for extrapolation, within limits, of results to future (and past) conditions of atmospheric  $p\text{CO}_2$ .

Lastly, we will demonstrate that the obtained results are, as far as this can be assessed, fully compatible with the seminal work of Takahashi et al. (2009), and with the results of the recent inversion-based estimates of Gruber et al. (2009). Furthermore, only minor quantitative and qualitative differences are observed with the work of Waugh et al. (2006) and Sabine et al. (2004). The tracer-based study of Khatiwala et al. (2009) is shown to be in close agreement with the current work.

### 7.9.1. Trends determined in $C_T^{\text{meas}}$

The presented TSR technique is a variant of the MLR technique in order to discern, within hydrographic and biogeochemical variability, trends in  $C_T^{\text{meas}}$ , which are subsequently ascribed to accumulation of anthropogenic  $\text{CO}_2$  for the atmosphere. However, the MLR technique is susceptible to biases and secular trends in input parameters (e.g., Levine et al., 2008), which conceivably mask or enhance, to unknown extent, the obtained results.

The MLR methodology was devised for - and is especially applicable to (Wallace, 1995; Levine et al., 2011) - data from (sets of two) cruises separated in time by only a moderate amount of time (5-10 years). Over such short intervals, the magnitude of hydrographic and biogeochemical variability is large compared to the expected increase in  $C_T$ , and no trends are expected to be directly detectable, unless by resorting to the use of MLR. For example, the large (physically and biologically driven) effects of seasonality on  $C_T$  are to a large extent incorporated into the coefficients of the derived MLR. Because of this,  $C_{\text{res}}^{\text{TSR}}$  should vary only minimally over the seasons, and would be more easily observed to gradually rise over the years. On the other hand,  $C_T^{\text{meas}}$  itself may vary strongly over the seasons, and therefore no trend over time may be apparent through this variability - especially so if cruises are performed over different seasons in different years.

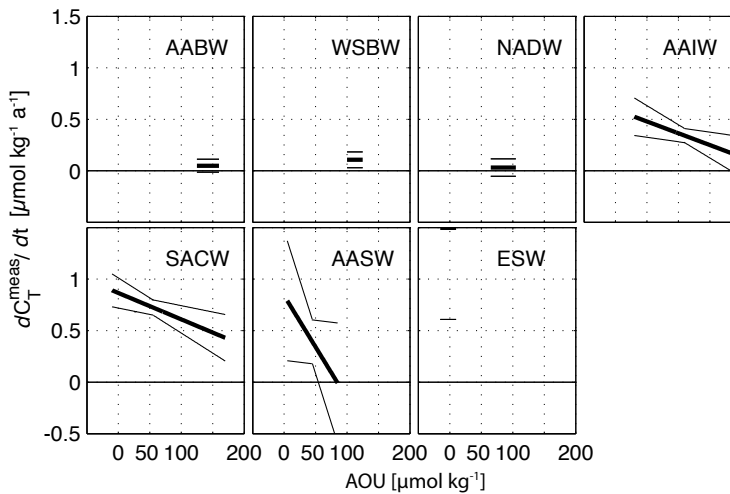
Because the current study considers data over a relatively large time interval (35 years), it may be expected that the increase in  $C_T$  (from uptake of  $\text{CO}_{2,\text{ant}}$  from the atmosphere) is evident despite such natural variability. To test this expectation, we performed an analysis set up exactly like the TSR approach, with the adaptation that the surface fitting (section 7.7)

is not performed for time-vs-AOU-vs- $C_{\text{res}}^{\text{TSR}}$ , but rather for time-vs-AOU-vs- $C_{\text{T}}^{\text{meas}}$ . In this approach, the generation of  $C_{\text{T}}^{\text{TSR}}$  and calculation of  $C_{\text{res}}^{\text{TSR}}$  (section 7.6) is not required anymore.

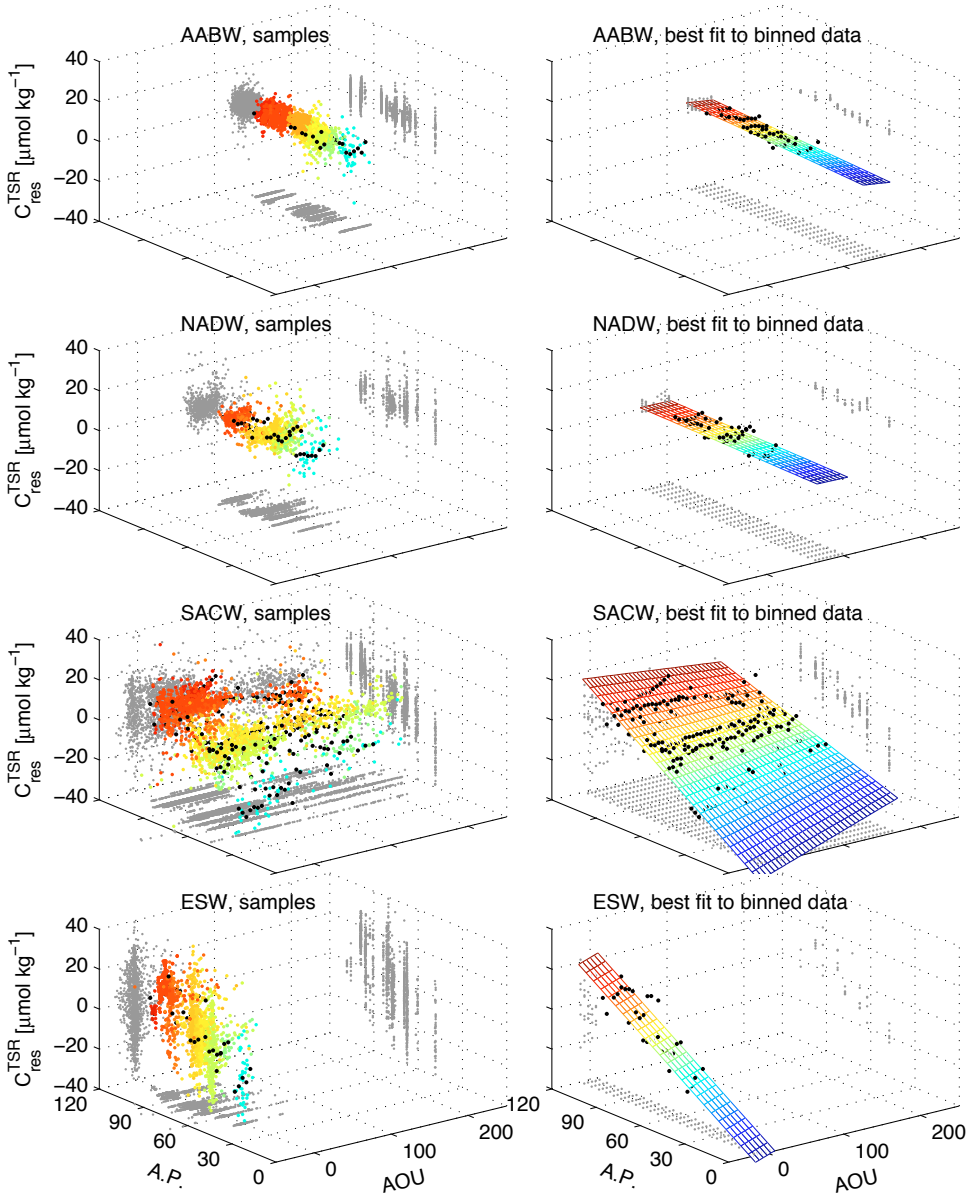
The determined shapes of the fitted surfaces (one for each water mass) are, as may be expected, wholly different between the two approaches. Nonetheless, we still expect to find an increase in  $C_{\text{T}}$  over time - at least for those water masses that are well ventilated, and if the noise from natural variability is not too strong. Additionally, we again expect to observe a dependency of the time trend of  $C_{\text{T}}$  on AOU (i.e.,  $dC_{\text{T}}/dt$  would decrease with increasing AOU). Any result of this exercise may be further treated in the same way as done before.

The results of this 'simplified' analysis are shown in Table 7.6 (third column) and Figure 7.15. The latter may be compared to Figure 7.11. It is evident that the results obtained using  $C_{\text{T}}^{\text{meas}}$  are highly comparable with the preceding results obtained using  $C_{\text{res}}^{\text{TSR}}$ . The inferred rate of increase of the total inventory of  $C_{\text{ant}}$  ( $d^{\text{INV}}C_{\text{ant}}/dt$ ) in the South Atlantic Ocean is nearly identical between methods:  $389 \pm 80$  vs.  $401 \pm 130$   $\text{PgC a}^{-1}$  for the  $C_{\text{res}}^{\text{TSR}}$ - and  $C_{\text{T}}^{\text{meas}}$ -methods, respectively. For all water masses, results are comparable, although the uncertainty of the determination is some 60% larger for the  $C_{\text{T}}^{\text{meas}}$ -based approach than for the 'full' TSR method. Thus the earlier obtained results are inferred to be robust. Additionally, this exercise corroborates the assumption that the use of MLR improves the sensitivity of detection of trends in  $C_{\text{T}}$ , presumably because the MLR captures and compensates for a significant part of the natural variability.

Nonetheless, some discrepancies between the two sets of results are observed. The largest (relative) difference is observed for the rate of storage of  $C_{\text{ant}}$  in the equatorial surface water (ESW), namely from  $+36 \pm 9$   $\text{TgC a}^{-1}$  ( $C_{\text{res}}^{\text{TSR}}$ -method) to  $+64 \pm 37$   $\text{TgC a}^{-1}$  ( $C_{\text{T}}^{\text{meas}}$ -method). More than any other, the ESW is a water mass that has a highly variable  $C_{\text{T}}$ , spanning a range from 1900 to 2100  $\mu\text{mol kg}^{-1}$ . This large variability leads to a high uncertainty of the fit. The



**Figure 7.15** Same as Figure 7.11, but showing time trends in  $C_{\text{T}}^{\text{meas}}$ , rather than in  $C_{\text{res}}^{\text{TSR}}$ . The likeness between the two results is taken to corroborate the validity of the used TSR methodology. Note the larger uncertainties in this figure compared to Figure 7.11. For a discussion see text section 7.9.2.



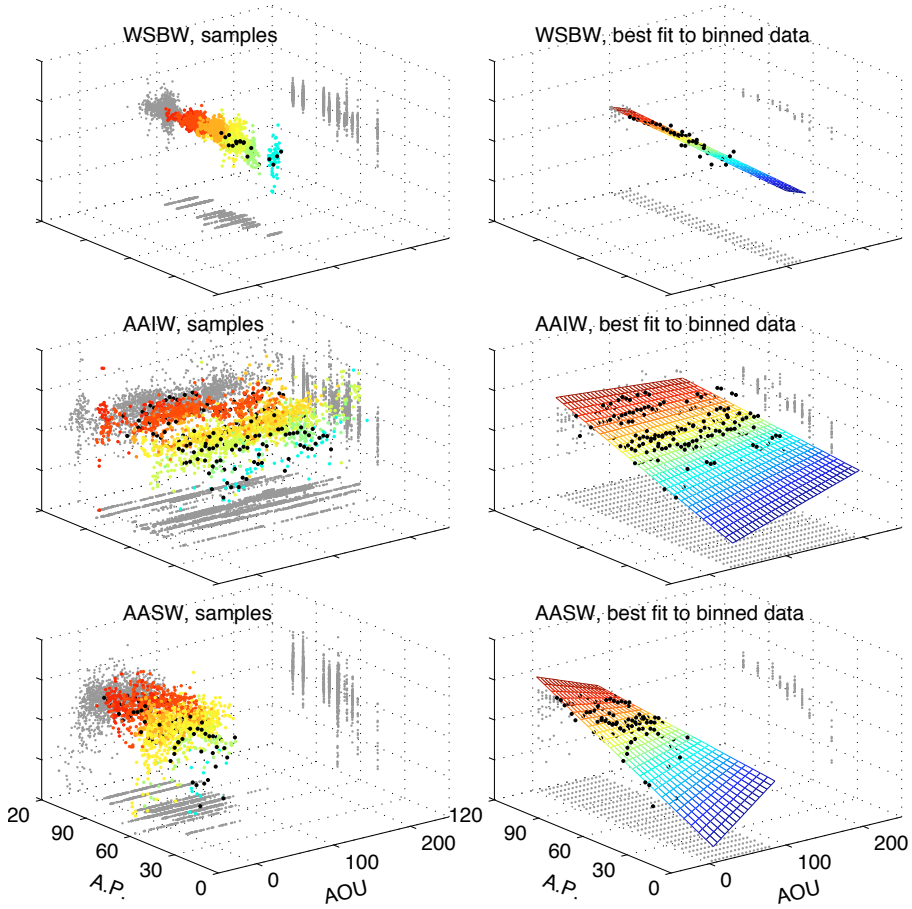
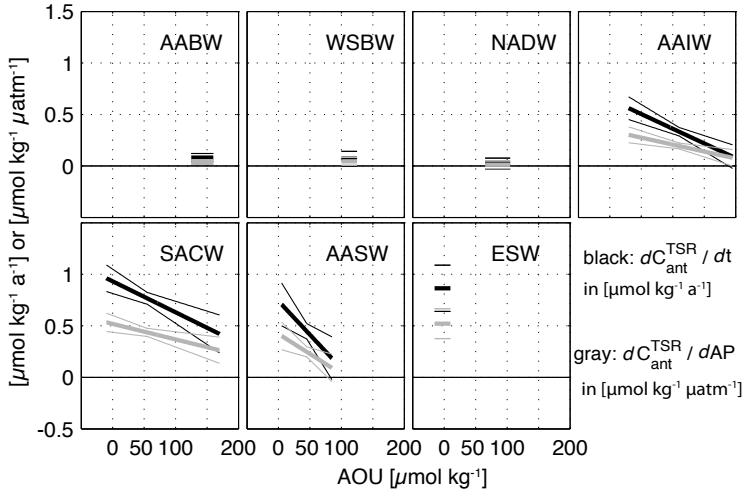


Figure 7.16 Same as Figure 7.10, but showing the surface fits of  $C_{\text{res}}^{\text{TSR}}$  versus AOU and AP (the atmospheric perturbation of anthropogenic  $\text{CO}_2$ ), rather than versus AOU and time. This approach is considered to improve the linearity of the relationships, and therefore to improve the surface fitting. For a discussion see text section 7.9.2.



**Figure 7.17** Identical to Figure 7.11, but with added trends of  $C_{\text{ant}}^{\text{TSR}}$  versus the anthropogenic perturbation of atmospheric  $\text{CO}_2$  (AP). See text section 7.9.2 for a discussion.

result for this water mass is therefore regarded to be inferior to the TSR-based result (since  $C_{\text{res}}^{\text{TSR}}$  does not show such a very large range). By contrast, the results for the two very large, often sampled, well ventilated and homogenous water masses (the AAIW and SACW), are statistically indistinguishable between the two methods.

It may be of some interest to note that the method also allows for the determination of trends in back-calculated  $C_{\text{ant}}$  (e.g., with the TrOCA method; Touratier et al., 2004a,b), or in back-calculated preformed  $C_T$  ( $C_T^0$ ; Brewer, 1978; Chen and Millero, 1979). As a result of the application of the TrOCA technique in this context, we infer significant increases of  $C_{\text{ant}}$  in the NADW and AABW. These increases are also reported by Rios et al. (2012), from an analysis of 20 cruise datasets in the western South Atlantic Ocean, using the  $\phi C^*$  technique (Vasquez-Rodriguez et al., 2008). The reason that these strong increases are not observed in the present study in either  $C_T$  or  $C_{\text{res}}^{\text{TSR}}$  requires additional investigation, and is beyond the scope of the present study.

### 7.9.2. Inferring the inventory of $C_{\text{ant}}$ .

The TSR methodology does not yield an inventory of anthropogenic carbon ( $^{\text{INV}}C_{\text{ant}}$ ), but rather the rate of change of the inventory ( $d^{\text{INV}}C_{\text{ant}}/dt$ ). Therefore, no direct comparison can be made with earlier obtained inventories. We present here two options for obtaining an estimate of  $^{\text{INV}}C_{\text{ant}}$  that only require a very limited adaptation of the methodology. Firstly, we employ the concept of Transient Steady State (Tanhua et al., 2007) to straightforwardly derive a scaling factor between  $d^{\text{INV}}C_{\text{ant}}/dt$  and  $^{\text{INV}}C_{\text{ant}}$  and apply that factor. Secondly, the trends in  $C_{\text{res}}^{\text{TSR}}$  (section 7.7) will be re-assessed. This time, however, rather than being regressed versus time directly,

the regression is performed versus the atmospheric perturbation of anthropogenic  $\text{CO}_2$  (from here on referred to as the AP).

#### *Transient Steady State (TSS)*

The TSS concept (Gammon et al., 1982; Tanhua et al., 2007) states that after a sufficient amount of time, the rate of increase of a tracer at any point in the sub-surface ocean will be directly proportional to the rate of increase of that tracer at the sea surface, provided that the latter concentration is (approximately) exponentially increasing. When this ‘transient steady state’ is reached and the surface history is known, the unknown total concentration at any location at depth may be directly inferred from the (observed) rate of change of the concentration.

As a simple example, one could say that if the surface water concentration is known to have risen with 2% per year, a (significantly) determined increase in the ocean interior will also constitute 2% of the local total concentration. Hence, if we observe over 35 years a rate of change of  $1 \mu\text{mol kg}^{-1} \text{a}^{-1}$  in the SACW (for a total increase of  $35 \mu\text{mol kg}^{-1}$ ), over a period in which the atmospheric perturbation rose from 50 to  $105 \mu\text{atm}$  (the change of 55 being 52.3% of the total), we may state that the total concentration of  $C_{\text{ant}}$  at the surface is  $35/0.523=66.9 \mu\text{mol kg}^{-1}$ . Because the TSS approach consists of only a scaling factor, it may be applied to concentrations and inventories alike.

Over the 35 year period of our observations, the average annual increase of atmospheric anthropogenic  $\text{CO}_2$  was 2.2%. Assuming air-sea  $p\text{CO}_2$  equilibrium (see also section 7.9.3), the yearly increase in  $C_{\text{ant}}$  that is observed (or, rather, inferred) at any location at depth will constitute 2.2% of the total concentration. The determined rate of increase of the inventory of  $C_{\text{ant}}$  ( $d^{\text{INV}}C_{\text{ant}}/dt$ , section 7.8.4) is thus 2.2% of the  $^{\text{INV}}C_{\text{ant}}$  of the South Atlantic Ocean. This simple scaling factor thus suggests  $^{\text{INV}}C_{\text{ant}} = 0.39(\pm 0.08)/0.022 \text{ PgC a}^{-1} = 17.7 \pm 3.6 \text{ PgC}$ .

#### *Regression versus the atmospheric perturbation*

It may be argued (Rios et al., 2012) that the TSR methodology for determining linear increases of  $C_{\text{ant}}$  over time is not particularly valid over longer periods of time. The atmospheric concentration of  $C_{\text{ant}}$  increases exceedingly rapidly over this period, and the uptake by the surface ocean is generally assumed to reflect that exponential behavior. Performing a linear fit may significantly over- or underestimate the actual trend, especially when the sampling intensity was not constant over the investigated period (see Figure 7.4). Therefore, in addition to performing a regression of  $C_{\text{res}}^{\text{TSR}}$  versus time (section 7.7), we perform this regression versus the concentration of anthropogenic atmospheric  $\text{CO}_2$  (i.e., the atmospheric perturbation (AP; in  $\mu\text{atm}$ ) above the pre-industrial  $p\text{CO}_2$  of  $280 \mu\text{atm}$ ), as suggested by Rios et al. (2012). This requires only a slight modification of the steps outlined in section 7.7, while the rest of the methodology remains unaltered. In doing this, we obtain an estimate of the rate of storage of  $C_{\text{ant}}$  in  $\mu\text{mol kg}^{-1} \mu\text{atm}^{-1}$  (as opposed to the earlier result in  $\mu\text{mol kg}^{-1} \text{a}^{-1}$ ).

This adaptation of the originally presented approach has several benefits (Rios et al., 2012). Firstly, as stated, it allows for improved linear fitting of data over long time periods. Secondly, it allows the determined rate of increase of the concentration of  $C_{\text{ant}}$  to be converted to the concentration itself. For example, if at a certain location in the ocean interior, the rate of increase of  $C_{\text{ant}}$  is determined to be  $0.6 \mu\text{mol kg}^{-1} \mu\text{atm}^{-1}$ , then at a total perturbation (since the beginning of the Industrial Revolution) of  $100 \mu\text{atm}$ ,  $C_{\text{ant}}$  may be calculated to be  $60 \mu\text{mol kg}^{-1}$ .

Lastly, the method allows for straightforward scaling of the inferred oceanic accumulation of  $C_{\text{ant}}$  to past and future concentrations of atmospheric anthropogenic  $\text{CO}_2$ .

Like most other methods, the 'AP'-method requires the assumption of a steady state ocean, and of a constant  $p\text{CO}_2$  disequilibrium between atmosphere and sea surface. We note that neither condition is known to be met in the real ocean.

Applying this method, we obtain an overall rate of storage of  $218 \pm 55 \text{ TgC } \mu\text{atm}^{-1}$  (see Table 7.6, fourth column, and Figures 7.16 and 7.17 for results for individual water masses). At the rate of increase of the atmospheric perturbation in the year 1994 (on average  $1.5 \mu\text{atm a}^{-1}$  over 1990-1998), this translates to a *time* rate of storage of  $0.33 \pm 0.08 \text{ PgC a}^{-1}$ . This estimate is slightly lower than the earlier presented estimate of  $0.39 \pm 0.08 \text{ PgC a}^{-1}$ , derived with the unmodified TSR technique, but statistically the estimates are not significantly different. For more recent years, during which the mean rate of increase of  $\text{CO}_2$  was approximately  $2.0 \mu\text{atm a}^{-1}$ , the determined trends translate into a rate of storage of  $0.44 \pm 0.11 \text{ PgC a}^{-1}$ .

Assuming that the rate of storage obtained from regressing against the atmospheric perturbation is valid for the timespan of 1973 to 2008, we calculate, using the corresponding values of the AP, the values of  $^{\text{INV}}C_{\text{ant}}$  for each year. In 1973 (AP:  $\sim 48 \mu\text{atm}$ ), the  $^{\text{INV}}C_{\text{ant}}$  of the South Atlantic Ocean was  $\sim 10.5 \text{ PgC}$ , rising to  $22.2 \pm 5.6 \text{ PgC}$  in 2008. A time history of  $C_{\text{ant}}$  based on this approach is shown in Figure 7.18.

### 7.9.3. Comparison with estimates of other investigators.

Several attributes of this study may be compared with results from other investigators. Among these are the results of the OMP, the inferred rates of uptake of  $C_{\text{ant}}$  and the (rate of change of the) inventory of  $C_{\text{ant}}$ . However, since OMP results to large extent reflect the largely arbitrary decisions about the exact source water type definitions (and the amount of them), this following

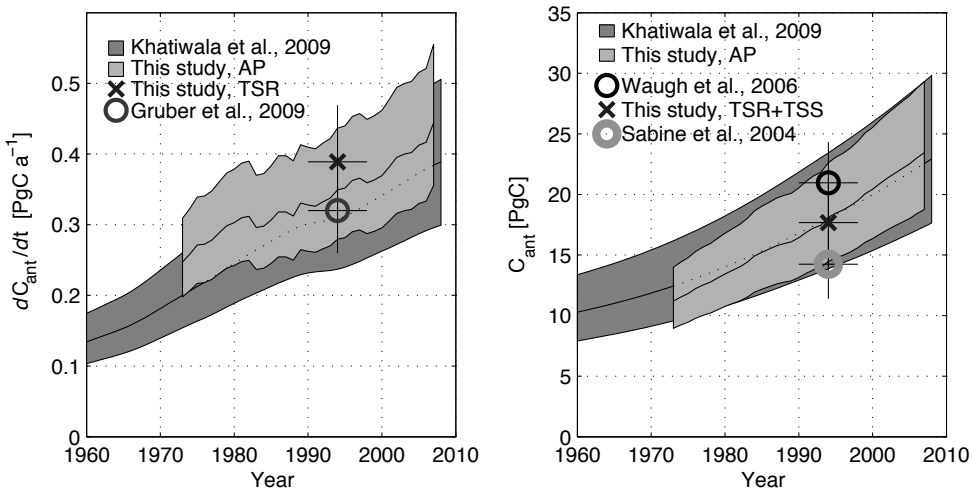


**Figure 7.18.** Summary of the results of several studies. Left panel: estimates of the rate of increase in the inventory of  $C_{\text{ant}}$ . Right panel: estimates of the inventory of  $C_{\text{ant}}$ . For a discussion see text section 7.9.3.



section will be limited to a discussion of the determined (rates of change of) the concentrations of  $C_{\text{ant}}$ , and of derived quantities thereof (inventories).

Studies of gas flux across the air-sea interface (e.g., Takahashi et al., 2009) are generally restricted to an assessment of the contemporary flux (i.e., the combined natural and anthropogenic fluxes). Our analysis explicitly attempts to resolve the anthropogenic flux. In the case that no large between-ocean basin flux of  $C_{\text{ant}}$  takes place, and the net natural flux is known, the air-sea flux would equal the rate of storage, and a comparison between Takahashi et al. (2009) and the present study would be feasible. However, lateral transport of ocean interior  $C_{\text{ant}}$  between the South Atlantic Ocean and the other oceans (the North Atlantic and the Indian and Pacific oceans) is commonly acknowledged to exist (e.g., England et al., 1993; Tomczak, 2003; Takahashi et al., 2009; Gruber et al., 2009). Furthermore, the Southern Ocean is considered to have been a source of  $\text{CO}_2$  in preindustrial times. Therefore, without first applying the TSR methodology to at least all southern hemispheric oceans, no such comparison between storage rates and surface-fluxes will yield new insights.

Nonetheless, a comparison with Takahashi et al. (2009) may be informative in a different respect. These authors report narrowly constrained rates of the increase of  $p\text{CO}_2$  (reproduced in Table 7.7), for Southern Ocean surface waters in austral winter (days of year 172 to 326) between 1986 to 2007, presumably resulting from the uptake of  $\text{CO}_{2,\text{ant}}$  from the atmosphere. These rates are associated with increases in  $C_T$ , and depend mainly on the temperature, alkalinity and salinity of the seawater. A comparison shows that the rates of increase in  $C_T$  observed in the present study are compatible with the rates of increase in  $p\text{CO}_2$  determined by Takahashi et al. (2009).

From the flux data presented by Takahashi et al. (2009), we estimate a total contemporary (i.e., natural + anthropogenic) flux for the South Atlantic Ocean of about  $-0.16 \text{ PgC a}^{-1}$  (here, negative values indicate flux from atmosphere to ocean). For the sake of argument we briefly assume that the storage of  $C_{\text{ant}}$ , as determined in the present study, entirely results from surface uptake within the local basin. We may under these assumptions infer the natural (or pre-industrial) flux from the Southern Ocean to the atmosphere to have been as large as  $+0.23 \text{ PgC a}^{-1}$  (the natural flux equals the contemporary flux minus the anthropogenic flux, i.e.,  $F_{\text{nat}} = -0.16 - 0.39 = 0.23 \text{ PgC a}^{-1}$ ). This finding illustrates the inversion of the role of the Southern Ocean over the industrial era, from a source to a sink of atmospheric  $\text{CO}_2$ .

In the remainder of this section we compare the presented estimates of  $d^{\text{INV}}C_{\text{ant}}/dt$  and  $^{\text{INV}}C_{\text{ant}}$  with results from other earlier investigations. These estimates are summarized in Figure 7.18.

**Table 7.7.** Rates of increase of  $p\text{CO}_2$ , as reported by Takahashi et al. (2009; T09), and their concomitant increases in  $C_T$  (calculated at relevant T, S and  $A_T$ ) are compared with the rates as determined in the present study by the surface fitting procedure in the cores of water masses (at  $\text{AOU} = 0 \text{ } \mu\text{mol kg}^{-1}$ ; text section 7.7, see also Figure 7.10 and 7.11).

Temperature	T09	T09	TSR
$^{\circ}\text{C}$	$\mu\text{atm a}^{-1}$	$\mu\text{mol kg}^{-1} \text{ a}^{-1}$	$\mu\text{mol kg}^{-1} \text{ a}^{-1}$
0.8-1.5	$+1.82 \pm 0.39$	$+0.70 \pm 0.15$	$+0.72 \pm 0.17$ (AAIW/AASW)
4.5-5.5	$+1.85 \pm 0.35$	$+0.74 \pm 0.14$	$+0.67 \pm 0.16$ (AAIW)
equatorial	$+1.25 \pm 0.30$	$+0.76 \pm 0.14$	$+0.91 \pm 0.18$ (ESW)

The study performed by **Sabine et al. (2004)** suggested that  $C_{\text{ant}}$  in the Southern Ocean is nearly absent at any depth along the water column. Several subsequent studies (e.g., Matsumoto and Gruber, 2005; Waugh et al., 2006) have nonetheless presented evidence for  $C_{\text{ant}}$  in these waters, and have attributed the discrepancy to an artifact of the  $\Delta C^*$  methodology as employed by Sabine et al. (2004).

Briefly, the  $\Delta C^*$  method requires the user to determine the pre-industrial level of  $C_T$  for the isopycnal interval(s) under consideration. Specifically in the Southern Ocean, the determination of such baselines is a complicated process (Matsumoto and Gruber, 2005; van Heuven et al., 2001; LoMonaco et al., 2005a,b). In part because most deep waters of the global ocean contain a large fraction of water derived from the Antarctic formation regions, biases in the assumed baselines propagate into the wider ocean, and indeed Sabine et al. (2004) present  $C_{\text{ant}}$  to be close to zero throughout the deep ocean (with the North Atlantic ocean being a marked exception). The inventory for the South Atlantic Ocean, determined by Sabine et al. (2004) is therefore on the low side of the comparison, although within the range of the other estimates (Figure 7.18, panel b, gray circle; generated from data available at [cdiac.ornl.gov](http://cdiac.ornl.gov)).

**Waugh et al. (2006)** use ocean interior CFC measurements to estimate the inventory of  $C_{\text{ant}}$  with the Transit Time Distribution (TTD) method (Hall et al., 2002; McNeill et al., 2003). Based on skill assessments of the TTD technique using oceanic general circulation models (oGCMs), Waugh et al. (2006) conclude that the method produces a global inventory estimate that is biased circa 20% too high. They subsequently reduce their findings by 20% uniformly over the global ocean. The datapoint in Figure 7.18 (black circle in panel b; generated from data available at [cdiac.ornl.gov](http://cdiac.ornl.gov)), which represents the results from that study for the South Atlantic Ocean, has also received this -20% correction, but is still somewhat higher than the other estimates. This is not unexpected, because Waugh et al. (2006) note that the great majority of the bias of the global inventory is believed to be contributed by the Southern Ocean. They propose that, in regions downstream of the deep water formation zones in the Southern Ocean, the TTD method overestimates the concentration of  $C_{\text{ant}}$  by up to 60%, due to the assumption of a constant  $p\text{CO}_2$  disequilibrium between the surface waters and the atmosphere. This assumption is commonly made in ocean carbon studies, and is likely to be valid for the large majority of the surface of the oceans. However, specifically for the Southern Ocean, modeling exercises (e.g., Matear et al., 2003) and measurements (Klatt et al., 2002 for CFCs) indicate strong undersaturation (of up to 50%) may be present in these formation waters.

**Gruber et al. (2009)** report on an elaborate assessment of  $C_{\text{ant}}$  estimates in an inversion setup. The authors use rates of oceanic transport (obtained from a diverse suite of general circulation models) to infer the fluxes of  $\text{CO}_2$  and  $C_{\text{ant}}$  between atmosphere and ocean, and within the ocean, that are required to reproduce the distribution of  $C_{\text{ant}}$  that was inferred by Sabine et al. (2004). On a global scale, their results are highly comparable with the fluxes estimated by Takahashi et al. (2009). However, discrepancies are observed in the Southern Ocean, conceivably due to a lack of data that affects both approaches. Additional uncertainty is introduced by the fact that the inversion study attempts to 'explain' the  $C_{\text{ant}}$  estimates yielded by the  $\Delta C^*$  approach, which itself is subject to uncertainties, as detailed above. Because the inversion method essentially attempts to reproduce the  $\Delta C^*$ -derived  $C_{\text{ant}}$  fields, any biases therein would be reflected in the

resultant fluxes. From Figure 6 in Gruber et al. (2009) we roughly estimate the storage in the South Atlantic (south of the equator) in 1995 to be approximately  $320 \pm 20\%$  TgC  $\text{a}^{-1}$ . This estimate is in fair agreement with our TSR-based result of  $389 \pm 80$  TgC  $\text{a}^{-1}$  but probably on the low side.

**Khatiwala et al. (2009)**, use an advanced variant of the TTD method to determine a time-resolved history of oceanic  $C_{\text{ant}}$  from the beginning of the industrial revolution to the present day. Firstly, they use a diverse suite of tracers in a maximum entropy deconvolution scheme to optimally constrain how the ocean interior is ventilated from the surface. That is, Khatiwala et al. (2009) determine for each location in the ocean interior, how much water from each part of the sea surface arrives there after how much time. The resulting ‘ventilation functions’ ( $G$ ) optimally account for the concentrations of six conservative tracers as observed in the ocean interior ( $S$ ,  $T$ ,  $\text{PO}_4^*$ , CFC-11, CFC-12,  $\Delta^{14}\text{C}$ ), given their known concentration histories at the sea surface. Additionally, Khatiwala et al. (2009) estimate the concentration history of  $C_{\text{ant}}$  at the ocean’s surface (subdivided into 26 patches) using the  $p\text{CO}_2$  dataset of Takahashi et al. (2009), under certain constraints (partly derived from models) regarding how the air-sea disequilibrium evolves as a functions of the atmospheric perturbation of  $\text{CO}_2$ . Lastly, the ventilation functions  $G$  are used to propagate the  $C_{\text{ant}}$  concentrations history with time from the surface into the three-dimensional ocean interior. The method yields the time- and space-resolved history of oceanic  $C_{\text{ant}}$  as well as the fluxes through each of the 26 surface patches.

The work of Khatiwala et al. (2009) relaxes several of the assumptions that have impacted the accuracy of earlier methods. Firstly, the method requires no knowledge of remineralization ratios. Wanninkhof et al. (1999) illustrate that uncertainty about (and spatial variability of) these ratios leads to a substantial uncertainty in estimates of  $C_{\text{ant}}$  when using back calculation techniques (such as  $\Delta\text{C}^*$ ). Secondly, the method of Khatiwala et al. (2009) allows the air-sea  $p\text{CO}_2$  disequilibrium to evolve over time, and to be different for each of the 26 discerned surface patches. As argued above, the assumption of a constant  $p\text{CO}_2$  disequilibrium is considered an important cause of the over-estimation of the global  $^{\text{INV}}C_{\text{ant}}$  by Waugh et al. (2006). Lastly, the method explicitly accounts for water mass mixing and diffusive-advective transport through the use of Green functions. The lack thereof comprised another disadvantage of the  $\Delta\text{C}^*$  methodology (though not intractable, see Matsumoto and Gruber, 2005).

**Table 7.8.** Comparison of the rates of increase of the column inventory of  $C_{\text{ant}}$  along  $30^\circ\text{S}$ , as determined over 1993-2003 by Murata et al. (2008; M08) and as determined in the present study (TSR; as taken from the data underlying figure 7.13). The third column results are in good agreement for the western side of the section, the TSR method shows significantly higher values in the eastern half of the section. A conceivable cause for this is the greater ventilation age of the eastern mode waters, as suggested by M08, which conceivably is not fully resolved in our study due to insufficient representation of the distinct formation locales of the eastern and western mode (and central) waters.

Longitudinal range	$\Delta^{\text{C}}C_{\text{ant}}$ (M08) 2003-1993 mol $\text{m}^{-2}$	$d^{\text{C}}C_{\text{ant}}/dt$ (M08) mol $\text{m}^{-2} \text{a}^{-1}$	$d^{\text{C}}C_{\text{ant}}/dt$ (TSR) mol $\text{m}^{-2} \text{a}^{-1}$
50°W – 35°W	8.8	0.88	0.87
35°W – 15°W	7.1	0.71	0.94
15°W – 2°E	4.9	0.49	0.9
2°E – 15°E	4.3	0.43	0.88

Nonetheless, some minor criticism may be leveled at the method of Khatiwala et al. (2009) in that the prescribed Green function for the shape of the TTD may not accurately represent the ventilation of (specifically) the Southern Ocean. Evidence for this may be seen in the (minor) loss of ability of the method to infer  $C_{\text{ant}}$  in model data for this region (supplementary material of Khatiwala et al., 2009). However, this error accounts to less than about 5% of the local inventories, and is hardly consequential for the global results. The work of Khatiwala et al. (2009), although not based on ocean interior  $C_T$  data, therefore likely is the best current estimate of the time rates, concentrations and inventories of  $C_{\text{ant}}$  currently available.

In Figure 7.18, our results based on the TSR and TSR+TSS methods (dark X's in the left and right panel, respectively) are seen to match within uncertainties with the time histories provided by Khatiwala et al. (2009). Specifically, the evolution of  $d^{\text{INV}}C_{\text{ant}}/dt$  (i.e., left panel) obtained with the regression against the atmospheric perturbation is only about 10% higher than that of Khatiwala et al. (2009). The time history of  $^{\text{INV}}C_{\text{ant}}$  (right panel), derived using the AP approach, matches almost perfectly.

**Murata et al. (2008)** report on inferred increases in concentration and column inventory of  $C_{\text{ant}}$  (by correcting for variable biological respiration) between 1993 and 2003 along a transect between South America and Africa along 30 °S. They report rates of increase of the column inventory (i.e.,  $d^{\text{C}}C_{\text{ant}}/dt$ , in  $\text{mol m}^{-2} \text{a}^{-1}$ ) at four locations (see Table 7.8), with a mean rate of  $0.6 \pm 0.1 \text{ mol m}^{-2} \text{a}^{-1}$ . Murata et al. (2008) find Subantarctic Mode Water (SAMW, synonymous to the SACW used in the present study), to show higher rates of storage of  $C_{\text{ant}}$  in the western than in the eastern basin. The higher rates observed by Murata et al. (2008) in the western basin are suggested to result from the more recent ventilation of these waters than those in the eastern basin. No such difference is observed by Murata et al. (2008) for the deeper located AAIW, which is considered to be derived from a single ventilation region in the southeastern South Pacific (Talley, 1996). The results of our study (last column in Table 7.8, from data underlying Figure 13), are comparable in the western South Atlantic ocean, but are significantly higher than those of Murata et al. (2008) in the eastern basin. If indeed the observation of Murata et al. (2008) is accurate, this is an indication that our accuracy could be improved by considering separately the Central Waters of the eastern and western basins.

## 7.10. Conclusions

We present and apply an advanced version of the Time Series Residuals method (Van Heuven et al., 2011) for the determination of the time rate of increase of  $C_{\text{ant}}$  in the South Atlantic Ocean. We obtain rates of storage of  $C_{\text{ant}}$  ( $dC_{\text{ant}}/dt$ ) of about  $1 \mu\text{mol kg}^{-1} \text{a}^{-1}$  in the most recently ventilated surface waters, and rates that are indistinguishable from zero in the less ventilated North Atlantic Deep Water. The time rate of change of the total inventory of  $C_{\text{ant}}$  of the South Atlantic Ocean is found to be  $389 \pm 80 \text{ TgC a}^{-1}$ . Although the large majority of this storage is accounted for by the Central and Intermediate water masses, the rates of storage in the Weddell Sea Bottom Water and the Antarctic Bottom Water are also significant, amounting to  $81 \pm 40$  and  $19 \pm 18 \text{ TgC a}^{-1}$ , respectively.

In addition to determining the trend in  $C_{\text{res}}^{\text{TSR}}$ , we also determine trends directly in the measured values of  $C_T$ , thereby relaxing several of the assumptions of the TSR method.

The resulting rates are broadly comparable albeit with substantially increased uncertainties ( $d^{\text{INV}}C_T/dt$ :  $401 \pm 130 \text{ TgC a}^{-1}$ ), enhancing confidence in the TSR method.

The Transient Steady State method (TSS; Tanhua et al., 2007) allows for calculation of  $C_{\text{ant}}^{\text{TSR}}$  from  $dC_{\text{ant}}^{\text{TSR}}/dt$ , under the generally reasonable assumption that TSS has been reached in the South Atlantic Ocean. The hereby obtained  $C_{\text{ant}}^{\text{TSR}}$  allows for comparison with results from earlier investigations.

Modifying the method (following Rios et al., 2012) to express the rate of increase of  $C_{\text{ant}}$  not as a function of time, but of the atmospheric perturbation of anthropogenic  $\text{CO}_2$ , conceptually improves the detectability of trends and has the additional benefit of allowing the scaling of the results to future concentration of atmospheric  $p\text{CO}_2$ . Moreover, the absolute concentrations of  $C_{\text{ant}}$  may be inferred. Applying this modification, we find a rate of increase of  $0.22 \pm 0.06 \text{ PgC } \mu\text{atm}^{-1}$ . Multiplying this with the AP of  $82 \mu\text{atm}$  in the year 1994, we obtain an inventory of  $C_{\text{ant}}$  in the South Atlantic Ocean of  $17.7 \text{ PgC}$ , accumulated between the onset of the Industrial Revolution (1750) and 1994.

The integrated results ( $0.39 \pm 0.08 \text{ PgC a}^{-1}$  and  $0.22 \pm 0.06 \text{ PgC } \mu\text{atm}^{-1}$ ) as well as many of the smaller scale details (such as the increase in surface water  $C_{\text{ant}}$  or local increases in column inventories of  $C_{\text{ant}}$ ) are all broadly or even closely in line with results obtained by earlier investigators (Gruber et al., 2009; Takahashi et al., 2009; Khatiwala et al., 2009). Differences between our study and those of Waugh et al. (2006) and Sabine et al. (2004) are discussed to conceivably result from certain assumptions made by the latter two methods that are considered to impair their applicability to Southern Ocean waters.

To the best of my knowledge, this is the first result where an estimate of  $dC_{\text{ant}}/dt$  is derived without requiring assumptions about the degree of  $p\text{CO}_2$ - or  $p\text{O}_2$ -disequilibrium in deep-water formation regions. With minor modifications to the method, we additionally obtain an estimate of  $^{\text{INV}}C_{\text{ant}}$ . The convincing agreement with, but conceptual independence from, the work of Khatiwala et al. (2009), further strengthens and constrains the evidence for significant storage of  $C_{\text{ant}}$  in the South Atlantic Ocean.

## 7.11. Recommendations for future research

The convincing results obtained in the South Atlantic Ocean certainly warrant the application of the TSR method to other ocean basins. However, due to the use of OMP analysis, water mass stability over time is required. This demand may limit the applicability of the TSR method in the North Atlantic Ocean, which is known to feature highly variable rates of formation of Labrador Sea Water, the dominant water mass in the intermediate depths of that basin. A variant of the TSR method that does not employ OMP analysis may be applied there, with the slight disadvantage of a conceivably larger uncertainty of the results – this may not be crucial because of the larger  $C_{\text{ant}}$  signal in the North Atlantic.

The spatial resolution and accuracy of the method may be improved by separately determining  $dC_{\text{ant}}/dt$  in the western and eastern sides of the basin. For instance, a preliminary application of that approach suggests that the  $dC_{\text{ant}}/dt$  in the SACW is higher in the western basin than in the eastern basin, in accordance with the results of Murata et al. (2008). Such refinements will contribute to a better spatial resolution of the pattern of storage of  $C_{\text{ant}}$  in the South Atlantic Ocean. However, in order to retain a sufficiently high number of datapoints

## Chapter 7

for the assessment of the AOU-versus- $dC_{\text{ant}}/dt$  dependency under such higher-resolution OMP analyses, more cruise data will be required. Luckily, deep section chemical data is being collected routinely even in the far South Atlantic Ocean, so the proposed improvement may likely be implemented in the future.

Further improvements may be sought in the use of a more sophisticated age tracer (instead of AOU), more advanced water mass identification schemes, and more advanced curve fitting procedures (instead of the multi-linear approach used in section 7.7). Although we are convinced that the large-scale result of the currently employed analysis setup is robust, we anticipate refinements in spatial resolution to be possible. Additionally, at reduced levels of uncertainty comes the possibility of the determination of trends on timescales shorter than those of the full 35 years spanned by the currently used dataset. Such sub-era analyses might corroborate or falsify the proposed slowdown in recent years of the rate of oceanic storage of anthropogenic  $\text{CO}_2$  compared to the increase in the atmosphere (e.g., Le Quéré et al., 2007).







# Chapter 8

## **Synthesis and recommendations for future research**



This thesis reports on aspects of the work performed with the aim of assessing the rate of storage of anthropogenic CO<sub>2</sub> in the oceans. These aspects are (i) the collection of new data, (ii) the construction of a highest-quality basin-scale data product from new and historical data and (iii) the combined use of these data to investigate the accumulation of CO<sub>2,ant</sub> in the Weddell Gyre and the South Atlantic Ocean. This section summarizes and discusses the reported work, and makes recommendations for future studies.

### 8.1. Analytical work

The shipboard implementation of the commonly used, highly precise and accurate analytical techniques for measuring C<sub>T</sub> and A<sub>T</sub> was detailed in Chapter 3. About 8000 oceanographic samples have been collected and analyzed during several research cruises, totaling about 9 months of at sea (Table 3.1). In almost all cases, these efforts were matched by additional analyses of dissolved oxygen and nutrients. Often, samples for CFC-11 and CFC-12 were additionally collected and analyzed, in all cases by the colleagues of the Institute for Umweltp Physik (IUP) at the University of Bremen, Germany. Many of these datasets have already been released to publically accessible data repositories.

Short-term precision of the analyses of both C<sub>T</sub> and A<sub>T</sub> is approximately  $\pm 2 \mu\text{mol kg}^{-1}$ . This value is considered the best that may be attained during ship-based work. Analytical accuracy of the analysis of C<sub>T</sub> is considered to be approximately equally good, at  $\pm 2 \mu\text{mol kg}^{-1}$ . Accuracy of analyses of A<sub>T</sub> was approximately half as good at around  $\pm 4 \mu\text{mol kg}^{-1}$ . This, too, matches what is commonly reported to be the analytical limit for ship-based work. However, it is noted that the accuracy during this thesis work was set by correction against certified reference material (CRM). Especially for analysis of A<sub>T</sub> (which may be affected by non-linear errors), this method of calibration is inferior to the use of CRM to *verify* independently attained accuracy.

#### *Analytical work: recommendations*

Although results are of satisfactory quality, significant modifications to instrumentation and procedures are recommended in Chapter 3. These fairly specific modifications should may be implemented in short order. Some more general (and more involved), recommendations will be made in the remainder of this section.

As argues in Chapter 3, the concurrent analysis of a sample on *two* machines allows for a better quantification of analytical precision and accuracy than may be obtained using a single instrument. The continuation of concurrent use of instruments is highly recommended. However, an alternative and conceivably superior (because independent) constraint to measurement accuracy may be available in the analysis of a third CO<sub>2</sub>-system parameter: pH. This spectrophotometric analysis is straightforward and precise, inherently accurate, and the required equipment is already present at NIOZ in the form of a couple of SAMI in-situ pH sensors. After a minor, required modification (the installation of a heat exchanger in the sample inlet line to bring the sample to analysis temperature), this additional analysis will be of significant value as a constraint on the accuracy with which the state of the carbonate

system is analyzed. Analysis may be performed on the same bottles from which the VIND-TAs tap their samples, or dedicated subsamples may be collected in the appropriate vessels (SOP6b of Dickson et al., 2007).

Calculation of  $A_T$  from titration data, is currently performed by the many research groups using a wide variety of software routines. An informal investigation into the various routines currently in use has been conducted by myself and others. All routines are based on the same thermodynamic considerations and, generally, employ the comparable mathematical methods. Nonetheless, subtle differences exist, mostly pertaining to the choice of dissociation constants for the non-abundant ions. Moreover, the programs in use are often badly documented, hindering user comprehension. Although guidelines for the development of the mathematical innards of these routines are provided in SOP3 of Dickson et al. (2007), implementation may differ between groups. For these reasons, the development of a well-documented, flexible, multi-platform routine for the calculation of  $A_T$  from titration results would be of significant benefit to the community. Ideally, such software should be maintained and hosted by the authoritative Carbon Dioxide Information and Analysis Centre (CDIAC, <http://cdiac.ornl.gov>), which currently already hosts several related software programs. Pursuance of this development should be of definitive benefit to the quality of the global  $A_T$  analysis effort.

### 8.2. Database synthesis

**Chapter 4 and 5** detailed the methodology that was developed and used to synthesize a large, internally consistent dataset of CO<sub>2</sub> relevant parameters spanning 30 years. The source data for this CARINA (Carbon In the North Atlantic Ocean; Key et al., 2010) effort consisted of 188 cruise datasets, obtained mostly by European researchers between 1980 and 2005. High-quality data from the recent international CLIVAR project (Climate Variability and Predictability, <http://www.clivar.org/>) were included to serve as a framework of ‘master’ cruises against which the 188 others could be compared. The CARINA data product is comprised of three, partially overlapping, datasets for the Arctic Oceans, Atlantic Ocean and Southern Ocean. These data are available in a common, well-documented format, thereby facilitating their use by scientists from fields ranging from experimental biological oceanography to Earth system model development. Data quality was optimized in a two step approach, pertaining to precision and accuracy, respectively.

Data collection and primary quality control (QC1) of the 188 datasets was performed by Dr. Robert Key of Princeton University, NJ., USA. First, the submitted data was brought into a standard format. Necessary changes generally regarded the numbering of station and cast identifiers, the matching of various reported parameters to a single depth, unit conversions and calibration scale conversions (for CFCs and pH). Subsequent QC1 (Chapter 5, Tanhua et al., 2010) consisted of the flagging of obviously outlying individual datapoints (occasionally flagging complete datasets due to exceedingly large uncertainties or variable bias). All 188 cruise datasets so processed have been made available in a common format through the CLIVAR and Carbon Hydrographic Data Office (<http://cchdo.ucsd.edu/>).

Subsequently, secondary quality control was performed (Chapter 5; Tanhua et al., 2010b). The goal hereof was to determine the adjustments that needed to be applied to the individual cruise datasets in order to minimize the offsets between the cruises. The meth-

odology that is used for this is the inversion approach outlined by Johnson et al. (2001). The first step is to determine, for each property of interest (salinity,  $C_T$ ,  $A_T$ ,  $O_2$ ,  $NO_3$ ,  $PO_4$  and Si), the offsets between cruises (i.e., the *relative biases between cruises*, not the absolute biases of cruises). This was accomplished by comparing the deep-ocean property values wherever two cruises have sampled the same location (generally within 200 kilometers), irrespective of the year or season of sampling (the assumption here is that deep-ocean property values are invariant over timescale of several few years, and that therefore no offset is expected at these depths). This strategy yielded, for most properties, more than 2000 offsets between different combinations of the 188 cruises in the dataset. For example, cruise *a* would be determined to have  $C_T$  values that are  $7 \pm 2 \mu\text{mol kg}^{-1}$  higher than that of cruise *b*, but  $2 \pm 5 \mu\text{mol kg}^{-1}$  lower than that of cruise *c*. This information, in and of itself gives little clues as to the absolute bias of each cruise. Therefore, in a second step, an inversion algorithm (Menke 1984; Wunsch 1996) is used to determine for each property those adjustments to cruises that, if applied, would minimize the mean of all the offsets within the database.

The inversion approach allows several subtle constraints to be applied. Firstly, the arbitrary ‘pinning’ of known-to-be-accurate cruises, meaning that their values may not be considered for adjustment. In effect, that defines these cruises as ‘master’ cruises to which the rest of the database will be adjusted, providing for a known calibration of the resulting database. Secondly, offsets may be weighted. We opted to reduce the weight of offsets as a function of the time between sampling of the cruises. Additionally, weight was decreased with the uncertainty with which an offset was determined. Various offset determination methods and inversion schemes were tried and compared, mostly resulting in comparable results. The adjustments that the inversion routines suggested were thoroughly vetted by the CARINA team members, before being applied. The internal consistency of the resulting database is shown to be significantly higher than that of the QC1-dataset (Chapter 5, Table 3). Of specific relevance to this thesis are the improvements to  $C_T$  and  $A_T$ . These improvements were, respectively, from  $\pm 5.0$  to  $3.2 \mu\text{mol kg}^{-1}$  and from  $6.7$  to  $3.9 \mu\text{mol kg}^{-1}$ .

Processing after QC2 consisted of simplification of quality flags, interpolation of missing carbon-relevant data ( $O_2$ , nutrients) wherever possible, calculation of derived quantities (densities, et cetera) and full calculation of the state of the carbonate system (Chapter 2) wherever possible.

#### *Database synthesis: recommendations*

The CARINA data product is comprised of three, partially overlapping, datasets for the Arctic Oceans, Atlantic Ocean and Southern Ocean. The earlier GLODAP project (Key et al., 2004) also consisted of three sub-datasets (Atlantic, Pacific, Indian). The related *PACIFICA* program (led by Dr. Masao Ishii, MRI-JMA, Tsukuba, Japan) aims to provide by late 2012 a similarly optimized data product for the Pacific Ocean. Performing a true global analysis of storage rates of  $CO_{2,ant}$  is significantly complicated by the necessity of merging these various products and the subsequent removal of those cruises that are present in duplicate. Such global analyses will greatly benefit from the proposed *Global Ocean Carbon Synthesis* project (GOCS, led by Dr. Nicolas Gruber, ETH Zürich, Switzerland). This effort aims to combine all the above sources of data, as well as data acquired in the most recent years, into a single large data product. This carbon data obtained during the thesis work postdated the cut-off for CARINA data (pre-

mid-2005), so as of yet is not included in any large-scale data compilation. The contribution of these data to the GOCS effort is highly recommended.

An important methodological advance in such a newly undertaken dataset synthesis effort could be the implementation of MLR-based methods to assess measurement biases (such as used for  $C_T$  in this thesis, Chapter 7, section 6), replacing or supplementing the ‘crossover’ methodology used in CARINA. The proposed methodology has been successfully used in Olsen et al. (2006) and Olsen (2009), and its wider use during GOCS may benefit the final inversions by allowing estimates of offsets between cruises to be made of fairly wide spatial extent. In such a scheme, one would not infer offsets between two cruises, but rather assess the differences between measurements of a cruise and the values predicted for that cruise based on a statistical relationship obtained from other cruises within the same region. Although such residuals are indicative not necessarily of biases in the assessed parameters (but of the independent parameters), iterative use could yield the minimal adjustments to be performed to maximize dataset consistency.

### 8.3. Assessing the rate of storage of anthropogenic $\text{CO}_2$

**Chapter 6** describes the careful preparation of a dataset comprising 10 cruises performed between 1973 and 2008 along the Prime Meridian in the Weddell Gyre in the Southern Ocean. Data of these cruises originates from the CARINA and GLODAP synthesis efforts. Added to these are several original datasets that in part have been collected during this thesis work (*PFS Polarstern* expedition ANT-XXIV/3, Feb-Apr 2008). The 10 quasi-coincident (overlapping) datasets are projected onto a common meridional section, and the linear time trends in  $C_T$  are quantified at each grid point of the section. The approach yields an unambiguous, albeit low, time rate of change of  $C_T$  in the deep Weddell Gyre of  $+1.2 \pm 0.6 \mu\text{mol kg}^{-1} \text{decade}^{-1}$  over this 35 years time interval. This trend is not observed at the intermediate depths of the water column, as expected due to the ‘bottom-up’ convectively driven ventilation of the Weddell Gyre. The spatial distribution of the accumulation is shown to bear a strong resemblance to that of the accumulation of CFC-12, an inert anthropogenic gas that is taken up from the atmosphere and measured in the ocean with very high signal-to-noise ratio. This resemblance is an indication that the inferred time trends in  $C_T$  result from uptake of  $\text{CO}_{2,\text{ant}}$  from the atmosphere, and therefore less likely to be the result of biogeochemical or hydrographic variability.

A statistical technique is presented with the aim of unambiguously attributing the time trend in  $C_T$  to results from accumulation of  $C_{\text{ant}}$ . The application of this Time Series Residuals technique (TSR) however does not yield the a convincing attribution. Nonetheless, because the increase is shown not to be easily attributable to either biogeochemical or hydrographical variability, by default the attribution to accumulation of  $C_{\text{ant}}$  is maintained. From an extrapolation to the wider Weddell Gyre, we infer that  $12 \text{ PgC a}^{-1}$  (circa 0.1% of current anthropogenic emissions) of anthropogenic  $\text{CO}_2$  are sequestered in the deep Weddell Gyre (i.e., excluding the storage in the upper 500 meters). The error estimates of this result are somewhat subjectively estimated to be about 50%. This uncertainty stems in part from incomplete spatial representation of the Weddell Gyre by the studied section, and partly from the substantial uncertainty of the determined trends themselves. Notwithstanding that uncertainty, the inferred trends



are considered to provide a unambiguous constraint on the rate of storage of  $C_{\text{ant}}$  in the deep Weddell Gyre.

The gradual increase of  $C_T$  (supposedly due to accumulation of  $\text{CO}_{2,\text{ant}}$ ) at 0 °E in the deep Weddell Gyre constitutes the major finding of Chapter 6. It corroborates the expectation that the deep Weddell Gyre constitutes at most a modest sink for  $\text{CO}_{2,\text{ant}}$ , taken up at the sea surface (Poisson and Chen, 1987, Hoppema et al., 2001). The relatively low rate that was observed appears at first sight incompatible with the findings of Lo Monaco et al. (2005), based on measurements obtained at the eastern edge of the Weddell Gyre at 30 °E. These authors find significant concentrations of  $C_{\text{ant}}$ , which would not be attainable without a high rate of storage. Causes of this incongruence are speculative, but fall in two categories. Firstly, the employed methods (for inferring  $dC_{\text{ant}}/dt$  or  $C_{\text{ant}}$ ) may be inaccurate. Secondly, and more interestingly, conceivable real-world differences in the efficacy  $\text{CO}_2$  uptake by the surface waters that contribute to the bottom waters at these two locations may exist. The large majority of the bottom waters at the location of the study of Chapter 6 are derived from along the continental edge of the Weddell Gyre, whilst the water of the study of Lo Monaco may to a much larger extent be derived from the continental edge to the east of the 30 °E section (Schodlok et al., 2001). Conceivably, differences in ice cover, convection or other processes may be involved in an enhanced rate of transport of  $C_{\text{ant}}$  around the 30 °E section. Research expeditions, aimed at quantification of the  $C_{\text{ant}}$  content of downwelling waters may be required to resolve this incongruence, as well as other unresolved, highly pertinent questions relating to the ventilation of the deep Southern Ocean.

Although Chapter 6 demonstrated the viability of determining trends in measured  $C_T$  in the deep Weddell Gyre (note that no results are presented for the upper water column), the likelihood of being able to successfully replicate this work in the shallower water column, in the Weddell Sea or elsewhere, is low. The high variability at shallow depths (<1 km), caused by currents, would likely obscure the small signal of  $C_{\text{ant}}$  accumulation. Therefore, the direct differencing technique appears restricted to application in the deep ocean.

In **Chapter 7**, the Time Series Residuals method (TSR; introduced in Chapter 6) is modified for application at basin scale, along the full depth of the water column. It is applied to a database of the South Atlantic Ocean (here defined as all waters between the Equator and the Antarctic continent, between 30 °E and Drake Passage at 65 °W). The database contains 53 cruises, spanning the years 1973 to 2009. Seven distinct water masses are discerned by means of extended Optimum Multiparameter Analysis (eOMPA; Karstensen and Tomczak, 1998). The modified TSR methods aims to quantify the rate of increase of  $C_{\text{ant}}$  in each of these water masses.

Within each water mass,  $dC_{\text{ant}}/dt$  is assumed to be highest at the ventilation region (i.e., the surface outcrop) and to become gradually smaller further within the interior (because the interior waters were ventilated at times of lower atmospheric  $\text{CO}_2$ ). In order to quantify this characteristic of  $C_{\text{ant}}$  accumulation, the time rate of change of  $C_{\text{ant}}$  is expressed as a function of apparent oxygen utilization (AOU), which here is thus considered a tracer of ventilation age (the time since a water sample was last at the surface).

As expected, the rates  $dC_{\text{ant}}/dt$  are clearly observed to decrease with increasing AOU. In the surface outcrops of water masses, the analysis reveals values of  $dC_{\text{ant}}/dt$  to increase (at

circa  $1 \mu\text{mol kg}^{-1} \text{a}^{-1}$ ), in approximate equilibrium with the increasing atmospheric  $p\text{CO}_2$ . Rates close to zero were observed for the North Atlantic Deep Water (NADW). Both these observations are consistent with expectations. We note that values of  $dC_{\text{ant}}/dt$  for the deep water masses of southern origin (Antarctic Bottom Water, Weddell Sea Bottom Water) are slightly above zero – suggesting the accumulation of significant amounts of  $C_{\text{ant}}$  in these voluminous water masses. The finding of accumulation of  $C_{\text{ant}}$  in the WSBW is compatible with the observations in Chapter 6. However, in that Chapter, we did not find a significant time trend of  $C_T$  in the Weddell Sea Deep Water, which is a principal contributor to the AABW.

The quantification on the basis of AOU of  $dC_{\text{ant}}/dt$  for each water mass, allows these rates to be straightforwardly projected onto the World Ocean Atlas 2005 (WOA05; Garcia et al., 2005). The WOA05 climatology does not itself contain any  $\text{CO}_2$ -data, but does contain a high-resolution, three-dimensional AOU data product. The resulting grid of data of  $dC_{\text{ant}}/dt$  is integrated in two ways to yield the time rate of change of **a**) the column inventory of  $C_{\text{ant}}$  ( $d^{\text{CI}}C_{\text{ant}}/dt$ , in  $\text{mol C m}^{-2} \text{a}^{-1}$ ) and **b**) the rate of change of the total inventory (in  $\text{mol C a}^{-1}$ ) of the South Atlantic Ocean.

We calculate the overall rate of storage of  $C_{\text{ant}}$  in the South Atlantic Ocean (poleward of the Equator extending to the Antarctic continent) to be  $0.39 \pm 0.08 \text{ PgC a}^{-1}$ . The zonal mean of the time rate of change of the column inventory of  $C_{\text{ant}}$  ( $d^{\text{CI}}C_{\text{ant}}/dt$ ) is shown to exhibit a maximum of circa  $1 \text{ mol C m}^{-2} \text{a}^{-1}$  in the latitudinal range between  $35^\circ\text{S}$  and  $50^\circ\text{S}$ , i.e., to the north of the Polar Front. This feature results from subduction of  $C_{\text{ant}}$ -rich intermediate waters at the polar front, and their subsequent equatorward advection. The large amounts of  $C_{\text{ant}}$  taken up at higher latitudes are hereby to a large extent stored in the intermediate latitudes. Rates of storage of  $0.5 \text{ mol C m}^{-2} \text{a}^{-1}$  are encountered both to the north and south of this main ‘storage belt’. The western basin of the South Atlantic Ocean features a slightly larger storage of  $C_{\text{ant}}$  than the Eastern Basin, as may be expected from the distinct formation processes of the intermediate waters in the western and eastern basin (Talley, 1996; Poole and Tomczak, 1999; Murata et al., 2008).

In most respects, our results compare favorably with other recent estimates of accumulation of  $C_{\text{ant}}$  in the South Atlantic Ocean. Wanninkhof et al. (2010) studied such accumulation along a meridional section ) used the eMLR-technique. Murata et al., 2008 employed a back-calculation techniques along a zonal section along  $30^\circ\text{S}$ . In general, the results from the three studies are highly congruent. As a distinct improvement over previous results, our study offers - to the best of my knowledge - unprecedented spatial scale and extent. The conceptually fully independent study of Khatiwala et al. (2009), which does not rely on ocean interior  $C_T$ , additionally closely resembles the results obtained in the present study. Taken together, this body of evidence confirms the notion that the South Atlantic Ocean (poleward of the Equator, west of  $30^\circ\text{E}$  and east of Drake Passage at  $65^\circ\text{W}$ ) constitutes a strong sink for anthropogenic  $\text{CO}_2$  at a rate of approximately  $0.4 \pm 0.1 \text{ PgC a}^{-1}$  in 1994.

The presented TSR method is a valuable tool in discerning the steady accumulation of  $C_{\text{ant}}$ . The method allows the accumulation of  $\text{CO}_{2,\text{ant}}$  to be sharply distinguished within the natural biogeochemical and hydrographical variability of the ocean. This is exemplified by the comparison shown in table 7.6, where the consideration of these extra processes (rather than observing only trends in  $C_T$ ) reduces by about 40% the uncertainty of the inferred rate of increase of  $C_{\text{ant}}$  in the South Atlantic Ocean ( $389 \pm 80$  vs  $401 \pm 130 \text{ PgC a}^{-1}$ ).

A major finding Chapter 7 is that the presented TSR method is capable to assess trends in  $C_{\text{ant}}$  over large spatial scales, using very large datasets. Estimates obtained from such larger amounts of cruises (as opposed to only from two cruises) renders the result less susceptible to biases of data from individual cruises, and may improve spatial coverage.

The broader application of the TSR method (or comparable) will benefit the validation of estimates of accumulation of  $C_{\text{ant}}$  from high-resolution tracer-based techniques (e.g., Waugh et al., 2006; Khatiwala et al., 2009), and from computer models (e.g., Gruber et al., 2009, and references therein). Moreover, the TSR-technique may prove to be a valuable tool in diagnosing temporal changes in carbon uptake by the surface ocean. For instance, the reduction in the strength of the North Atlantic sink for  $C_{\text{ant}}$  observed in sea surface data (e.g., Schuster and Watson, 2007; Metzl et al., 2010; McKinley et al., 2011) will need corroboration from the ocean interior, to where this reduction should be propagated. We note that the current application of the TSR technique in the South Atlantic Ocean has not been able to accurately resolve trends on timescales shorter than about 20 years (and only trends over 35 years have been presented). However, in the much more densely sampled North Atlantic Ocean (Key et al., 2010), the required amount of temporal detail is likely to be attainable.

#### *Assessing the rate of storage of anthropogenic CO<sub>2</sub>: recommendations*

The ability of the section-comparison method presented in **Chapter 6** to detect trends in  $C_T$  (and by inference in  $C_{\text{ant}}$ ) of bottom waters is evident. In addition to the presented application in the Weddell Sea Bottom Water, the method may be used to infer trends in  $C_{\text{ant}}$  in the well-ventilated Denmark Strait Overflow Water (DSOW) between Iceland and Scotland. This water mass has been sampled many times, starting in 1972 with GEOSECS (although the accuracy of the  $C_T$  data obtained at these northern GEOSECS stations is commonly questioned; e.g., Peng and Wanninkhof, 2010). At least 15 subsequent occupations with measurements of  $C_T$  and ancillary properties are available along part of that section. About a dozen of these are may be found in Perez et al., 2010. Additionally, there are the data from cruises of RV Pelagia: 64PE175 in 2001 (although the data of  $C_T$  are of questionable quality due to the use of an experimental analytical technique; Stoll et al., 2001), 64PE240 (2005, this Thesis, Chapter 3), 64PE275 (2007, this Thesis, Chapter 3) and 64PE342 (2011, sampled by NIOZ (Mr. K. Bakker) on my behalf, will be analyzed in late 2012).

Among the few other regions of conceivable application is the repeat coverage available along the bottom waters south of Tasmania (data of  $C_T$  available from about 8 occupations since 1968; McNeill et al., 2001).

A definite improvement to the modified TSR approach as used in **Chapter 7** would be to use the alternative approach to expressing the rates of increase of  $C_{\text{ant}}$  that is already briefly explored. Following Rios et al. (2012),  $C_{\text{ant}}$  is regressed against not against time, but against the atmospheric perturbation of anthropogenic CO<sub>2</sub> (the AP) above the 'natural' level of 280  $\mu\text{atm}$ . The resulting quantity,  $dC_{\text{ant}}/d\text{AP}$  has units of  $\mu\text{mol kg}^{-1} \mu\text{atm}^{-1}$ . Benefits of this method are **a**) the implicit linearization of the regression (which should allow for a better fit), **b**) the enhanced possibility of using the result to project rates of increase as a function of future AP, **c**) the possibility of inferring from  $dC_{\text{ant}}/d\text{AP}$ , the total inventory of  $C_{\text{ant}}$  in any given year (simply by multiplying with the then-current AP).

On a more fundamental note, the rigorous use of reference materials or techniques during the analyses of nutrients (Aoyama et al., 2008) and oxygen (Reinthal et al., 2006) is highly recommended (Chapters 4 and 6, this thesis). The determination of the increase of the anthropogenic components of  $C_T$  will likely benefit greatly from the increased accuracy that will result from this practice.

### 8.4. Perspectives

In the present work we derive – from a uniquely large dataset – an estimate of the rate of storage of anthropogenic  $CO_2$  in the South Atlantic Ocean. Similar numbers from other parts of the global ocean are becoming available in the recent literature (e.g., Peng et al., 2003; Perez 2010; Vazquez-Rodriguez, 2012; Wanninkhof et al., 2010; Peng and Wanninkhof, 2010; Murata, 2007, 2008). Although obtained using a variety of methods, this body of work, taken together, begins to paint a coherent, global picture of the evolving accumulation of  $CO_2$  in the oceans. The relevance of this information for our understanding of the effect of humanity's perturbation of the carbon cycle can hardly be overstated (Sarmiento et al., 2010).

Although ship-based profiling work is likely to remain for the foreseeable future the backbone of ocean interior carbon cycle science, rapid advances are being made in the field of autonomous, in-situ data collection systems. Instrumentation for the in-situ analysis of pH,  $C_T$ ,  $pCO_2$  and  $A_T$  is being developed and in some cases already experimentally deployed (e.g., Byrne et al., 2002; Wang et al., 2007; Seidel et al., 2008). Additionally, measurement of dissolved oxygen and nitrate is also being successfully implemented (Körtzinger et al., 2004). Platforms for such instrumentation range from static moorings, via moored or free-floating profilers to autonomous gliders. The increased spatial and/or temporal resolution yielded by these observation system will prove invaluable to this field (Johnson et al., 2009; Gruber et al., 2010) and these developments should be supported to the greatest possible extent.

The accuracy of the new instrumentation will for the foreseeable future be inferior to the laboratory-based state of the art. This necessitates regular calibration against ship-based 'ground truth'. Such calibration may conceivably be performed semi-automatically using adaptations of the crossover analysis (Chapter 5) or multivariate linear regression (Chapter 7). Investigating this potential may prove of significant benefit to the rapid dissemination of the obtained results to the wider community, thereby maximizing the scientific potential of the novel measurement techniques.

Due to these new data collection efforts, the volume of available ocean interior carbon-relevant data will likely grow at an increasing rate. This will allow more temporally detailed assessment of rates of increase. It may be envisioned that routine analysis of the growing global database, by techniques like TSR, will regularly provide (for example on a two-yearly basis) an updated estimate of the increase in the oceanic  $C_{ant}$  inventory over the most recent years. Such an estimate will provide another important constraint on global carbon cycle studies, for which atmospheric and sea-surface synthesis products are already being routinely released (e.g., atmospheric concentration of  $CO_2$  and related properties as updates to Keeling et al. (2001), and sea surface  $CO_2$ -fluxes: Takahashi et al. (2009)).





# Chapter 9

## Summary





### *The natural carbon cycle*

The element carbon (C) is naturally exchanged at very high rates between and within the oceans, the land (biomass, soil) and the atmosphere. The flows (or *fluxes*) between these *bio-spheric reservoirs* are predominantly driven by temperature variations of the sea surface, by the growth and decay of trees and plants on land, and by the occurrence of massive algal blooms in the oceans. Nonetheless, because of the seasonal reversal of these fluxes, the amounts of carbon in the atmosphere, land and ocean reservoirs have remained relatively stable over the several thousand years since the most recent ice age. The *natural carbon cycle* is thus considered to have been in *steady state*.

### *The modern perturbation*

Causing a strong departure from this steady state, human society has begun, around 1750, to add significant amounts of carbon to the atmosphere (in the form of carbon dioxide, CO<sub>2</sub>) by the burning of fossil fuels. These fossil fuels (mainly coal, oil and methane gas) are obtained from deep-earth reservoirs, which do not have significant natural contact with the three bio-spheric reservoirs. Thus, in the process of fossil fuel extraction and combustion, humanity is adding additional carbon to the carbon cycle. The additional, or *anthropogenic* CO<sub>2</sub> (CO<sub>2</sub><sup>ant</sup>, i.e., CO<sub>2</sub> from human activity) will be gradually divided over the atmosphere, land and ocean reservoirs by the natural exchange processes.

Up to the present day, human society has emitted to the atmosphere more than 1.3 trillion tonnes of CO<sub>2</sub> by the burning of fossil fuels and production of cement (Boden et al., 2010). The rate of emission of CO<sub>2</sub><sup>ant</sup> is still increasing and currently approaches 36 billion tonnes of CO<sub>2</sub> per year, or about a million kilos of CO<sub>2</sub> per second. Land use change (mainly deforestation) results in additional large emissions of CO<sub>2</sub> to the atmosphere (Houghton et al., 2008). Over the last ~250 years, the atmospheric concentration of CO<sub>2</sub> has increased already by ~40% from the natural level of ~280 ppm (parts per million) to ~393 ppm in 2012.

### *Observed and expected consequences*

In the atmosphere, CO<sub>2</sub> acts to block the spaceward radiation of heat. The anthropogenic increase of atmospheric CO<sub>2</sub> thereby increasingly ‘insulates’ the Earth. The observed upward trends of land and ocean temperature are considered to be consequences of this buildup of CO<sub>2</sub><sup>ant</sup> in the atmosphere (Solomon et al., 2007).

Many changes that are associated with this ‘global warming’ have been documented. Among these are an increase in sea surface height, and decreases in sea ice extent and glacier and ice sheet mass (Solomon et al., 2007). Further consequences that more directly relate to human wellbeing (for example droughts and flooding) are expected with high likelihood under most scenarios of future development (IPCC, 2012).

Lastly, the uptake of increasing amounts of CO<sub>2</sub> by the ocean causes ‘ocean acidification’ (Feely et al., 2004). The associated increase in the solubility of calcareous shells may lower the fitness of various organisms that are at the basis of the food chain (Doney et al., 2009). This process is hypothesized to negatively impact the health of oceanic ecosystems, and thereby the societies that depend on these ecosystems for income or food. However, because

organisms may adapt and evolve in response to these changing environmental conditions (e.g., Lohbeck et al., 2012), the future consequences of ‘ocean acidification’ are not currently well understood.

### *The current state of global carbon cycle research*

In order to fully comprehend the changing global carbon cycle, the processes that distribute the  $\text{CO}_2^{\text{ant}}$  between atmosphere, land and ocean need to be better understood. Over the period 2000 to 2010, about only 46% of all anthropogenic emissions of  $\text{CO}_2$  (thus including emissions from land use change) are found to remain in the atmosphere. The ‘missing’ 54% are being removed from the atmosphere by the ocean and/or the terrestrial biosphere. Based in part on model-based calculations, these land and ocean *sinks* are estimated to be of approximately equal size (Le Queré et al., 2009). However, the capacity of the ocean for continued high rates of uptake is expected to be limited by basic chemistry, and may be expected to begin to lag behind the rate of emissions (e.g., Sarmiento et al., 1995; Thomas et al., 2007). Recent sea surface measurement campaigns have shown a high variability in (and a tentative reduction of) the relative rate at which  $\text{CO}_2^{\text{ant}}$  enters the ocean (e.g., Takahashi et al., 2009; Watson et al., 2009; Metzl et al., 2010). However, such air-sea gas exchange studies generally represent only a relatively small area over a short time span, and therefore do not straightforwardly allow for an assessment of the global net uptake of  $\text{CO}_2^{\text{ant}}$  by the oceans.

An accurate, data-based assessment of the rate of the resulting increase of  $\text{CO}_2^{\text{ant}}$  in the ocean *interior* would therefore be of high value as an additional constraint on the strength of the oceanic sink for  $\text{CO}_2^{\text{ant}}$ . However, the rate of ocean storage of  $\text{CO}_2^{\text{ant}}$  is not determined easily either. Various processes involved in the ocean carbon cycle affect the large natural concentration of dissolved  $\text{CO}_2$ , thereby making the small anthropogenic addition difficult to observe.

Nonetheless an accurate, data-based assessment of the rate of storage of  $\text{CO}_2^{\text{ant}}$  in the ocean interior is coming within reach due to the growing availability of high quality, internally consistent datasets, collected over a timespan of already almost 40 years (from 1972 to the present day).

### *Goals of this thesis*

This thesis work aimed to provide a data-based estimate of the rate of storage of  $\text{CO}_2^{\text{ant}}$  within the ocean. The performed work consisted of (i) the collection at sea of new, high-quality data of ocean interior  $\text{CO}_2$  concentrations and related properties, (ii) the construction of a highest-quality data product from new and historical data from the Atlantic Ocean and (iii) the combined use of these data to investigate the rate of storage of  $\text{CO}_2^{\text{ant}}$  in the Weddell Gyre (located to the southeast of South America, bordering Antarctica) and in the larger South Atlantic Ocean. These regions are considered to be of large importance for the uptake of anthropogenic  $\text{CO}_2$  at the sea surface and for its transport into the interior of the ocean.

### *Summary of results*

During 7 research expeditions, some 8000 measurements have been made of ocean interior concentrations of dissolved  $\text{CO}_2$  (*dissolved inorganic carbon*) and related properties. These data are shown to be of highly satisfactory precision and accuracy. Together with existing datasets, they

may be used to infer the desired data-based estimate of the rate of storage of  $\text{CO}_2^{\text{ant}}$  in the oceans.

With a team of international scientists, a large database has been constructed of  $\text{CO}_2$ -relevant data from the ocean interior, collected during 188 research expeditions over the years 1973 to 2005. Many of these data were not previously publicly available. In order to maximize the accuracy of this database, a suite of semi-automatic computational routines was developed to facilitate the minimization of the offsets between the cruises, following a mathematical inversion method (Johnson et al., 2001). These routines provide recommendations for adjustments to the individual cruises data which would – when applied – minimize the offsets between the cruises in the deep ocean. These recommendations were carefully inspected by teams of highly experienced investigators, in order to make sure that only true analytical bias was compensated, without erasing real-world changes in the deep ocean. The minimization approach is shown to have significantly improved the internal consistency of the final data product compared to the original data of the individual source cruises. The final data product has been released to the international research community as the CARINA-database (Carbon in the North Atlantic).

A detailed, local study has been made of the rate of storage of  $\text{CO}_2^{\text{ant}}$  using data collected on ten research expeditions, performed between 1973 and 2008 along the  $0^\circ$ -meridian in the Weddell Gyre in the Southern Ocean. One of these ten datasets was collected during this thesis work (*PFS Polarstern* expedition ANT-XXIV/3, Feb-Apr 2008).

The assessment unambiguously reveals the gradual storage of  $\text{CO}_2^{\text{ant}}$  in the Weddell Sea Bottom Water (WSBW), at a rate of  $1.2 \pm 0.6$  micromoles of carbon per kilogram of seawater per decade ( $1.2 \pm 0.6 \mu\text{mol kg}^{-1} \text{decade}^{-1}$ ) over the period 1973-2008. Moreover, the spatial distribution of this accumulation along the section has been determined. This distribution strongly resembles that of the accumulation of CFC-12, an inert anthropogenic gas that is taken up from the atmosphere and is very well measurable in the ocean. This resemblance is an indication that the observed time trends in the amount of dissolved  $\text{CO}_2$  are indeed the result of enhanced uptake of  $\text{CO}_2$  from the atmosphere. The observed time trends provide a strong constraint for the amount of  $\text{CO}_2^{\text{ant}}$  in the deep Weddell Gyre, for which previous estimates differed significantly. An extrapolation to the wider Weddell Gyre suggests that the rate of storage of  $\text{CO}_2^{\text{ant}}$  in the water layers deeper than 500 meter is approximately  $0.012 \pm 0.006$  PgC per year (1 PgC =  $10^{15}$  grams, or 1 billion tonnes, of carbon). This is approximately 0.2% of the mean rate of emissions of  $\text{CO}_2^{\text{ant}}$  over the period 1973-2008.

Subsequently, using a larger dataset of 53 cruises, the rate of storage of  $\text{CO}_2^{\text{ant}}$  is investigated in the South Atlantic Ocean as a whole (defined here as all waters located between the Equator, the Antarctic continent,  $30^\circ\text{E}$  and Drake Passage at  $65^\circ\text{W}$ ). A careful assessment of seven distinct water masses in this ocean basin shows that  $\text{CO}_2^{\text{ant}}$  increases rapidly in the near-surface part of water masses, which likely have experienced recent air-sea gas exchange with the atmosphere. The 'older' water in the interior layers of the water mass exhibit a much lower time trend of  $\text{CO}_2^{\text{ant}}$  over the 40 years for which measurements are available.

Approximately two thirds of the total storage of  $\text{CO}_2^{\text{ant}}$  is observed in water masses at shallow and intermediate depth (0-1500 meters), while the more voluminous deep and bottom

water masses store about one third of the  $\text{CO}_2^{\text{ant}}$  taken up from the atmosphere. The overall mean rate of storage of  $\text{CO}_2^{\text{ant}}$  in the South Atlantic Ocean (as defined above) is determined to have been  $0.39 \pm 0.08$  PgC per year over the period 1973-2008. That equals  $\sim 6\%$  of the mean anthropogenic emission to the atmosphere over this period (6.3 PgC per year). The highest depth-integrated rate of the storage (approximately 1 mole, or 12 grams, of carbon per square meter per year) is observed in the latitudinal range between  $35^\circ\text{S}$  and  $50^\circ\text{S}$ . This is slightly to the north of where air-sea gas exchange studies observe the highest influx of  $\text{CO}_2$  into the ocean. This displacement is due to the northward movement of the water masses after they sink down from the surface around  $50^\circ\text{S}$  as part of the large-scale ocean circulation.

These results compare favorably with other recent estimates of storage of  $\text{CO}_2^{\text{ant}}$ , made in smaller regions of the South Atlantic Ocean (Murata et al., 2008; Wanninkhof et al., 2010), but offer improved spatial detail and extent. The conceptually fully independent study of Khatiwala et al. (2009), which is global in extent but does not use ocean interior measurements of  $\text{CO}_2$ , additionally closely resembles the results obtained in the present study.

The result corroborates our understanding that the South Atlantic Ocean is responsible for the storage of circa 20% of all anthropogenic  $\text{CO}_2$  that is being taken up by the global ocean. The future monitoring of this rate of storage will be of significant importance for further constraining the evolution of the strength of the ocean sink for anthropogenic  $\text{CO}_2$ .

### *Conclusions*

This thesis demonstrates that large chemical-oceanographic datasets can be optimized for internal consistency by a (semi-)automated procedure. Newly collected data of high quality will contribute to the increasing accuracy at which the rate of storage of anthropogenic  $\text{CO}_2$  in the oceans may be quantified.

It is additionally shown that it is possible to convincingly determine the rate of storage of  $\text{CO}_2^{\text{ant}}$  in the ocean interior in an ocean basin that exhibits strong biogeochemical and hydrographical variability, and which has been sampled only sparsely both in space and time. The developed methodology may prove valuable (especially when additionally applied to the other ocean basins) for the assessment of the role of the oceans in the perturbed global carbon cycle.







## **Nederlandse samenvatting**





*De natuurlijke koolstofcyclus*

Het element koolstof (C) wordt in grote hoeveelheden uitgewisseld tussen – en in – de oceanen, de biomassa op het land, en de atmosfeer. De stofstromen (of *fluxen*) tussen deze *biosferische reservoirs* worden voornamelijk gedreven door de (seizoenale) variatie van de temperatuur van het zeeoppervlak, de groei en afbraak van bomen en planten op land, en de groei van algen in zee. Echter, juist vanwege deze seizoenale omkering van deze fluxen is de *gemiddelde* hoeveelheid koolstof in elk van de reservoirs (atmosfeer, land, oceaan) betrekkelijk stabiel gebleven gedurende de meedere duizenden jaren sinds het einde van de meest recente ijstijd. De natuurlijke koolstofkringloop wordt aldus verondersteld in *dynamisch evenwicht* te hebben verkeerd.

*De moderne verstoring*

Dit dynamisch evenwicht werd fors verstoord toen de zich industrialiserende samenleving vanaf ongeveer het jaar 1750 grote hoeveelheden koolstof is gaan uitstoten naar de atmosfeer (in de vorm van koolstofdioxide, CO<sub>2</sub>), voornamelijk door de verbranding van fossiele brandstoffen. Deze fossiele brandstoffen (voornamelijk kool, olie en aardgas) worden gedolven uit reservoirs diep in de aardkorst, welke van nature geen noemenswaardig contact hebben met de eerdergenoemde biosferische reservoirs. Door de winning en verbranding van fossiele brandstoffen is de mens dus bezig om extra koolstof toe te voegen aan de koolstofkringloop. Deze *antropogene* CO<sub>2</sub> (CO<sub>2</sub><sup>ant</sup>, antropogeen betekent zoveel als ‘door de mens gemaakt’) zal geleidelijk worden verdeeld tussen de atmosferische, terrestrische en oceanische reservoirs door de natuurlijke uitwisselingsprocessen.

Tot op heden heeft de mensheid al meer dan 1300 miljard ton CO<sub>2</sub> uitgestoten door gebruik van fossiele brandstoffen en door productie van cement (Boden et al., 2010). Veranderend landgebruik (voornamelijk ontbossing) veroorzaakt additionele uitstoot van CO<sub>2</sub> naar de atmosfeer (Houghton et al., 2008). De totale uitstootsnelheid neemt nog altijd toe en nadert momenteel de 36 miljard ton CO<sub>2</sub> per jaar, ofwel ongeveer een miljoen kilo CO<sub>2</sub> per seconde. Gedurende de afgelopen 250 jaar is de atmosferische CO<sub>2</sub>-concentratie met ongeveer 40% toegenomen van het natuurlijke (ofwel *pre-industriële*) niveau van ~280 ppm (parts per million, deeltjes per miljoen) tot ~393 ppm in 2012.

*Waargenomen en verwachte gevolgen*

In de atmosfeer remt CO<sub>2</sub> de uitstraling van warmte van het aardoppervlak richting de ruimte. De antropogene stijging van de atmosferische CO<sub>2</sub>-concentratie ‘isoleert’ de aarde in toenemende mate. De waargenomen stijging van land- en zeetemperatuur worden algemeen aangenomen consequenties te zijn van de ophoping van CO<sub>2</sub> in de atmosfeer (Solomon et al., 2007).

Veel veranderingen die geassocieerd zijn met de opwarming van de aarde zijn reeds gedocumenteerd. Hieronder bevinden zich de geleidelijke stijging van de zeespiegel en afnames in zeeijsoppervlak en ijkapmassa (Solomon et al., 2007). Verdere consequenties die (nog) directer van invloed zijn op het menselijk welzijn (bijvoorbeeld droogte en overstromingen) worden met hoge waarschijnlijkheid verwacht onder de meeste scenario's van toekomstige ontwikkeling (IPCC, 2012). Bovendien veroorzaakt de opname van toenemende hoeveelheden CO<sub>2</sub> door de oceaan zogenaamde ‘oceanverzuring’ (Feely et al., 2004). De daarmee gepaard

gaande toename in de oplosbaarheid van kalkschelpjes kan de overlevingskansen verlagen van organismen die aan de basis van de oceanische voedselketen staan (Doney et al., 2009). Dit proces zal mogelijk negatieve gevolgen hebben op de gezondheid van ecosystemen in zee, en daarmee eveneens op de menselijke gemeenschappen die van deze ecosystemen afhankelijk zijn voor voedsel en inkomsten. Echter, omdat organismen de mogelijkheid hebben zich aan te passen en te evolueren in reactie op verandering in hun milieu (zie bijvoorbeeld Lohbeck et al., 2012) zijn de toekomstige gevolgen van oceaanzuivering vooralsnog niet goed te voorspellen.

#### *De stand van zaken in het onderzoek naar de koolstofkringloop*

Om de veranderende koolstofcyclus volledig te kunnen begrijpen, is een beter begrip noodzakelijk van de processen die de uitgestoten  $\text{CO}_2^{\text{ant}}$  verdelen tussen atmosfeer, land en oceaan. Van de antropogene uitstoot van  $\text{CO}_2$  tijdens de periode 2000 tot 2010 resteert slechts zo'n 46% in de atmosfeer. De 'missende' 54% zijn uit de atmosfeer verwijderd door de oceaan en/of de terrestrische biosfeer. Onder andere gebaseerd op modelberekeningen worden deze oceaan- en land-putten ongeveer op gelijke grootte geschat (Le Quéré et al., 2009). Echter, de capaciteit van de oceaan voor voortdurende opname grote hoeveelheden  $\text{CO}_2$  wordt beperkt door de de oplossings-chemie van koolstof in de oceaan, en wordt verwacht steeds verder achterop te geraken ten opzichte van de snelheid van uitstoot van  $\text{CO}_2$  door de mensheid (zie bijvoorbeeld Sarmiento et al., 1995; Thomas et al., 2007). Recente meetcampagnes op zee hebben een grote variabiliteit (en ogenschijnlijk een afname) laten zien in de relatieve snelheid waarmee  $\text{CO}_2^{\text{ant}}$  de oceaan binnendringt (zie bijvoorbeeld Takahashi et al., 2009; Watson et al., 2009; Metzl et al., 2010). Echter, dergelijke gas-uitwisselings-meetcampagnes representeren slechts een klein gebied gedurende een zeer beperkte tijd, en lenen zich derhalve niet goed voor het verkrijgen van een schatting van de wereldwijde netto  $\text{CO}_2^{\text{ant}}$ -opname door de oceaan.

Een nauwkeurige, op data gebaseerde bepaling van de snelheid van de resulterende toename van  $\text{CO}_2^{\text{ant}}$  in de oceaan zou derhalve van grote waarde kunnen zijn om de uiteindelijke grootte van de oceanische put voor  $\text{CO}_2^{\text{ant}}$  nader te bepalen. Echter, ook de snelheid van opslag van  $\text{CO}_2^{\text{ant}}$  in de oceaan is niet eenvoudig te bepalen. Verschillende processen die onderdeel zijn van de oceanische koolstofcyclus beïnvloeden de (zeer grote) natuurlijke hoeveelheid opgelost  $\text{CO}_2$  en maakten daardoor de betrekkelijk kleine antropogene toevoeging lastig om waar te nemen.

Desalniettemin komt een nauwkeurige, op data gebaseerde bepaling van de opslagsnelheid van  $\text{CO}_2^{\text{ant}}$  in de diepe oceaan binnen handbereik, als gevolg van de groeiende beschikbaarheid van kwalitatief hoogwaardige en onderling geharmoniseerde datasets, verzameld over een tijdspanne van nu al bijna 40 jaar (1972 tot heden).

#### *Doelstelling van dit proefschrift*

Dit promotieonderzoek heeft als doel het verkrijgen van een op metingen gebaseerde schatting van de opslagsnelheid van  $\text{CO}_2^{\text{ant}}$  in de oceanen. Het uitgevoerde onderzoek besloeg (i) het verzamelen op zee van nieuwe, hoogwaardige metingen van de hoeveelheden opgelost  $\text{CO}_2$  en gerelateerde eigenschappen in de diepe Atlantische oceaan en (ii) het samenstellen van een zeer hoogwaardig dataproduct uit nieuwe en historisch meetgegevens van de Atlantische Ocean, en (iii) het gebruik van deze gecombineerde gegevens om de opslagsnelheid te

bepalen van  $\text{CO}_2^{\text{ant}}$  in de Weddell Gyre (gelegen ten zuid-oosten van Zuid-Amerika, grenzend aan Antarctica) en in de Zuid Atlantische Oceaan als geheel. Deze regio's worden van groot belang geacht voor de opname van antropogeen  $\text{CO}_2$  door het zeeoppervlak en voor het daaropvolgende transport de diepzee in.

#### *Samenvatting van resultaten*

Gedurende 7 onderzoeksvaartritten zijn zo'n 8000 metingen verricht van de concentraties van opgelost  $\text{CO}_2$  (en gerelateerde eigenschappen) in watermonsters verzameld in de diepe oceaan. Deze data worden getoond de voor dit werk gewenste precisie en nauwkeurig te bezitten. Tegenover reeds bestaande datasets kan deze nieuwe data derhalve gebruikt worden voor het maken van de gewenste schatting van de opslagsnelheid van  $\text{CO}_2^{\text{ant}}$  in de oceanen.

Met een internationaal team van wetenschappers is een grote database samengesteld van  $\text{CO}_2$ -relevante gegevens uit de diepe oceaan, verzameld tijdens 188 onderzoeksvaartritten gedurende de jaren 1972 tot 2005. Veel van deze data waren voorheen niet publiek beschikbaar. Teneinde de nauwkeurigheid van deze database te optimaliseren is een collectie van semi-geautomatiseerde berekeningsroutines ontwikkeld. Deze routines maken het mogelijk om afwijkingen tussen de verschillende vaartritten te minimaliseren door toepassing van een mathematische inversie methode (Johnson et al., 2001). De routines verschaffen suggesties voor aanpassingen van de data van individuele vaartritten welke – bij toepassing ervan – de afwijkingen in de diepe oceaan minimaliseren. Deze suggesties zijn in detail geïnspecteerd door groepen van ervaren onderzoekers teneinde er zeker te zijn dat alleen analytische afwijkingen werden gecompenseerd, zonder dat per ongeluk ook de werkelijk optredende veranderingen in de diepe oceaan zijn verwijderd. De gehanteerde methodiek wordt getoond de interne consistentie van het uiteindelijke dataproduct sterk te hebben vergroot in vergelijking met de originele data van de individuele vaartritten. Het uiteindelijke dataproduct is beschikbaar gemaakt voor de internationale onderzoeksgemeenschap als de CARINA-database (Carbon in the North Atlantic).

Een gedetailleerde, lokale studie van de opslagsnelheid van  $\text{CO}_2^{\text{ant}}$  is gemaakt met data verzameld tijdens 10 onderzoeksvaartritten uitgevoerd tussen 1973 en 2008 langs de  $0^\circ$ -meridiaan in de Weddell Gyre in de Zuid-Atlantische Oceaan. Eén van de 10 gebruikte datasets is verzameld tijdens dit promotieonderzoek (PFS *Polarstern* expeditie ANT-XXIV/3, Feb-Apr 2008). De gemaakte analyse toont de geleidelijke opslag (accumulatie) aan van  $\text{CO}_2^{\text{ant}}$  in het Weddell Zee Bodemwater (Engels: *Weddell Sea Bottom Water*, WSBW) met een snelheid van ongeveer  $1.2 \pm 0.6$  micromol koolstof per kilogram zeewater per 10 jaar ( $1.2 \pm 0.6 \mu\text{mol kg}^{-1} \text{decade}^{-1}$ ) over de periode 1973-2008. Daarnaast werd de ruimtelijke verdeling van deze opslag langs de sectie bepaald. Deze verdeling blijkt sterke overeenkomsten te vertonen met die van de accumulatie van CFC-12, een inert antropogeen gas dat net als  $\text{CO}_2^{\text{ant}}$  uit de atmosfeer wordt opgenomen en zeer precies meetbaar is in zeewater. Deze overeenkomst is een indicatie dat de waargenomen toename (over de tijd) van opgelost  $\text{CO}_2$  inderdaad het gevolg is van de voortdurend toegenemende opname van  $\text{CO}_2$  uit de atmosfeer. De waargenomen opslagsnelheid vormt een duidelijke restrictie voor schattingen van de waarde van de totale hoeveelheid  $\text{CO}_2^{\text{ant}}$  die zich reeds in de Weddell Gyre heeft opgehoopt – een waarde waarvoor schattingen sterk verschillen. Een extrapolatie naar de Weddell Zee als geheel suggereert dat de opslagsnelheid in het water

dieper dan 500 meter ongeveer  $0.012 \pm 0.06$  PgC per jaar is ( $1 \text{ PgC} = 10^{15}$  gram, ofwel 1 miljard ton koolstof). Dit is gelijk aan ongeveer 0.2% van de gemiddelde uitstootsnelheid van  $\text{CO}_2^{\text{ant}}$  over de periode 1973-2008.

Hieropvolgend is, met gebruik van een grotere dataset van 53 vaartochten, de opslag snelheid van  $\text{CO}_2^{\text{ant}}$  bepaald in de Zuid Atlantische Oceaan als geheel (hier gedefinieerd als alle wateren die zich bevinden tussen de evenaar, het Antarctisch continent,  $30^\circ\text{O}$  en Drake Passage rond  $65^\circ\text{W}$ ). Een zorgvuldige beschouwing van zeven verschillende watermassa's in dat oceaan-basin laat zien dat  $\text{CO}_2^{\text{ant}}$  snel toeneemt in het deel van watermassa's nabij het oceaanoppervlak, alwaar recentelijk gasuitwisseling heeft plaatsgevonden met de moderne atmosfeer. Het 'oudere' water dieper in het binnenste van de watermassa's laat een veel tragere toename in de hoeveelheid  $\text{CO}_2^{\text{ant}}$  zien gedurende de 40 jaar waarvoor metingen beschikbaar zijn. Deze resultaten worden op basis van een hoogwaardige klimatologie geëxtrapoleerd teneinde een gedetailleerde ruimtelijke verdeling te verkrijgen van de opslagsnelheid van  $\text{CO}_2^{\text{ant}}$  in de Zuid-Atlantische Oceaan.

De gemiddelde snelheid (over 1973-2008) van de totale opslag door de Zuid Atlantische Oceaan (zoals hierboven gedefinieerd) bedraagt  $0.39 \pm 0.08$  PgC per jaar. Dat is gelijk aan ongeveer 6% van de gemiddelde antropogene uitstootsnelheid over die periode (ongeveer 6.3 pgC per jaar). Ongeveer tweederde van de totale opslag van  $\text{CO}_2^{\text{ant}}$  wordt waargenomen in de ondiepe en intermediaire watermassa's (0-1500 meter diepte), terwijl de meer volumineuze diep- en bodem-watermassa's ongeveer één derde van de uit de atmosfeer opgenomen  $\text{CO}_2^{\text{ant}}$  bevatten.

De hoogste (diepte-geïntegreerde) opslagsnelheid wordt waargenomen tussen de breedtegraden  $35^\circ\text{Z}$  en  $50^\circ\text{Z}$ , en bedraagt ongeveer 1 mol koolstof per vierkante meter per jaar ( $\text{mol m}^{-2} \text{ a}^{-1}$ ). Deze regio bevindt zich ten noorden van het gebied waar gasuitwisselingsstudies een zeer sterke opname van  $\text{CO}_2$  door de oceaan waarnemen. Dit ogenschijnlijke verschil wordt verklaard door de noordwaardse verplaatsing van de betreffende watermassa's nadat deze wegzinken van het oppervlak rond  $50^\circ\text{Z}$ , als onderdeel van de grootschalige oceaancirculatie.

De behaalde resultaten vertonen sterkte overeenkomsten met andere recente schattingen van de opslag (en opnamesnelheid) van  $\text{CO}_2^{\text{ant}}$  door de oceaan, gemaakt in kleinere regio's van de Zuid Atlantische Oceaan (Murata et al., 2008; Wanninkhof et al., 2010), maar biedt verbeterd ruimtelijk detail en dekking. Resultaten van een conceptueel volledig onafhankelijke studie door Khatiwala et al. (2009), die geen gebruik maakt van koolstofmetingen in de diepe oceaan, komen ook goed overeen met de hier behaalde resultaten.

De resultaten versterken de bewijsvoering voor eerdere beweringen dat de Zuid Atlantische Oceaan verantwoordelijk is voor de opslag van circa 20% van alle antropogene  $\text{CO}_2$  die door de oceanen wordt opgenomen. De toekomstige monitoring van de opslagsnelheid wordt van groot belang geacht voor het kunnen bepalen van de ontwikkeling van oceanische put voor antropogeen  $\text{CO}_2$ .

### *Conclusies*

Dit proefschrift demonstreert dat grote chemisch-oceanografisch datasets kunnen worden geoptimaliseerd voor interne consistentie door middel van (semi-)automatische procedures. Nieuw

verzamelde data van hoge kwaliteit kunnen bijdragen aan het toenemen van de nauwkeurigheid waarmee de opslagsnelheid van antropgeen CO<sub>2</sub> in de oceanen kan worden vastgesteld.

Eveneens wordt gedemonstreerd dat het mogelijk is om de opslagsnelheid van CO<sub>2</sub><sup>ant</sup> in de diepe oceaan op overtuigende wijze vast te stellen in een oceanobasin dat een sterke biogeochemische en hydrografische variabiliteit vertoont en slechts betrekkelijk sporadisch bemonsterd is. De ontwikkelde methodiek kan, zeker wanneer eveneens toegepast op de andere oceanobasins, van grote waarde zijn voor de bepaling van de rol van de oceanen in de verstoorde koolstofkringloop.





## References





- Aminot, A. and D.S. Kirkwood (1995). *Report on the results of the fifth ICES Intercomparison Exercise for Nutrients in Seawater*. ICES Cooperative Research Report No. 213.
- Anderson, L.A. and J.L. Sarmiento (1994). Redfield ratios of remineralization determined by nutrient data-analysis. *Global Biogeochemical Cycles* 8(1), 65-80.
- Anderson, L.G., O. Holby, R. Lindegren and M. Ohlson (1991). The transport of anthropogenic carbon dioxide into the Weddell Sea. *Journal of Geophysical Research* 96, 16679-16687.
- Antonov, J.I., R.A. Locarnini, T.P. Boyer, A.V. Mishonov and H.E. Garcia (2006). World Ocean Atlas 2005, Volume 2: Salinity. In: S. Levitus (Ed.), *NOAA Atlas NESDIS 62*. U.S. Government Printing Office, Washington, D.C. 182 pp.
- Aoyama M., J. Barwell-Clarke, S. Becker, M. Blum, E.S. Braga, S.C. Coverly, E. Czobik, I. Dahllhof, M.H. Dai, G.O. Donnell, C. Engelke, G.C. Gong, G.-H. Hong, D.J. Hydes, M.M. Jin, H. Kasai, R. Kerouel, Y. Kiyomono, M. Knockaert, N. Kress, K.A. Kroglund, M. Kumagai, S. Letorme, Y. Li, S. Masuda, T. Miyao, T. Moutin, A. Murata, N. Nagai, G. Nausch, M.K. Ngirchchol, A. Nybakk, H. Ogawa, J. van Ooijen, H. Ota, J.M. Pan, C. Payne, O. Pierre-Duplessix, M. Pujó-Pay, T. Raabe, K. Saito, K. Sato, C. Schmidt, M. Schuett, T.M. Shammon, J. Sun, T. Tanhua, L. White, E.M.S. Woodward, P. Worsfold, P. Yeats, T. Yoshimura, A. Youenou and J.Z. Zhang (2008). *The 2006 Intercomparison exercise for reference material for nutrients in seawater in a seawater matrix*. Technical Reports of the Meteorological Research Institute No. 58, 104pp.
- Archer, D. and V. Brovkin (2005). Fate of fossil fuel CO<sub>2</sub> in geologic time. *Journal of Geophysical Research* 110(C9), 65–80.
- Arrhenius, S. (1896). On the influence of carbonic acid in the air upon the temperature of the Earth. *Publications of the Astronomical Society of the Pacific* 9(54), 14–24.
- Bainbridge, A.E. (Ed.; 1981). *GEOSECS Atlantic Expedition, Vol. 1, Hydrographic Data 1972-1973*. IDOE/ NSF. 121pp.
- Bakker, D.C.E., M. Hoppema, M. Schroeder, W. Geibert and H.J.W. de Baar (2008). A rapid transition from ice covered CO<sub>2</sub>-rich waters to a biologically mediated CO<sub>2</sub> sink in the eastern Weddell Gyre. *Biogeosciences* 5, 1373-1386.
- Bandstra, L., B. Hales and T. Takahashi (2006). High-frequency measurements of total CO<sub>2</sub>: Method development and first oceanographic observations. *Marine Chemistry* 100(1-2), 24–38.
- Boden, T.A., G. Marland and R.J. Andres (2011). *Global, Regional, and National Fossil-Fuel CO<sub>2</sub> Emissions*. Carbon Dioxide Information Analysis Center, Oak Ridge National Laboratory, U.S. Department of Energy, Oak Ridge, Tennessee.
- Böning, C.W., A. Dispert, M. Visbeck, S. Rintoul and F.U. Schwarzkopf (2008). Response of the Antarctic Circumpolar Current to recent climate change. *Nature Geoscience* 1, 864–869.
- Brewer, P.G. and J.C. Goldman (1976). Alkalinity changes generated by phytoplankton growth. *Limnology and Oceanography* 21(1), 108-117.
- Brewer, P.G. (1978). Direct observation of the oceanic CO<sub>2</sub> increase. *Geophysical Research Letters* 5, 997-1000.
- Broecker, W.S. (1971). A kinetic model for the chemical composition of sea water. *Quaternary Research* 1(2), 188–207.
- Broecker, W.S. (1974). "NO", a conservative water-mass tracer. *Earth and Planetary Science Letters* 23, 100-107.
- Broecker, W.S. and T.-H. Peng (1982). *Tracers in the Sea*. Eldigio Press, Lamont-Doherty Geological Observatory, Palisades, NY. 690pp

- Bu, X. and M.J. Warner (1995). Solubility of chlorofluorocarbon 113 in water and seawater. *Deep-Sea Research Part I* 42(7), 1151–1161.
- Budillon, G., M. Pacciaroni, S. Cozzi, P. Rivaro, G. Catalano, C. Ianni and C. Cantoni (2003). An optimum multiparameter mixing analysis of the shelf waters in the Ross Sea. *Antarctic Science* 15(1), 105–118.
- Bullister, J.L. and D.P. Wisegarver (1998). The solubility of carbon tetrachloride in water and seawater. *Deep-Sea Research Part I* 45(8), 1285–1302.
- Bullister, J.L., D.P. Wisegarver and F.A. Menzia (2002). The solubility of sulfur hexafluoride in water and seawater. *Deep-Sea Research Part I* 49(1), 175–187.
- Byrne, R.H., X. Liu, E. Kaltenbacher and K. Sell (2002). Spectrophotometric measurement of total inorganic carbon in aqueous solutions using a liquid core waveguide. *Analytica Chimica Acta* 451(2), 221–229.
- Byrne, R.H. and W. Yao (2008). Procedures for measurement of carbonate ion concentrations in seawater by direct spectrophotometric observations of Pb(II) complexation. *Marine Chemistry* 112(1-2), 128–135.
- Canadell, J.G., C. Le Quééré, M.R. Raupach, C.B. Field, E.T. Buitenhuis, P. Ciais, T.J. Conway, N.P. Gillett, R. Houghton and G. Marland (2007). Contributions to accelerating atmospheric CO<sub>2</sub> growth from economic activity, carbon intensity, and efficiency of natural sinks. *Proceedings of the National Academy of Sciences* 104(47), 18866–18870.
- CarboOcean Scientific Steering Committee (2004). CarboOcean Science Plan. [www.carboocean.org](http://www.carboocean.org)
- Chen, C.T.A. and F.J. Millero (1979). Gradual increase of oceanic CO<sub>2</sub>. *Nature* 277, 205–206.
- Chen, C.T.A. (1993). The oceanic anthropogenic CO<sub>2</sub> sink. *Chemosphere* 27(6), 1041–1064.
- Chipman, D.W., T. Takahashi and S.C. Sutherland (1986). *Carbon chemistry of the South Atlantic Ocean and the Weddell Sea: The results of the Atlantic Long Lines (AJAX) Expeditions, October 1983 – February 1984*. Lamont-Doherty Geological Observatory, Columbia University, Palisades, NY. 185pp.
- Clayton, T.D. and R.H. Byrne (1993). Spectrophotometric seawater pH measurements: Total hydrogen ion concentration scale calibration of m-cresol purple and at-sea results. *Deep-Sea Research Part I* 40(10), 2115–2129.
- Cleveland, W. S. and S.J. Devlin (1988). Locally weighted regression: An approach to regression analysis by local fitting. *Journal of the American Statistical Association* 83, 596–610.
- Cooley, S.R. and P.L. Yager (2006). Physical and biological contributions to the western tropical North Atlantic Ocean carbon sink formed by the Amazon River plume. *Journal of Geophysical Research* 111(C8), C08018.
- Deacon, G.E.R. (1984). *The Antarctic Circumpolar Ocean*. Cambridge University Press, Cambridge, New York. 180pp.
- Dickson, A.G. (1981). An exact definition of total alkalinity and a procedure for the estimation of alkalinity and total inorganic carbon from titration data. *Deep-Sea Research Part A* 28, 609–623.
- Dickson, A.G. (1990). *The ocean carbon dioxide system: Planning for quality data*. US JGOFS News 2.
- Dickson, A.G. and C. Goyet (1994). *Handbook of methods for the analysis of the various parameters of the carbon dioxide system in seawater*. Version 2. DOE, ORNL/CDIAC-74.
- Dickson, A.G. (2001). Reference material for oceanic CO<sub>2</sub> measurements. *Oceanography* 14(4), 21–22.
- Dickson, A.G., J.D. Afghan and G.C. Anderson (2003). Reference materials for oceanic CO<sub>2</sub> analysis: a method for the certification of total alkalinity. *Marine Chemistry* 80, 185–197.
- Dickson, A.G., C.L. Sabine and J.R. Christian (Eds.; 2007). *Guide to best practices for ocean CO<sub>2</sub> measurements*. PICES Special Publication 3. 191 pp.
- Dickson, A.G. (2010). Standards for ocean measurements. *Oceanography* 23(3), 34–47.

- Doney, S.C., K. Lindsay, K. Caldeira, J.-M. Campin, H. Drange, J.-C. Dutay, M. Follows, Y. Gao, A. Gnanadesikan, N. Gruber, A. Ishida, F. Joos, G. Madec, E. Maier-Reimer, J.C. Marshall, R.J. Matear, P. Monfray, A. Mouchet, R. Najjar, J.C. Orr, G.-K. Plattner, J. Sarmiento, R. Schlitzer, R. Slater, I.J. Totterdell, M.-F. Weirig, Y. Yamanaka and A. Yool (2004). Evaluating global ocean carbon models: The importance of realistic physics. *Global Biogeochemical Cycles* 18, GB3017.
- Doney, S.C., V.J. Fabry, R.A. Feely and J.A. Kleypas (2009a). Ocean Acidification: The Other CO<sub>2</sub> Problem. *Annual Review of Marine Science* 1(1), 169–192.
- Doney, S.C., I. Lima, J. K. Moore, K. Lindsay, M.J. Behrenfeld, T.K. Westberry, N. Mahowald, D.M. Glover and T. Takahashi (2009b). Skill metrics for confronting global upper ocean ecosystem-biogeochemistry models against field and remote sensing data. *Journal of Marine Systems* 76(1-2), 95–112.
- Etheridge D.M, L.P. Steele, R.L. Langenfelds, R.J. Francey, J.M. Barnola and V.I. Morgan (1996). *Journal of Geophysical Research Atmosphere* 101, 4115–4128.
- Fahrbach, E., S. Harms, G. Rohardt, M. Schröder and R. Woodgate (2001). Flow of bottom water in the northwestern Weddell Sea. *Journal of Geophysical Research* 106, 2761-2778.
- Fahrbach, E., M. Hoppema, G. Rohardt, M. Schröder and A. Wisotzki (2004). Decadal-scale variations of water mass properties in the deep Weddell Sea. *Ocean Dynamics* 54, 77-91.
- Fahrbach, E. and H.J.W. de Baar (2010). The expedition of the research vessel “Polarstern” to the Antarctic in 2008 (ANT-XXIV /3). *Reports on Polar and Marine Research* 606. 232pp.
- Feely, R.A., C.L. Sabine, K. Lee, W. Berelson, J. Kleypas, V.J. Fabry and F.J. Millero (2004). Impact of anthropogenic CO<sub>2</sub> on the CaCO<sub>3</sub> system in the oceans. *Science* 305(5682), 362-366.
- Feely, R.A., S.C. Doney and S.R. Cooley (2009). Ocean acidification: Present conditions and future changes in a high-CO<sub>2</sub> world. *Oceanography* 22(4), 36-47.
- Fine, R.A. (2011). Observations of CFCs and SF<sub>6</sub> as Ocean Tracers. *Annual Review of Marine Science* 3, 173–95.
- Foster, T. and E. Carmack (1976). Temperature and salinity structure in the Weddell Sea. *Journal of Physical Oceanography* 6, 36-44.
- Friedlingstein, P., R.A. Houghton, G. Marland, J. Hackler, T.A. Boden, T.J. Conway, J.G. Canadell, M.R. Raupach, P. Ciais and C. Le Quéré (2010). Update on CO<sub>2</sub> emissions. *Nature Geoscience* 3(12), 811–812.
- Friis, K., A. Körtzinger, J. Pätsch and D.W.R. Wallace (2005). On the temporal increase of anthropogenic CO<sub>2</sub> in the subpolar North Atlantic. *Deep-Sea Research Part I* 52, 681-698.
- Gammon, R.H., J. Cline and D. Wisegarver (1982). Chlorofluoromethanes in the Northeast Pacific Ocean: Measured vertical distributions and application as transient tracers of upper ocean mixing. *Journal of Geophysical Research* 87(C12), 9441–9454.
- Garcia, H.E., R.A. Locarnini, T.P. Boyer and J.I. Antonov (2006a). World Ocean Atlas 2005, Volume 3: Dissolved Oxygen, Apparent Oxygen Utilization, and Oxygen Saturation. In: S. Levitus (Ed.), *NOAA Atlas NESDIS 63*. U.S. Government Printing Office, Washington, D.C. 342 pp.
- Garcia, H.E., R.A. Locarnini, T.P. Boyer and J.I. Antonov (2006b). World Ocean Atlas 2005, Volume 4: Nutrients (phosphate, nitrate, silicate). In: S. Levitus (Ed.), *NOAA Atlas NESDIS 64*. U.S. Government Printing Office, Washington, D.C. 396 pp.
- Geibert, W., P. Assmy, D.C.E. Bakker, C. Hanfland, M. Hoppema, L.E. Pichevin, M. Schroeder, J.N. Schwarz, I. Stimac, R. Usbeck and A. Webb (2010). High productivity in an ice melting hot spot at the eastern boundary of the Weddell Gyre. *Global Biogeochemical Cycles* 24, GB3007.
- Gloor, M., J.L. Sarmiento and N. Gruber (2010). What can be learned about carbon cycle climate feedbacks from the CO<sub>2</sub> airborne fraction? *Atmospheric Chemistry and Physics* 10(16), 7739–7751.

- Gnanadesikan, A., J.P. Dunne, R.M. Key, K. Matsumoto, J.L. Sarmiento, R.D. Slater and P.S. Swathi (2004). Oceanic ventilation and biogeochemical cycling: Understanding the physical mechanisms that produce realistic distributions of tracers and productivity. *Global Biogeochemical Cycles* 18, GB4010.
- Gouretski, V.V. and K. Jancke (2001). Systematic errors as the cause for an apparent deep water property variability: global analysis of the WOCE and historical hydrographic data. *Progress in Oceanography* 48, 337–402.
- Gruber, N., J.L. Sarmiento and T. Stocker (1996). An improved method for detecting anthropogenic CO<sub>2</sub> in the oceans. *Global Biogeochemical Cycles* 10, 809–837.
- Gruber, N. (1998). Anthropogenic CO<sub>2</sub> in the Atlantic Ocean. *Global Biogeochemical Cycles* 12, 165–192.
- Gruber, N., M. Gloor, S.E. Mikaloff Fletcher, S.C. Doney, S. Dutkiewicz, M.J. Follows, M. Gerber, A.R. Jacobson, F. Joos, K. Lindsay, D. Menemenlis, A. Mouchet, S.A. Müller, J.L. Sarmiento and T. Takahashi (2009). Oceanic sources, sinks, and transport of atmospheric CO<sub>2</sub>. *Global Biogeochemical Cycles* 23(1), 1–21.
- Gruber, N., A. Körtzinger, A. Borges, H. Claustre, S.C. Doney, R.A. Feely, M. Hood, M. Ishii, A. Kozyr and P. Monteiro (2010). Toward an integrated observing system for ocean carbon and biogeochemistry at a time of change. *Proceedings of OceanObs'09: Sustained Ocean Observations and Information for Society, Venice, Italy, 21–25 September 2009* 1, 8.
- Hall, T.M., T.W.N. Haine and D.W. Waugh (2002). Inferring the concentration of anthropogenic carbon in the ocean from tracers. *Global Biogeochemical Cycles* 16(4), 1131.
- Hall, T.M., D.W. Waugh, T.W.N. Haine, P.E. Robbins and S. Khatiwala (2004). Estimates of anthropogenic carbon in the Indian Ocean with allowance for mixing and time-varying air-sea CO<sub>2</sub> disequilibrium. *Global Biogeochemical Cycles* 18, GB1031.
- Haraldsson, C., L.G. Anderson, M. Hassellöv, S. Hulth and K. Olsson (1997). Rapid, high-precision potentiometric titration of alkalinity in ocean and sediment pore waters, *Deep-Sea Research Part I* 44(12), 2031–2044.
- Hauck, J., M. Hoppema, R.G.J. Bellerby, C. Völker and D. Wolf-Gladrow (2010). Data-based estimation of anthropogenic carbon and acidification in the Weddell Sea on a decadal timescale. *Journal of Geophysical Research* 115, C03004.
- Hoppema, M., E. Fahrbach, M. Schröder, A. Wisotzki and H.J.W. de Baar (1995). Winter-summer differences of carbon dioxide and oxygen in the Weddell Sea surface layer. *Marine Chemistry* 51, 177–192.
- Hoppema, M., E. Fahrbach, M.H.C. Stoll and H.J.W. de Baar (1998). Increase of carbon dioxide in the bottom water of the Weddell Sea, Antarctica. *Marine Chemistry* 59, 201–210.
- Hoppema, M., W. Roether, R. Bellerby and H.J.W. de Baar (2001a). Direct measurements reveal insignificant storage of anthropogenic CO<sub>2</sub> in the abyssal Weddell Sea. *Geophysical Research Letters* 28(9), 1747–1750.
- Hoppema, M., O. Klatt, W. Roether, E. Fahrbach, K. Bulsiewicz, C. Rodehacke and G. Rohardt (2001b). Prominent renewal of Weddell Sea Deep Water from a remote source. *Journal of Marine Research* 59, 257–279.
- Hoppema, M. (2004). Weddell Sea as a globally significant contributor to deep-sea sequestration of natural carbon dioxide. *Deep-Sea Research Part I* 51, 1169–1177.
- Hoppema, M., R. Middag, H.J.W. de Baar, E. Fahrbach, E.M. van Weerlee and H. Thomas (2007). Whole season net community production in the Weddell Sea. *Polar Biology* 31, 101–111.
- Houghton, R.A. (2003). Revised estimates of the annual net flux of carbon to the atmosphere from changes in land use and land management 1850–2000. *Tellus B* 55, 378–390.
- Huhn, O., H. Hellmer, M. Rhein, C. Rodehacke, W. Roether, M.P. Schodlock and M. Schröder (2008). Evidence of deep- and bottom-water formation in the western Weddell Sea. *Deep-Sea Research Part II* 55, 1098–1116.

- Field, C.B., V. Barros, T.F. Stocker, D. Qin, D.J. Dokken, K.L. Ebi, M.D. Mastrandrea, K.J. Mach, G.-K. Plattner, S.K. Allen, M. Tignor and P.M. Midgley (Eds.; 2012). *Managing the Risks of Extreme Events and Disasters to Advance Climate Change Adaptation. A Special Report of Working Groups I and II of the Intergovernmental Panel on Climate Change*. Cambridge University Press. 582 pp.
- Ito, T., M. Follows and E. Boyle (2004). Is AOU a good measure of respiration in the oceans? *Geophysical Research Letters* 31, L17305.
- Jiménez-López, C., E. Caballero, F. Huertas and C. Romanek (2001). Chemical, mineralogical and isotope behavior, and phase transformation during the precipitation of calcium carbonate minerals from intermediate ionic solution at 25 °C. *Geochimica et Cosmochimica Acta* 65(19), 3219–3231.
- Johnson, G.C., P.E. Robbins and G.E. Hufford (2001). Systematic adjustments of hydrographic sections for internal consistency. *Journal of Atmospheric and Oceanic Technology* 18(7), 1234–1244.
- Johnson, K.M., A.E. King and J.M. Sieburth (1985). Coulometric TCO<sub>2</sub> Analyses for Marine Studies; an Introduction. *Marine Chemistry* 16, 61–82.
- Johnson, K.M., K.D. Wills, D.B. Butler, W.K. Johnson and C.S. Wong (1993). Coulometric total carbon dioxide analysis for marine studies - maximizing the performance of an automated gas extraction system and coulometric detector. *Marine Chemistry* 44(2-4), 167–187.
- Johnson, K.M., A.G. Dickson, G. Eiseid, C. Goyet, P. Guenther, R.M. Key, F.J. Millero, D. Purkerson, C.L. Sabine, R.G. Schottle, D.W.R. Wallace, R.J. Wilke and C.D. Winn (1998). Coulometric total carbon dioxide analysis for marine studies: assessment of the quality of total inorganic carbon measurements made during the US Indian Ocean CO<sub>2</sub> Survey 1994–1996. *Marine Chemistry* 63(1–2), 21–37.
- Johnson, K.S., W.M. Berelson, E.S. Boss, Z. Chase, H. Claustre, S.R. Emerson, N. Gruber, A. Körtzinger, M.J. Perry and S.C. Riser (2009). Observing biogeochemical cycles at global scales with profiling floats and gliders: Prospects for a global array. *Oceanography* 22(3), 216–225.
- Kaltin, S., C. Haraldsson and L.G. Anderson (2005). A rapid method for determination of total dissolved inorganic carbon in seawater with high accuracy and precision. *Marine Chemistry* 96(1-2), 53–60.
- Karstensen, J. and M. Tomczak (1998). Age determination of mixed water masses using CFC and oxygen data. *Journal of Geophysical Research* 103(C9), 18599–18606
- Kawase, M. and J.L. Sarmiento (1985): Nutrients in the Atlantic thermocline. *Journal of Geophysical Research* 90, 8961–8976.
- Keeling, C.D. (1960). The concentration and isotopic abundances of carbon dioxide in the atmosphere. *Tellus* 12(2), 200–203.
- Keeling, C.D., S.C. Piper, R.B. Bacastow, M. Wahlen, T.P. Whorf, M. Heimann and H.A.J. Meijer (2001). *Exchanges of atmospheric CO<sub>2</sub> and <sup>13</sup>CO<sub>2</sub> with the terrestrial biosphere and oceans from 1978 to 2000. I. Global aspects*. SIO Reference Series, No. 01-06. UCSD Scripps Institution of Oceanography. 88pp.
- Key, R.M., A. Kozyr, C.L. Sabine, K. Lee, R. Wanninkhof, J.L. Bullister, R.A. Feely, F.J. Millero, C. Mordy and T.-H. Peng (2004). A global ocean carbon climatology: Results from Global Data Analysis Project (GLODAP). *Global Biogeochemical Cycles* 18, GB4031.
- Key, R.M., T. Tanhua, A. Olsen, M. Hoppema, S. Jutterström, C. Schirnick, S. van Heuven, A. Kozyr, X. Lin, A. Velo, D.W.R. Wallace and L. Mintrop (2010). The CARINA data synthesis project: Introduction and overview. *Earth System Science Data* 2, 105–121.
- Khatiwala, S., M. Visbeck and P. Schlosser (2001). Age tracers in an ocean GCM. *Deep-Sea Research Part I* 48(6), 1423–1441.



- Khatiwala, S., F. Primeau and T. Hall (2009). Reconstruction of the history of anthropogenic CO<sub>2</sub> concentrations in the ocean. *Nature* 462(7271), 346–349.
- Klatt, O., W. Roether, M. Hoppema, K. Bulsiewicz, U. Fleischmann, C. Rodehacke, E. Fahrbach, R.F. Weiss and J.L. Bullister (2002). Repeated CFC sections at the Greenwich Meridian in the Weddell Sea. *Journal of Geophysical Research* 107, C3030.
- Klatt, O., E. Fahrbach, M. Hoppema and G. Rohardt (2005). The transport of the Weddell Gyre across the Prime Meridian. *Deep-Sea Research Part II* 52, 513–528.
- Körtzinger, A., L. Mintrop and J.C. Duinker (1998). On the penetration of anthropogenic CO<sub>2</sub> into the North Atlantic Ocean. *Journal of Geophysical Research* 103(C9), 18689.
- Körtzinger, A., J. Hedges and P. Quay (2001). Redfield ratios revisited: removing the biasing effect of anthropogenic CO<sub>2</sub>. *Limnology and Oceanography* 46(4), 964–970.
- Körtzinger, A., J. Schimanski, U. Send and D.W.R. Wallace (2004). The ocean takes a deep breath. *Science* 306(5700), 1337–1337.
- Lamb, M.F., C.L. Sabine, R.A. Feely, R. Wanninkhof, R.M. Key, G.C. Johnson, F.J. Millero, K. Lee, T.-H. Peng, A. Kozyr, J.L. Bullister, D. Greeley, R.H. Byrne, D.W. Chipman, A.G. Dickson, C. Goyet, P.R. Guenther, M. Ishii, K.M. Johnson, C.D. Keeling, T. Ono, K. Shitashima, B. Tilbrook, T. Takahashi, D.W.R. Wallace, Y.W. Watanabe, C.D. Winn and C.S. Wong (2002). Consistency and synthesis of Pacific Ocean CO<sub>2</sub> survey data. *Deep-Sea Research Part II* 49, 21–58.
- Le Quéré, C., C. Rödenbeck, E.T. Buitenhuis, T.J. Conway, R. Langenfelds, A. Gomez, C. Labuschagne, M. Ramonet, T. Nakazawa, N. Metzl, N.P. Gillett and M. Heimann (2007). Saturation of the Southern Ocean CO<sub>2</sub> sink due to recent climate change. *Science* 319(5863), 1735–1738.
- Le Quéré C, M.R. Raupach, J.G. Canadell and G. Marland (2009). Trends in the sources and sinks of carbon dioxide. *Nature Geosciences* 2, 831–836.
- Lee, K., F.J. Millero and D.M. Campbell (1996). The reliability of the thermodynamic constants for the dissociation of carbonic acid in seawater. *Marine Chemistry* 55, 233–245.
- Lee, K., L.T. Tong, F.J. Millero, C.L. Sabine, A.G. Dickson, C. Goyet, G.-H. Park, R. Wanninkhof, R.A. Feely and R.M. Key (2006). Global relationships of total alkalinity with salinity and temperature in surface waters of the world's ocean. *Geophysical Research Letters* 33, L19605.
- Lenton, A., F. Codron, L. Bopp, N. Metzl, P. Cadule, A. Tagliabue and J. LeSommer (2009). Stratospheric ozone depletion reduces ocean carbon uptake and enhances ocean acidification. *Geophysical Research Letters* 36, L12606.
- Levine, N., S.C. Doney, R. Wanninkhof, K. Lindsay and I.Y. Fung (2008). Impact of ocean carbon system variability on the detection of temporal increases in anthropogenic CO<sub>2</sub>. *Journal of Geophysical Research* 113, C03019.
- Levitus, S. (1982). *Climatological atlas of the world ocean*. NOAA Professional Paper #13, Rockville, MD. 191 pp.
- Levitus, S., J. Antonov and T. Boyer (2005). Warming of the world ocean, 1955–2003. *Geophysical Research Letters* 32(2), L02604.
- Lewis, E. and D.W.R. Wallace (1998). *Program Developed for CO<sub>2</sub> System Calculations*. ORNL/CDIAC-105. Carbon Dioxide Information Analysis Center, Oak Ridge National Laboratory, U.S. Department of Energy, Oak Ridge, Tennessee.
- Lo Monaco, C., N. Metzl, A. Poisson, C. Brunet and B. Schauer (2005a). Anthropogenic CO<sub>2</sub> in the Southern Ocean: Distribution and inventory at the Indian-Atlantic boundary (World Ocean Circulation Experiment line I6). *Journal of Geophysical Research* 110, C06010.
- Lo Monaco, C., C. Goyet, N. Metzl, A. Poisson and F. Touratier (2005b). Distribution and inventory of anthropogenic CO<sub>2</sub> in the Southern Ocean: Comparison of three data-based methods. *Journal of Geophysical Research* 110, C09502.

- Locarnini, R.A., A.V. Mishonov, J.I. Antonov, T.P. Boyer and H.E. Garcia (2006). World Ocean Atlas 2005, Volume 1: Temperature. In: S. Levitus (Ed.), *NOAA Atlas NESDIS 61*. U.S. Government Printing Office, Washington, D.C. 182 pp.
- Lohbeck, K.T., U. Riebesell and T.B.H. Reusch (2012). Adaptive evolution of a key phytoplankton species to ocean acidification. *Nature Geoscience* 5(5), 346–351.
- Lovenduski, N.S., N. Gruber, S.C. Doney and I.D. Lima (2007). Enhanced CO<sub>2</sub> outgassing in the Southern Ocean from a positive phase of the Southern Annular Mode. *Global Biogeochemical Cycles* 21, GB2026.
- Mackas, D.L., K.L. Denman and A.F. Bennett (1987). Least Squares Multiple Tracer Analysis of Water Mass Composition. *Journal of Geophysical Research* 92(C3), 2907–2918.
- Marland, G., T.A. Boden and R.J. Andres (2008). Global, Regional, and National Fossil Fuel CO<sub>2</sub> Emissions. In *Trends: A Compendium of Data on Global Change*. Carbon Dioxide Information Analysis Center, Oak Ridge National Laboratory, U.S. Department of Energy, Oak Ridge, Tennessee, U.S.A.
- Martz, T.R., H.W. Jannasch and K.S. Johnson (2009). Determination of carbonate ion concentration and inner sphere carbonate ion pairs in seawater by ultraviolet spectrophotometric titration. *Marine Chemistry* 115(3–4), 145–154.
- Matear, R.J. and B.I. McNeil (2003). Decadal accumulation of anthropogenic CO<sub>2</sub> in the Southern Ocean: A comparison of CFC-age derived estimates to multiple-linear regression estimates. *Global Biogeochemical Cycles* 17(4), 1113.
- Matear, R.J., C.S. Wong and L. Xie (2003). Can CFCs be used to determine anthropogenic CO<sub>2</sub>? *Global Biogeochemical Cycles* 17(1), 1013.
- Matsumoto, K., J.L. Sarmiento, R.M. Key, O. Aumont, J.L. Bullister, K. Caldeira, J.-M. Campin, S.C. Doney, H. Drange, J.-C. Dutay, M.J. Follows, Y. Gao, A. Gnanadesikan, A., N. Gruber, A. Ishida, F. Joos, K. Lindsay, E. Maier-Reimer, J.C. Marshall, R.J. Matear, P. Monfray, A. Mouchet, R. Najjar, G.-K. Plattner, R. Schlitzer, R. Slater, P.S. Swathi, I.J. Totterdell, M.-F. Weirig, Y. Yamanaka, A. Yool and J.C. Orr (2004). Evaluation of ocean carbon cycle models with data-based metrics. *Geophysical Research Letters* 31, L07303.
- Matsumoto, K. and N. Gruber (2005). How accurate is the estimation of anthropogenic carbon in the ocean? An evaluation of the  $\Delta C^*$  method. *Global Biogeochemical Cycles* 19, GB3014.
- Matsumoto, K. (2007). Radiocarbon-based circulation age of the world oceans. *Journal of Geophysical Research* 112, C09004.
- McElligott, S., R.H. Byrne, K. Lee, R. Wanninkhof, F.J. Millero and R.A. Feely (1998). Discrete water column measurements of CO<sub>2</sub> fugacity and pH<sub>T</sub> in seawater: A comparison of direct measurements and thermodynamic calculations. *Marine Chemistry* 60, 63–73.
- McKinley, G.A., A.R. Fay, T. Takahashi and N. Metzl (2011). Convergence of atmospheric and North Atlantic carbon dioxide trends on multidecadal timescales. *Nature Geoscience* 4(9), 606–610.
- McNeil, B.I., R.J. Matear and B. Tilbrook (2001). Does carbon-13 track anthropogenic CO<sub>2</sub> in the Southern Ocean? *Global Biogeochemical Cycles* 15, 597–613.
- McNeil, B.I., R.J. Matear, R.M. Key, J.L. Bullister and J.L. Sarmiento (2003). Anthropogenic CO<sub>2</sub> uptake by the ocean based on the global chlorofluorocarbon data set. *Science* 299, 235–239.
- McNeil, B.I., N. Metzl, R.M. Key, R.J. Matear and A. Corbiere (2007). An empirical estimate of the Southern Ocean air-sea CO<sub>2</sub> flux. *Global Biogeochemical Cycles* 21, GB3011.
- Mehrbach, C., C.H. Culberson, J.E. Hawley and R.N. Pytkowicz (1973). Measurement of the apparent dissociation constants of carbonic acid in seawater at atmospheric pressure. *Limnology and Oceanography* 18, 897–907.
- Menke, W. (1984). *Geophysical Data Analysis: Discrete Inverse Theory*. Academic Press, 260 pp.



- Metzl, N. (2009). Decadal increase of oceanic carbon dioxide in Southern Indian Ocean surface waters (1991-2007). *Deep-Sea Research Part II* 56, 607-619.
- Metzl N., A. Corbière, G. Reverdin, A. Lenton, T. Takahashi, A. Olsen, T. Johannessen, D. Pierrot, R. Wanninkhof, S.R. Ólafsdóttir, J. Olafsson and M. Ramonet (2010). Recent acceleration of the sea surface  $f\text{CO}_2$  growth rate in the North Atlantic subpolar gyre (1993–2008) revealed by winter observations. *Global Biogeochemical Cycles* 24, GB4004.
- Mikaloff Fletcher, S.E., N. Gruber, A.R. Jacobson, S.C. Doney, S. Dutkiewicz, M. Gerber, M.J. Follows, F. Joos, K. Lindsay, D. Menemenlis, A. Mouchet, S.A. Muller and J.L. Sarmiento (2006). Inverse estimates of anthropogenic  $\text{CO}_2$  uptake, transport, and storage by the ocean. *Global Biogeochemical Cycles* 20, GB2002.
- Millero, F.J., J. Zhang, K. Lee and D. Campbell (1993). Titration Alkalinity of Seawater. *Marine Chemistry* 44(2), 153–165.
- Millero, F.J., D. Pierrot, K. Lee, R. Wanninkhof, R.A. Feely, C.L. Sabine, R.M. Key and T. Takahashi (2002). Dissociation constants for carbonic acid determined from field measurements. *Deep-Sea Research Part I* 49, 1705–1723.
- Millero, F.J., T. Graham, F. Huang, H. Bustos-Serrano and D. Pierrot (2006). Dissociation constants of carbonic acid in seawater as a function of salinity and temperature. *Marine Chemistry* 100(1-2), 80–94.
- Millero, F.J., R. Woosley, B. DiTrollo and J. Waters (2009). The effect of ocean acidification on the speciation of metals in natural waters. *Oceanography* 22, 72-85.
- Mintrop, L., F.F. Perez, M. Gonzalez-Davila, M.J. Santana-Casiano and A. Kortzinger (2000). Alkalinity determination by potentiometry: Intercalibration using three different methods. *Ciencias Marinas* 26(1), 23-37.
- Mojica Prieto, F.J. and F.J. Millero (2002). The values of  $\text{pK}_1 + \text{pK}_2$  for the dissociation of carbonic acid in seawater. *Geochimica et Cosmochimica Acta* 66(14), 2529–2540.
- Mucci, A. (1983). The solubility of calcite and aragonite in seawater at various salinities, temperatures, and one atmosphere total pressure. *American Journal of Science* 283(7), 781–799.
- Murata, A., Y. Kumamoto, K. Sasaki, S. Watanabe and M. Fukasawa (2008). Decadal increases of anthropogenic  $\text{CO}_2$  in the subtropical South Atlantic Ocean along 30°S. *Journal of Geophysical Research* 113, C06007.
- Ólafsson, J., S.R. Ólafsdóttir, A. Benoit-Cattin, M. Danielsen, T.S. Arnarson and T. Takahashi (2009). Rate of Iceland Sea acidification from time series measurements. *Biogeosciences* 6, 2661-2668.
- Olsen, A., A.M. Omar, R.G.J. Bellerby, T. Johannessen, U. Ninnemann, K.R. Brown, K.A. Olsson, J. Ólafsson, G. Nondal, C. Kivimäe, S. Kringstad, C. Neill and S. Ólafsdóttir (2006). Magnitude and origin of the anthropogenic  $\text{CO}_2$  increase and  $^{13}\text{C}$  Suess effect in the Nordic seas since 1981. *Global Biogeochemical Cycles* 20, 1-12.
- Olsen, A. (2009). Nordic Seas total dissolved inorganic carbon data in CARINA. *Earth System Science Data* 1, 35-43.
- Orr, J.C., E. Maier-Reimer, U. Mikolajewicz, P. Monfray, J.L. Sarmiento, J.R. Toggweiler, N.K. Taylor, J. Palmer, N. Gruber, C.L. Sabine, C. Le Quéré, R.M. Key and J. Boutin (2001): Estimates of anthropogenic carbon uptake from four three-dimensional global ocean models. *Global Biogeochemical Cycles* 15, 43–60.
- Orr, J.C., V.J. Fabry, O. Aumont, L. Bopp, S.C. Doney, R.A. Feely, A. Gnanadesikan, N. Gruber, A. Ishida, F. Joos, R.M. Key, K. Lindsay, E. Maier-Reimer, R.J. Matear, P. Monfray, A. Mouchet, R.G. Najjar, G.-K. Plattner, K.B. Rodgers, C.L. Sabine, J.L. Sarmiento, R. Schlitzer, R.D. Slater, I.J. Totterdell, M.-F. Weirig, Y. Yamanaka and A. Yool (2005). Anthropogenic ocean acidification over the twenty-first century and its impact on calcifying organisms. *Nature* 437, 681-686.

- Park, P.K. (1969). Oceanic CO<sub>2</sub> system: an evaluation of ten methods of investigation. *Limnology and Oceanography* 14(2), 179–186.
- Peacock, S. (2004). Debate over the ocean bomb radiocarbon sink: Closing the gap. *Global Biogeochemical Cycles* 18, GB2022.
- Peacock, S. and M. Maltrud (2006). Transit-time distributions in a global ocean model. *Journal of Physical Oceanography* 36(3), 474–495.
- Peng, T., R. Wanninkhof, J.L. Bullister, R.A. Feely and T. Takahashi (1998). Quantification of decadal anthropogenic CO<sub>2</sub> uptake in the ocean based on dissolved inorganic carbon measurements. *Nature* 396, 560–563.
- Peng, T., R. Wanninkhof and R.A. Feely (2003). Increase of anthropogenic CO<sub>2</sub> in the Pacific Ocean over the last two decades. *Deep-Sea Research Part II* 50, 3065–3082.
- Peng, T. and R. Wanninkhof (2010). Increase in anthropogenic CO<sub>2</sub> in the Atlantic Ocean in the last two decades. *Deep-Sea Research Part I* 57(6), 755–770.
- Perez, F.F. and F. Fraga (1987). A precise and rapid analytical procedure for alkalinity determination. *Marine Chemistry* 21, 169–182.
- Perez, F.F., M. Vázquez-Rodríguez, E. Louarn, X.A. Padin, H. Mercier and A.F. Ríos (2008). Temporal variability of the anthropogenic CO<sub>2</sub> storage in the Irminger Sea. *Biogeosciences* 5, 1669–1679.
- Perez, F.F., M. Vázquez-Rodríguez, H. Mercier, A. Velo, P. Lherminier and A.F. Ríos (2010). Trends of anthropogenic CO<sub>2</sub> storage in North Atlantic water masses. *Biogeosciences* 7(5), 1789–1807.
- Peters, G.P., G. Marland, C. Le Quéré, T. Boden, J.G. Canadel and M.R. Raupach (2012). Rapid growth in CO<sub>2</sub> emissions after the 2008–2009 global financial crisis. *Nature Climate Change* 2, 2–4.
- Pierrot, D., C. Neill, K. Sullivan, R. Castle, R. Wanninkhof, H. Luger, T. Johannessen, A. Olsen, R.A. Feely and C.E. Cosca (2009). Recommendations for autonomous underway pCO<sub>2</sub> measuring systems and data-reduction routines. *Deep-Sea Research Part II* 56(8–10), 512–522.
- Poisson, A. and C.T.A. Chen (1987). Why is there little anthropogenic CO<sub>2</sub> in the Antarctic Bottom Water? *Deep-Sea Research Part A* 34, 1255–1275.
- Poole, R. and M. Tomczak (1999). Optimum multiparameter analysis of the water mass structure in the Atlantic Ocean thermocline. *Deep-Sea Research Part I* 46(11), 1895–1921.
- Postma, H. (1964). The exchange of oxygen and carbon dioxide between the ocean and the atmosphere. *Netherlands Journal of Sea Research* 2(2), 258–283.
- Prinn, R.G., R.F. Weiss, P.J. Fraser, P.G. Simmonds, D.M. Cunnold, F.N. Alyea, S. O'Doherty, P. Salameh, B.R. Miller, J. Huang, R.H.J. Wang, D.E. Hartley, C. Harth, L.P. Steele, G. Sturrock, P.M. Midgley and A. McCulloch (2000). A history of chemically and radiatively important gases in air deduced from ALE/GAGE/AGAGE. *Journal of Geophysical Research* 105, 17751–17792.
- Raupach, M.R., G. Marland, P. Ciais, C. Le Quéré, J.G. Canadell, G. Klepper and C.B. Field (2007). Global and regional drivers of accelerating CO<sub>2</sub> emissions. *Proceedings of the National Academy of Sciences* 104(24), 10288.
- Redfield, A.C., B.H. Ketchum and F.A. Richards (1963). The influence of organisms on the composition of sea-water. In: Hill, M.N. (Ed.), *The composition of seawater. Comparative and descriptive oceanography*. Harvard University Press.
- Reinthal, T., K. Bakker, R. Manuels, J. van Ooijen and G.J. Herndl (2006). Fully automated spectrophotometric approach to determine oxygen concentrations in seawater via continuous-flow analysis. *Limnology and Oceanography: Methods* 4, 358–366.

- Riebesell, U., K.G. Schulz, R.G.J. Bellerby, M. Botros, P. Fritsche, M. Meyerhöfer, C. Neill, G. Nondal, A. Oschlies, J. Wohlers and E. Zöllner (2007). Enhanced biological carbon consumption in a high CO<sub>2</sub> ocean. *Nature* 450(7169), 545–548.
- Ríos, A.F., A. Velo, P.C. Pardo, M. Hoppema and F.F. Perez (2012). An update of anthropogenic CO<sub>2</sub> storage rates in the western South Atlantic basin and the role of Antarctic Bottom Water. *Journal of Marine Systems* 94(C), 197–203.
- Roche, M. and F.J. Millero (1998). Measurement of total alkalinity of surface waters using a continuous flowing spectrophotometric technique. *Marine Chemistry* 60(1-2), 85–94.
- Ronski, S. and G. Budéus (2005). Time series of winter convection in the Greenland Sea. *Journal of Geophysical Research* 110, C04015.
- Roussenov, V., R.G. Williams, M.J. Follows and R.M. Key (2004). Role of bottom water transport and diapycnic mixing in determining the radiocarbon distribution in the Pacific. *Journal of Geophysical Research* 109, C06015.
- Sabine, C.L., R.M. Key, K. Johnson, F.J. Millero, A. Poisson, J.L. Sarmiento, D.W.R. Wallace and C.D. Winn (1999). Anthropogenic CO<sub>2</sub> inventory of the Indian Ocean. *Global Biogeochemical Cycles* 13, 179-198.
- Sabine, C.L., R.A. Feely, R.M. Key, J.L. Bullister, F.J. Millero, K. Lee, T.-H. Peng, B. Tilbrook, T. Ono and C.S. Wong (2002a). Distribution of anthropogenic CO<sub>2</sub> in the Pacific Ocean. *Global Biogeochemical Cycles* 16(4), 1083.
- Sabine, C.L., R.M. Key, R.A. Feely and D. Greeley (2002a). Inorganic carbon in the Indian Ocean: Distribution and dissolution processes. *Global Biogeochemical Cycles* 16(4), 1067.
- Sabine, C.L., R.A. Feely, N. Gruber, R.M. Key, K. Lee, J.L. Bullister, R. Wanninkhof, C.S. Wong, D.W.R. Wallace, B. Tilbrook, F.J. Millero, T.-H. Peng, A. Kozyr, T. Ono and A.F. Rios (2004). The oceanic sink for anthropogenic CO<sub>2</sub>. *Science* 305, 367–370.
- Sabine, C.L., R.M. Key, A. Kozyr, R.A. Feely, R. Wanninkhof, F.J. Millero, T.-H. Peng, J.L. Bullister and K. Lee (2005). *Global Ocean Data Analysis Project: Results and Data*. ORNL/CDIAC-145, NDP-083, Carbon Dioxide Information Analysis Center, Oak Ridge National Laboratory, US Department of Energy, Oak Ridge, Tennessee. 110 pp.
- Sabine, C.L., R.A. Feely, F.J. Millero, A.G. Dickson, C. Langdon, S. Mecking and D. Greeley (2008). Decadal changes in Pacific carbon. *Journal of Geophysical Research* 113, C07021.
- Sabine, C.L. and T. Tanhua (2010). Estimation of Anthropogenic CO<sub>2</sub> Inventories in the Ocean. *Annual Review of Marine Science* 2(1), 175–198.
- Sarmiento, J.L., C. Le Quéré and S.W. Pacala (1995). Limiting future atmospheric carbon dioxide. *Global Biogeochemical Cycles* 9(1), 121–137.
- Sarmiento, J.L. and N. Gruber (2006). *Ocean biogeochemical dynamics*. Princeton University Press. 503pp.
- Sarmiento, J.L., J. Simeon, A. Gnanadesikan, N. Gruber, R.M. Key and R. Schlitzer (2007). Deep ocean biogeochemistry of silicic acid and nitrate. *Global Biogeochemical Cycles* 21, GB1S90.
- Sarmiento, J.L., M. Gloor, N. Gruber, C. Beaulieu, A.R. Jacobson, S.E. Mikaloff Fletcher, S. Pacala and K. Rodgers (2010). Trends and regional distributions of land and ocean carbon sinks. *Biogeosciences* 7(8), 2351–2367.
- Schmitt, J., R. Schneider, J. Elsig, D. Leuenberger, A. Lourantou, J. Chappellaz, P. Köhler, F. Joos, T.F. Stocker, M. Leuenberger and H. Fischer (2012). Carbon isotope constraints on the deglacial CO<sub>2</sub> rise from ice cores. *Science* 336(6082), 711-714.
- Schnack-Schiel, S. (Ed.; 1987). The winter-expedition of the research vessel “Polarstern” to the Antarctic (ANT-V/1-3). *Reports on Polar Research* 39, 259 pp.
- Schneider, B., R. Schlitzer, G. Fischer and E. M. Nöthig (2003). Depth-dependent elemental compositions of particulate organic matter (POM) in the ocean. *Global Biogeochemical Cycles* 17(2), 1032.

- Schuster, U. and A.J. Watson (2007). A variable and decreasing sink for atmospheric CO<sub>2</sub> in the North Atlantic. *Journal of Geophysical Research* 112, C11006.
- Seidel, M.P., M.D. DeGrandpre and A.G. Dickson (2008). A sensor for in situ indicator-based measurements of seawater pH. *Marine Chemistry* 109(1-2), 18–28.
- Shiller, A.M. (1981). Calculating the Oceanic CO<sub>2</sub> Increase: A Need for Caution. *Journal of Geophysical Research* 86(C11), 11083–11088.
- Sitch, S., C. Huntingford, N. Gedney, P.E. Levy, M. Lomas, S.L. Piao, R. Betts, P. Ciais, P. Cox, P. Friedlingstein, C.D. Jones, I.C. Prentice and F.I. Woodward (2008). Evaluation of the terrestrial carbon cycle, future plant geography and climate-carbon cycle feedbacks using five dynamic global vegetation models (DGVMs). *Global Change Biology* 14, 2015–2039.
- Solomon, S., D. Qin, M. Manning, Z. Chen, M. Marquis, K.B. Averyt, M. Tignor and H.L. Miller (Eds.; 2007). *Climate Change 2007: The Physical Science Basis. Contribution of Working Group I to the Fourth Assessment Report of the Intergovernmental Panel on Climate Change*. Cambridge University Press.
- Steinfeldt, R., T. Tanhua, J.L. Bullister, R.M. Key, M. Rhein and J. Kähler (2010). Atlantic CFC data in CARINA. *Earth System Science Data* 2, 1–15.
- Stoll, M.H.C., R.W. Rommets and H.J.W. de Baar (1993). Effect of selected calculation routines and dissociation constants on the determination of total carbon dioxide in seawater. *Deep-Sea Research Part I* 40(6), 1307–1322.
- Stoll, M.H.C., K. Bakker, G. Nobbe and R. Haese (2001). Continuous-flow analysis of dissolved inorganic carbon content in seawater. *Analytical Chemistry* 73(17), 4111–4116.
- Sweeney, C., E. Gloor, A.J. Jacobson, R.M. Key, G. McKinley, J.L. Sarmiento and R. Wanninkhof (2007). Constraining global air-sea exchange for CO<sub>2</sub> with recent bomb <sup>14</sup>C measurements. *Global Biogeochemical Cycles* 21, GB2015.
- Swift, J. (2008). *A guide to submitting CTD/hydrographic/tracer data and associated documentation to the CLIVAR and Carbon Hydrographic Data Office*. UCSD Scripps Institution of Oceanography. 37pp.
- Takahashi, T., S.C. Sutherland, R. Wanninkhof, C. Sweeney, R.A. Feely, D.W. Chipman, B. Hales, G. Friederich, F. Chavez, C.L. Sabine, A. Watson, D.C.E. Bakker, U. Schuster, N. Metzl, H. Yoshikawa-Inoue, M. Ishii, T. Midorikawa, Y. Nojiri, A. Koertzing, T. Steinhoff, M. Hoppema, J. Olafsson, T.S. Arnarson, B. Tilbrook, T. Johannessen, A. Olsen, R. Bellerby, C.S. Wong, B. Delille, N.R. Bates and H.J.W. de Baar (2009). Climatological mean and decadal change in surface ocean pCO<sub>2</sub> and net sea-air CO<sub>2</sub> flux over the global oceans. *Deep-Sea Research Part II* 56, 554–577.
- Talley, L.D. (1996). Antarctic intermediate water in the South Atlantic. In: G. Wefer (Ed.), *The South Atlantic: Present and Past Circulation*. Springer, New York.
- Tanhua, T., A. Biastoch, A. Körtzinger, H. Lüger, C. Böning and D.W.R. Wallace (2006). Changes of anthropogenic CO<sub>2</sub> and CFCs in the North Atlantic between 1981 and 2004. *Global Biogeochemical Cycles* 20, GB4017.
- Tanhua, T., A. Körtzinger, K. Friis, D.W. Waugh and D.W.R. Wallace (2007). An estimate of anthropogenic CO<sub>2</sub> inventory from decadal changes in oceanic carbon content. *Proceedings of the National Academy of Sciences* 104, 3037–3042.
- Tanhua, T., D.W. Waugh and D.W.R. Wallace (2008). Use of SF<sub>6</sub> to estimate anthropogenic CO<sub>2</sub> in the upper ocean. *Journal of Geophysical Research* 113, C04037.
- Tanhua, T. (2009). *MATLAB program developed for secondary quality control of hydrographic data*. Carbon Dioxide Information Analysis Center, Oak Ridge National Laboratory, US Department of Energy, Oak Ridge, Tennessee.
- Tanhua, T., R. Steinfeldt, R.M. Key, P. Brown, N. Gruber, R. Wanninkhof, F.F. Perez, A. Körtzinger, A. Velo, U. Schuster, S. van Heuven, J.L. Bullister, I. Stendardo, M. Hoppema, A.

- Olsen, A. Kozyr, D. Pierrot, C. Schirnick and D.W.R. Wallace (2010a). Atlantic Ocean CARINA data: overview and salinity adjustments. *Earth System Science Data* 2, 17-34.
- Tanhua, T., S. van Heuven, R.M. Key, A. Velo, A. Olsen and C. Schirnick (2010b). Quality control procedures and methods of the CARINA database. *Earth System Science Data* 2, 35-49.
- Thomas, H. (2002). Remineralization ratios of carbon, nutrients, and oxygen in the North Atlantic Ocean: A field databased assessment. *Global Biogeochemical Cycles* 16(3), 24.
- Thomas H., A.E.F. Prowe, S. van Heuven, Y. Bozec, H.J.W. de Baar, L.-S. Schiettecatte, K. Suykens, M. Koné, A.V. Borges, I.D. Lima and S.C. Doney (2007). Rapid decline of the CO<sub>2</sub> buffering capacity in the North Sea and implications for the North Atlantic Ocean. *Global Biogeochemical Cycles* 21, GB4001.
- Tomczak, M. (1981). A multi-parameter extension of temperature/salinity diagram techniques for the analysis of non-isopycnal mixing. *Progress in Oceanography* 10, 147-171.
- Tomczak, M. (1999). Some historical, theoretical and applied aspects of quantitative water mass analysis. *Journal of Marine Research* 57, 75-303.
- Tomczak, M. and J.S. Godfrey (2003). *Regional Oceanography: an Introduction*. Second edition. Daya Publishing House, India.
- Touratier, F. and C. Goyet (2004a). Applying the new TrOCA approach to assess the distribution of anthropogenic CO<sub>2</sub> in the Atlantic Ocean. *Journal of Marine Systems* 46, 181-197.
- Touratier, F. and C. Goyet (2004b). Definition, properties, and Atlantic Ocean distribution of the new tracer TrOCA. *Journal of Marine Systems* 46, 169-179.
- Touratier, F., L. Azouzi and C. Goyet (2007). CFC-11,  $\Delta^{14}\text{C}$  and  $^3\text{H}$  tracers as a means to assess anthropogenic CO<sub>2</sub> concentrations in the ocean. *Tellus B* 59, 318-325.
- van Heuven, S.M.A.C., D. Pierrot, J.W.B. Rae, E. Lewis and D.W.R. Wallace (2009). *MATLAB Program Developed for CO<sub>2</sub> System Calculations*. ORNL/CDIAC-105b. Carbon Dioxide Information Analysis Center, Oak Ridge National Laboratory, U.S. Department of Energy, Oak Ridge, Tennessee. (updated in 2011)
- van Heuven, S.M.A.C., M. Hoppema, O. Huhn, H. A. Slagter, and H.J.W. de Baar (2011). Direct observation of increasing CO<sub>2</sub> in the Weddell Gyre along the Prime Meridian during 1973-2008. *Deep-Sea Research II* 58, 2613-2635.
- Varekamp, J., R. Kreulen, R. Poorter and M. Bergen (1992). Carbon sources in arc volcanism, with implications for the carbon cycle. *Terra Nova* 4(3), 363-373.
- Vázquez-Rodríguez, M., F. Touratier, C.L. Lo Monaco, D.W. Waugh, X. Padin, R.G.J. Bellerby, C. Goyet, N. Metzl, A.F. Ríos and F.F. Perez (2009). Anthropogenic carbon distributions in the Atlantic Ocean: data-based estimates from the Arctic to the Antarctic. *Biogeosciences* 6, 439-451.
- Vázquez-Rodríguez, M. (2009). *On the Anthropogenic CO<sub>2</sub> in the Atlantic Ocean*. Ph.D thesis. Universidad de Vigo, Vigo, Spain.
- Velo, A., F.F. Pérez, X. Lin, R.M. Key, T. Tanhua, M. de la Paz, S. van Heuven, S. Jutterström and A.F. Ríos (2010). CARINA data synthesis project: pH data scale unification and cruise adjustments. *Earth System Science Data* 2, 133-155.
- Volk, T. and M.I. Hoffert (1985). Ocean carbon pumps: Analysis of relative strengths and efficiencies in ocean-driven atmospheric CO<sub>2</sub> changes. In: E.T. Sundquist and W.S. Broecker (eds.), *The Carbon Cycle and Atmospheric CO<sub>2</sub>: Natural Variations Archean to Present*. AGU Geophysical Monograph Series 32.
- Walker, S., R. Weiss and P. Salameh (2000). Reconstructed histories of the annual mean atmospheric mole fractions for the halocarbons CFC-11, CFC-12, CFC-113 and carbon tetrachloride. *Journal of Geophysical Research* 105, 14285-14296.
- Wallace, D.W.R. (Ed.; 1995). *Monitoring global ocean carbon inventories*. OOSDP Background Report No. 5, Texas A&M University, College Station, Texas, USA.



- Wang Z.A, X. Liu, R.H. Byrne, R. Wanninkhof, R.E. Bernstein, E.A. Kaltenbacher and J. Patten (2007). Simultaneous spectrophotometric flow-through measurements of pH, carbon dioxide fugacity, and total inorganic carbon in seawater. *Analytica Chimica Acta* 596, 23-36.
- Wanninkhof, R. and K. Thoning (1993). Measurement of fugacity of CO<sub>2</sub> in surface water using continuous and discrete sampling methods. *Marine Chemistry* 44(2-4), 189-204.
- Wanninkhof, R., S.C. Doney, T.H. Peng, J.L. Bullister, K. Lee and R.A. Feely (1999a). Comparison of methods to determine the anthropogenic CO<sub>2</sub> invasion into the Atlantic Ocean. *Tellus B* 51, 511-530.
- Wanninkhof, R., E. Lewis, R.A. Feely and F.J. Millero (1999b). The optimal carbonate dissociation constants for determining surface water pCO<sub>2</sub> from alkalinity and total inorganic carbon. *Marine Chemistry* 65, 291-301
- Wanninkhof, R., W.E. Asher, D.T. Ho, C. Sweeney and W.R. McGillis (2009). Advances in Quantifying Air-Sea Gas Exchange and Environmental Forcing. *Annual Review of Marine Science* 1(1), 213-244.
- Wanninkhof, R., S.C. Doney, J.L. Bullister, N.M. Levine, M. Warner and N. Gruber (2010). Detecting anthropogenic CO<sub>2</sub> changes in the interior Atlantic Ocean between 1989 and 2005. *Journal of Geophysical Research* 115(C11), C11028.
- Warner, M.J. and R.F. Weiss (1985). Solubilities of chlorofluorocarbons 11 and 12 in water and seawater. *Deep-Sea Research Part I* 32(12), 1485-1497.
- Watanabe, A., H. Kayanne, K. Nozaki, K. Kato, A. Negishi, S. Kudo, H. Kimoto, M. Tsuda and A.G. Dickson (2004). A rapid, precise potentiometric determination of total alkalinity in seawater by a newly developed flow-through analyzer designed for coastal regions. *Marine Chemistry* 85, 75-87.
- Watson, A.J, U. Schuster, D.C.E Bakker, N.R. Bates, A. Corbiere, M. Gonzalez-Davila, T. Friedrich, J. Hauck, C. Heinze, T. Johannessen, A. Kortzinger, N. Metzl, J. Olafsson, A. Olsen, A. Oschlies, X.A. Padin, B. Pfeil, J.M. Santana-Casiano, T. Steinhoff, M. Telszewski, A.F. Rios, D.W.R. Wallace and R. Wanninkhof (2009). Tracking the Variable North Atlantic Sink for Atmospheric CO<sub>2</sub>. *Science* 326(5958), 1391-1393.
- Waugh, D.W., T.M. Hall, B.I. McNeil, R.M. Key and R.J. Matear (2006). Anthropogenic CO<sub>2</sub> in the oceans estimated using transit time distributions. *Tellus B* 58, 376-389.
- Weiss, R. (1970). The solubility of nitrogen, oxygen and argon in water and seawater. *Deep Sea Research and Oceanographic Abstracts* 7, 721-735.
- Weiss, R. (1974). Carbon dioxide in water and seawater: the solubility of a non-ideal gas. *Marine Chemistry* 2, 203-215.
- Weppernig, R., P. Schlosser, S. Khatiwala and R. Fairbanks (1996). Isotope data from Ice Station Weddell: Implications for deep water formation in the Weddell Sea. *Journal of Geophysical Research* 101, 25-25.
- Wilke, R., D.W.R. Wallace and K. Johnson (1993). Water-Based, Gravimetric Method for the Determination of Gas Sample Loop Volume. *Annals of Chemistry* 65(17), 2403-2406.
- Wunsch, C. (1996). *The Ocean Circulation Inverse Problem*. Cambridge University Press. 437 pp.
- Yool, A., A. Oschlies, A.J.G. Nurser and N. Gruber (2010). A model-based assessment of the TrOCA approach for estimating anthropogenic carbon in the ocean. *Biogeosciences* 7, 723-751.
- Zeebe, R.E. and D.A. Wolf-Gladrow (2001). *CO<sub>2</sub> in seawater: equilibrium, kinetics, isotopes*. Elsevier Oceanography Series 65. 346pp.





## **Acknowledgements / dankwoord**





One of the many joys of making the final touches on this thesis (lay-out, maps, methods section) is that the whole period of research sits in front of me at a single time. Looking at that, and having to scrape my mind about which ports we sailed out of and into, with whom and doing what, brings back many happy memories of these activities and the people involved. These last pages are intended to thank these and more people, who all contributed in one way or another to my finishing this thesis.

First and foremost, Hein de Baar, first promotor, I am very grateful for the many exciting opportunities you provided me with over the past years. Your continuous support (either direct: feeding me apple pie and espresso while spelling out paragraph after paragraph; or invisible in the form of surprise invitations to interesting and/or important meetings) and your seemingly endless patience have allowed me to find my way in the field of chemical oceanography. It's been a marvelous time.

Harro Meijer, second promotor, the hospitable environment of your lab and your enthusiasm about the new oceanographic isotope research I try to do there are very much appreciated – your support has been invaluable during the many months I needed to finish this thesis.

I'd like to thank the thesis assessment committee, consisting of professors Leif Anderson, Monika Rhein and Herman Ridderinkhof, for its willingness to review and comment on the manuscript.

Many colleagues, at home and abroad, have helped me gain my footing in the world of oceanography. From among these: John Dacey, I loved your lab and your place. Your independent, creative style of doing research was an inspiration. Henk Zemmeling, you have supported me during the first few of years of my studies, and it was a loss that you left the lab in 2008 – I'm sure I could've learned much more from you (not in the least in the area of writing up). Mario Hoppema, I'd like to thank you for the many insights you have given me, and for all the time you devoted to the careful and exact assessments of the many figures and draft texts I've sent you. Your comments have helped me to sharpen my reasoning. Toste Tanhua, you got me started using MATLAB in the spring of 2007, which has allowed me to do more funky data analyses than I may ever find use for. Thanks for that and the many opportunities for collaboration you've offered.

Additional thanks go out to Bob Key, Are Olsen, Benjamin Pfeill and the many others that have made attending the various CarboOcean workshops and symposia so valuable, interesting and pleasant.

I am grateful to all my current colleagues at the Centre for Isotope Research – in particular my roommate Charlotte – for all the fun, enthusiasm, and support and understanding whenever I was not there or not available due to kids or thesis.

As much as I feel at home in my current workplace, I hold many memories of the happy group of (ex-) PhDs at the department of Ocean Ecosystems at the Biological Centre in Haren.

Peter, Han, Paul, Willem, Karin, Anouk, Henk-Jan, Deniz, Gemma, Ika and all others, thanks for the great fun we had. I also owe thanks to Winfried Gieskes, Wim Klaassen, Jacqueline Stefels, Anita Buma and Eize Stamhuis – all of whom have at some time contributed to my study and work related to this thesis.

My third – though occasional – workplace during these years was at the Royal Netherlands Institute for Sea Research on Texel, which has proven to be always very welcoming. I'd like to thank all local students and co-workers for livening up my many brief stays there. In that context, I'd like to thank Karel Bakker above all others for his hospitality, helpfulness and humor. Jan van Ooijen, Evaline van Weerlee and - again - Karel Bakker, thank you for the interesting discussions and advice about precision, accuracy and all other things metrological. Your world-class nutrient lab has been a great inspiration (and has yielded many thousands of measurements supporting this work). Klaas Timmermans, Josje Snoek, Babette, Mascha, Astrid, Lesley and Elizabeth, thanks for making the NIOZ CO<sub>2</sub> lab such a pleasant place to have worked in.

During the last seven years, many months were spent on board the research vessels *Pelagia* and *Polarstern*. I am grateful to the officers and crew who have without exception been helpful, dedicated and friendly. This thesis could not exist without your professionalism.

Captain Schwarze, officers and crew, Eberhard Fahrbach, Hein de Baar and fellow passengers of Polarstern expedition ANT-XXIV/3, thank you very much for your great care and support during the dark days in Atka Bay and afterwards. Willem and Stefan, you will be remembered.

Alice, thank you for having me by your side during your days in Polarstern's hospital and I'm glad you are doing as well as you are.

The CO<sub>2</sub> measurements on board were not generally performed alone (rather, alone in shifts). I'd like to thank my highly-regarded fellow container dwellers Friederike, Henk, Maaïke, Astrid, Hans and Lesley for their dedication, support, and friendship.

Expedition leaders Thomas, Veth, Lemke, Brummer, Kieke, Fahrbach, de Baar, Gerringa and Rijkenberg, thanks for excellent planning, care and collaboration. I am grateful to Hendrik van Aken for having offered the opportunity to join several of his expeditions. NIOZ technicians and analysts Willem, Leon, Lorendz, Martin, Ruud, Sander, Santiago, Sven, you've offered great support – many expeditions would have ended mere days after leaving port if not for your skill and commitment.

Cabin-mates Rodrigo, Erwin and Rob, fellow passengers Lukas, Claire, Anne-Carlijn, Maarten, Patrick L., Patrick S., and all others not mentioned here: thanks for the great times we've had on board – you have made these trips unforgettable.

Dan vanaf hier in het Nederlands: Anne Chris, Kirsten, Renske, Marco, Ivo (de oude), Anne Marthe, Hendrike, Martijn, Anneke, Reinout en Alinde, lieve (ex-)biologische vrienden en al jullie niet genoemde partners (voor zover niet onderling verweven), maar ook Berend & Marjolein, Els & Eelke, Ika & Chris en Himme & Lisette, dank voor alle leuke, smakelijke en/ of avontuurlijke dingen die we afgelopen jaren gedaan hebben, alsmede voor het niet ál te

regelmatig vragen hoe lang ik nog over m'n boekje dacht te gaan doen. Zonder de door jullie geboden steun en afleiding zou het schrijven van dit proefschrift vast nooit gelukt zijn.

Paranimf #1, lieve Ika, we lachen al met elkaar sinds de keer dat ik je dat gedoe met die dissociatieconstanten moest uitleggen op een van je eerste dagen als *aio*, een jaar nadat ik begon. Dank voor alle leuke dingen die we daarna samen hebben gedaan en nog steeds doen, dat ik als eerste mocht eindigen, en dat je altijd zo betrouwbaar, vol vertrouwen en enthousiast bent.

Himme, paranimf #2, muzikale offshore-scheefsbouwer, wij gaan nog veel langer terug, en ik kan me mijn eerste keer lachen met je niet herinneren – pech. Dank voor de constante bron van verantwoord vermaak die je biedt/bent, voor je niet-aflatende interesse voor – en je relativerende kijk op – deze iets nerdige variant van werken op zee. Kenmerkend stoer en optimistisch van je dat je dit wetenschappelijk werk zonder meer wilt helpen verdedigen.

Papa, mama, Renée, Rolf, mijn lieve ouders-en-eega's, jullie zijn enthousiast en ondersteunend geweest in elke fase van mijn studie en promotieonderzoek. Hoe vaak ik ook in de rats, aan de grond of op een schip zat, jullie hebben mij altijd alle ruimte gegeven en nooit het geloof (of in ieder geval de hoop) opgegeven dat er uiteindelijk een boekje zou liggen. Heel veel dank daarvoor.

Hugo, stoere broer van me, ik ben zo trots als een aap/pauw op je – prachtig om te zien hoe jij je tegen de stroom in ontwikkeld hebt, en hoe snel je nog steeds doorgroeit. Ik hoop jou en Myrthe snel weer te kunnen komen opzoeken.

Tieme, Cokkie, Marianne, Joost, mijn lieve schoonouders, -zus en soort van zwager, jullie worden hartelijk bedankt voor je niet-aflatende ondersteuning, jullie humor en de broodnodige relativering.

Lieve Eefje, ik ben je onbeschrijflijk dankbaar voor de liefde die ik van je krijg, voor je net-niet-eindeloze geduld en je tactvolle volharding in het motiveren en re-organiseren van deze regelmatig- en wanhopig-vastlopende perfectionist – zonder jouw steun en aansporing zou deze promotie nooit zijn voltooid. We zijn gedurende de wording van dit proefschrift veranderd van een in eerste instantie kansloos-geacht lange-afstands-treinrelatie-studentenstel tot een heus gezinnetje met een carport en twee prachtige kleine jochies. Ik hoop ook al het volgende samen met je te mogen meemaken.

Hidde, papa is blij dat je zo'n leuk en lief ventje bent. Je hebt nu al een brede interesse, en ik hoop dat we samen nog veel mooie en leuke dingen gaan zien en doen.

Ivo, zo klein als je nu nog bent, je schaterende lachje brengt nóg meer geluk in ons gezin. Ook met jou hoop ik nog veel bijzonders te mogen meemaken. Dank je wel dat je papa tot haast hebt gemaakt.

Groningen, 31 december 2012.





## **CV & Bibliography**



## Curriculum Vitae

Steven was born in the city of Leiden in the Netherlands on March 15<sup>th</sup>, 1980. He attended both primary and high school in the nearby town of Sassenheim. Although drawn to exact studies in Delft, he opted to study Biology at Leiden University, starting in 1998. After two years he moved to Groningen to specialize in marine biology at Rijksuniversiteit Groningen (RuG). The two-week lecture series *Introductory Oceanography* and the associated practicals piqued his interest in the role of the oceans within the 'Earth system', and two not-so-biologically-oriented internships followed. The first of those, at RuG, concerned the assessment of CO<sub>2</sub>-fluxes across the surface of the Wadden Sea using the 'eddy-covariance' technique. His second internship was performed at Woods Hole Oceanographic Institution in Massachusetts, USA. That work aimed to assess the drivers of the air-sea gas flux of dimethylsulphide (DMS), by sampling simultaneously for biology and dissolved gasses at multiple depths from a small, remote controlled boat. Steven graduated at RuG in 2005. By that time quite enamored by oceanography, he jumped at the chance to perform the adventurous PhD study that led to this thesis.

His current employment at the Centre for Isotope Research at Groningen University entails the measurement of ratios of carbon isotopes in seawater.

Steven has been living together with Eveline in Groningen since 2006. They have two lovely young sons, Hidde and Ivo.

## Bibliography

- van Heuven, S., M. Hoppema, O. Huhn, H.A. Slagter and H.J.W. de Baar (2011). Direct observation of increasing CO<sub>2</sub> in the Weddell Gyre along the Prime Meridian during 1973–2008. *Deep-Sea Research II*, 58, 2613–2635.
- van Heuven, S., D. Pierrot, J.W.B. Rae, E. Lewis and D.W.R. Wallace (2009; updated in 2011). *MATLAB Program Developed for CO<sub>2</sub> System Calculations*. ORNL/CDIAC-105b. Carbon Dioxide Information Analysis Center, Oak Ridge National Laboratory, U.S. Department of Energy, Oak Ridge, Tennessee.
- Hoppema, M., A. Velo, S. van Heuven, T. Tanhua, R.M. Key, X. Lin, D.C.E. Bakker, F.F. Perez, A.F. Ríos, C. Lo Monaco, C.L. Sabine, M. Álvarez and R.G.J. Bellerby (2009). Consistency of cruise data of the CARINA database in the Atlantic sector of the Southern Ocean. *Earth System Science Data*, 1, 63–75.
- Huhn, O., M. Rhein, M. Hoppema and S. van Heuven (2013). Decline of deep and bottom water ventilation and slowing down of anthropogenic carbon storage in the Weddell Sea, 1984–2011. (accepted for publication in *Deep-Sea Research I*).
- Key, R.M., T. Tanhua, A. Olsen, M. Hoppema, S. Jutterström, C. Schirnack, S. van Heuven, A. Kozyr, X. Lin, A. Velo, D.W.R. Wallace and L. Mintrop (2010). The CARINA data synthesis project: Introduction and overview. *Earth System Science Data*, 2, 105–121.
- Klunder, M.B., D. Bauch, P. Laan, H.J.W. de Baar, S. van Heuven and S. Ober (2012). Dissolved iron in the Arctic shelf seas and surface waters of the Central Arctic Ocean: Impact of Arctic river water and ice-melt. *Journal of Geophysical Research*, 117, C01027.



- Lo Monaco, C., M. Álvarez, R.M. Key, X. Lin, T. Tanhua, B. Tilbrook, D.C.E. Bakker, **S. van Heuven**, M. Hoppema, N. Metzl, A.F. Ríos, C.L. Sabine and A. Velo (2010). Assessing the internal consistency of the CARINA database in the Indian sector of the Southern Ocean. *Earth System Science Data*, 2, 51-70.
- Neven, I.A., J. Stefels, **S. van Heuven**, H.J.W. de Baar and J.T.M. Elzenga (2011). High plasticity in inorganic carbon uptake by Southern Ocean phytoplankton in response to ambient CO<sub>2</sub>. *Deep-Sea Research II*, 58, 2636-2646.
- Pierrot, D., P. Brown, **S. van Heuven**, T. Tanhua, U. Schuster, R. Wanninkhof and R.M. Key (2010). CARINA TCO<sub>2</sub> data in the Atlantic Ocean. *Earth System Science Data*, 2, 177-187.
- Olsen, A., R.M. Key, E. Jeansson, E. Falck, J. Olafsson, **S. van Heuven**, I. Skjelvan, A.M. Omar, K.A. Olsson, L.G. Anderson, S. Jutterström, F. Rey, T. Johannessen, R.G.J. Bellerby, J. Blindheim, J.L. Bullister, B. Pfeil, X. Lin, A. Kozyr, C. Schirnack, T. Tanhua and D.W.R. Wallace (2009). Overview of the Nordic Seas CARINA data and salinity measurements. *Earth System Science Data*, 1, 25-34.
- Provoost, P., **S. van Heuven**, K. Soetaert, W.P.M. Laane and J.J. Middelburg (2010). Long-term record of pH in the Dutch coastal zone: a major role for eutrophication-induced changes. *Biogeosciences*, 7, 3869-3878.
- Rutgers van der Loeff, M.M., P. Cai, I. Stimac, R. Middag, M. Klunder and **S. van Heuven** (2011). <sup>234</sup>Th in surface waters: distribution of particle export flux across the Antarctic Circumpolar Current and in the Weddell Sea during the GEOTRACES expedition ZERO and DRAKE. *Deep-Sea Research II*, 58, 2749-2766.
- Sabine, C.L., M. Hoppema, R.M. Key, B. Tilbrook, **S. van Heuven**, C. Lo Monaco, N. Metzl, M. Ishii, A. Murata and S. Musielewicz (2010). Assessing the internal consistency of the CARINA data base in the Pacific sector of the Southern Ocean. *Earth System Science Data*, 2, 195-204.
- Tanhua, T., R. Steinfeldt, R.M. Key, P. Brown, N. Gruber, R. Wanninkhof, F.F. Pérez, A. Körtzinger, A. Velo, U. Schuster, **S. van Heuven**, J.L. Bullister, I. Stendardo, M. Hoppema, A. Olsen, A. Kozyr, D. Pierrot, C. Schirnack and D.W.R. Wallace (2010). Atlantic Ocean CARINA data: overview and salinity adjustments. *Earth System Science Data*, 2, 17-34.
- Tanhua, T., **S. van Heuven**, R.M. Key, A. Velo, A. Olsen and C. Schirnack (2010). Quality control procedures and methods of the CARINA database. *Earth System Science Data*, 2, 35-49.
- Thomas H., A.E.F. Prowe, **S. van Heuven**, Y. Bozec, H.J.W. de Baar, L.-S. Schiattecatte, K. Suykens, M. Koné, A.V. Borges, I.D. Lima and S.C. Doney (2007). Rapid decline of the CO<sub>2</sub> buffering capacity in the North Sea and implications for the North Atlantic Ocean. *Global Biogeochemical Cycles*, 21, GB4001.
- Velo, A., F.F. Pérez, X. Lin, R.M. Key, T. Tanhua, M. de la Paz, **S. van Heuven**, S. Jutterström and A. F. Ríos (2010). CARINA data synthesis project: pH data scale unification and cruise adjustments. *Earth System Science Data*, 2, 133-155.



